Universitat
Internacional
de Catalunya

Influence of Cu(II) and Glycodendrimers on Amyloid-beta Peptide Aggregation

Oxana Klementieva

ADVERTIMENT. La consulta d’aquesta tesi queda condicionada a l’acceptació de les següents condicions d'ús: La difusió d’aquesta tesi per mitjà del servei TDX (www.tesisenxarxa.net) ha estat autoritzada pels titulars dels drets de propietat intel·lectual únicament per a usos privats emmarcats en activitats d’investigació i docència. No s’autoritza la seva reproducció amb finalitats de lucre ni la seva difusió i posada a disposició des d’un lloc aliè al servei TDX. No s’autoritza la presentació del seu contingut en una finestra o marc aliè a TDX (framing). Aquesta reserva de drets afecta tant al resum de presentació de la tesi com als seus continguts. En la utilització o cita de parts de la tesi és obligat indicar el nom de la persona autora.

ADVERTENCIA. La consulta de esta tesis queda condicionada a la aceptación de las siguientes condiciones de uso: La difusión de esta tesis por medio del servicio TDR (www.tesisenred.net) ha sido autorizada por los titulares de los derechos de propiedad intelectual únicamente para usos privados enmarcados en actividades de investigación y docencia. No se autoriza su reproducción con finalidades de lucro ni su difusión y puesta a disposición desde un sitio ajeno al servicio TDR. No se autoriza la presentación de su contenido en una ventana o marco ajeno a TDR (framing). Esta reserva de derechos afecta tanto al resumen de presentación de la tesis como a sus contenidos. En la utilización o cita de partes de la tesis es obligado indicar el nombre de la persona autora.

WARNING. On having consulted this thesis you’re accepting the following use conditions: Spreading this thesis by the TDX (www.tesisenxarxa.net) service has been authorized by the titular of the intellectual property rights only for private uses placed in investigation and teaching activities. Reproduction with lucrative aims is not authorized neither its spreading and availability from a site foreign to the TDX service. Introducing its content in a window or frame foreign to the TDX service is not authorized (framing). This rights affect to the presentation summary of the thesis as well as to its contents. In the using or citation of parts of the thesis it’s obliged to indicate the name of the author.

Influence of Cu(II) and Glycodendrimers on Amyloid-beta Peptide Aggregation

Oxana Klementieva

Influence of Cu(II) and Glycodendrimers on Amyloid-beta Peptide Aggregation

Oxana Klementieva

A thesis submitted to
Universitat Internacional de Catalunya
For the degree of
DOCTOR OF PHILOSOPHY

UIC
Thesis Director

Dr. A. Gella

UAB
Thesis Co-Director

Dr. J. Cladera

November 2011

Universitat Internacional de Catalunya
Facultat de Medicina i Ciències de la Salut

Abstract

Senile plaques of Alzheimer's disease (AD) patients are composed primarily of the amyloid-β peptide (Aβ), and within these plaques Cu(II) ions are found concentrated and directly bound to Aβ. Cu(II) homeostasis is severely impaired in AD patients and recent *in vivo* studies implicate Cu(II) in the aetiology of AD. However the role of Cu(II) ions in AD is currently highly disputed.

A nowadays widely accepted point of view is that those amorphous aggregates of Aβ peptide are the toxic Aβ species forming in the initial states of the oligomerization process. Aβ fibrils, the end product of this process and the structural basis of amyloid plaques, would be non-toxic. One way of action against the damaging effects of amyloid peptides on neuronal functioning consists in finding molecules which are able either to block the formation of the toxic oligomers, to disrupt their structure or to lock the amyloid into what may be a non-cytotoxic form of the aggregate. It has been shown that glycodendrimers have a decreased toxicity with respect to other charged dendrimers and have a great potential as antiamiloydogenic agents.

Influence of Cu(II) on Aβ aggregation and amyloidogenic properties of glyco dendrimers are the two aspects which were investigated in this thesis. In Chapter 3.1 AFM, TEM, SEM, SAXS, FTIR and fluorescence spectroscopy were used to study a morphology and a secondary structure of Aβ-Cu(II) aggregates. Finally, the toxic effects of Aβ40-Cu(II) aggregates were studied in a PC12 and SH-SY5Y cell lines. Aβ40 aggregated with Cu(II) was found to have enhanced cell toxicity compared with those of Aβ40 alone. Therefore this study finds considerable support for an altered amyloid hypothesis where Cu(II) dyshomeostasis has a central role in AD.

In Chapter 3.2 of this thesis it is shown that maltose dense shell dendrimers can be efficiently used to inhibit Alzheimer's amyloid peptide cell toxicity by facilitating the clustering of amyloid fibrils. Maltose dendrimers are confirmed to be non-toxic to PC12 and SH-SY5Y cell lines and to inhibit the normal degree of toxicity of Aβ40 fed to the cells in its fibrillar form. The results show that both maltose dendrimers effectively interfere with the Aβ40 polymerization, in a way that is mainly dependent on the maltose surface charge density. Therefore these results allow a better understanding of the potential use of dendrimers as antyamiloidogenic agents and call the attention towards the necessity to carefully evaluate the toxicity of the different antiamyloid compound-peptide complexes.

**This thesis is dedicated to my children, Gleb and Oleg,
who have encouraged me to put hard work
into everything I strive for.**

Acknowledgements

The origin of the book you hold lies in the early autumn of 2008 when Dr. Nuria Durany offered me to join to her research group at the Universitat Internacional de Catalunya. Her interest in Alzheimer's disease research has been so inspiriting that I was also griped. It did not take me a long to make mi mind and begin a journey toward the doctorate title.

Before I even started writing this thesis, I already knew that part where I say "thank you" would not be easy to write. The well-known "thank you" paradox states: the more persons and details you mention, the higher the probability that you forget someone. Therefore, I would like to express my one big "THANK YOU" to everyone who contributed in one way or another to the successful end of my journey and made the past three years predominantly interest ones.

However. to make it a bit more personal after all, I would like to mention some people for their very special contribution to this work. My grate thanks and appreciation go to my supervisors, Dr. J. Cladera, Dr. N. Durany and Dr. A. Gella who have dedicated to my research and supported me in a very friendly manner without their generosity, patience and knowledge this thesis would have never completed. My colleagues from Universitat Internacional de Catalunya and Universitat Autonoma de Barcelona always helped me always and a lot, they have provided me with a very pleasant working atmosphere for which I am truly grateful. I would like to thank the members of the committees who have generosity given their time and expertise to read my work and comment on it.

My special thanks go to my friends, thought they could not help me with the research itself, they gave me much needed distraction from it. My biggest gratitude goes to my to my parents and my father-in-low for their unconditional love and immense confidence in me. Last but not least my warmest thanks are to my husband, Konstantin, for possibility to live in Spain, to work and to write this thesis, for reading my drafts, for unforgettable comments, for providing me with a lot useful help, for standing by me and sharing with me hardest, but most important and pleasant job of raising our sons, Gleb and Oleg, who are my pride and joy.

Sant Cugat dell Vales, January 2012
Oxana Klementieva,

Abbreviations

The three-letter and single-letter standard amino acid codes are used to describe amino acid residues.

AD Alzheimer’s disease

Aβ Amyloid-β peptide

Aβ16 Amyloid-β peptide containing first 16 residues

Aβ28 Amyloid-β peptide containing first 28 residues

Aβ40 Amyloid-β peptide containing first 40 residues

Aβ42 Amyloid-β peptide containing 42 residues

AFM Atomic Force Microscopy

APP Amyloid precursor protein

Å Angstrom

APOE Apolipoprotein E

AICD APP intracellular domain

AFU Arbitrary fluorescence units

AFM Atomic force microscopy

CSF Cerebrospinal fluid

CD Circular dichroism

c Concentration

CTF Co-Factor theory

D2O Deuterated water

DLS Dynami Light Scattering

DMSO Dimethyl sulfoxide

DMEM Dulbecco’s Modified Eagle Medium

em Emission

EM Electron microscopy

EPR Electron paramagnetic resonance

ER Endoplasmic reticulum

ex Excitation

fAD Familial Alzheimer’s disease

FTIR Fourier transform infrared

HEPES (N-[2-hydroxyethyl] piperazine-N’-[2 ethanesulfonic acid])

M Molar

mg Milligram

mL Millilitre

mM Millimolar

M Molar

MTT4,5-Dimethylthiazol-2-yl)-2,5-Diphenyltetrazolium Bromide

nm Nanometre

nM Nanomolar

NFT Neurofibrillary tangles

NMDA N-methyl D-aspartate

NMDAR N-methyl D-aspartate receptor

PAMAM polyamidoamine

PAMAM0 poly(amidoamine) dendrimer with neutrally charged surface

PAMAM+ Poly(amidoamine) dendrimer with positively charged surface

PPI polypropylene imine

PPI-G4 polypropylene imine dendrimer of the fourth generation

PPI-G5 polypropylene imine dendrimer of the fifth generation

PS Presenilin

PS1 Presenilin-1

PS2 Presenilin-2

ROS Reactive oxygen species

rpm Rotations per minute

SAXS Small Angle Scattering

SDS Sodium dodecyl sulfate

SPs Senile plaques

TFE Trifluoroethanol

ThT Thioflavin T (4-(3,6-dimethylbenzothiazol-2-yl)-N,N-dimethyl-aniline

UPR Unfolded Protein Response

UV Ultraviolet

UV/Vis Ultraviolet/Visible

µL Microlitre

µM Micromolar

Table of Contents

1 Introduction

1.1 IMPACT OF ALZHEIMER'S DISIEASE

1.1.1 Introduction

Because of the ageing of populations worldwide, one of the major health concerns in the coming decades will be age-related neurodegenerative disorders (dementias). Dementia is a decline in mental ability that usually progresses slowly, in which memory, thinking, and judgement are impaired, and personality may deteriorate. Dementia is one of the most important causes of disability in the elderly. According to the European Parliament Commission and the Council of 22 July 2009 on a European initiative on Alzheimer's disease the most common types of dementia are:

- Alzheimer's disease (AD) (50 to 70 % of cases, this already high number of sufferers of AD is underestimated due to difficulties in early diagnosis.);
- Vascular dementia;
- Dementia caused by successive strokes;
- Frontotemporal dementia;
- Pick's disease;
- Binswanger's disease;
- Lewy-Body dementia;

Alzheimer's disease and other dementias are reaching epidemic proportions, with a large human, social, and economic burden. It was estimated that 35.6 million people worldwide was suffering from dementia in all its forms in 2010, and that this number will nearly double every 20 years, possibly reaching 65 million in 2030, (2010 report by Alzheimer's Disease International). The number of people suffering now from dementia in Europe is estimated to be 9.9 million. According to European Parliament resolution of 19 January 2011 on a *European initiative on Alzheimer's disease and other dementias*[1]. The total direct medical and social care costs of Alzheimer's disease in Europe amount to (approximately 99.7 billion Euros.

Spain is one of the fastest ageing societies in the world. According to the ageing index, the proportion of the Spanish population aged 65 years and over (16.8% in 2004) have doubled in the last 30 years ranking seventh among European countries. Therefore, the burden of chronic neurodegenerative disorders, particularly AD, is expected to grow exponentially. The analysis indicated that some 600,000 and 400,000 people have dementia and AD in Spain, respectively (de Pedro-Cuesta et al. 2009).

---

[1] http://www.europarl.europa.eu/sides/getDoc.do?pubRef=-//EP//TEXT+TA+P7-TA-2011-0016+0+DOC+XML+V0//EN

Alzheimer’s disease is an irreversible neurodegenerative disorder, characterized by a gradual loss of the cognitive functions inexorably leading to dementia. From an early stage characterized by a mild loss of recent memory, the disease advances to more devastating symptoms such as faulty judgements and even personality changes, to terminate in a complete loss of reasoning ability and self sufficiency. Death normally ensues 8 to 10 years after diagnosis. AD is often referred to as early- or late-onset depending on whether it appears before or after age 65, and is normally distinguished in familial, i.e., inherited, and sporadic, which is caused by a combination of genetic, lifestyle and environmental factors. About 75% of AD patients have the sporadic form, which has normally a late-onset. The familial form (fAD), which affects the remaining 25%, can have instead either an early-onset (about 5% of all familial cases) or a late-onset (Corder et al. 1993).

Caring for patients with AD creates a financial burden to both society and caregivers. In addition to the monetary cost associated with the illness, caregivers of AD patients also experience significant emotional distress (Donaldson et al., 1998). As the disease progresses and the patient becomes more debilitated, the amount of time spent caring for the patient will also increase, resulting in additional burden on the caregivers. Most European countries are already spending about 1% of their gross domestic product on dementia. These percentages of gross domestic product are already high, but they are set to triple in the next 40 years[2].

1.1.2 History of Alzheimer's disease

When Auguste Deter died in 1906, Alois Alzheimer, who had closely followed her mental degradation over the previous 5 years, obtained her brain and performed a post-mortem study. By using a silver-staining method just developed by Bielschowsky, Alzheimer identified aggregations of fibrils and what he called ‘miliary foci’. Alterations of that nature had been already observed by others in post-mortem brains, but Alzheimer was the first to relate them to his patient’s dementia. He described the case a year later and Auguste Deter remained in medical history as the first clinical case of what has been ever since referred to as Alzheimer’s disease. For an English translation of Alzheimer’s 1907 paper, see (Alzheimer et al., 1995).

Strikingly, isolation of the major protein in the AD plaques, amyloid-beta-peptide (Aβ), did not occur until 1984 (Glenner and Wong, 1984). Another major event is the development of the amyloid cascade hypothesis in 1992 (Holmes et al., 2008), which hypothesises that formation of fibres and plaques by Aβ is the key event in AD (discussed in more detail later in this chapter). Since 1985 there have been large strides forward in understanding the disease, but a therapeutic that halts or reverses progression of the disease remains elusive. In Figure 1.1 a time line of some

---

[2] Didier Houssin, Minister of France, Congress *Europe against Alzheimer’s disease* 2008 http://www.plan-alzheimer.gouv.fr/-a-european-priority-.html

selected developments in AD is outlined. There are many important findings that have been omitted, but the key developments considered to be relevant to this thesis are shown.

Time

1906: Alois Alzheimer establishes that dementia is associated with neurofibrillary tangles and amyloid plaques (Alzheimer et al., 1995).
1984: Aβ is isolated from amyloid cores (Glenner and Wong, 1984).
1986: Amyloid precursor protein (APP) gene identified (St George-Hyslop et al. 1987; R. E. Tanzi et al. 1988).
1990: Mutations identified in APP which can cause early onset AD (Naiki et al., 1989).
1993: Role for apoE in AD suggested (Strittmatter et al., 1993).
1995: Presenilin genes 1 and 2 discovered (Levy-Lahad et al., 1995; Sherrington et al., 1995)
1997: The common core structure of amyloid fibrils is shown by X-ray diffraction (Sunde et al. 1997)
1998: Cu(II) shown to aggregate Aβ and concentrated in amyloid plaques (C S Atwood et al. 1998)
2002: Copper levels increased in AD patients serum (Squitti et al., 2002)
2003: Cu(II) shown directly bound to Aβ histidine in amyloid plaques (Dong et al. 2003).
2005: Molecular structure of fibrils varies and is self-propagating (Makin and Serpell, 2005a).
2007: Aβ fibrils contain a steric zipper (Sawaya et al. 2007).
2008: Plaques in mice shown to cause toxicity (Meyer-Luehmann et al., 2008).
2008: Metal Hypothesis of AD (Bush and Tanzi, 2008)
2009: Oxidative stress is essential for Aβ toxicity in drosophilia (Rival et al. 2009).
2010: Co-factor theory, a new approach (R. J. McDonald, Craig, and Hong 2010).
2011: Granular Non-fibrillar Aggregates toxicity in AD (Benseny Cases et al., 2011).

Figure 1.1 Selected advances from the field of AD relative to Cu(II) ions, dendrimers and Aβ.

1.1.3 Aetiology of Alzheimer's disease

At this time, we do not yet know what causes Alzheimer's disease or how to stop its progression. It has been shown that Alzheimer's disease:

- is not a part of normal ageing
- affects both men and women
- is more common in people as they age -- most people with the disease are over 65
- is not caused by hardening of the arteries

- is not caused by stress

As Alzheimer’s disease progresses and affects different areas of the brain, various abilities become impaired. The result is changes in abilities and/or behaviour. At present, once an ability is lost, it is not known to return.

1.1.3.1 Diagnosis

Since no single test or biochemical measurement can securely lead to a diagnosis of AD, intellectual deterioration is diagnosed as possible or probable AD on the basis of a careful analysis of the symptoms, the medical history of both patient and his/her relatives, a variety of neuropsychological tests and from the exclusion of alternative conditions, generally attained via neuroimaging. Almost universally physicians today follow the NINCDS-ADRDA Criteria for diagnosis of Alzheimer’s disease published in 1984 by the National Institute of Neurological and Communicative Disorders and Stroke (NINCDS) and the Alzheimer's Disease and Related Disorders Association (ADRDA), which specify eight cognitive domains that are compromised in AD – memory, language, perceptual skills, attention, constructive abilities, orientation, problem solving and functional abilities – and give guidelines for impairment assessment and diagnosis.

1.1.3.2 AD macroscopic pathology

Atrophy is the major macroscopic characteristic of the AD brain. Ventricles are dilated, gyri appear narrower and sulci wider than in a normal brain. The loss of tissue, which roughly correlates with the degree of cognitive decline, is so severe that an AD brain can weigh less than 1000g. Frontal, parietal and temporal lobes are all involved, the hippocampus in particular being severely affected. The primary sensory-motor cortex appears affected with some delay, whereas the occipital lobe is relatively spared (Figure 1.2). The disease affects memory and mental functioning (e.g. thinking and speaking, etc.), but can also lead to other problems such as confusion, changes of mood and disorientation in time and space. Over time, the disease destroys large areas of the brain, leaving its victims with little comprehension or awareness.

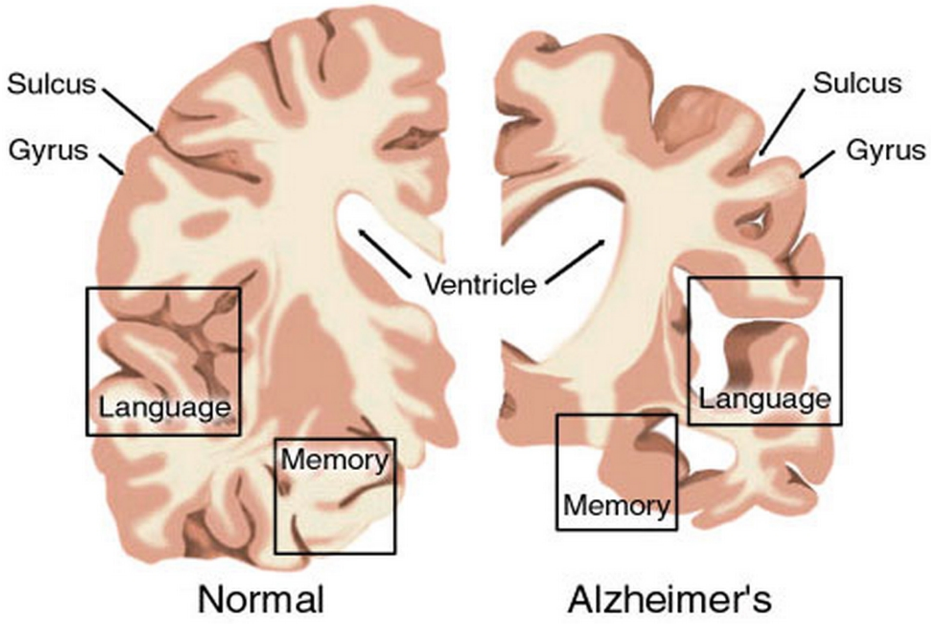

Figure 1.2 Brain With Alzheimer's Disease These images represent a cross-section of the brain as seen from the front. The cross-section on the left represents a normal brain and the one on the right represents a brain with Alzheimer's disease. (image taken from web site of *American Health Assistance Foundation*

1.1.4 **AD microscopic pathology**

The ‘miliary foci’ and fibril aggregations that Alzheimer observed are today normally referred to as senile plaques (SPs) and neurofibrillary tangles (NTFs), and remain the hallmarks of AD. The ultimate result of the presence of plaques and tangles in AD is a severe neuronal loss that can reach 60% in the hippocampus and 80% in the nucleus basalis and in some frontal and temporal areas (R.Squitti and C.Salustri 2011).

SPs are clusters of protein fibrils that form in the extracellular space, made of an amyloidal core, abnormal neurites and glial cells. The amyloidal core is mainly an aggregation of amyloid-beta peptide (Aβ), a 4 kDa peptide 39 to 43 amino acids long, which is produced by the proteolytic cleavage of the Amyloid Precursor Protein (APP), a transmembrane protein present in many cell types and highly concentrated on neuron synapses (See Chapter 1.3).

SPs are roughly spherical with a diameter reaching up to 200 μm (Figure 1.3), and are normally distinguished in ‘diffuse’ and ‘compact’: Diffuse SPs are amorphous deposits of non-fibrillar ‘pre-amyloid’ Aβ, which produce no alteration of the neuropil. Compact SPs, more often referred to as ‘neuritic’, show instead an amyloid core surrounded by dystrophic neuritis. The latter appear as clusters of radially oriented neuronal processes.

There are at least 3 subtypes of neuritic SPs: Primitive, which lack the amyloidal core; Classical, in which a dense amyloid core is surrounded by dystrophic neuritis, which in turn appear interconnected by low density amyloidal fibrils; Burned-out, which have only the dense amyloidal core and at most a few neurites. This subdivision mirrors what researches believe is SPs' evolution: after being released, Aβ segments forms diffuse plaques in the extracellular space until elements such as cytokines, ApoE, proteoglycans and others become embedded with the complex causing it to degenerate into neuritic plaques. In other words, SPs start as diffuse and then evolve into neuritic, first primitive, then classical, and finally burned out.

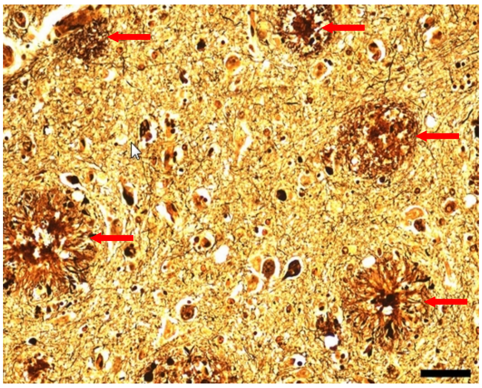

Figure 1.3 Microscopic examination of fibrillar deposits in Alzheimer's disease. The characteristic microscopic findings of Alzheimer's disease include "senile plaques" which are collections of degenerative presynaptic endings along with astrocytes and microglia. These plaques are best seen with a silver stain. Fibrils are the main component of amyloid deposits known as senile plaques. Senile plaques are lesions 10–200 mm in diameter with a dense core of fibrillar amyloid. These plaques are surrounded by degenerating and swollen nerve terminals Scale bars indicate 50 microns (Schenk et al. 1999).

SPs appear to have also an anatomical hierarchy: higher-order association areas have the highest density of SPs, whereas the primary sensory-motor cortex the lowest. Striatum and cerebellum show a rather high density of SPs, but they are all of the diffuse type. The hippocampus appears relatively spared.

Only neuritic SPs are specific to AD, whereas diffuse SPs are found also in the brains of nondemented elderly individuals (R.Squitti and C.Salustri 2011).

NFTs are aggregates of modified protein tau in the intracellular space. In normal conditions, the protein tau binds to microtubules, contributes to the progress of their formation and is a key element in their stability. In AD, tau undergoes hyper-phosphorylation which causes the protein to aggregate (Grundke-Iqbal et al., 1986). Moreover, upon hyper-phosphorylation, tau loses its binding capability so that the microtubules disintegrate. Tau is not the focus of this thesis and so will only be mentioned briefly. For a more in-depth review please see (Alies et al., 2011) (Avila, 2006, 2006).

In AD, the areas most affected by NFTs are hippocampus, sibiculum, amygdala, entorhinal and transentorhinal corteces. In the neocortex, higher-order association areas are more affected than the unimodal association areas, and the primary sensory-motor cortex is relatively spared. NFTs are also numerous in the nucleus basalis, limbic nuclei of the thalamus, locus ceruleus, substantia nigra, and the raphe nuclei of the brainstem. It is important to remember, that NFTs are not AD specific and are frequent also in non-demented elderly individuals.

During the last 20 years, considerable progress has been made in unravelling the aetiology of AD. Several factors that increases the risk of developing AD have been reported, including ageing, head injuries, family history of AD or Down syndrome's, sex (higher prevalence of AD in women), vascular diseases, educational attainment, exposure to environmental toxins and infectious processes (Lombardi et al., 1998; Whalley, 2001). Other contributing factors include genetic predisposition, β-amyloid deposition, microglial cell activation, altered immune response, oxidative stress, deficiencies in endogenous antioxidants, alteration in metal ions, energy depletion and nutritional compromises (Selkoe 2001). Epidemiological and molecular genetic data suggest that although there are multiple causes of AD, genetic factors play an important role (Munoz and Feldman, 2000). Four genes have been identified to be associated with an increased risk (Gasparini et al., 2001)it has been suggested that AD could result from a multi-factorial process involving both a genetic predisposition and an exposure to environmental factors (Grant et al., 2002). There is a large body of evidence that abnormalities at various stages of the processing and distribution of this peptide can result in amyloid plaques that lead to damage of cholinergic neurons in the medial septum as well as hippocampal and cortical neurons (Braak and Braak, 1991).

The Aβ accumulation subsequently induces tau aggregation, phosphorylation, neuronal death and dementia, suggesting tau aggregation is downstream of Aβ fibril formation (Price and Morris, 1999). These findings are strongly in favour of Aβ as the disease causing agent. Among the different Aβ aggregated species which form along the aggregation process, increasing experimental evidence points to globular oligomers as the cytotoxic agents. One way of action against the perverse effects of amyloid peptides on neuronal functioning consists in finding molecules which are able either to block the formation of the toxic oligomers, to disrupt their structure or to lock the amyloid into what may be a non-cytotoxic form of the aggregate.

1.2 PROTEIN MISFOLDING PATHWAYS

1.2.1 Protein folding

Proteins are essential elements for life. They are building blocks of all organisms and the operators of cellular functions. Humans produce a repertoire of about 30.000 different proteins, each with a different role. Each protein has its own unique sequence and shape (native conformation) in order to fulfil its specific function. The appearance of incorrectly shaped (misfolded) proteins is associated with various, often highly debilitating diseases for which no sufficient cure is available yet.

Protein folding is the process by which the newly synthesized protein molecule folds into its unique three-dimensional structure. The primary product of the protein synthesis is the linear amino acid chain, which lacks any three-dimensional structure. To become functional, the protein has to be packed into its particular native conformation. In the cell, a variety of proteins named chaperones assist the newly synthesized polypeptide to attain its native conformation. Protein folding is a very complex process and the molecular mechanisms responsible for protein assembly are of the most elemental open question in biochemistry. The energy landscape theory that was first proposed by Joseph Bryngelson and José N. Onuchic (Bryngelson et al., 1995; Onuchic et al., 1997), states that folding of a protein does not follow a singular, specific pathway; it is in fact a rather complex self-organizing process that generally does not occur through an obligate series of intermediates, but through routes down a folding funnel (Onuchic et al., 1995). The energy of the different conformations decreases with the development of organized, native-like properties. On the highest energy level, proteins do not comprise ordered structures. As the proteins fold more into the native conformation and the secondary structural arrangements appear at certain positions of the polypeptide chain, they shift to a lower energy phase. At the end of the correct folding procedure, as the proteins obtain their correctly packed native conformations with a unique set of α-helical and β-sheet motifs, they find their energy minimum. The drive for the energy minimum makes the correct protein folding highly efficient and very rapid. Thermodynamically, the folding process is described as an energy funnel (Leopold et al., 1992), where the unfolded states are characterized by a higher degree of conformational entropy and free energy than the native. The façade of this folding funnel is unique for a specific polypeptide sequence under a particular set of conditions. By definition, entropy is a measure of chaos, the amount of all different conformational states that the protein can attain. Free energy stands for the amount of thermodynamic energy in a system which can be converted into work. The unfolded state is associated with more chaos, higher entropy and free energy, which leads to the instability of the three dimensional structure. Therefore, as folding proceeds, the narrowing of the funnel represents a decreased number of conformational states as well as lower free energy. At the bottom of the funnel, which is also known as the global minimum, the folding alternatives are reduced to a single conformation.

1.2.2 Protein misfolding

Protein misfolding is a common event in living cells. In young and healthy cells, the misfolded protein load is disposed of by protein quality control (PQC) systems. In ageing cells and in cells from certain individuals with genetic diseases, the load may overwhelm the PQC capacity, resulting in accumulation of misfolded proteins. Dependent on the properties of the protein and the efficiency of the PQC systems, the accumulated protein may be degraded or assembled into toxic oligomers and aggregates. To illustrate this concept, there is a number of very different protein misfolding diseases including AD, Parkinson's disease, α-1-antitrypsin deficiency, familial neurohypophyseal diabetes insipidus, phenylketonuria, and short-chain acyl-CoA dehydrogenase deficiency. Despite the differences, an emerging paradigm suggests that the cellular effects of protein misfolding provide a common framework that may contribute to the elucidation of the cell pathology and guide intervention and treatment strategies of many genetic and age-dependent diseases (Gregersen et al., 2006). Misfolding is influenced by the amino acid composition and certain mutations are known to accelerate the process. Moreover, it also depends on environmental conditions, since once they are exposed to specific environmental changes such as increased temperature, high or low pH, agitation, elevated glucose or oxidative agents, proteins can lose their native conformation more rapidly. The process, wherein the native state is disrupted is called denaturation and it generally results in the unfolding of the proteins. Due to the lack of arrangement, unfolded proteins are non-functional. Importantly, the unfolded state is thermodynamically unfavourable and unstable. Seeking for lower energy levels and more stability, unfolded proteins have a tendency to aggregate. (Figure 1.4).

Under certain circumstances such as pH or temperature change, mechanical stress, glycation or oxidation; proteins undergo conformational changes that results in unfolding and partial misfolding that is associated with the tendency to aggregate. During aggregation, proteins can obtain a range of different structural appearances, which are generally enriched in cross-β structure, including intermediates varying from unordered amorphous aggregates to ordered fibrils that are called amyloid.

Subsequent to protein unfolding, aggregation consists of two parts. The first one is the nucleation, when proteins reversibly attach to a growing core. When the nucleus crosses the threshold of a critical mass, the second part begins, wherein further protein molecules attach irreversibly to the core developing a large aggregate. Studies with small fibril-forming peptides have shown that during aggregation, the free energy change depends on the concentration of monomer. At low concentrations the monomeric, at high concentrations the aggregated state is favoured because of the large barrier that needs to be overcome to resolve the aggregates (Nelson et al., 2005) which makes the aggregate highly stable. Protein aggregation can result in various different structural appearances with intermediates (oligomers) varying from unordered amorphous aggregates to highly ordered fibrils that are called amyloid.

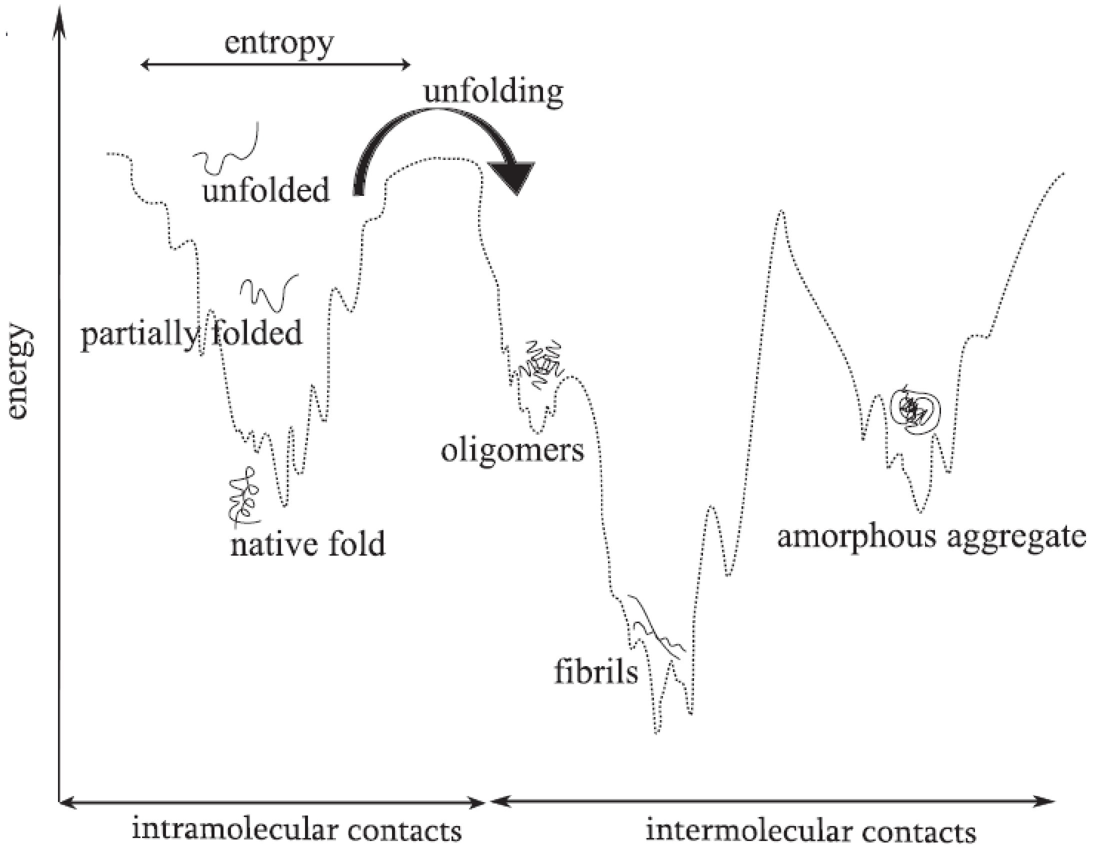

Figure 1.4 Energy state of protein folding under physiological and misfolding conditions. The shape of the graph shows energy state of the protein conformations moving toward its native or misfolded condition through multiple inter- and intramolecular contact arrangements. Recent experiments have allowed the placement of different 'intermediate' structures on both pathways although detailed structural models for many of these species are not yet available. Furthermore, the species involved in converting kinetically stabilized globular structures into the thermodynamic global free energy minimum in the form of amyloid fibrils for different proteins is currently not defined (Jahn and Radford, 2005)

1.3 AMYLOID-BETA PEPTIDE

1.3.1 Aβ peptide

The two fundamental characteristics of the AD brain are extracellular amyloid plaques and intracellular neurofibrillary tangles. Approximately 90 % of the amyloid plaques consist of the aggregated form of Aβ (Masters et al., 1985). The remaining 10 % is a variety of other components including membrane lipids from degenerated axons, metal ions, and traces of other components from the interstitium (C S Atwood et al. 2002). Amyloid aggregates are a hallmark of central nervous systems affected by Alzheimer's disease. The amyloid peptides Aβ40 and Aβ42 are the two main components in such aggregates. When studied in vitro, amyloid aggregates follow a nucleation-dependent polymerization reaction. Among the different aggregated species which form along the aggregation process, increasing experimental evidence points to globular oligomers as the cytotoxic agents (Haass and Selkoe, 2007). One way of action against the perverse effects of amyloid peptides on neuronal functioning consists in finding molecules which are able either to block the formation of the toxic oligomers, to disrupt their structure or to lock the amyloid into what may be a non-cytotoxic form of the aggregate. The sequence of Aβ40 is:

D$_1$AEFRH$_6$DSGY$_{10}$EVH$_{13}$H$_{14}$QKLVFFAEDVGSNK$_{28}$GAIIGLMVGGVV$_{40}$IA$_{42}$

The Aβ peptide has a hydrophobic C-terminal and a hydrophilic N-terminal, residues 17-21, the central hydrophobic cluster, (green letters) and residues 30-40 in the C-terminal tail have a hydrophilic cluster (blue letters) with a high propensity for fibril formation. It is disordered in water solution but deviates from a complete random conformation by a few non-random regions. NMR studies have indicated a turn-like structure at residue 8-12 and hydrophobic interactions between side-chains in the 16-24 regions with a bend-like structure at 20-24 (Riek et al., 2001).

In AD Aβ peptide undergoes a misfolding pathway to form amyloid fibrils. It is generally agreed that this pathway is based on a nucleation event followed by elongation. Considering that fibrils are much more stable thermodynamically than the monomeric form of Aβ, it is surprising that we do not all develop Aβ fibrils and AD at a much younger age.

1.3.2 Aβ peptide: location and function

Aβ is constitutively produced in the brain throughout life in all humans. It is present in the cerebrospinal fluid (CSF) and plasma in humans with a typical concentration of 5 nM (Vigo-Pelfrey et al., 1993). Aβ is predominately generated in the golgi bodies through the amyloidogenic processing of the amyloid precursor protein (APP), then trafficked to the cell membrane (Gasparini et al., 2001).

Aβ is most often characterized as an incidental catabolic by product that lacks a normal physiological role. However, Aβ has been shown to be a specific ligand for a number of different receptors and other molecules, transported by complex trafficking pathways, modulated in response to a variety of environmental stressors (Teng and Tang, 2005), and able to induce pro-inflammatory and apoptotic activities (Paris et al., 2000). Recent findings suggest Aβ is a hitherto unrecognised AMP that may normally function in the innate immune system that stands in stark contrast to current models of Aβ-mediated pathology and has important implications for ongoing and future AD treatment strategies (Soscia et al., 2010). Interestingly, the application of Aβ to cortical neurons promoted endocytosis of NMDA (N-methyl-Daspartic) receptors (Snyder et al., 2005). These receptors occur at the post-synaptic membrane at glutamatergic synapses, and are vulnerable to excitotoxicity in AD. Excitoxicity can occur when NMDA receptors are overactivated, such as by a pathological excess of the neurotransmitter glutamate. Over-activation results in high levels of Cu(II) ions entering the cell which activates a number of enzymes that go on to damage cell structures. Having a metal binding capacity Aβ might also participate in normal metal homeostasis (Bush, 2003). Thus Aβ's normal function may be to depress synaptic function, protecting against excitotoxicity (Sarrel J., 2010).

1.3.3 Amyloid precursor protein

Aβ is a fragment of a protein that is snipped from APP, a membrane surface protein produced by healthy cells (Figure 1.5). Much is still unknown about APP, such as its precise role in normal physiology. Many possibilities have been reported. It has been suggested that APP may be a receptor, and/or that it may serve as a link between kinesin molecular motors and synaptic vesicles. Roles as an adhesion protein, and a function relating to promotion of neurite growth have also been proposed. Gene transcriptional activity has been attributed to APP as well (Schenk et al., 1999).

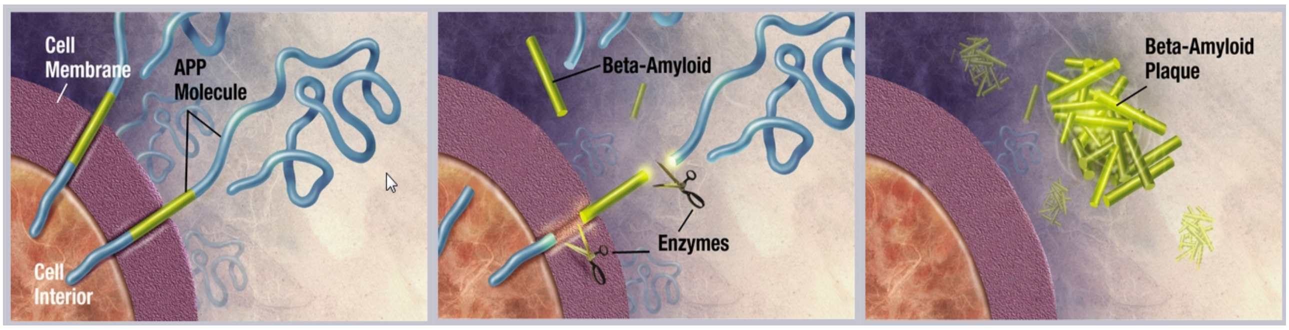

Figure 1.5 Beta-amyloid is cleaved by beta- and gamma- secretase enzymes. In a healthy brain, these β-amyloid fragments are broken down and eliminated. However, in AD, these sticky fragments accumulate and fold into hard, insoluble clumps/fibrils, forming plaques on the surface of the neuron (Schenk et al., 1999).

APP is a type I transmembrane protein, with its large N-terminal domain in the extracellular space, ubiquitously expressed in a variety of cells types (Mattson, 1997), encoded on chromosome 21 in humans (Kang et al., 1987). There are three main isoforms of the protein found in the brain, APP_{695}, APP_{751} and APP_{770}, where APP_{695} is the predominant form expressed in neurons (Tanzi et al., 1988). Multiple roles for APP have been suggested, broadly falling into three categories:

- acting as a contact receptor, with a role in forming functional synapses through cell adhesion
- a trophic role in its secreted form after cleavage, promoting cell proliferation and motility
- a role in metal ion homoeostasis. APP shares structural homology to copper chaperones and may function as a Cu(I) binding neuronal metallochaperone (Bayer et al., 2006) or as a cell surface metalloreductase, as APP is capable of reducing Cu(II) to Cu(I) (Barnham et al., 2003)

APP trafficking is shown in Figure 1.6 APP matures through the constitutive secretory pathway, during which it undergoes N-glycosylation (glycans attached to a nitrogen in asparagine or arginine side chains) in the endoplasmic reticulum and Oglycosylation (glycans attached to the hydroxy oxygen of serine, threonine and tyrosine side-chains) in the golgi bodies. Upon exiting the golgi body, APP is trafficked to the plasma membrane. Once APP reaches the cell surface, it is internalised and either trafficked via the endocytic/recycling pathway back to the cell surface, or degraded in the lysosome. APP trafficking is likely to vary depending on the cell type, and the intracellular organelles/transport vesicles involved in APP trafficking in neurons require further characterisation (Thinakaran and Koo 2008)

During trafficking APP can undergo one of two processing events (Figure 1.6). The non-amyloidogenic pathway, without the production of Aβ, is the sequential processing of APP by α and γ-secretases and occurs mainly at the cell surface (Sisodia 1992) The amyloidogenic pathway is the cleavage of APP by β-secretase then γ-secretase, resulting in Aβ secretion and occurs during trafficking through the endocytic organelles (Koo and Squazzo, 1994).

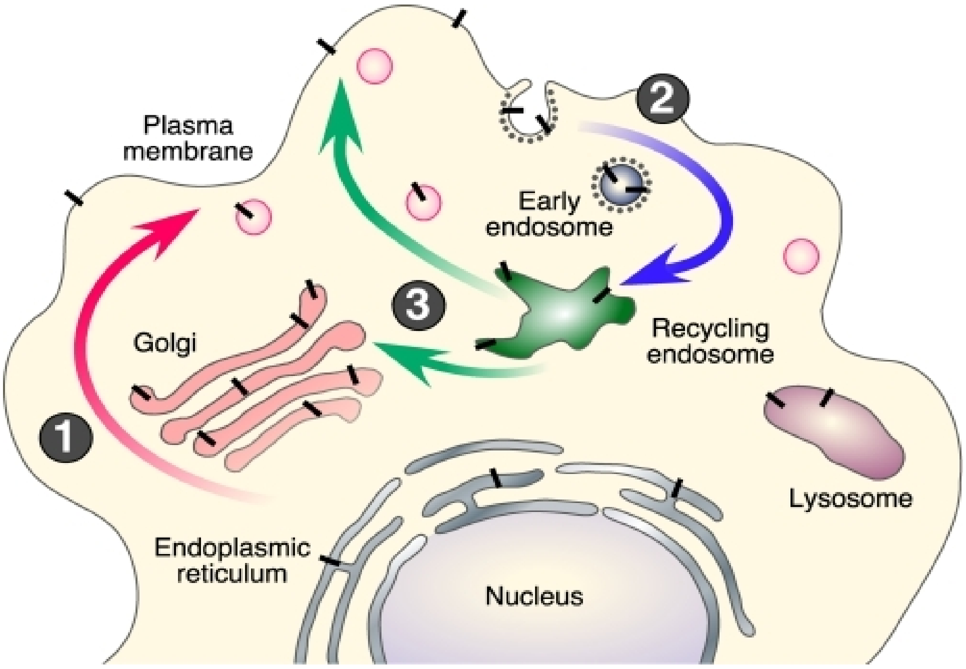

Figure 1.6 A diagram of intracellular trafficking of APP. APP molecules (black bars) are trafficked through the constitutive secretory pathway where they undergo post-translational modifications in the endoplasmic reticulum and golgi body, then are trafficked to the plasma membrane (step 1). APP is then internalised (step 2) and trafficked through the endocytic and recycling compartments back to the cell membrane (step 3). The non-amyloidogenic pathway mainly occurs at the cell surface where α-secretases reside. Alternatively the amyloidogenic pathway occurs in endocytic organelles where β-secretase and γ-secretase are present (Thinakaran and Koo 2008)

In the Figure 1.7 schematically shown the amyloidogenic and non-amyloidogenic pathways of APP cleavage. In the non-amyloidogenic pathway APP is cleaved at the cell membrane by α-secretase (Sisodia 1992). The α-secretase site in APP is between residues 687 and 688 of APP, α-secretase cleavage results in the release of an APP extracellular domain (Parvathy et al., 1999), than γ-secretase releases the soluble 3kDa N-terminal fragment p3 extracellularly and APP intracellular domain into the cytoplasm. The p3's function is yet to be elucidated, but it has been shown to be non-toxic to neuronal cells (Minogue et al. 2009).

Amyloidogenic processing of APP involves sequential cleavage by β-secretase and secondly γ-secretase. The 99-amino-acid C-terminal fragment of APP generated by β-secretase cleavage can be internalized and further processed by γ-secretase to produce Aβ in the endocytic compartments (Vassar et al., 1999). Depending on the exact point of cleavage by γ-secretase, two main forms of Aβ comprising of either 1-40 or 1-42 amino acid residues, are produced. Moreover, minor amounts of shorter Aβ peptides such as Aβ38 and Aβ37 have also been detected (Walter et al., 2001). Cleavage of C99 by γ-secretase releases an APP intracellular domain that can translocate to the nucleus where it may regulate gene expression, including the induction of apoptotic genes (Leissring et al., 2002). The enzymatic complex γ-secretase, which cleaves APP within a transmembrane region, involves four different proteins: presenilin, nicastrin, Aph-1 and Pen-2. Actually, it is widely accepted that the presenilins, particularly PS1 facilitate the proteolytic cleavage of APP to generate Aβ (Benedek et al., 2004). Therefore, mutations leading to PS1 with different altered sites appear to be responsible for the erroneous cleavage of APP and generation of Aβ petides.

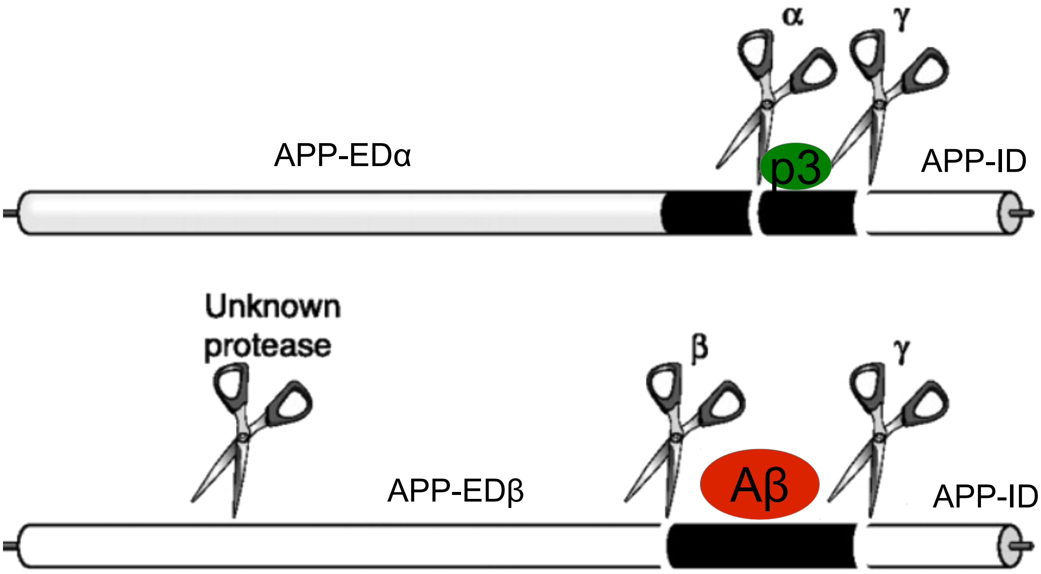

Figure 1.7. Proteolytic processing of APP by secretases. A full-length APP is an integral membrane protein. Cleavage sites of α-, β-, and γ-secretase are indicated by scissors. Cleavage by α-secretase yields a soluble ectodomain of APP (APP-EDα) and a membrane-bound carboxy-terminal fragment which after cleavage by γ-secretase yields p3 and the APP intracellular domain (APP-ID). β-secretase cleavage yields APP-EDβ, and a fragment which after cleavage by γ-secretase yields Aβ and APP-ID (De Strooper 2010).

1.3.4 Hypotheses on the causes of AD

1.3.4.1 Classical hypothesis

There are three major classic hypotheses on the origin of AD. **The cholinergic hypothesis** (Francis et al., 1999), which is the oldest and the one on which the majority of currently available drug therapies are based, proposes that AD is caused by a reduced synthesis of the neurotransmitter acetylcholine. **The amyloid cascade hypothesis** (Hardy and Allsop, 1991) postulates instead that the fundamental cause of the disease is the deposition of Aβ, which is supported by the evidence that mutations in the gene for APP, which is known to cause Aβ aggregation, are linked to AD. **The tau hypothesis**, based on a study demonstrating that deposition of Aβ plaques does not correlate well with neuron loss (Schmitz et al., 2004), proposes that abnormalities in the tau protein initiate the disease cascade.

Safety and efficacy of more than 500 pharmaceutical treatments are being investigated in clinical trials worldwide on the basis of these three hypotheses. In 2008, two separate clinical trials showed positive results in modifying the course of the disease in mild to moderate AD: one with the metal complexing agent PBT2 (Lannfelt et al., 2008) and one with methylthioninium chloride , a drug that inhibits tau aggregation, which unfortunately failed to confirm the positive results in its phase III (R.Squitti and C.Salustri 2011).

Genetic studies of familial AD (fAD) provide perhaps the strongest evidence supporting the amyloid hypothesis. Mutations in APP, presenilin 1 (PS1), and presenilin 2 (PS2) account for all the cases of fAD, whereas the E4 allele in the ApoE gene increases the risk of getting the disease. To date, approximately 180 familial AD mutations have been identified in PS1, 20 fAD mutations in PS2 and 36 fAD mutations in APP (www.molgen.ua.ac.be/ADMutations). Most of the mutations in APP and presenilins seem to increase Aβ generation and/or increase Aβ42 levels. Mutations in APP are localized at or near the cleavage sites that give rise to Aβ, although some mutations are mapped in the middle of the Aβ peptide and are thought to increase fibrillization. Mutations in PS1 and PS2, unlike those in APP, are distributed throughout the molecule. The question whether these mutations represent a toxic gain-of-function or a loss-of-function of APP and presenilins remains unsettled (De Strooper 2010; J Hardy 1997; Van Broeck, Van Broeckhoven, and Kumar-Singh 2007; M S Wolfe et al. 1998). Genetic evidence strongly supports Aβ as the causative agent of Alzheimer's disease but the role of Aβ in the progression of AD is still unclear. The amyloid hypothesis dominates the AD research field because it is the best described and most scrutinized model, and is supported by a large volume of data. The classical view of amyloid hypothesis shown in Figure 1.8 adapted from (Pimplikar, 2009). The classical view of the amyloid cascade hypothesis proposes Aβ as the starting point of the cascade. According to the amyloid cascade hypothesis, accumulation of Aβ in the brain is the primary influence driving AD pathogenesis. The rest of the disease process, including formation of neurofibrillary tangles containing tau protein, is proposed to result from an imbalance between Aβ production and Aβ clearance. In this hypothesis genetic and environmental factors result in Aβ aggregation and synaptic injury. Downstream of Aβ deposition altered kinase/phosphatase activities occur, resulting in hyperphosphorylation of the protein tau. Finally oxidative injury and neuronal dysfunction results in widespread cell death and dementia (Hardy and Higgins, 1992; Hardy, 1997)

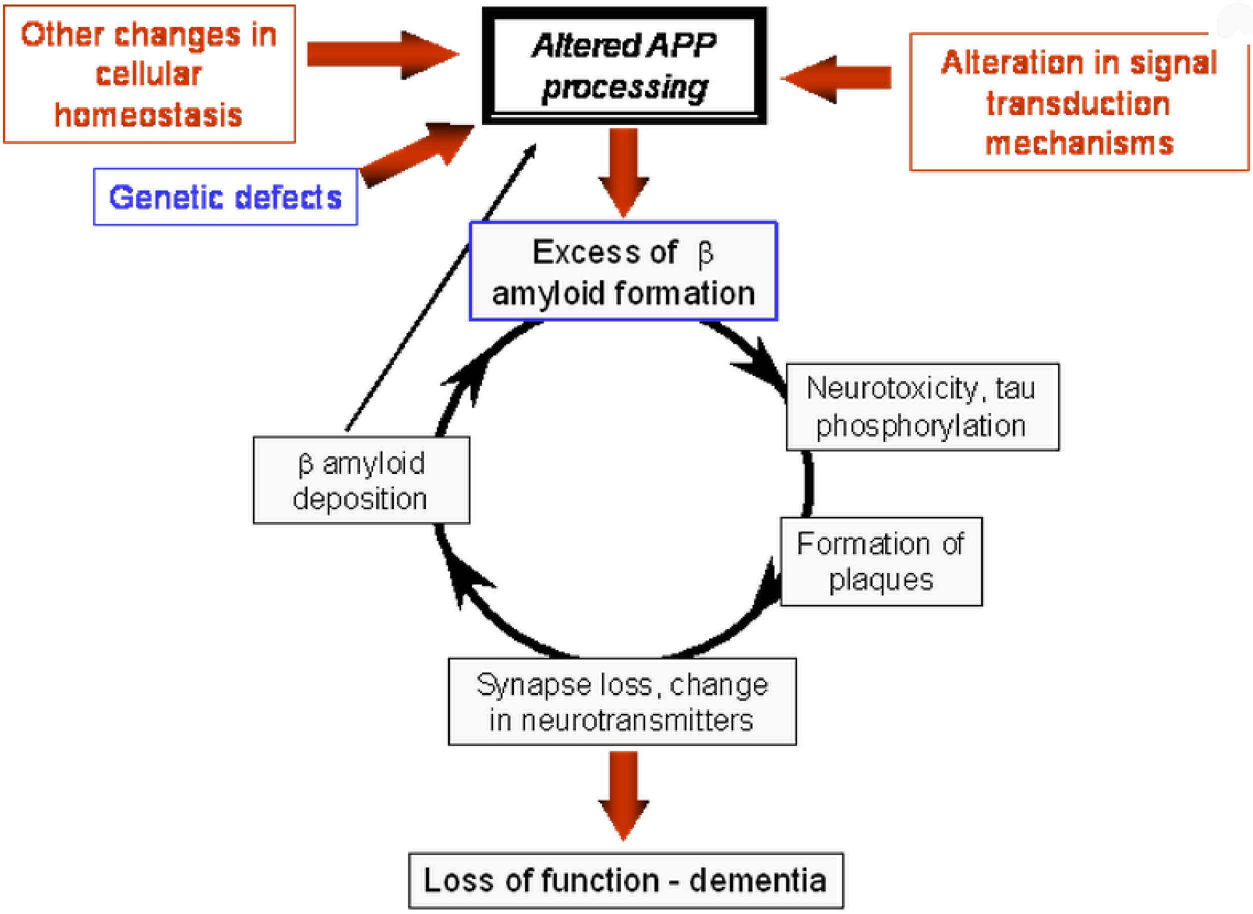

Figure 1.8 The amyloid cascade hypothesis. The central event for the amyloid cascade hypothesis is the excessive formation of **Aβ**. The source of excessive **Aβ** formation is the amyloid precursor **APP** and multiple factors may contribute to its aberrant processing. Here we have indicated genetic alterations since it has been largely demonstrated that mutations associated with familial forms of Alzheimer's disease, result in aberrant metabolism and excess production of Aβ .Defective signal transduction mechanisms, neurotransmitter changes and other perturbations of normal cellular homeostasis may also contribute to aberrant APP processing. Most of these alterations have been detected and characterized in the brain and/or peripheral tissues of AD patients and constitute a significant example of the pharmacological modulability of the regulated processing of APP (Racchi and Govoni, 2003).

Amyloid cascade hypothesis is not universally accepted. One reason for this development is the accumulation of new data that are inconsistent with the main tenets of the hypothesis but because of the enormous amount of data in the literature, it is easy to seek support for either view by selectively focusing on the data favourable to one's view and ignoring the studies that runs contrary to it.

The recent **co-factors theory (CTF)** of aetiology of AD differs from the other dominant models in the field. The theory proposes that AD is the consequence of interactions between various combinations of co-factors. These co-factors include genes, plaques and tangles, neurotrasmitter changes, vascular abnormalities, stress hormones, circadian rhythmus, head trauma, seizures, prions, estrogen, apoptosis, oxidative stress and glucose metabolism. The various co-factors were divided into two major categories. One set of factors, passive factors, can create a neuronal environment that makes neurons more susceptible to damaging agents or forces. An example of passive factor is cholinergic depletion of the hippocampus. Another set of factors, active factors are damaging agents of forces that can produce neuronal death. An example of an active factor is seizure activity. The basic prediction of the original model (McDonald, 2002) were severe memory impairments linked with hippocampal dysfunction. The new concept is the idea that different combination of co-factors can differently activate mechanisms of brain dysfunction and neurodegeneration. For example:

(1.) a factor amplifying the same mechanisms as another already present factor;

(2.) a factor activating multiple mechanisms and another factor activating independent parallel mechanism;

(3.) a single factor activating multiple mechanisms and another factor activating the same mechanisms as well as different mechanisms.

The CFT is a potential explanation of why current treatment approaches work on some patients and not on other. The idea is that a particular case might have various layer of factors, some of which be reduced with current treatment strategies but not others (McDonald, Craig, and Hong 2010).

1.3.4.2 The metal hypothesis

Recently, researchers have uncovered an important role played in AD neurodegeneration by transition metals via their properties to cause oxidative stress. In fact, copper and iron are known to participate in Fenton-type reactions that generate uncontrollable reactive oxygen species (ROS) capable of damaging and destroying molecular and cellular compartments (Atwood et al. 2004). Authors have widely reported enhanced metal concentrations in specific areas of AD patients' brains, in particular of iron, copper and zinc in cerebrospinal fluid (CSF) (Smith et al., 2007), of iron in the basal ganglia (Bartzokis et al. 2000).. It has been also observed that APP possesses selective zinc and copper binding sites which mediate redox activity, causing precipitation of Aβ even at low concentrations (Bush et al., 1994).

Also Aβ possesses selective high and low-affinity metal-binding sites. They can bind equimolar amounts of copper and zinc but, in conditions of acidosis, copper completely displaces zinc from Aβ (Atwood et al., 2000). Wheras on the one hand Aβ deposition in plaques is an age-dependent phenomenon, on the other hand Aβ production does not appear to increase with age. This seems to indicate that other age-dependent changes, as for example changes in metal homeostasis, may play a key role in Aβ transformation and neurotoxicity. Since copper and zinc are both modulators of the glutamatergic neurotransmission (Bush and Tanzi, 2008), abnormalities in metal homeostasis can have detrimental effects on synaptic processes, such as metal reuptake or storage in the synaptic cleft. All this evidence has eventually led to the proposal of a Metal Hypothesis of AD(Bush and Tanzi, 2008), which is based on the concept that it is the interaction of Aβ with specific metals, especially copper, that drives AD pathogenesis by promoting aggregation and neurotoxicity. By now, this view has become fully accepted and there is general agreement on the existence of a link between AD and oxidative stress phenomena triggered by transition metals. The Metal hypothesis of AD is now supported by the results of numerous clinical studies (Squitti et al., 2002, 2004; Squitti and Salustri, 2009)

1.3.5 Amyloid fibrils

The molecular pathway by which Aβ forms soluble oligomers and insoluble fibrils and protofibrils *in vivo* is not clear. The currently available information is based on two experimental approaches. The *in vitro* approach involves the use of synthetic Aβ peptides under controlled conditions, whereas the *in vivo* approach relies on isolating such oligomers from tissue culture media, brain extracts, etc.

All amyloid fibrils possess cross-beta structure and consist of one particular protein or peptide. A parallel arrangement of beta-sheets with β-strands perpendicular to the axis of the fibril appears to be the major structural feature of amyloid fibrils (Tycko 2006; Kajava, Aebi, and Steven 2005; Balbach et al. 2002). However, the native structures of amyloidogenic proteins differ greatly and several amyloidogenic proteins are intrinsically disordered or contain highly flexible unfolded regions (e. g. Aβ), Several amyloidogenic proteins are stabilized by intramolecular disulfide bonds. The nature of the structural elements guiding amyloid formation is poorly understood. Such structural analysis is important in order to understand the pathological function of amyloid and to find inhibitors that prevent the formation of toxic species or their interaction with targets such as cell membranes or the extracellular matrix. Despite the many mechanisms nature has generated to prevent protein misfolding and aggregation there are a large number of diseases caused by the aberrant folding of proteins, so-called misfolding diseases. In a subset of these diseases proteins undergo conformational changes and self-associate into stable, insoluble, fibrils with β-sheet structure called amyloid fibrils (Figure 1.9). These structures are highly protease resistant and the cell is often unable to degrade them. All amyloid fibrils are composed of β-sheets with their constituent hydrogen bonded strands, parallel or anti-parallel, running perpendicular to the axis of the fibril (Figure 1.9). This cross-β structure was first observed by X-ray diffraction (Eanes and Glenner, 1968) where amyloid fibrils show two distinct signals, one at 4.7 Å and one between 10-11 Å. The 4.7 Å signal corresponds to the hydrogen bonding distance between the 15 strands in each sheet and the other signal indicates the spacing between different interacting sheets. Recently, methods like solid-state NMR (Boix 2006 and references therein) and cryo-electron microscopy (Serpell and Smith, 2000) have further helped in characterizing the fibril structure from a number of proteins. Mature fibrils are usually made up of 2-6 fibrilar subunits named protofilaments which, slightly twisted around each other, form unbranched fibers, 7-12 nm in diameter (Makin and Serpell 2005).

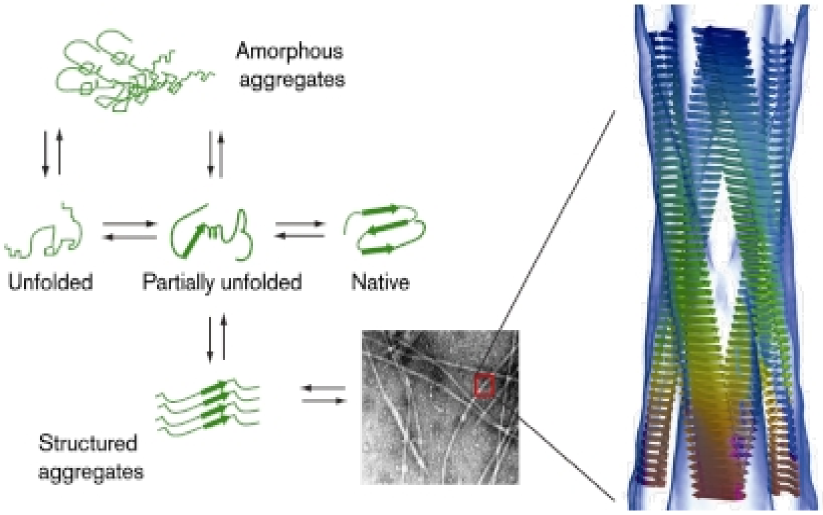

Figure 1.9. Protein folding and misfolding. It is believed that amorphous, unstructured aggregates can form from unfolded as well as partially unfolded states. Structured aggregates most likely form from partially structured intermediates. These aggregates can go on to form amyloid-like fibrils. These insoluble fibrils are composed of β-sheets parallel to the fibril axis and are usually made up of 2-6 protofilaments, twisted around each other. (Fibril model adapted from (Jiménez et al., 1999).

Jarrea and Lansbury (1993) have proposed that kinetically, Aβ peptide fibrillogenesis can be described as a two step process: nucleation and growth. Nucleation is a slow self-association of monomeric Aβ in a random coil conformation to form an oligomeric nucleus with β-sheet secondary structure. Once the nucleus has formed, fibril starts to grow. Our group reported that Aβ40 peptide at the beginning of fibrillation has a mixture of unordered and α-helical structures which converts rapidly into the intermolecular non-fibrillar beta-structure. Figure 1.10 is a data combination of two experiments: the white background bit in the figure corresponds to the data reported by Kirkitadze et al. (U, α and β variation detected using CD spectroscopy, see Fig. 1 in (Kirkitadze et al., 2001); the hatched background bit in the figure represents the ThT and FTIR data reported by (Benseny-Cases et al., 2007). The key point is that most of the total amount of β-structures that form during the aggregation process are already present by the end of the nucleation phase. The high molecular weight oligomers' structure is already β but non-fibrillar. During the elongation phase, such non-fibrillar β-structures (they do not bind ThT; for ThT -fibril binding see Chapter 2, section 2.2.1.5) transform into fibrillar b-structures (they bind ThT).

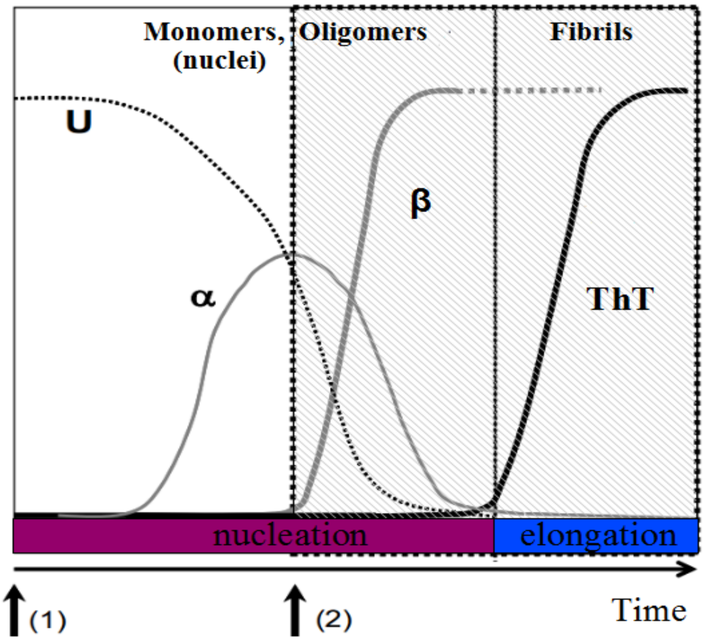

Figure 1.10 The secondary structural changes during Aβ40 peptide fibrillization, compared to the kinetics of the process measured using ThT. The arrow labelled (1) denotes the starting point in Kirkitadze's experiments, whereas the arrow labelled (2) denotes the starting point in N. Benseny-Cases's experiments. According to the corresponding curves it is shown that during a period of time corresponding to a nucleation phase (purple bar) the content of α-helical structures decreases down to its minimum meanwhile the content of β-structures reaches its maximum but fibrillar b-structure content grows in elongation phase (blue bar).

For amyloid fibril formation to occur the native protein needs to be destabilized. It is believed that amorphous aggregates can from both unfolded and intermediate states whereas structured aggregates like amyloid fibrils most likely originate from partially folded intermediates. A nucleation-dependent process of amyloid fibrils is characterized by a critical concentration below which no aggregation will occur, a lag phase when oligomers (nuclei) are formed from misfolded monomers, followed by a more rapid elongation phase and finally a steady state phase where monomers and fibrils are at equilibrium (Figure 1.11). The lag phase can be abolished by adding a preformed nucleus, a so-called seed. It has been suggested that the fundamental unit of all amyloid fibrils is a dry steric zipper formed by two tightly interdigitated β-sheets. The process of fibril formation then probably starts by the un-masking of several zipper-forming segments, permitting them to stack into sheets – if this is a naturally occurring event it would be compatible with the slow nucleation event (Sawaya et al., 2007).

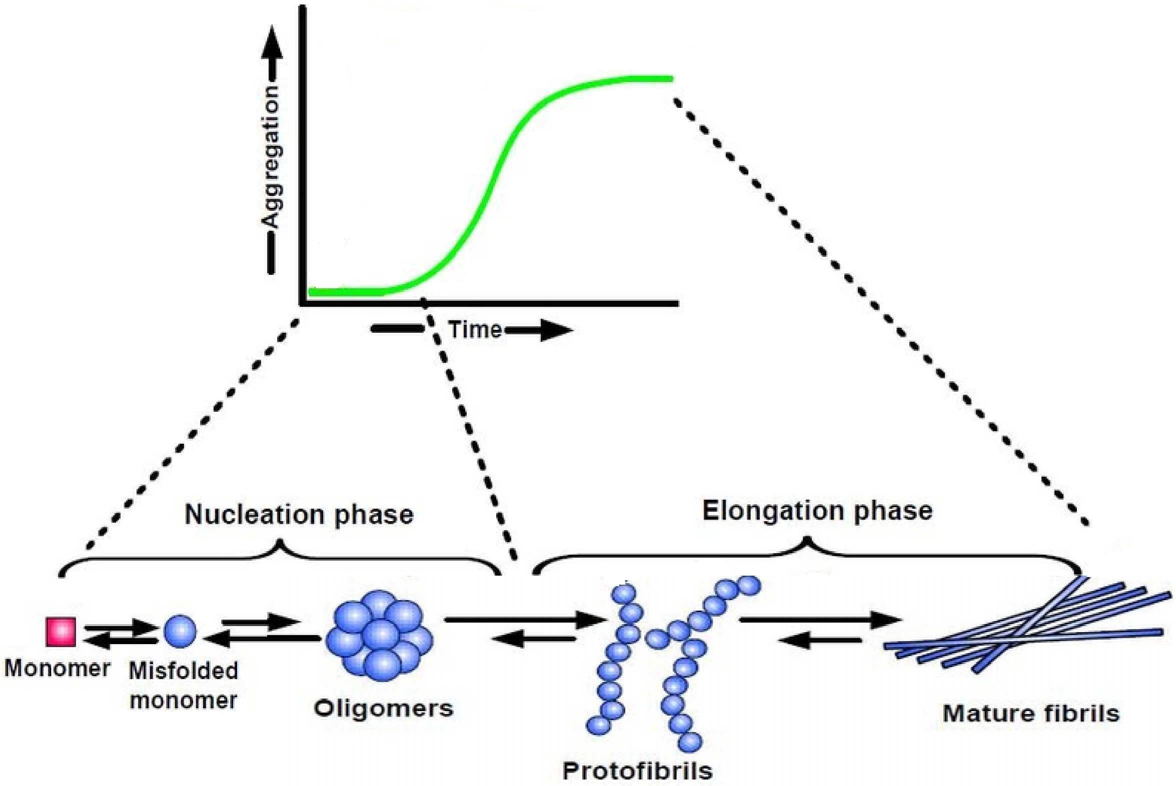

Figure 1.11. Formation of amyloid fibrils is a nucleation dependent process. This type of event is characterized by a slow lag-phase: Aβ monomers initially forming low molecular weight soluble oligomers, then during an elongation phase these oligomers further aggregate into insoluble protofibrils, fibrils and plaques.

1.3.6 Toxicity of Aβ

1.3.6.1 Secondary structure of Aβ and toxicity

As it was mentioned above Aβ is generated during normal cellular metabolism and is present in the brains and secreted to the extracellular space of the human brain and also found in cerebrospinal fluid (CSF) of normal humans throughout life (Haass et al., 1992). Several lines of evidence indicate the physiological role of Aβ in neuronal activity (Pearson and Peers, 2006). Thus, the presence of Aβ in the CSF of nondemented individuals and in the media from neuronal cell cultures during normal metabolism indicates that Aβ has a role in the central nervous system in addition to having a potential pathological role in AD. Therefore, the mere presence of Aβ simply does not cause neurodegeneration; rather neuronal injury appears to develop because of the ordered self-association of Aβ molecules which become neurotoxic. The fact that monomeric Aβ become neurotoxic only upon self-association is well supported by the recent research on amyloid toxicity in resolving the specific neurotoxic structures derived from Aβ's self-association and their relative contributions to AD pathogenesis (Haass and Selkoe, 2007).

Studies using synthetic Aβ peptides provide additional support for the role of prefibrillar and fibrillar Aβ assemblies in AD pathogenesis. The first nonfibrillar assemblies identified were protofibrils; these heterogeneous structures range from spherical assemblies of ~5 nm in diameter to short, flexible rods of up to 200 nm in length (Walsh et al., 1997). The protofibrils and fibrils are principally different from each other depending on their size and relative solubility. The protofibrils appear to behave as true fibrils intermediates in that they can both form fibrils and dissociate to low molecular weight species. They are known to be neurotoxic, acute application of protofibrils *in vivo* rapidly alter the synaptic physiology, whereas chronic application causes cell death (Hartley et al., 1999, 2008).

The secondary structure of Aβ fibrils, like all amyloid proteins, is composed of β-sheet. This is due to β-sheets being the most thermodynamically stable secondary structure for oligomers (Perczel, Hudáky, and Pálfi 2007). X-ray fibre diffraction patterns can be used to detect the structure of fibrils and significantly, they indicate that β-strands align perpendicularly to the fibril axis, and this 'cross-β motif' is a defining feature of all fibres (Figure 1.12) (Sunde et al., 1997; Serpell et al., 1999).

Aβ undergoes a misfolding pathway in AD to form amyloid fibrils. The nucleating event that triggers fibril formation is still unclear. Four proposed nucleating events are described below:

1. α-helix formation,
2. Folding nucleus formation,
3. Micelle formation
4. Paranuclei formation

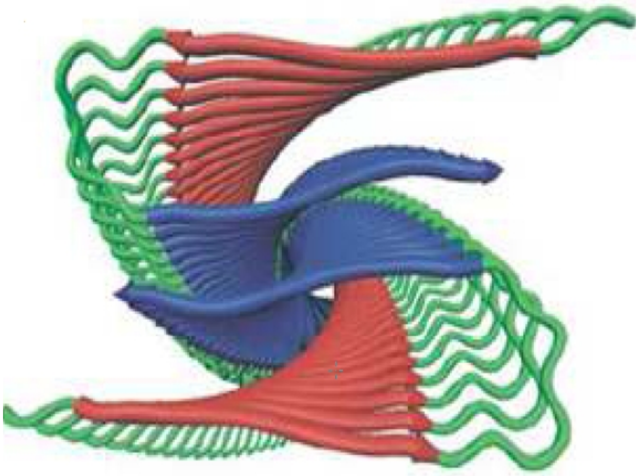

Figure 1.12. Structural model for the formation of a protofilament. Cartoon representation of the four layered amyloid β-sheet fibril. Each cross-β unit is a double-layered structure, with parallel β-sheets formed by residues 12–21 (red arrows) and 30–40 (blue arrows) (Boix, 2006).

1. α-helix formation (Soto et al. 1995). Soluble Aβ has been proposed to be in equilibrium between α-helix and β sheet secondary structure. The transition to β-sheet may be the nucleating factor, with the ability to form fibrils only occurring once β-sheet structure has been obtained. Increasing the propensity for α-helical secondary structure results in a reduction in fibril formation ability and likewise amino acid substitutions that disfavour α-helical formation accelerate formation of fibrils.

2. Folding nucleus formation (Lazo et al. 2005). An intramolecular nucleation event in both Aβ40 and Aβ42 has been suggested, where Val24-Lys28 forms a "folding nucleus" by forming a turn.

3. Micelle formation (Lomakin et al. 1996). In this model if a critical Aβ40 concentration is reached or exceeded, then nucleation occurs through the formation of micelles, with a hydrodynamic radii (R_h) of 7 nm. It is assumed that these micelles act as sites of nucleation. At Aβ40 concentrations less than the critical protein concentrations, micelles do not form and subsequently, nucleation is heterogeneous, with multiple nucleation pathways, possibly through seeding on impurities.

Once formed, the nuclei advance by a series of elongation steps to low molecular weight oligomers which then increase in size to oligomers and fibres. Electron microscopy and solid state NMR showed that fibrils grown under quiescent conditions had a maximum diameter of 9 ± 1 nm, a periodic twist and were toxic to neuronal cell cultures. Conversely, fibrils grown under agitated conditions had a diameter of 5 ± 1 nm, non-twisting and were not toxic to cell cultures (Petkova et al., 2005). Once formed, the fibrils can then associate further to form the SPs observed in AD brains.

1.3.6.2 Nature of the toxic species

The mechanism by which Aβ is toxic is hotly debated. Plaques are one of the most obvious features of the Alzheimer's disease brain, and initially were considered the toxic species, however there are several pieces of evidence that cast doubt as to their responsibility for the neurodegeneration observed. Firstly, plaque formation is not unique to the disease state, and studies have shown that there is not always a link between the presence of amyloid plaques and cognitive decline (Yankner et al., 2008). Recently it was shown that granular non-fibrillar aggregates (GNAs) are possible toxic species in Alzheimer's disease. GNAs form on the surface of negatively charged biological membranes and as a consequence of an acidic environment, off the polymerization pathway at neutral pH. Aβ40 GNAs disturb the bilayer structure of model membranes and seem to be more toxic to cells with negatively charged membranes (Benseny Cases et al., 2011). The different species that have been isolated from the fibril formation pathway and suggested to be toxic are discussed below.

A major problem with studies that aim to characterising a particular species or group that forms during fibril formation is that under experimental conditions (usually conducted at much higher Aβ concentrations than would occur *in vivo*) Aβ will aggregate rapidly. This difficulty in confidently identifying one stable intermediate which can be reliably isolated explains why some of the "toxic species" include a large range of oligomeric sizes. Thus unless methods are used to stabilise each species (though this itself will change the nature of the sample), it is probable that aggregation will continue throughout the experiment and thus monomers will aggregate to form small oligomers, which will become large oligomers and so on.

1.3.6.3 Possible mechanisms of Aβ toxicity

Accumulation of the Aβ is generally believed to be central to the induction of Alzheimer's disease, but the relevant mechanism(s) of toxicity are still unclear. Here presented mechanisms are three major areas where Aβ is thought to promote toxicity: membrane alterations, intracellular interactions, oxidative stress and endoplasmic reticulum stress.

A. Membrane Alterations:

Within APP, Aβ resides partially in the membrane. Consequently Aβ has a predominantly polar N terminus, and largely hydrophobic C terminus. This hydrophobic tail has led to the hypothesis that the toxicity is due to Aβ interactions with cell membranes (Simakova and Arispe, 2007). There are several ways this could lead to toxicity:

1. Membrane insertion will disrupt the structure and function of the plasma membrane (Arispe et al., 2007).

2. The conductance of lipid bilayers and cell membranes will increase in the presence of Aβ oligomers, through Aβ indirectly thinning the membrane, or causing localised structural defects (Sokolov et al., 2006).

3. Aβ forms ion channels, resulting in increased conductance of Ca2+ and other cations. This results in cell death via triggering Ca2+ sensitive apoptosis signalling pathways (Arispe et al., 2007).

B. Intracellular Interactions

An emerging role for intracellular Aβ is that it exerts toxicity at very early stages in AD dysfunction. Theoretically the intracellular environment should favour fibril formation, due to the lower pH of certain intracellular organelles and crowding effects. Increases in intraneuronal Aβ deposits in transgenic mice occurred at the same time as abnormalities in behaviour and physiology (Camargo et al., 2005), but before plaque or tangle formation.

The theory that intracellular changes begin the cascade of neurodegeneration is an attractive one. However studies of the Aβ secretory pathway show that most Aβ produced is secreted from the cell. Indeed intraneuronal Aβ42 levels actually decrease with increasing development of AD (Gouras et al., 2000). Thus extracellular Aβ would have to be re-internalised, and it is debatable whether intracellular Aβ would reach concentrations high enough to cause the significant toxicity that would be expected from the trauma observed in AD brains.

C. Oxidative Stress

Increased levels of oxidative damage are characteristic of AD brains. Oxidative stress has also been observed to occur before the formation of amyloid plaques (Nunomura et al., 1999). In early studies, Aβ was suggested to generate ROS (reactive oxygen species) spontaneously (Hensley et al., 1994). However further studies using electron paramagnetic resonance spin-trapping, found no evidence of spontaneous formation of peptide-derived free radicals during the incubation of Aβ40 (Turnbull et al., 2001), and it now seems highly unlikely that Aβ is capable of generating ROS alone. It was then suggested that Aβ could produce ROS in the presence of transition metals through Fenton/Haber-Weiss reactions (Huang et al., 1999). The ability of Cu(II) to undergo Fentons/Haber-Weiss reactions and generate ROS is described late in this chapter. Aβ has a methionine at position 35 and in Aβ isolated from plaques the methionine is oxidised. Potentially, Met35 could donate electrons for metal ion reduction, and in doing so initiate a redox cycle. But the exact toxic mechanism is still unclear and it is possible the theories are closely interconnected (Dong et al., 2003).

D. Endoplasmic reticulum stress.

Under physiological conditions,aberrant proteins are targeted for degradation by the ubiquitin proteasome system (UPS) or the autophagic-lysosomal system. Both systems are part of a complex network that maintains the protein

homeostasis, also called proteostasis. The accumulation of protein aggregates in AD and many other neurodegenerative disorders indicates a severe disturbance in the proteostasis network. In the endoplasmic reticulum (ER) aberrant proteins are exported to the cytosol and subsequently degradated by the UPS; a process called ER-associated degradation (ERAD). In addition, ER stress conditions induce autophagy. Increased levels of aberrant proteins in the ER activate the unfolded protein response (UPR), a stress response aimed to restore proteostasis in the ER. The ER stress results from disrupted protein folding triggered by protein mutation or oxidation, reduced proteasome activity, and altered Ca2+ homeostasis. It was revealed increased splicing of X-box binding protein-1 (XBP-1), an UPR transcription factor, in AD compared with age-matched control. Among target genes of XBP-1, expression of protein disulfide isomerase (PDI) was increased in AD, also suggesting disturbed activation of the UPR in AD (Lee et al., 2010). As it shown in Figure 1.13 UPR activation enhances autophagy.

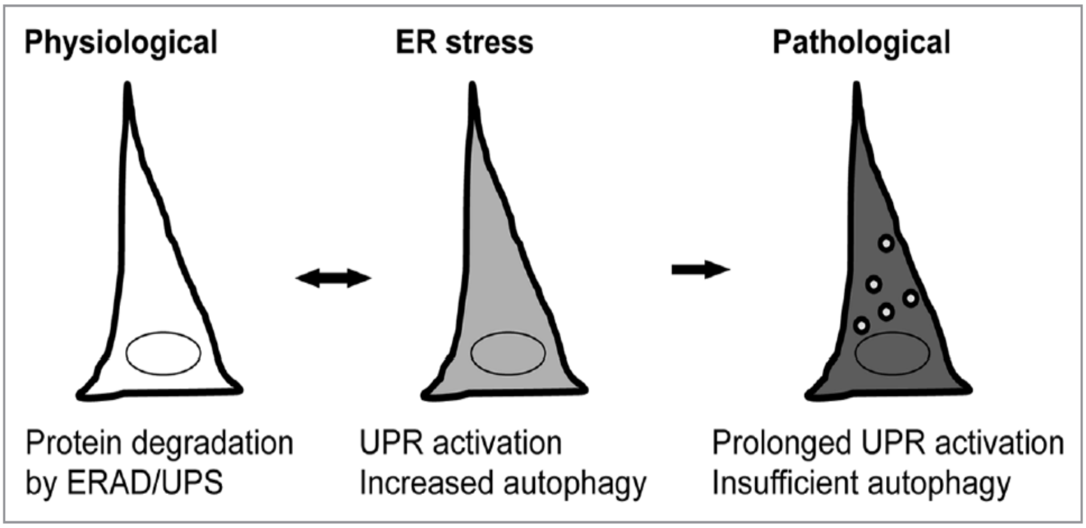

Figure 1.13. ER stress preferentially activates autophagy in neuronal cells. Under physiological conditions, aberrant ER proteins are removed by ERAD and degraded by the UP S. A disturbance of ER homeostasis resulting in activation of the UP R will activate the autophagy pathway. In AD neurons, the autophagic capacity may not be sufficient due to age-related impairment of the autophagic-lysosomal system and/or increased demand for autophagy by (prolonged) activation of the UPR. (Scheper, Nijholt, and Hoozemans 2011)

1.4 COPPER

1.4.1 The chemistry of copper

The interaction between Aβ and Cu(II) is the major theme of this thesis, thus this section of the introduction discusses copper in the body, its redox chemistry and aspects of metal-ligand binding. Copper is a crucial cofactor in enzymes such as cytochrome c and superoxide dismutase, and it can drive a range of processes in the body that are essential for life. It can exist in biological systems in two states: reduced Cu(I) and oxidized Cu(II). Defects in copper homeostasis are directly responsible for human disease, for example mutations in the *ATP7a* or *ATP7b* genes, which encode Cu-transporting ATPase pumps, result in Menkes and Wilson's disease respectively. Menkes disease is a lethal disorder of intestinal copper hyperaccumulation with severe copper deficiency in peripheral tissues. Wilson's disease results in hepatic and neuronal copper overload, which requires chronic therapy to enhance copper excretion or reduce copper absorption (Wang et al., 2011).

1.4.2 Copper life cycle

Copper is the 29th element of the Periodic table. Its electronic configuration is $3d^{10}$ $4s^1$. Cuprous ion Cu(I), has completely filled d-orbitals with 10 electrons ($3d^{10}$), while the cupric ion (Cu(II) has only 9 electrons in the d orbitals, ($3d^9$) with one electron being unpaired. Consequently bivalent copper (Cu(II)) is paramagnetic and represents the most stable oxidation state of copper

(Valko et al., 2005).

In adult humans, the net absorption of dietary copper is approximately 1 mg per day. Dietary copper joins some 4-5 mg of endogenous copper flowing into the gastrointestinal tract through various digestive juices. Most of this copper returns to the circulation and to the tissues (including liver). Much lower amounts of copper flow into and out of other major parts of the body (including heart, skeletal muscle, and brain). Newly absorbed copper is transported to body tissues in two phases, borne primarily by plasma protein carriers (albumin, transcuprein, and ceruloplasmin). In the first phase, copper goes from the intestine to the liver and kidney; in the second phase, copper usually goes from the liver (and perhaps also the kidney) to other organs (Linder et al., 1998). It was discovered that Cu(II) may be released postsynaptically at glutamatergic synapses in hippocampus, in the site for initial Aβ deposition in AD (Schlief et al., 2005).

About 85-95% of copper tightly binds to ceruloplasmin, whereas the remainder loosely binds to and is exchanged among albumin, α2 macroglobulin, amino acids, peptides and several micronutrients. We will refer to the portion that binds to ceruloplasmin as ‘bound’ copper, and to the portion that binds to the loose compounds as ‘free’ copper (Linder et al., 1998), following a custom of Wilson’s Disease clinical care.

Copper, in excess of cellular needs, mediates free radical production and direct oxidation of lipids, proteins, and DNA. Therefore the balance between intracellular and extracellular contents of copper is driven by cellular transport systems that regulate uptake, export and intracellular compartmentalization (Valko, Morris, and Cronin 2005).

1.4.3 Copper in the brain

Since copper is an integral part of many proteins necessary for neurological functioning, the role of copper in oxidative mediated stress in neurodegenerative diseases was intensively studied. The role of copper has been implicated in neurodegenerative disorders such as AD, Parkinson’s disease and amyotrophic lateral sclerosis (Cookson and Shaw, 1999). The mechanism of copper transport into the brain is unclear. Interestingly, in comparison to Cu(II) in the blood, studies comparing radiolabelled free copper, copper-albumin, and copper-ceruloplasmin showed that free copper was the major species entering the brain (Choi and Zheng, 2009). The blood brain barrier (BBB) is the major entrance for copper to the brain, whereas the blood-cerebrospinal fluid (BSF) barrier regulates copper homeostasis in the cerebrospinal fluid (CSF).

Once copper has crossed the BBB/BSF barrier the high affinity copper transporters mediate Cu (I) transport into neurons. The mammalian mechanism of reducing extracellular Cu(II) to Cu(I) is still unclear. Although free Cu(II) may be the major species entering the brain, once inside the cell redox active metals such as Cu(I) are usually tightly chaperoned – there are no free Cu(I)/ Cu(II) ions in the cell (Rae et al. 1999).

1.4.4 Redox chemistry of copper

Copper is essential for life. It plays a pivotal role in the central nervous system, in which a low concentration of copper results in incomplete development, whereas an excess of copper is injurious.

Copper is a redox active metal as it can change its valence state under biological conditions. The one electron difference between Cu(I) and Cu(II) allows copper to promote radical reactions. Dissolved molecular oxygen in the body is liable to react with redox active metals such as copper to produce ROS. Superoxides ($O_2\bullet-$) are one type of ROS that are produced in the mitochondrial transport chain, and dealt with by superoxide dismutase (SOD). SOD is a copper-containing enzyme which catalyses dismutation of $O_2\bullet-$ to hydrogen peroxide (H_2O_2) by the copper ions in SOD undergoing oxidation and reduction:

$$\text{Enzyme–Cu(II)} + (O_2\bullet\text{-}) \longrightarrow \text{Enzyme-Cu(I)} + O_2$$

$$\text{Enzyme-Cu(I)} + (O_2\bullet\text{-}) + 2(H+) \longrightarrow \text{Enzyme–Cu(II)} + H_2O_2$$

Hydrogen peroxide is widespread in the cell and is only a weak oxidising or reducing agent, and generally poorly reactive. However it can react with iron and copper to form damaging species, such as the hydroxyl radical (OH•), via Fenton's cycling and the Haber-Weiss reaction (below):

$$\text{Cu(I)} + H_2O_2 \longrightarrow \text{Cu(II)} + (OH\bullet) + (OH\text{-}) \quad \text{(Fenton reaction)}$$

$$(O_2\bullet\text{-}) + H_2O_2 \xrightarrow{\text{Met Catalyst}} O_2 + (OH\bullet) + (OH\text{-}) \quad \text{(metal-catalysed Haber Weiss-reaction)}$$

Thus, through redox cycling, copper has the potential to produce a range of harmful species which can go on to generate a variety of oxidative damage in the cell (Figure1.14). Accumulation of ROS can result in the modification of proteins, lipids and DNA leading ultimately to cell death.

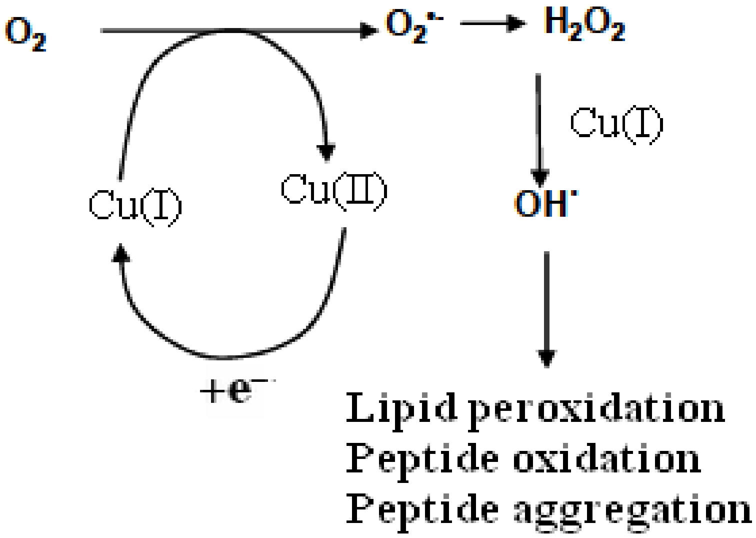

Figure 1.14 Diagram of Cu(II) induced oxidative stress. Dissolved molecular oxygen is liable to react with redox active metals such as copper. In the reduced state Cu(I) will reduce O_2 to superoxide O_2• - which is then dismutated or disproportionated to H_2O_2, for example by superoxide dismutase. If H_2O_2 is not cleared by scavenging mechanisms (e.g. catalase or glutathione peroxidase) it can generate the highly reactive hydroxyl radical (OH•˙) upon reaction with an encountered reduced metal Cu(I) (Sigel, 2006).

1.4.5 Evidence for a role for copper in AD

Neurodegenerative metallochemistry has developed on the observation that APP possesses selective zinc and copper binding sequences that the APP is a copper protein. APP binds copper in two domains, one located in the extracellular N-terminal region and the other in the C-terminal region within the Aβ peptide (Squitti and Zito, 2009). Ithas been proposed that APP reduces Cu2+ to Cu1+ upon coordination, thus promoting thenon-amyloidogenic cleavage pathway(K. Barnham et al. 2003). Depletion of intracellular copper results in a reduction of APP gene expression (Bellingham et al. 2004).

One of the main characteristics of AD includes altered metal ion concentrations in the brain, such as Cu (Bayer et al., 2006). Copper levels are significantly elevated in the brains of AD patients (Lovell et al., 1998). Raman spectroscopy of senile plaque cores isolated from AD brains displayed vibrational frequencies arising from copper and zinc ions directly bound to the histidine imidazole rings of Aβ in the plaques (J. Dong et al. 2003). In addition, synchrotron X-ray fluorescence has identified hot spots in which Cu is concentrated within Aβ associated amyloid plaques (Miller et al., 2006). Finally copper levels in serum are much higher in patients with AD than controls (Squitti and Salustri, 2009). Copper binds to Aβ with a high affinity via histidine (His 6, 13 and 14) interacting with tyrosine (Tyr 10) residues (Streltsov et al. 2008). This all indicates that disrupted metal ion homeostasis occurs in AD (Bush 2003).

There are two commonly expressed objections to the role of copper in AD. The first objection is that AD is not associated with elevated exposure to environmental copper. It is important to clarify this misconception. The total concentration of copper within the brain is potentially more than sufficient to be neurotoxic. As a consequence, the brain has efficient homeostatic mechanisms in place to maintain compartmentalization of metal ions, which when compromised cause neurodegenerative diseases such as Wilson’s and Menkes’ disease. There is evidence to suggest that homeostatic mechanisms for metal ions are impaired in AD patients, and AD is characterized by altered metal ion-dependent processes and metal ion concentrations in the brain (Cuajungco and Lees, 1997). The second objection is that the affinity of Aβ for Cu(II) is too low to bind these metals at their extracellular concentrations. This is also a misconception, since extracellular levels of Cu(II) may reach as high as 15 μM (Lovell et al., 1998), whereas it was shown that Aβ affinity for Cu(II) is at the submicromolar level and is reported to be much higher in amyloid plaques (Syme et al. 2004).

1.5 AD TREATMENT

1.5.1 Current therapeutics for AD

So far no one single factor has been identified as a cause for Alzheimer's disease. It is likely that a combination of factors, including age, genetic inheritance, environmental factors, diet and overall general health, are responsible. In some people, the disease may develop silently for many years before symptoms appear and the onset of clinical disease may require a trigger. Most often, AD is diagnosed in people over 65 years of age (Brookmeyer et al., 1998), although the less-prevalent early-onset Alzheimer's can occur much earlier. The disease affects memory and mental functioning (e.g. thinking and speaking, etc.), but can also lead to other problems such as confusion, changes of mood and disorientation in time and space. At first the symptoms such as difficulty with memory and loss of intellectual abilities may be so slight that they go unnoticed, both by the person concerned and his or her family and friends. However, as the disease progresses, the symptoms become more and more noticeable and start to interfere with routine work and social activities. Practical difficulties with daily tasks such as dressing, washing and going to the toilet gradually become so severe that in time the person becomes totally dependent on others. Over time, the disease destroys large areas of the brain, leaving its victims with little comprehension or awareness. The mean life expectancy following diagnosis is approximately seven years (Mölsä et al., 1986). Alzheimer's disease always ends in death, typically from pneumonia or lack of nutrition (Waldemar et al., 2007). Currently no treatments to delay or halt the progression of the disease are, as of yet, available. As of 2010, more than 800 clinical trials are in the process of being carried out for identification of a possible treatment for AD (http://www.clinicaltrials.gov), but it is unknown if any of the tested intervention strategies will show promising results. A number of non-invasive, life-style habits have been suggested for the prevention of Alzheimer's disease, such as mental stimulation, exercise, and a balanced diet are suggested, as both a possible prevention and a sensible way of managing the disease but there is a lack of adequate evidence for a link between these recommendations and reduced degeneration ("Can Alzheimer's disease be prevented" 2006 National Institute on Ageing).

There are two types of possible treatment to fight this disease: preventive and curative. In the first case AD can have different causes that are generic, toxic, environmental, metabolic and infectious in origin. These causes are often independent but cumulative. And each requires a target treatment. Research therefore centres on obtaining the earliest possible diagnostic, eliminating exogenious causes, and applying specific treatment.

Currently to aid management of AD there are four drugs approved by regulatory agencies such as the U.S. Food and Drug Administration (FDA) and the European Medicines Agency (EMEA). Three of the drugs (Donepezil, Galantamine and Rivastigmine) are acetylcholinesterase inhibitors. Acetylcholinesterase inhibitors have been developed in response to post-mortem and biopsy studies which found decreases in acetylcholine synthesis and release in AD brains (Bowen et al., 1977). By inhibiting acetylcholinesterase activity, more acetylcholine is available at the synapse and subsequently cognitive function is improved.

Memantine, the fourth drug, is an N-methyl-D-aspartic acid receptor (NMDAR) antagonist. It was developed because NMDAR-mediated glutamate excitotoxicity is associated with the neuronal death characteristic of AD. Glutamate is the most abundant neurotransmitter in the body, and is bound at chemical synapses by the NMDAR, on the membranes of post-synaptic neurons. However excitotoxicity can occur when receptors for glutamate such as the NMDAR are overactivated. Overactivation from excess glutamate allows high levels of calcium ions to enter the cell, activating a number of enzymes, which damage cell structures, resulting in cell death. The extent of AD symptoms correlates well with the neuronal death caused by excess glutamate. Thus using an NMDA receptor antagonist such as memantine should prevent excess glutamate binding and subsequent excitotoxicity. A drug called Ebixa (trade name for the drug memantine) is the only drug that is suitable for use in people in the middle to later stages of dementia.

Side-effects of all those mentioned drugs may include hallucinations, confusion, dizziness, headaches and tiredness.

Unfortunately there is nowadays no specific treatment strategy of cure for Alzheimer's disease capable of demonstrating empirical efficacy and safety has yet to emerge. Because current treatments are mainly symptomatic, drugs may only stabilize some of the symptoms of Alzheimer's disease for a limited period of time (Augy, Bonin-Guillaume, and Blin 2006), the research to expand our basic knowledge to develop AD modifying therapies and understanding of the state of Amyloid beta-peptide is more than academic interest. AD progression indicates that new parameters need to be investigated which could incommode particular molecular polymorphic forms of Amyloid beta-peptides.

1.5.2 Current therapeutic research

Aβ antibodies are being investigated. Here presented only a few examples concerning this field. The seminal study in this area used transgenic mice which over-express mutant human APP (Val717Phe) (Schenk et al., 1999). Synthetic human Aβ42 was used as an immunogen (active immunisation). Treatment began before plaque formation was observed. Eight of the nine transgenic mice immunised with Aβ42 developed serum antibody titres against Aβ42 of greater than 1:10000. The result of this was that immunisation with Aβ42 almost completely prevented Aβ deposition, with seven of the nine mice having no detectable Aβ deposits in their brains. Additionally there was a near total reduction in the Aβ burden in the hippocampus. In contrast, control animals that had been immunised with phosphate buffered saline only contained numerous Aβ deposits and had a significantly greater Aβ burden ($P = 0.0005$). The Aβ42 immunised mice lacked all the hallmarks of neurodegeneration characteristic of AD, including an absence of dystrophic neurites, and dramatically reduced astrocytosis. Presumably immunisation either prevents deposition and/or promotes clearance of Aβ in the brain. The same study also observed the effect of immunisation after plaque formation had occurred, and found immunisation with Aβ significantly slowed the development of existing pathologies in the animals.

Passive immunisation has also been closely studied. The ability of Aβ binding proteins to act as an Aβ "sink" was assessed. The antibody m266 showed a low picomolar affinity and thus could bind Aβ in the presence of physiological buffers and endogenous Aβ binding proteins. The same transgenic mouse model as used in the Schenk study above was used to assess the effects of m266 *in vivo*. Unbound Aβ plasma levels were reduced from 140 pg/ml in control mice to essentially undetectable levels in mice treated with m266, suggesting all plasma Aβ was bound to m266. Additionally the amount of Aβ bound to m266 increased over several days to ~ 1000 fold above endogenous plasma Aβ levels. This strongly implies that circulating m266 facilitates the transfer of Aβ into the plasma from the CNS (DeMattos et al., 2001). The same group produced a follow-up study where they determined the effect of m266 on learning and memory.

However a further study using passive immunization in transgenic mice found that although administration of Aβ immunisation significantly reduced amyloid, it also induced a two-fold increase in cerebral microhaemorrhages and a significant increase in haemorrhage severity over controls. This may results from passive immunization compounding the weakening of cerebral blood vessels which occurs during amyloid deposition (Pfeifer et al., 2002). Furthermore a phase II clinical study using a serum Aβ antibody (AN1792) was halted when 6 % of the patients developed meningoencephalitis (Orgogozo et al., 2003).

A further study was carried out with the antibody An1792, and found that immunisation of patients with An1792 was associated with a long term reduction in Aβ load and a variable degree of plaque removal. Unfortunately the study also found no support for immunisation improving cognitive function. Two individuals with the highest levels of Aβ antibodies and almost complete elimination of plaques still had clear end stage dementia before death, and there was no evidence of immunisation having an effect on long-term survival (Holmes et al., 2008). However the authors themselves concede that the small numbers of participants in the study may have masked potential smaller benefits of the treatment, thus it may be too early to write off immunisation as a possible AD therapeutic.

Another approach is decreasing Aβ production by targeting the secretases. γ-secretase inhibitors can be characterised into two generations of therapeutics. Firstly, administration of a γ-secretase cleavage site peptidomimetic resulted in a lowering of Aβ production (Wolfe et al., 1998). This substrate-based difluoro ketone was designed based on the APP γ –secretase cleavage site for Aβ42 and was demonstrated to be a specific inhibitor of Aβ biosynthesis in APP-transfected cells. However the peptidic and bulky properties of these mimics make them unlikely therapeutics for further development in *in vivo* studies, although they have provided valuable information on characterising γ-secretase's catalytic core (Lundkvist and Näslund, 2007). Early therapeutics had unfortunate side-effects with profound changes in gastrointestinal tract tissue morphology and altered lymphocyte development, probably due to impaired Notch signalling (Wong et al. 2004). The Notch signalling pathway is essential during embryogenesis (Artavanis-Tsakonas et al., 1995).

A different strategy to using γ-secretase inhibitors is the development of γ-secretase modulators. Tarenflurbil is an enantiomer of a non-steroidal anti-inflammatory drug (NSAID). NSAIDs include drugs such as ibuprofen and aspirin. NSAIDs interact directly with the γ-secretase complex. The mechanism is unclear but the proteolytic cleavage site is altered, resulting in less Aβ42 and more Aβ(1-38). NSAIDs are attractive as therapeutics as they already have well-characterised toxicity profiles. However a large 18 month phase III trial of an NSAID showed no benefit, perhaps because taking the drug via oral administration resulted in insufficient brain concentrations (Eriksen et al., 2003).

In contrast, deletion of the β-secretase gene does not result in any serious toxicity and β-secretase is essential in generating Aβ, thus β-secretase inhibitors are considered to be one of the most promising targets for an AD therapeutic (Harrison et al., 2003). There are several encouraging studies using β-secretase inhibitors. GSK188909 is a BACE-1 inhibitor which was the first therapeutic shown to reduce brain amyloid levels in transgenic mice following oral administration (Hussain et al., 2007). Targeting BACE still seems to be the most viable approach for a single therapeutic in AD (Hunt and Turner, 2009).

1.6 DENDRIMERS

1.6.1 Definition of dendrimers

First discovered in the early 1980's by Donald Tomalia and co-workers (Tomalia and Majoros, 2003), these hyperbranched molecules were called dendrimers. The term originates from 'dendron' meaning a tree in Greek. Dendrimers are the new artificial macromolecules which have the structure like a tree. They are hyperbranched and monodisperse three-dimensional molecules, and have defined molecular weights and host–guest entrapment properties. Since dendrimers are synthesized from branched monomer units in a stepwise manner, it is possible to conduct a precise control on molecule size, shape, dimension, density, polarity, flexibility, and solubility by choosing different building/branching units and surface functional groups. Moreover, they can use small organic molecules and polymers as structural components, and thus acquire special physical and chemical properties (Cheng et al. 2008).

Up to now, dendrimers have been widely applied in many fields, such as supramolecular chemistry or host–guest chemistry (Al-Jamal et al., 2005), electrochemistry and photochemistry, nanoparticle synthesis, pollution management, dye decolorization, preparation of monomolecular membranes, curing of epoxy resins, catalysis, drug delivery, and gene transfection. ((Cheng et al., 2008) and references herein).

Dendrimers possess empty internal cavities and open conformations (for low-generation dendrimers), which make it possible to encapsulate hydrophobic drug molecules (Jansen et al., 1994). In addition, they have a much higher surface functional group density when compared with conventional macromolecules. These functional groups permit the application of dendrimers to enhance the solubility of many drugs (Yiyun and Tongwen, 2005).

Furthermore, the large number of surface functional groups on the outer shell dendrimer can significantly suppress the aggregation of amyloid proteins (Klajnert et al., 2008; Shukla et al., 2011).

1.6.2 Structures of dendrimers

Dendrimers consist of a series of chemical shells built on a small core molecule. It is the hyperbranching when going from the centre of the dendrimer towards the periphery, resulting in homostructural layers between the focal points (branching points). The number of focal points when going from the core towards the dendrimer surface is the generation number. For example, a dendrimer having five focal points when going from the centre to the periphery is denoted as the 5th generation dendrimer. Here, it abbreviated to simply a PPI-G5 e.g. a 5th generation of polypropylene imine. Dendrimers are very much like ordinary organic molecules for the first three generations. They are small and floppy without much consistent or specific three-dimensional structure. By G4 they are beginning to become spherical and to take on a preferred three dimensional structure. By G5 they have a consistent and specific three dimensional structure. Beyond G5 they are highly structured spheres. They are branched 3-D nanopolymers with controlled composition and architecture consisting of three components: a core, interior branch cells and terminal branch cell. These soft nanoparticles, with sizes in the range up to 100 nm, can serve as hosts for cations, anions and organic solutes. Generally, dendrimers are globe- or ellipsoidshaped.

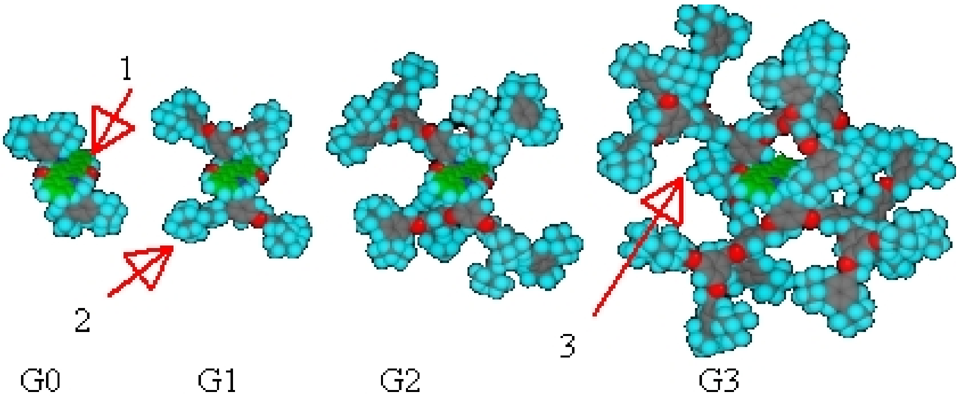

Figure 1.15 Representation of a fourth generation dendrimer. G0 is the core (1)(of dendrimer, G1-G3 – repetitions of branching unites (2). Internal cavities (3) make it possible to encapsulate hydrophobic drug molecules (McGrath, 2005)

The central core should be a molecule with at least two reactive functional groups. The repeated branches are organized in a series of radically concentric layers called ‘‘generations’’.The surface functional groups, which to a great degree determine dendrimer’s physical properties in solid state or in aqueous solutions, are located on the surface of dendrimer molecules. The number of surface functional groups, as well as the molecular weight and size of dendrimers, are related to its generation and can be controlled during synthesis (Figure 1.15)

1.6.3 Syntheses of dendrimers

Dendrimers are generally prepared using either a divergent method or a convergent one. There is a fundamental difference between these two construction concepts. In the divergent methods, dendrimer grows outwards from a multifunctional core molecule. The core molecule reacts with monomer molecules containing one reactive and two dormant groups giving the first generation dendrimer.

Then the new periphery of the molecule is activated for reactions with more monomers. The process is repeated for several generations and a dendrimer is built layer after layer. Divergent approach is successful for the production of large quantities of dendrimers. Problems occur from side reactions and incomplete reactions of the end groups that lead to structure defects. To prevent side reactions and to force reactions to completion large excess of reagents is required. It causes some difficulties in the purification of the final product. The convergent methods were developed as a response to the weaknesses of the divergent synthesis (B Klajnert and Bryszewska 2001). In the convergent approach, the dendrimer is constructed stepwise, starting from the end groups and progressing inwards. When the growing branched polymeric arms, called dendrons, are large enough, they are attached to a multifunctional core molecule (Figure 1.16). The convergent growth method has several advantages. It is relatively easy to purify the desired product and the occurrence of defects in the final structure is minimised. It becomes possible to introduce subtle engineering into the dendritic structure by precise placement of functional groups at the periphery of the macromolecule. The convergent approach does not allow the formation of high generations because steric problems occur in the reactions of the dendrons and the core molecule.

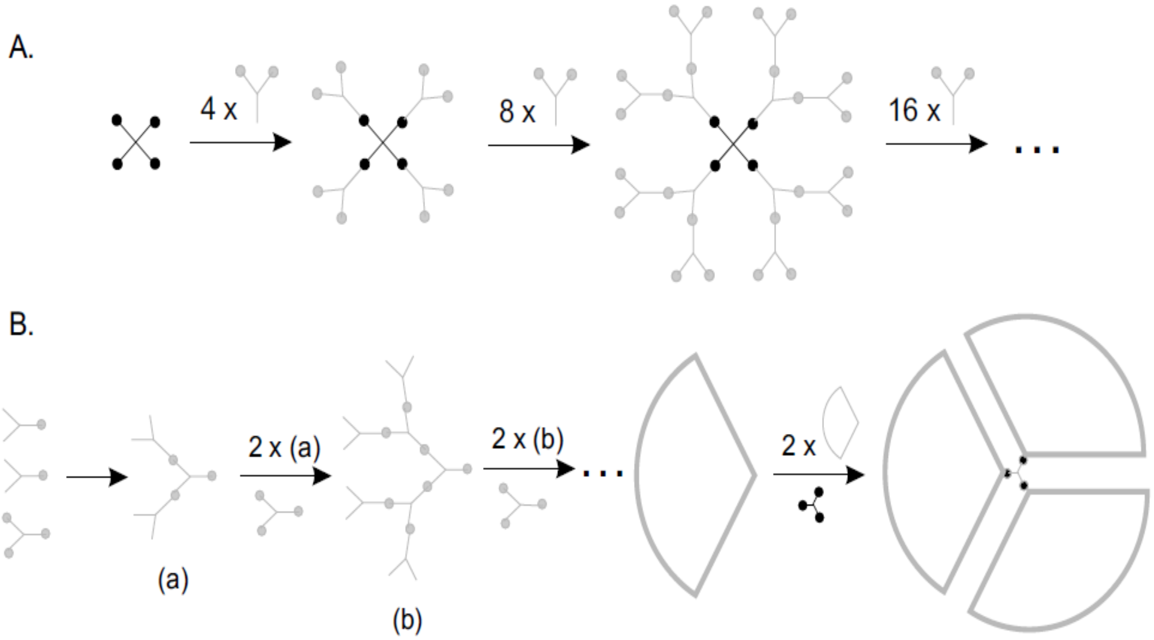

Figure 1.16 Two schemes for synthesis of dendrimers. A. The divergent growth method; B. The convergent growth method.

The first synthesised dendrimers were polyamidoamines (PAMAMs) (Alper, 1991) They are also known as starburst dendrimers. The term ‘starburst’ is a trademark of the Dow Chemicals Company.

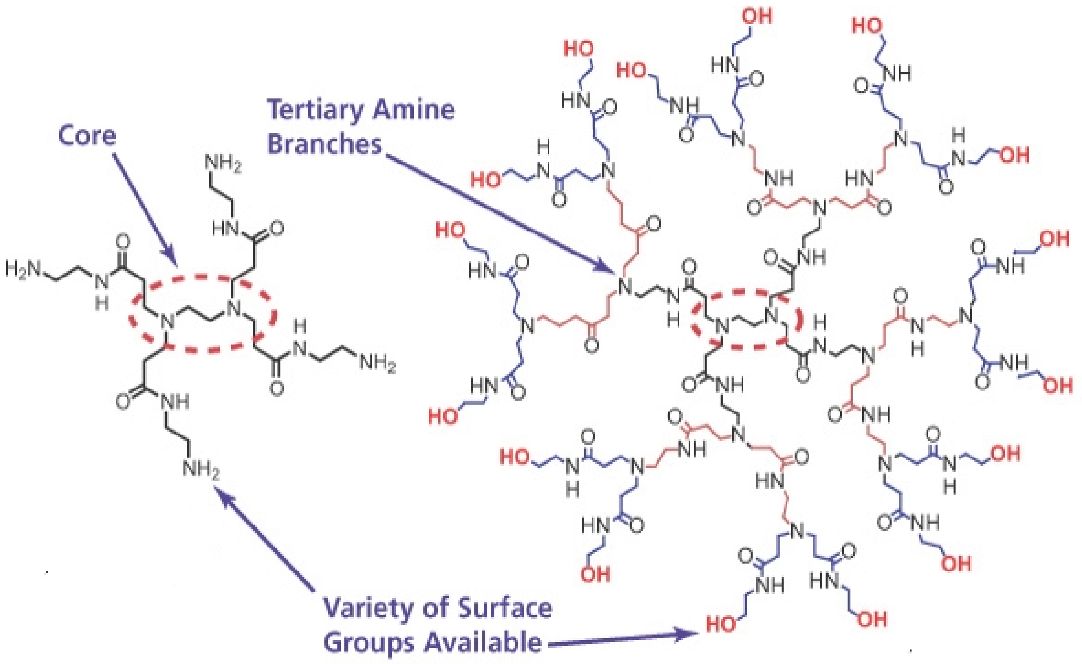

Figure 1.17 A structure of PAMAM dendrimer. Polyamidoamine (PAMAM) dendrimers are the most common class of dendrimers suitable for many materials science and biotechnology applications. PAMAM dendrimers consist of alkyl-diamine (2-carbon) core and tertiary amine branches (Image adapted from Sigma-Aldrich).

1.6.4 Properties of dendrimers

Dendrimers are monodisperse macromolecules, unlike linear polymers. The classical polymerization process which results in linear polymers is usually random in nature and produces molecules of different sizes, whereas size and molecular mass of dendrimers can be specifically controlled during synthesis. Because of their molecular architecture, dendrimers show some significantly improved physical and chemical properties when compared to traditional linear polymers. In solution, linear chains exist as flexible coils; in contrast, dendrimers form a tightly packed ball. Within the PAMAM dendrimer family, when they grow from generation 1–10 with 5 different core types and 10 functional surface groups (available by Sigma-Aldrich), the diameter of dendrimers with an ethylenediamine core increases from 1.1 to 12.4 nm (Svenson and Tomalia, 2005). Dendrimer solutions have significantly lower viscosity than linear polymers (Fréchet, 1994). The solubility of dendrimers is determined by the surface functional groups, dendrimer generation, repeated units, and even the core (Jorgensen and Nielson, 2010). The high density of functional groups (such as amine groups and carboxyl groups) on the surface of dendrimers may be expected to have potential applications in enhancing the solubility of hydrophobic drugs by electrostatic interaction. The presence of large numbers of functional groups on the surface of dendrimers makes them suitable for the covalent conjugation of numerous drugs with relevant functional group (Majoros et al., 2006).

In this work were studied the amiloidogenic properies of PAMAM (generation 4), PPI (generations 4 and 5) and fourth generation of cationic phosphorus-containing dendrimers (PCD). PCD are characterized by the presence in their backbone of aminothiophosphates at each branching point. PCD were selected following the study by **(Cortijo-Arellano, Ponce, Durany, and Cladera, 2008a)** The repetitive controlled divergent growth technique which forms the P-dendrimer backbone used these phosphorus atoms at each branching point. They have a hydrophilic surface and a hydrophobic backbone which allows very efficient membrane penetration (Loup et al., 1999).

The poly(amidoamine) (PAMAM) and PPI (polypropylene imine) dendrimers are commonly studied. Poly (amidoamine) dendrimers (PAMAM) are synthesized by the divergent method starting from ammonia or ethylenediamine initiator core reagents. Products up to generation 10 (a molecular weight of over 9,300,000 g/mol) have been obtained. PPI-dendrimers are oldest known dendrimer type developed initially by Vögtle (Giehm et al., 2008). PPI dendrimers are commercially available up to G5, and has found widespread applications in material science as well as in biology.

Currently, large amounts of pure PPI dendrimers are commercially available from Aldrich Chemical Co. and DSM.

An outstanding demonstration of the synthetic power of decorating the surface of dendrimers with “interesting” molecules comes, once again, by way of comparison of these nanodevices with proteins. Proteins, which have had the opportunity to evolve biocompatibility and systemic functions in multicellular organisms over hundreds of millions of years, have found it advantageous to decorate their surfaces with complex carbohydrates when they are displayed on the cell surface or secreted into the extracellular milieu. In the past few years, it has become clear that these sugars play many key roles in molecular recognition over short distances, such as interactions with the extracellular matrix and with neighbouring cells, as well providing system-wide communication (e.g., almost all protein hormones are glycosylated) (Kumar, 2007).

In this study PPI dendrimers decorated with maltose were used (Figure 1.18). When developing dendritic nanotools requiring bioactivity similar to that found in proteins, including the ability needed by a drug candidate to seek out and evoke responses at a specific but far-removed cell type in the body, it is wise to learn from nature and consider the inclusion of sugars to be an important design parameter.

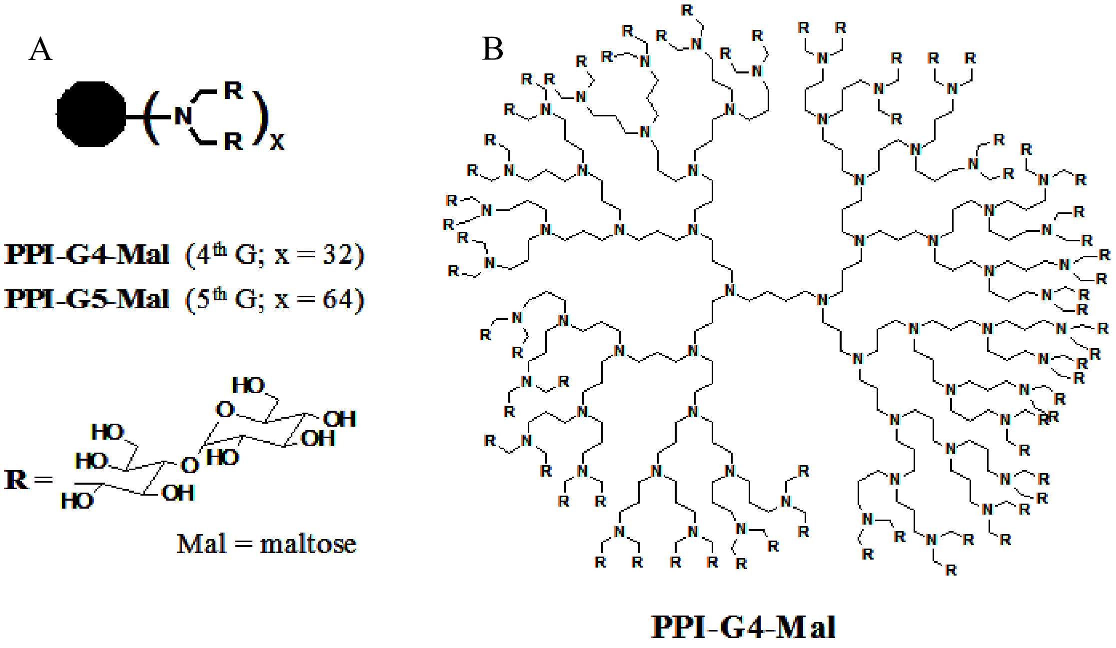

Figure 1.18 Schematic representation of structure of PPI-maltose dendrimers. (A) Idealized structure of 4th and 5th generation of PPI glycodendrimers used in the present study; (B) Chemical structure of PPI-G4 dendrimer This dendrimer starts from an ethylene diamine core with attached branches or arms. R is maltose molecule.

1.6.5 Applications

There are now more than fifty families of dendrimers, each with unique properties, since the surface, interior and core can be tailored to different sorts of applications. Many potential applications of dendrimers are based on their unparalleled molecular uniformity, multifunctional surface and presence of internal cavities. These specific properties make dendrimers suitable for a variety of high technology uses including biomedical and industrial applications of glycodendrimers

Generally, glycodendrimers possess highly potential perspective as drug-delivery system in (bio-)medical applications and in tailoring biological processes (Chabre and Roy, 2008). Previous studies have shown that dendrimers can be used as anti-amlyoid and anti-prion agents. In this context, glycodendrimers are also applicable as anti-prion agents (Klajnert et al., 2008).These facts motivated to use glycodendrimers as modulation agent in the fibrillation process of Aβ40 to exhibit a new application field of glycodendrimers.

Hypothesis

According to the amyloid cascade hypothesis amyloid peptides would play a central role in the onset and development of Alzheimer's disease. The toxicity of the peptide would strongly depend on the aggregation state of the peptide and peptide aggregation depends on several factors such as the presence of divalent metal cations. The interaction of the peptide divalent metal cations will affect the conformation of the peptidic aggregates and strongly influence their toxicity.

Nowadays, one of the main strategies in the design of strategies to fight against Alzheimer's disease is the discovery or synthesis of compounds that are either to block or to inhibit the toxic, aggregated forms of the amyloid peptides.

Aims of this thesis

Thus from first chapter it is clear that, although a great deal of progress has been made since 1985 when Aβ was first isolated, many important details are missing, and a great deal of controversy as to the role of Cu(II) and dendrimers remains. The five main aims of this thesis are outline below, but more detailed aims are within each of the two results chapters:

1. to investigate pH dependent structure and morphology of Aβ-Cu(II) aggregates.

2. to compare the fibril formation rates of Aβ in the presence and absence of Cu(II) and to establish the role of Cu(II) ions in Aβ aggregation.

3. to study the toxic effects of Aβ-Cu(II) complex.

4. to compare the fibril formation rates of Aβ in the presence and absence of dendrimers and to establish the role dendrimers in Aβ aggregation.

5. to study the toxic effects of Aβ in the presence of dendrimers to see if dendrimers enhance or reduce Aβ toxicity.

2 Materials and methods

2.1 REAGENTS

2.1.1 Chemicals

Fourth and fifth generation PPI dendrimers modified with a dense maltose shell (PPI-maltose) were prepared and characterized as described previously (Klajnert et al. 2008) and generously donated by Dr. D. Appelhans, Leibniz-Institut für Polymerforschung Dresden e.V

Copper(II) sulphate (99.9% CuSO4·5H2O) (Aldrich)
Dimethyl sulfoxide (DMSO, (CH3)2SO Sigma & Aldrich)
Deuterium Oxide (99.9% atom D min, D2O) (Merck)
Deuterium Chloride (99.9% atom D min, DCl) (Sigma & Aldrich)
Dulbecco modified Eagle's medium (Sigma)
Dulbecco modified Eagle's medium + Ham's F12 (Sigma)
Etanol (96%, C_2H_5OH) Merck
Glycine (H2NCH2COOH) (BDH)
HEPES (4-(2-Hydroxyethyl)piperazine-1-ethanesulfonic acid, N-(2-Hydroxyethyl)piperazine-N′-(2-ethanesulfonic acid)) (Sigma)
Horse Serum (Sigma)
Bovine Fetal Serum (Sigma)
Hydrochloric acid (Spectrosol, 11.6 M HCl) (Merck)
L-Glutamine (Gibco)
Methanol (99.93%, HPLC grade, CH3OH) (Merck)
MTT ((3-(4,5-Dimethylthiazol-2-yl)-2,5-diphenyltetrazolium bromide) (Sigma)
Nitrilotriacetic acid Sigma & Aldrich
Non essential aminoacids (Sigma)
Penicillin-Streptomycin Solution stabilized, with 10,000 units penicillin and 10 mg streptomycin/mL, sterile-filtered (Gibco)
Potassium Chloride (saturated solution, KCl) (Sigma-Aldrich)
Sodium hydroxide (Sigma)
Trypan Blue (Sigma)
Uranyl acetate (Sigma), obtained with kind permission from UAB Microscopy service;
Thioflavin T (Sigma-Aldrich Química SA (Madrid, Spain).
All chemicals were of analytical grade.

2.1.2 Other materials

Aβ28 [DAEFRHDSGYEVHHQKLVFFAEDVGSNKG] (JPT, Germany)
Aβ40 [DAEFRHDSGYEVHHQKLVFFAEDVGSNKGAIIGLMVGGVV] (JPT, Germany)

Poly(propylene imine) (PPI) dendrimers of fourth and fifth generation (SyMO-Chem (Eindhoven, Netherland).

Carbon coated 400 mesh copper grids (Fidelco)

2.1.3 Peptide preparation

Preparation of Aβ40 and Aβ28 stock solutions. 250 μM peptide was dissolved in HEPES buffer with 0.02% NH_3 at pH 11 and sonicated for 30 seconds. The stock solutions were kept at -80°C until used. The non-aggregated state of the peptide was checked by infrared spectroscopy as described in (Benseny-Cases et al., 2007). Peptide solution quality was controlled by FTIR, the infrared spectrum of Aβ40 showed an absorption peak centered at 1643 cm^{-1}, typical of unordered structures. The spectrum did not show any signs of peptide aggregation, which would result in an absorption band around 1620 $cm^{-}1$.

There are several different methods currently used for the solubilisation of Aβ. Chaotropic agents such as dimethylsulfoxide (DMSO) (Stine et al., 2003), organic acids such as trifluoroacetic acid (TFA) (Zagorski et al., 1999), organic cosolvents, usually trifluoroethanol (TFE) and hexafluoroisopropanol (HFIP) (Zagorski and Barrow, 1992) are common in the literature. Alternatively basic conditions, such as using sodium hydroxide (NaOH) to obtain a pH of 11 have also been shown to effectively solubilize Aβ40 and Aβ28.

A problem with using strong acids or organic solvents such as HFIP is that they can cause conformational changes that may influence fibrillogenesis. This adds to the variability that is already a major problem in fibril growth studies (Shen and Murphy, 1995). In addition the presence of these organic solvents or acids can be directly cytotoxic and thus interfere with toxicity studies, Using strongly basic conditions for solubilisation avoids these problems. An additional advantage of using high pH solubilisation conditions is that it avoids Aβ being near its isoelectric point. When Aβ is subsequently added to buffer at a neutral pH the solution passes through the isoelectric point (pI) of Aβ (pI 5.3), where the potential for Aβ aggregation and precipitation is maximised. This can result in highly variable kinetic behaviour and fibril morphologies (Wood et al., 1996). However, by using strongly basic conditions Aβ, aggregation can be avoided (Teplow 2006).

2.1.4 Buffer

The spectroscopic techniques used in this thesis have some influence on the choice of buffer. The studies presented here were typically performed in the 10 or 60 mM N-(2-Hydroxyethyl) piperazine-N'[2-ethanesulfonic acid]) (HEPES). HEPES was used also for its low affinity for Cu(II) (Sokolowska *et al.* 2005). Buffer was made to respective concentration in water.

2.1.5 pH measurements

The pH was adjusted using small amounts of 10-100 mM NaOH or HCl and measured using a benchtop pH-meter with an electrode with a 3 mm stem diameter and 55 mm in length to allow the pH of samples to be read whilst in 1 cm path length quartz cuvettes. For the fluorescence experiments the pH of the samples was determined before and after the experiment. The pH of most experiments was pH 7.4 to recreate physiological conditions as much as possible unless pH 11 Cu(II) binding condition.

2.1.6 Fibril growth conditions

2.1.6.1 Influences on fibril formation

Determining the mechanisms of fibril formation is crucial in understanding and perhaps controlling AD onset and progression. Formation of fibrils requires a considerable amount of organisation of Aβ monomers, and unfavourable forces that would destabilise Aβ fibrils must be compensated by forces that stabilise Aβ fibrils. There are a range of factors that can influence whether or not a protein will form fibrils, and how rapidly it will do so. Some of these factors have been optimised in the fibril growth studies described in this chapter, and so are discussed here in more detail.

The propensity of fibril formation to occur is based on a range of intrinsic and extrinsic factors. Intrinsic factors refer to properties of the peptide or protein itself which favour fibril formation, whereas extrinsic factors refer to external conditions such as pH, ionic strength, and protein concentration. These factors have been studied in some depth by various groups, and equations have been developed which can predict the aggregation rate of a protein.

2.1.6.2 Intrinsic factors

Hydrophobic interactions play an important role in folding and misfolding. Protein folding is thermodynamically driven to result in the most stable structure, and subsequently hydrophobic residues are clustered and buried, rather than on the protein surface. Replacement of nonpolar residues with polar residues results in inhibition of Aβ42 fibril formation and an increase in the peptide's solubility (Wurth et al., 2002). Additionally the study by Wurth et *al* showed that replacing non-polar residues with other non-polar residues had little or no effect, suggesting the hydrophobicity of residues is the most important factor in promoting fibril formation rather than specific amino acid interactions.

The NH and CO groups in the peptide backbone are thermodynamically more favourable in water compared to a non-polar environment, which causes conflict when they are next to hydrophobic side chains. To solve this thermodynamic mismatch, NH and CO groups form hydrogen bonds. Hydrogen bonds play a crucial part in influencing the propensity of proteins with β-sheet secondary structure to form fibrils. Rational design of peptides shows that β-sheet proteins favour intermolecular aggregation over intramolecular folding (Wang and Hecht, 2002). This is due to the difference in hydrogen bonding between the two different secondary structures. Whereas backbone hydrogen bonding in an α-helix can be mainly "satisfied" without needing to oligomerise, in β-strands the C=O and N-H groups form hydrogen bonds to N-H and C=O bonds on neighbouring strands.

Charge is also highly important in affecting the propensity for fibril formation. Two reasons why this could be are:

(1) Specific charge-charge interactions between imidizolium groups on histidine residues and the carboxylate groups on aspartate and glutamate could stabilise oligomers.

(2) Electrostatic repulsion: when the protein has a net positive or negative charge it is less likely to dimerise.

Experimental evidence suggests that electrostatic repulsion is more influential than specific charge-charge interactions. Fraser *et al* showed that substituting amino acids with opposite charges, e.g. histidine to aspartate, did not prevent fibril formation (Fraser et al., 1994), suggesting a loss of specificity will not prevent fibril formation.

2.1.6.3 Extrinsic factors

The influence of pH on fibril formation is closely linked to the importance of charge, as the external pH approaches a protein's pI, i.e. a net charge of 0, electrostatic repulsion will decrease and aggregation will increase. Salt can also affect fibril formation: as salt concentration increases, protein solubility decreases (salting out). This is due to increasing additions of salt reducing the number of water molecules available to the hydrophilic residues on the surface of the protein, causing protein-protein interactions to become stronger than solvent-protein interactions. Additionally salt ions can shield the ionic charges of the protein, reducing electrostatic repulsion. These two effects will increase protein self-association and the likelihood of fibril formation or protein aggregation. This is supported by fibril growth studies where monomer oligomerisation was found to be highly dependent on ionic strength (Johansson et al., 2006) and protofibril association required salt to minimise electrostatic repulsion between the two axial sides of the fibrils and allow lateral association to take place (Nichols et al., 2002; Lin et al., 2008). DuBay *et al* found that the accuracy of the fibril growth rate predictions from their equation improved when ionic strength was included (DuBay et al., 2004).

In addition to controlling the salt concentration, temperature and agitation are often manipulated in fibril growth experiments. Specific stages of Aβ fibril formation are highly temperature dependent. Raised temperatures shorten the lag phase and accelerate nucleation, but do not affect the elongation stage of fibril formation (Lin et al., 2008). Agitation is performed widely in the literature to aid formation of fibrils. Lee *et al* found an increase in fibril formation in the presence of agitation by a factor of 2-4 (Lee et al., 2007).

DuBay *et al* found that the rate of fibril formation increased with peptide concentration (DuBay et al., 2004). A higher protein concentration increases the likelihood of protein association. This could affect nucleus formation and also elongation. However a high protein concentration may favour aggregation over fibril formation. The concentration dependent nature of fibril formation can be likened to the crystallization of proteins, in which overly precipitative conditions for self-association will cause amorphous aggregates rather than ordered crystals to form. This fine line between fibril formation and aggregation may explain why some studies found no effect on fibril formation with increased protein concentration (Johansson et al., 2006).

Disagreements over which factors are more important in aiding or hindering fibril formation are common; this is especially true for metal ions. Studies showed more than a decade ago that Zn(II) and Cu(II) ions cause aggregation of Aβ (Atwood, et al. 1998, Bush, et al. 1994). However, further investigations suggested that Zn(II)and Cu(II) promote amorphous aggregation of Aβ and actually inhibit fibre formation and cell toxicity (Raman, et al. 2005, Yoshiike, et al. 2001). In this study, temperature, agitation, salt concentration, pH, metal and peptide concentration are all optimised and manipulated to promote fibril formation and minimise aggregation.

The solubilized peptide was unfrozen, diluted to the correct concentration and used immediately. A range of buffers were used, depending on the spectroscopic technique. Fibre growth kinetics are very sensitive to a number of factors that must be carefully controlled. They include the pH, concentration, agitation, temperature and ionic strength. Fibre growth experiments were typically with 25 μM Aβ(1-40) and the peptide was incubated at 37°C in 60 mM HEPES buffer with a gentle agitation using the same type of stirrers. This temperature, optimized agitation and buffer concentration allowed reproducible fibril formation growth curves, with a lag phase and a high concentration of fibrils at the end of incubation (as determined by ThT fluorescence).

Small adjustments were made with 10 mM NaOH or HCl to the stock Aβ solutions. The pH, a critical parameter in fibre growth rates, was measured before and after each fibre growth experiment; variations were ±0.05 pH units or less over the course of the experiment. Metal stock solutions were $CuSO_4$ 25 mM. The Thioflavin T (ThT) stock was dissolved in water to 5 mM, and kept foil wrapped and at 5°C. Then a small volume of ThT was added to the experimental sample to give final concentration in the fluorescence cuvette 35 µM.

For experiments in the presence of metal, a 5 mM stock CuSO4 solution was prepared in water and an aliquot was added to the peptide solutions. Metal-peptide ratio was 1 to 1.

2.2 EXPERIMENTAL METHODS

2.2.1 Spectroscopy techniques

2.2.1.1 Fluorescence spectroscopy

In the experiments described in this thesis, light in the UV has been used. In this region, the wavelength, λ, is the most common quantity used to represent the light energy.

Light is dualistic in nature. It can be described as an electromagnetic wave or as a package or quantum of energy - a photon. The aspects are equally valid and often one or the other is chosen to describe a specific phenomenon. The electromagnetic spectrum ranges from radio waves through infrared and visible light to X-rays and gamma radiation. The wavelength, λ, or the frequency, ν, are used to describe the radiation when the wave nature is considered, and the energy, E, is used when light is regarded as a stream of photons. These quantities are easily connected by the speed of light, *c*, and the Planck constant, *h*

$$E = h \cdot \nu = h \cdot \frac{c}{\lambda} \ [\mathrm{J}] \qquad c = \lambda \cdot \nu \ [\mathrm{m/s}]$$

During the 20th century, the theories of atomic physics and quantum mechanics were developed by Bohr, Schrödinger and others. These theories are fully capable of describing energy levels and transitions in atoms and molecules, but only the fundamentals are required for the understanding of this thesis. Quantum mechanics and atomic physics have continued to develop and for a more detailed description, the reader is referred to textbooks, e.g. (Haken and Wolf 2000; Friedrich 2006).

The hydrogen atom with one electron circulating around the charged nucleus is the simplest atomic system. According to the Pauli exclusion principle, there cannot be more than two electrons occupying any state, one with electronic spin up and one with spin down. When atoms bond together to form molecules, the total energy is lower than the sum of energy of the constituents. The description of energy levels becomes more complicated than for atoms, since energy states due to vibration and rotation motion are added. In Fig.2.1, the schematic picture of electronic levels and the addition of vibration and rotation levels is shown.

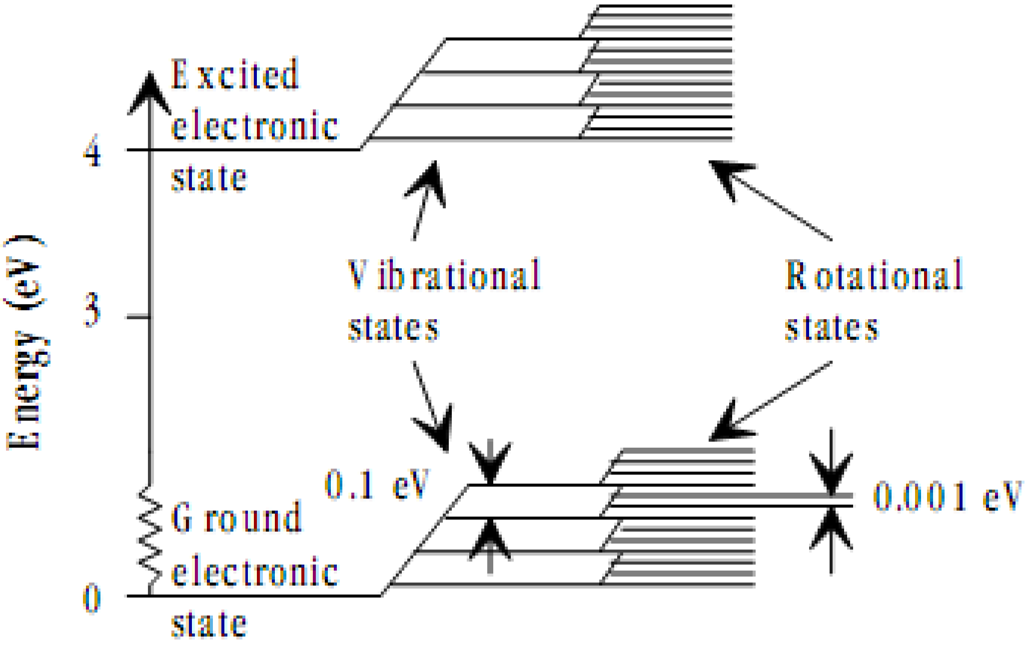

Figure 2.1 **Energy states in a molecule**. Electrons in atoms and molecules can change (make *transitions*) energy levels by emitting or absorbing a photon (of electromagnetic radiation) whose energy must be exactly equal to the energy difference between the two levels. Electrons can also be completely removed from a chemical species such as an atom, molecule, or ion. Complete removal of an electron from an atom can be a form of ionization, which is effectively moving the electron out to an orbital with an infinite principal quantum number, in effect so far away so as to have practically no more effect on the remaining atom (ion) Modified from (Lakowicz, 2006)

The configuration of the energy levels of a molecule determines many of the properties of that molecule. For instance, the energy separation between the electronic states determines the visible wavelengths that can be absorbed and thus the colour of the molecule. The transitions between the levels are the origin of many interesting phenomena like laser action, phosphorescence and fluorescence. Due to interaction with other molecules, the once excited electron is transferred to the lowest lying vibrational and rotational state within the excited state. When the molecule returns to any of the levels in the ground state, fluorescence light can be emitted.

The wavelength of the fluorescence will always be longer than the excitation light. Fluorescence light in solids and liquids is broad-banded due to the strong interaction between molecules and due to the large number of vibration and rotation levels. The excited molecule can also return non-radiatively through collisions and internal conversion. Together with inter-system crossing, these possibilities compete with fluorescence emission.

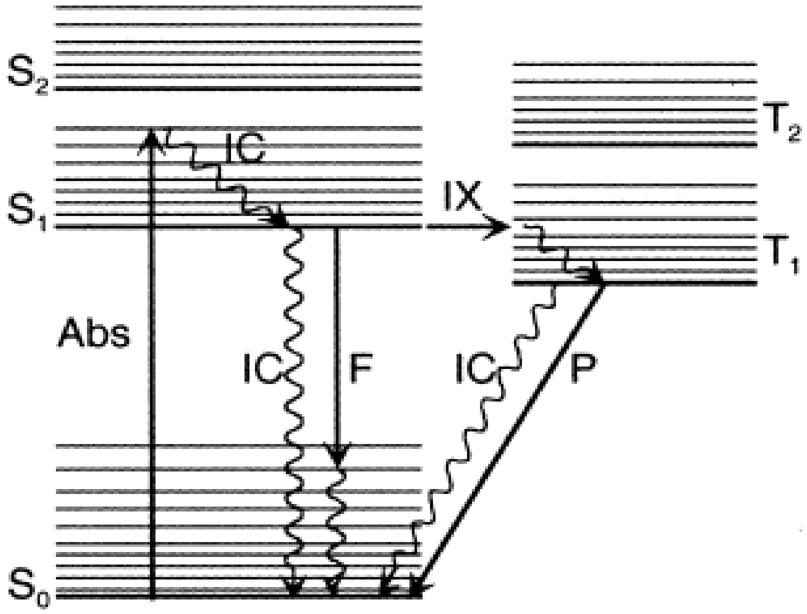

Figure 2.2. **Jablonski diagram** The diagram showing the absorption of a photon and some of the possible relaxation processes. S, T energy levels, IC, internal conversion; F, fluorescence; IX, intersystemcrossing; P, phosphorescence. Taken from(Lakowicz, 2006)

2.2.1.2 Fluorescence spectroscopy technique

The theory of fluorescence is briefly described below. For further details on the technique there are a number of good textbooks, e.g. (Lakowicz, 2006).

Fluorescence spectroscopy is one of the most powerful methods to study protein folding, dynamics, assembly, and interactions, as well as membrane structure. It has been successfully applied to investigate the complex mechanisms of protein aggregation including amyloid fibril formation and the interaction of amyloidogenic proteins with membranes, as well as their dynamic structures. The power of fluorescence spectroscopy lies in its broad applicability. Almost all proteins have natural fluorophores, tyrosine and tryptophan residues, which allow study of changes in protein conformation. Fluorescence spectroscopy requires a small amount of material and has a high signal-to-noise ratio. It is a convenient method to study fast protein conformational changes because the fluorescence emission lifetime is in the nanosecond range,which is relatively fast compared to most conformational transitions. It is also used in kinetics studies.

The time an average electron stays in a specific energy level is called the lifetime. Consequently, return to the ground state is spin-allowed and occurs rapidly by emission of a photon. The emission rates of fluorescence are typically 10^8 s^{-1}, so that a typical fluorescence lifetime is near 10 ns. The lifetime (t) of a fluorophore is the average time between its excitation and its return to the ground state. It is valuable to consider a 1-ns lifetime within the context of the speed of light. Light travels 30 cm in one nanosecond. Many fluorophores display subnanosecond lifetimes. Because of the short timescale of fluorescence, measurement of the time-resolved emission requires sophisticated optics and electronics. In spite of the experimental difficulties, time-resolved fluorescence is widely practiced because of the increased information available from the data, as compared with stationary or steady-state measurements. Phosphorescence is emission of light from triplet excited states, in which the electron in the excited orbital has the same spin orientation as the ground-state electron. Transitions to the ground state are forbidden and the emission rates are slow (10^3-10^0 s^{-1}), so that phosphorescence lifetimes are typically milliseconds to seconds. Even longer lifetimes are possible, as is seen from "glow-in-the-dark" toys: following exposures to light, the phosphorescent substances glow for several minutes while the excited phosphors slowly return to the ground state. Phosphorescence is usually not seen in fluid solutions at room temperature. This is because there exist many deactivation processes which compete with emission, such as nonradiative decay and quenching processes.

Fluorescence typically occurs from aromatic molecules. One widely encountered fluorophore is quinine, which is present in tonic water. If one observes a glass of tonic water which is exposed to sunlight, a faint blue glow is frequently visible at the surface. This glow is most apparent when the glass is observed at a right angle relative to the direction of the sunlight and when the dielectric constant is decreased by adding less polar solvents like alcohols. The quinine present in the tonic is excited by the ultraviolet (UV) light from the sun. Upon return to the ground state, the quinine emits blue light with a wavelength near 450 nm. The first observation of fluorescence from a quinine solution in sunlight was reported by Sir John Frederick William Herschel in 1845.

2.2.1.3 Fluorescence emission

A photon of energy $h\nu_{EM}$ is emitted, returning the fluorophore to its ground state S_0. Due to energy dissipation during the excited-state lifetime, the energy of this photon is lower, and therefore of longer wavelength, than the excitation photon $h\nu_{EX}$. The difference in energy or wavelength represented by ($h\nu_{EX} - h\nu_{EM}$) is called the Stokes shift. The Stokes shift is fundamental to the sensitivity of fluorescence techniques because it allows emission photons to be detected against a low background, isolated from excitation photons. In contrast, absorption spectrophotometry requires measurement of transmitted light relative to high incident light levels at the same wavelength (Figure 2.3)

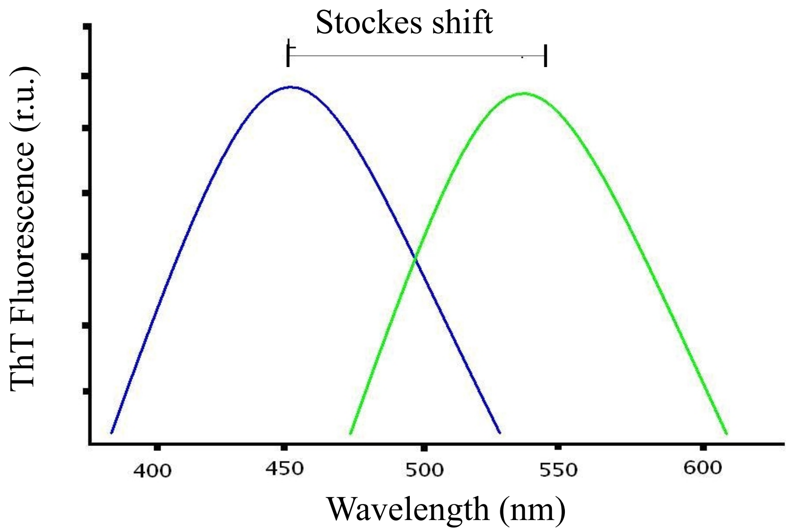

Figure 2.3 An idealized chart demonstrating the concepts of fluorescence excitation and emission spectra, as well as the Stokes shift. Stokes shift is the difference (in wavelength or frequency units) between positions of the band maxima of the absorption and emission spectrum (fluorescence) of the same electronic transition. Blue line: excitation spectrum, green: emission spectrum.

The entire fluorescence process is cyclical. Unless the fluorophore is irreversibly destroyed in the excited state (an important phenomenon known as photobleaching, see below), the same fluorophore can be repeatedly excited and detected. The fact that a single fluorophore can generate many thousands of detectable photons is fundamental to the high sensitivity of fluorescence detection techniques. For polyatomic molecules in solution, the discrete electronic transitions represented by $h\nu_{\mathrm{EX}}$ and $h\nu_{\mathrm{EM}}$ in Figure 2.2 are replaced by rather broad energy spectra called the fluorescence excitation spectrum and fluorescence emission spectrum. The bandwidths of these spectra are parameters of particular importance for applications in which two or more different fluorophores are simultaneously detected. The fluorescence excitation spectrum of a single fluorophore species in dilute solution is usually identical to its absorption spectrum. The absorption spectrum can therefore be used as a surrogate excitation spectrum data set. Under the same conditions, the fluorescence emission spectrum is independent of the excitation wavelength, due to the partial dissipation of excitation energy during the excited-state lifetime, as illustrated in Figure 2.2. The emission intensity is proportional to the amplitude of the fluorescence excitation spectrum at the excitation wavelength. Fluorescence intensity is measured in relative units (r.u.).

2.2.1.4 Intrinsic fluorophores

The second application for fluorescence spectroscopy was monitoring the intrinsic fluorescence of the tyrosine residue. Tryptophan (Trp) and tyrosine (Tyr) residues are naturally occurring fluorophores in proteins. Trp has the highest quantum yield and its emission maximum is sensitive to the polarity of its environment; consequently, Trp is a commonly used intrinsic fluorescent probe in studying protein folding and dynamics. The λ_{max} of a buried Trp is around 335 nm, whereas fully solvent accessible Trp has λ_{max} around 355 nm. Trp fluorescence lifetime measurements can overcome the limitations of steady-state measurements by allowing determination of the different lifetimes or anisotropy of different residues. Usually, the exponential decay does not follow a single exponent, indicating the existence of several different excited states of the fluorophore (Ragone et al., 1984). Tyr has significantly lower quantum yield than Trp and is usually only used as an intrinsic fluorescent probe in Trp-lacking proteins (as Aβ40), since energy transfer to Trp residues usually quenches the Tyr fluorescence. The Tyr emission maximum is near 305 nm and is not sensitive to the polarity of environment; however, Tyr emission depends on pH. The phenolic hydroxyl group has a pKa near 10 and at high pH is deprotonated. The deprotonation results in the formation of tyrosinate, which has a red-shifted emission spectrum (λ_{max} =340 nm). Phenylalanine (Phe) has a very low quantum yield, and is usually not used as a fluorescent probe. The close proximity of Phe to Tyr or Trp, and Tyr to Trp, can influence the quantum yield of Trp and Tyr through energy transfer. The emission spectra of proteins are sensitive to binding of substrates, protein-protein interactions and denaturation and changes in intrinsic fluorescence can be used to study structural changes (Lakowicz, 2006). Monitoring intrinsic Tyr fluorescence during fibril formation revealed changes in the shape and intensity of the Tyr emission spectrum. The decrease in tyrosine intensity parallels the assembly of Aβ40 into fibrils, due to formation of β-sheet which leads to the changing of neighborhood surrounding of Tyr10 which could act as proton acceptors and lead to quenching of tyrosine fluorescence (Munishkina and Fink, 2007).

2.2.1.5 Extrinsic fluorophores

Thioflavin T (4-(3,6-dimethylbenzothiazol-2-yl)-N,N-dimethyl-aniline, ThT), shown in Figure 2.4, is commonly used non-covalent extrinsic fluorescent probe in studies of protein folding and amyloid fibril formation. ThT is used as a specific probe for the presence of amyloid fibrils. It has a two-ring structure: the conjugated benzothiazol and aminobenzol rings are arranged in an almost planar orientation (ϕ∼30°) in the minimum energy conformation (Figure 2.4). During excitation, the rings rotate in order to obtain the most stable exited state conformation (ϕ∼90°), which has low fluorescence efficiency. Polar solvents and viscosity can affect the reorientation of the rings and as a result the ThT fluorescence. The binding to amyloid fibrils probably stabilizes the planar form of the molecule and leads to a 10–500-fold increase in ThT fluorescence intensity. It is tempting to speculate that ThT may bind between the beta- sheets of the fibril, however, no experimental data exist to support this assumption. Puzzlingly, ThT has two excitation (∼335 nm and ∼430 nm) and two corresponding emission peaks (∼425–455 nm and 483 nm): an increase of ThT concentration results in a red shift of the λ_{max} from 425 nm to 455 nm. Excitation at ~350 nm results in emission at ~438 nm, whereas excitation at ~440 nm leads to emission at 483 nm. Binding to amyloid fibrils induces a blue shift of the ThT λ_{max} from 483 nm to 478 nm. The excitation spectra show that only the peak around 430 nm increases upon ThT binding to fibrils. (Munishkina and Fink, 2007).

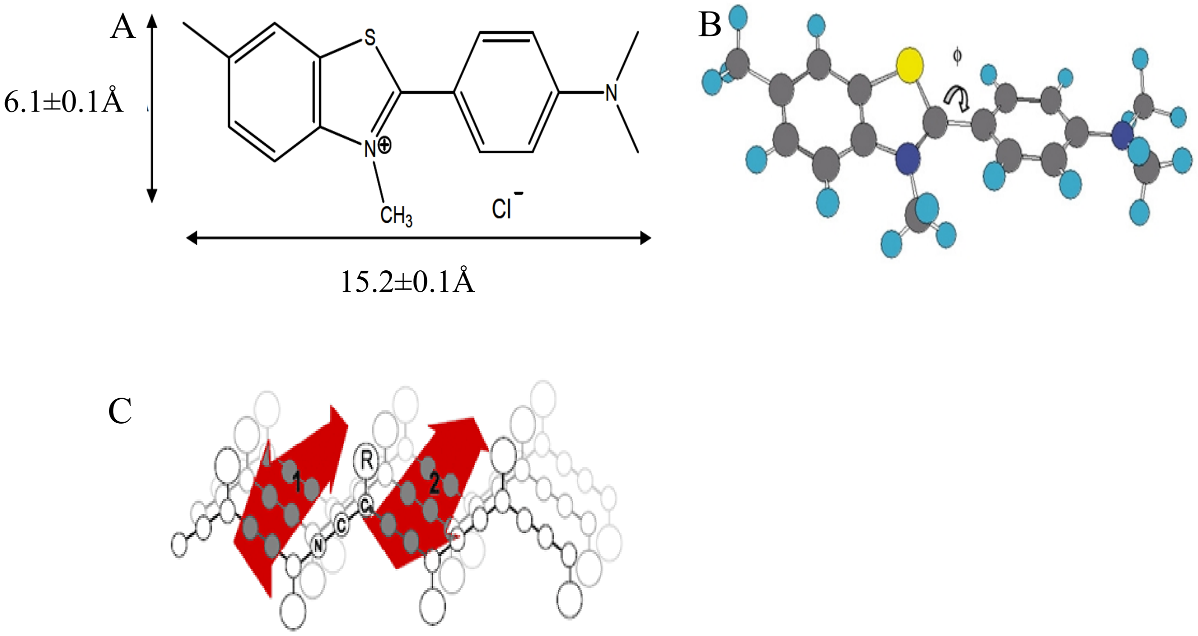

Figure 2.4 Thioflavin-T and diagram of a β-sheet. (A) Chemical structure of thioflavin-T. (B) Ball-and-stick model of ThT. The rotational angle is around 30 °. Carbons are dark grey, hydrogens are cyan, nitrogens are blue, and sulfur is yellow. (C) Dye interaction with the quaternary structure of a protein aggregate. Adjacent cross-strand side-chain ladders of a self-assembled antiparallel β-sheet of the protein aggregate is depicted. The sheet backbone is highlighted as N and C residues flanking the α-carbon. Side chains are indicated by the letter R within a circle. Binding to this common structural motif, present in aggregated protein, restricts dye rotation around the central carbon-carbon single bond separating the different aromatic portions of the molecule. Two possible dye binding orientation are depicted as red arrows in the diagram, though binding at atomic level resolution has yet to be fully delineated (ProteoStat®)

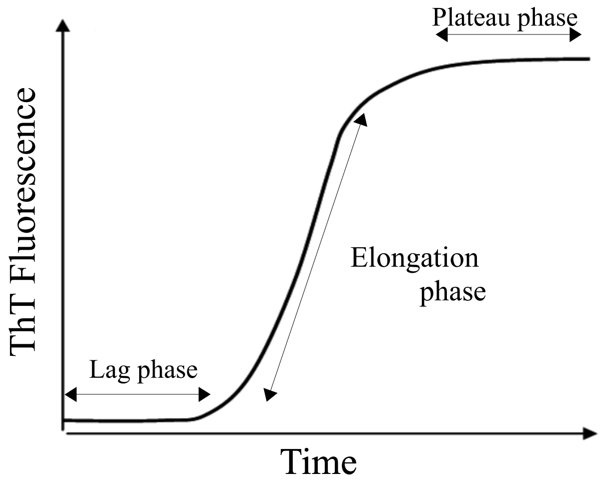

Figure 2.5 Fibril growth curves. A typical fibril growth curve, monitored by ThT fluorescence, with a lag phase and elongation phase and plateu of ThT fluorescence where the final fibrillar concentration (as measured by the ThT signal) does not change with time.

Today, measuring the characteristic ThT fluorescence at certain time points is probably the most widely used approach to follow fibril formation kinetics. For a nucleation dependent growth, a sigmoidal increase of the dyes fluorescence intensity is usually observed (Figure 2.5). Strategies imaging the fibril growth directly by total internal reflection microscopy have also been reported.

Currently there are no specific tools to distinguish oligomers that are direct precursors of fibrils, from oligomers that are off the fibril formation pathway. The formation of protofilaments and their assembly into mature fibril is also poorly understood, because we do not have specific markers that detect only protofilaments or only fibrils. A certain drawback using the ThT staining technique also has to be taken into account because of their aromatic and hydrophobic character. Dyes like ThT and Congo Red tend to form aggregates. These aggregates may nucleate the amyloid association process. Monitoring the time course of fibril formation, therefore, requires the preparation of individual dye containing samples at every time point. Thus, the application of ThT staining assays on a huge scale is highly restricted in terms of sample consumption.

2.2.1.6 Quenching

Fluorescence quenching can be dynamic or static. If the distance between the excited fluorophore and a quencher is fixed, the quenching is static. Dynamic (collisional) quenching depends on diffusion. The commonly used quenchers are iodine, oxygen, and acrylamide. Measuring the fluorophore accessibility to quenching by various types of quenchers allows estimation of the relative position of fluorophore in the protein or membrane. The quenching analysis employs the dependence of the fluorescence intensity on the concentration of a quencher. Dynamic quenching follows a linear concentration dependence, whereas static quenching deviates from linear dependence. Cu(II) is a well known quencher of fluorescence. The probable method of quenching is by the donation of an electron from the fluorophore (in this case tyrosine 10) to the quencher Cu(II). The quenching results from the formation of a nonfluorescent complex between the tyrosine and Cu(II). When this complex absorbs light, it returns to the ground state without emission of a photon (Figure 2.6).

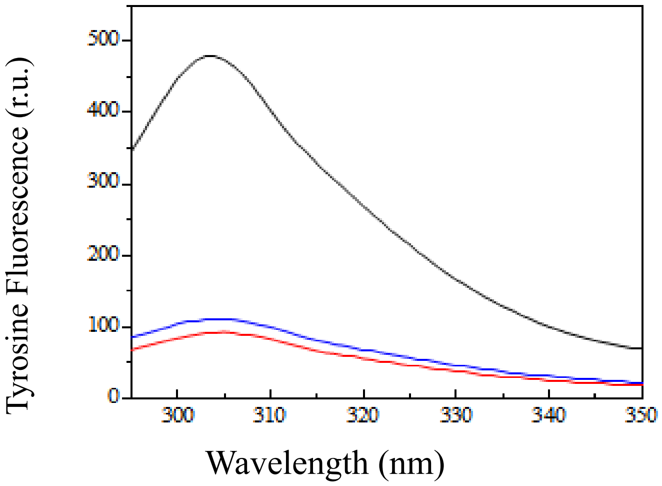

Figure 2.6 **Quenching of the tyrosine fluorescence of Cu(II).** Black curve: Tyrosine 10 spectra of Aβ40 were recorded in the absence of Cu(II). Red curve: Tyr10 spectra of Aβ40-Cu(II).

2.2.1.7 Instrumentation for fluorescence spectroscopy

For one cells experiments, the light from an excitation source passes through a filter or monochromator, and strikes the sample. A portion of the incident light is absorbed by the sample, and some of the molecules in the sample fluoresce. The fluorescence light is emitted in all directions. Some of this fluorescence light passes through a second filter or monochromator and reaches a detector, which is usually placed at 90° to the incident light beam to minimize the risk of transmitted or reflected incident light reaching the detector resulting in a fluorescence spectrum. No monochromator is perfect and it will transmit some stray light, that is, light with other wavelengths than the targeted. An ideal monochromator would only transmit light in the specified range and have a high wavelength-independent transmission. When measuring at a 90 angle, only the light scattered by the sample causes stray light. This results in a better signal-to-noise ratio Figure 2.7).

Fluorescent methods have three significant advantages over absorption spectroscopy. First, two wavelengths are used in fluorimetry, but only one in absorption spectroscopy. Emitted light from each fluorescent colour can be easily separated because each colour has unique and narrow excitation spectra. This selectivity can be further enhanced by narrowing the slit width of the emission monochromator so that only emitted light within a narrow spectral range is measured. Multiple fluorescent colours within a single sample can be quantified by sequential measurement of emitted intensity using a set of excitation and emission wavelength pairs specific for each colour.

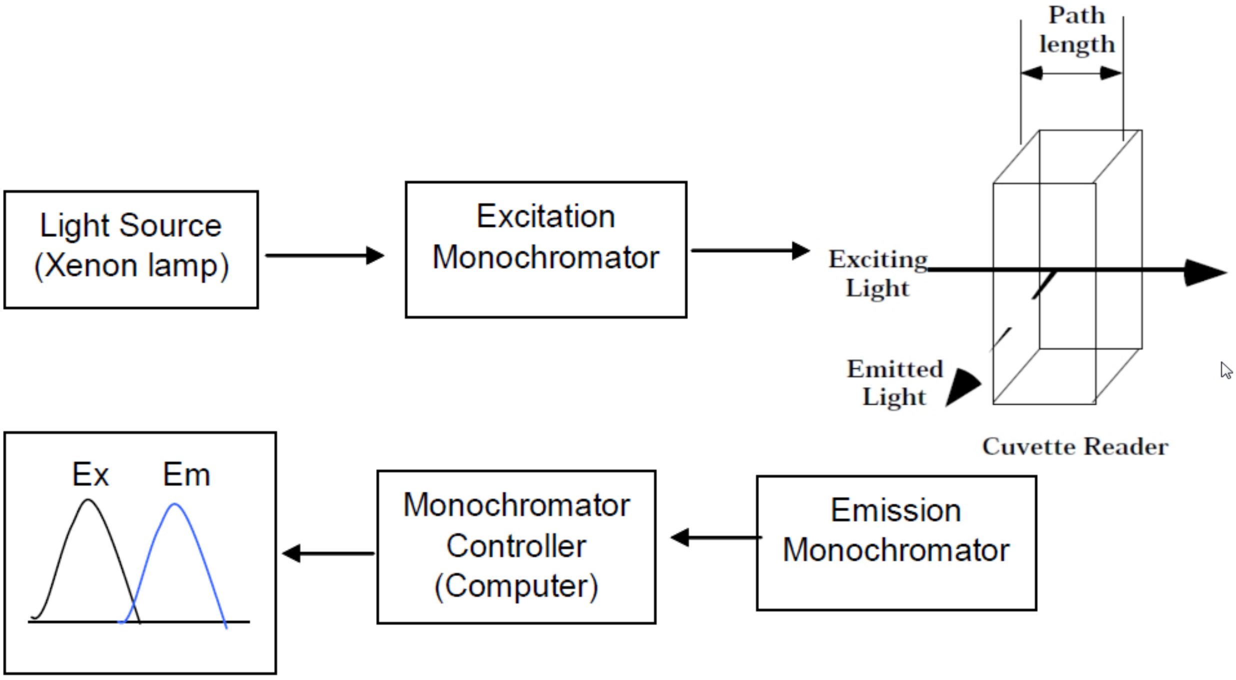

Figure 2.7 **Measuring of fluorescence.** Simplified scheme for a single sample holder spectrofluorometer (adapted from (Lakowicz, 2006). The cuvette reader excites the sample over the entire path length and reads the emitted light at right angles. The fluorescence was measured at a 90° angle relative to the excitation light

The second advantage of fluorescence over absorption spectroscopy is high signal to noise, since emitted light is read at right angles to the exciting light. For absorption spectrophotometry, the excitation source, sample and transmitted light are configured in line, so that the absorption signal is the small difference between the exciting light and the transmitted light, both of which are quite intense. The third advantage is that fluorescent methods have a greater range of linearity. Because of these differences, the sensitivity of fluorescence is approximately 1,000 times greater than absorption spectrophotometric methods.

A major disadvantage of fluorescence is the sensitivity of fluorescence intensity to fluctuations in pH and temperature. However, pH effects can be eliminated by using nonaqueous solvents, and normal room temperature fluctuations do not significantly affect the fluorescence intensities of commercial dye solutions. (Guilbault, 1973).

2.2.1.8 Preparation of sample

Fluorescence is a very sensitive technique. All fluorophores are subject to intensity variations as a function of temperature. Fluorescence variations due to pH changes are caused by the different ionizable chemical species formed by these changes. The results from these pH variations can be quite drastic since new ionization forms of the compound are produced. However, it is extremely susceptible to interference by contamination of trace levels of organic chemicals.

Potential sources of contamination are ubiquitous since any aromatic organic compound can be a possible source of fluorescence signal.

For experiments described in this thesis Thioflavin T (ThT) stock solutions, 8 mM, were prepared in 60 mM HEPES buffer and filtered through a 0.45 μm syringe driven filter unit (Millipore).

For fluorescence experiments, the solubilised peptide was diluted to 25 μM in the HEPES buffer. Cu(II) was added at different phases of fibril formation. Fibril growth was monitored using a PTI fluorimeter and FTIR spectrometer. For Thioflavin T (ThT) dye binding assay excitation and emission wavelengths were set at 450 and 490 nm, respectively. For Tyrosine fluorescence assays no ThT in the fluorescence cuvette was added. Excitation and emission wavelengths were set at 286 and 305 nm, respectively. The aggregation process was initiated by adding an aliquot of the peptide stock solution at pH 11 into the fluorescence cuvette containing 60 mM HEPES buffer at pH 7.2, in order to achieve a final peptide concentration of 25 μM and a final pH of 7.4. The fibril grow was monitored during at least 24 hours till the plateu of ThT florescence. When required, dendrimers were added into the cuvette before peptide addition. Fluorescence intensity of the ThT bound Aβ40 peptide, in the absence and in the presence of Cu(II) or dendrimers, was monitored over time at least 24 hours and that period was more than enough to reach a certain ThT fluorescence plateau. (Benseny-Cases et al., 2007; Cortijo-Arellano, Ponce, Durany, and Cladera, 2008a). For each experiment at least three independent measurements were done.

2.2.2 Fourier transform infrared spectroscopy

Infrared (IR) spectroscopy is one of the oldest and well established experimental techniques for the analysis of secondary structure of polypeptides and proteins (Stuart, 2004). Infrared spectroscopy has proven to be a powerful tool for studying biological molecules and the applications of this technique to biological problems is continually expanding, particularly with the advent of Fourier-transform infrared (FT-IR) spectroscopy in recent decades.

IR technique is based on the vibrations of the atoms of a molecule (Barth and Zscherp, 2002). This is a measurement of wavelength and intensity of the absorption of IR radiation by a sample. An IR spectrum is obtained by passing infrared radiation through a sample and determining what fraction of the incident radiation is absorbed at a particularly energy. The energy at which any peak in an absorption spectrum appears corresponds to the frequency of a vibration of a part of the sample molecule. This a chemical analytical technique, which measures the infrared intensity versus wavenumber $\nu = 1/\lambda$ where λ is the wavelength of light. Based upon the wavenumber, infrared light can be categorized as far infrared (4-400cm^{-1}), mid infrared (400-4,000cm^{-1}) and near infrared (4,000-14,000cm^{-1}) shown in Figure 2.8.

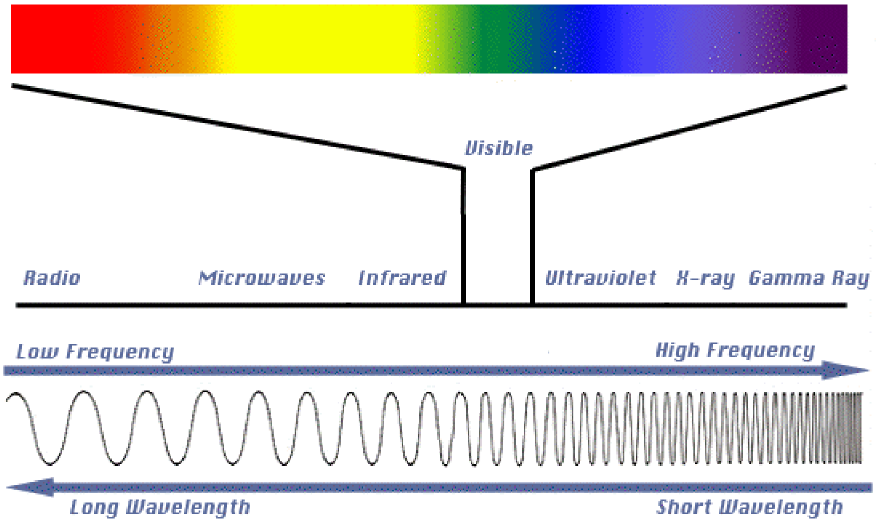

Figure 2.8 **Electromagnetic radiation spectrum**. The light our eyes see is a small part of a broad spectrum of electromagnetic radiation. On the immediate high energy side of the visible spectrum lies the ultraviolet, and on the low energy side is the infrared.

The IR spectral data of high polymers are usually interpreted in terms of the vibrations of a structural repeat unit (a chemical functional group) in a sample.(Elliott and Ambrose 1950; Krimm and Bandekar 1986). When an infrared light interacts with the matter, chemical bonds will stretch, contract and bend. As a result, a chemical functional group tends to adsorb infrared radiation in a specific wavenumber range regardless of the structure of the rest of the molecule. Photon energies associated with this part of the infrared (from 1 to 15 kcal/mole) are not large enough to excite electrons, but may induce vibrational excitation of covalently bonded atoms and groups. The covalent bonds in molecules are not rigid sticks or rods, but are more like stiff springs that can be stretched and bent. In addition to the facile rotation of groups about single bonds, molecules experience a wide variety of vibrational motions, characteristic of their component atoms. Consequently, virtually all organic compounds will absorb infrared radiation that corresponds in energy to these vibrations. Infrared spectrometers permit to obtain absorption spectra of compounds that are a unique reflection of their molecular structure.

A molecule composed of n-atoms has 3n degrees of freedom, six of which are translations and rotations of the molecule itself. This leaves 3n-6 degrees of vibrational freedom (3n-5 if the molecule is linear). Vibrational modes are often given descriptive names, such as stretching, bending, scissoring, rocking and twisting (Figure 2.9).

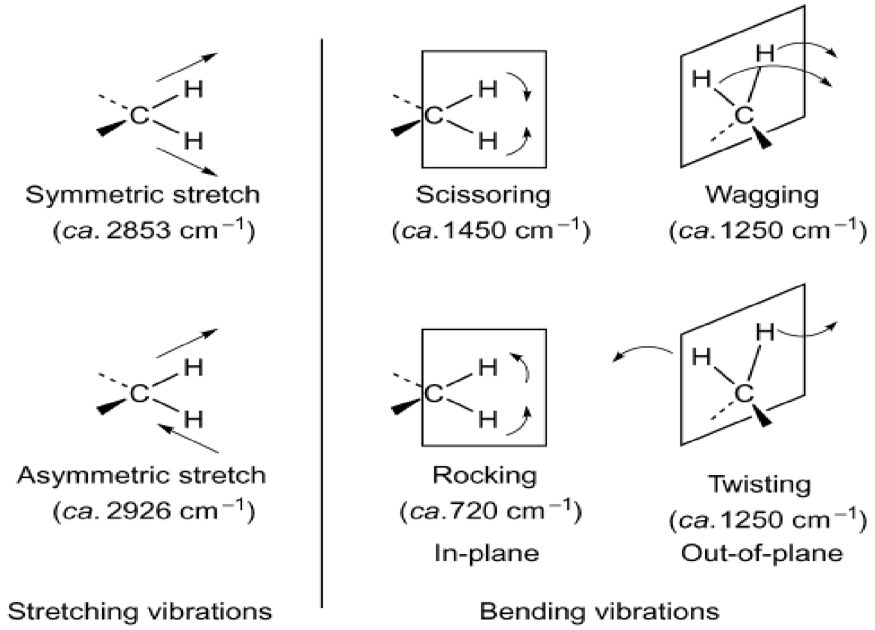

Figure 2.9 **Six different vibrational normal modes.**

The four-atom molecule of formaldehyde $H_2C{=}O$, the gas phase spectrum of which is shown below, provides an example of these terms. There are six fundamental vibrations (3*3-6), and these have been assigned to the spectrum absorptions (Figure 2.10).

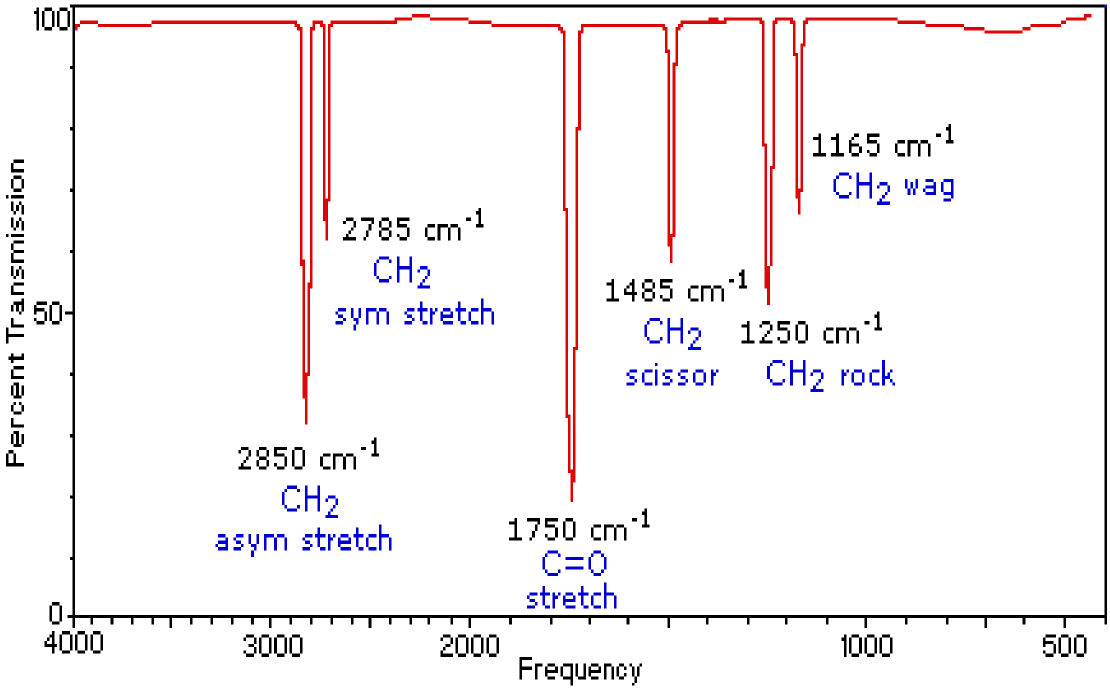

Figure 2.10 **A typical IR spectrum of gas phase of formaldehyde, $H_2C{=}O$**

The exact frequency at which a given vibration occurs is determined by the strengths of the bonds involved and the mass of the component atoms. In practice, infrared spectra do not normally display separate absorption signals for each of the 3n-6 fundamental vibrational modes of a molecule. The number of observed absorptions may be increased by additive and subtractive interactions leading to combination tones and overtones of the fundamental vibrations, in much the same way that sound vibrations from a musical instrument interact. Furthermore, the number of observed absorptions may be decreased by molecular symmetry, spectrometer limitations, and spectroscopic selection rules.

2.2.2.1 FTIR spectrophotometer

The early-stage IR instrument is of the dispersive type, which uses a prism or a grating monochromator. The dispersive instrument is characteristic of a slow scanning. A Fourier Transform Infrared (FTIR) spectrometer obtains infrared spectra by first collecting an interferogram of a sample signal with an interferometer, which measures all of infrared frequencies simultaneously. An FTIR spectrometer acquires and digitizes the interferogram, performs the FT function, and outputs the spectrum.

The heart of an FTIR Spectrophotometer is a Michelson Interferometer (Figure 2.11) built around the sample chamber. Radiation from an IR source is directed through the sample cell to a beam splitter. Half of the radiation is reflected from a fixed mirror while the other half is reflected from a mirror which moved continuously over a distance of about 2.5 micrometers. When the two beams are recombined at the detector, an interference pattern is produced. A single scan of the entire distance takes about 2 seconds and is stored in the computer. In order that several scans may be added, they must coincide exactly. Obviously, this would be impossible considering the thermal fluctuations and vibrations in the laboratory. In order to solve this problem, a helium-neon laser is simultaneously directed through the Michelson Interferometer and the interference pattern of the laser is used as a frequency reference.

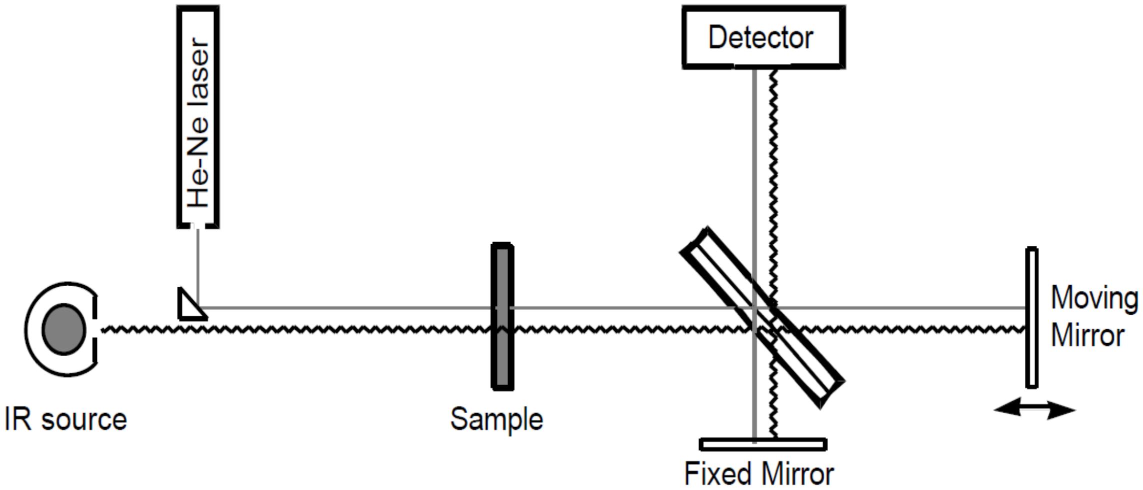

Figure 2.11 Diagram of the Michelson Interferometer used in an FTIR Spectrophotometer.

The interferogram signal is transmitted through or reflected off of the sample surface, the specific frequencies of energy are absorbed by the sample due to the excited vibration of function groups in molecules. The infrared signal after interaction with the sample is uniquely characteristic of the sample. The beam finally arrives at the detector.

2.2.2.2 Data analysis

In FTIR it is difficult to gain machine independent values and thus to compare exact values between spectrophotometers. For example, the percentage of the signal picked up by the detector is dependent upon the system, it will vary between different detectors, and with wavelength and time, as the detector inevitably deteriorates. Thus although the concentration of the sample will generally be related to the intensity of the signal, the units used in FTIR are usually described as arbitrary units.

The detected interferogram can not be directly interpreted. It has to be "decoded" with a wide-used mathematical technique in term of Fourier Transformation. The computer program can perform the Fourier transformation calculation and present an infrared spectrum, which plots absorption (or transmittance) versus wavenumber (Figure 2.12).

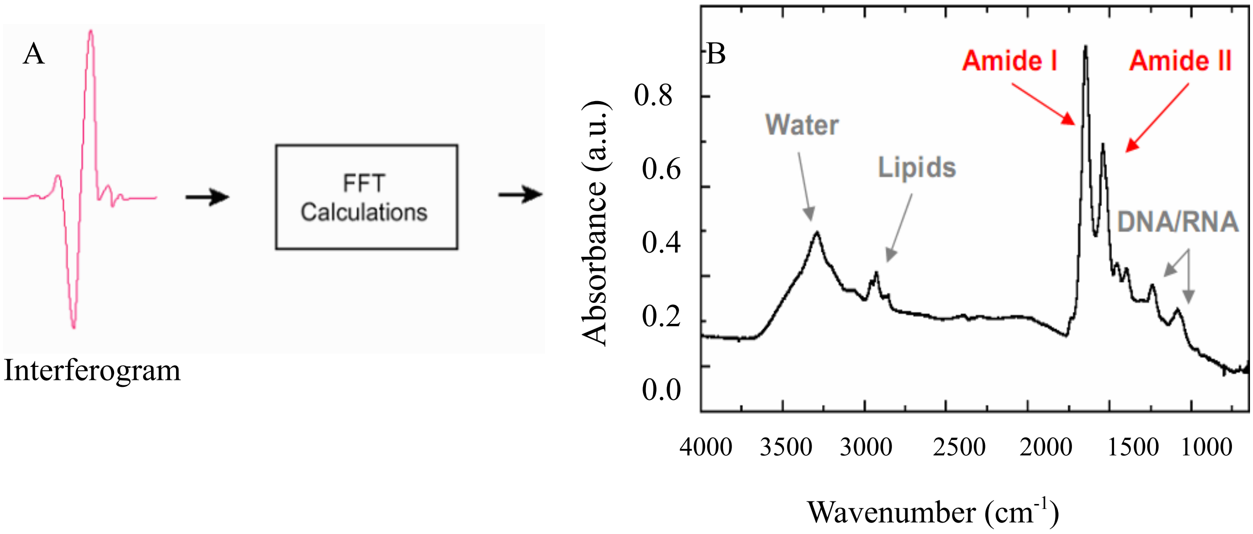

Figure 2.12 Translation of the symmetric interferogram into a spectrum by Fourier Transformation.(A) Interfrogram. (B) An infrared spectrum, which plots absorption (or transmittance) versus wavenumber.

When an interferogram is Fourier transformed, a single beam spectrum is generated. (The theoretical backgrounds of IR data handling techniques have been discussed in detail by Susi and Byler (Susi and Byler, 1983, 1986). A single beam spectrum is a plot of raw detector response versus wavenumber. A single beam spectrum obtained without a sample is called a background spectrum, which is induced by the instrument and the environments. Characteristic bands around 3500 cm^{-1} and 1630 cm^{-1} are ascribed to atmospheric water vapor, and the bands at 2350 cm^{-1} and

667 cm^{-1} are attributed to carbon dioxide. A background spectrum must always be run when analyzing samples by FTIR. When an interferogram is measured with a sample and Fourier transformed, a sample single beam spectrum is obtained. It looks similar to the background spectrum except that the sample peaks are superimposed upon the instrumental and atmospheric contributions to the spectrum. To eliminate these contributions, the sample single beam spectrum must be normalized against the background spectrum. Two criteria have been established to judge whether the spectrum is good or not (Dong et al., 1992). First, the bands originating from water vapor must be subtracted accurately from the protein spectrum between 1800 and 1500 cm^{-1}. Second, a straight baseline must be obtained from 2000 to 1750 cm$^{-1.}$ By using the two criteria, the average experimental errors of the spectra at the amide I and II band maxima could be less than 3% and 1.5%, respectively (Venyaminov and Kalnin, 1990).The identical scan conditions have to be used to record buffer reference spectrum and the spectrum of protein solution. In addition, water vapor, as well as water (or buffer) itself, must be subtracted accurately from the protein spectrum. As mentioned above, using a straight base line between 2000 and 1750 cm^{-1} as the standard to judge the complete water subtraction would lead to a higher quality of protein spectra.

During FTIR experiments H_2O is a great problem: in fact, the band corresponding to the O-H bending mode is at 1644 cm^{-1}, obscuring the amide I band. If the protein solvent is H_2O, the O-H bonds absorb so greatly that it is impossible to subtract the H_2O signal. To solve this problem, standard FTIR experiments are usually performed in deuterated buffers. The wavenumber of O-D bonds stretching, indeed, is lowered by 400 cm^{-1}, to be about 1244 cm^{-1}, totally out from the Amide I band.

2.2.2.3 Data interpreting

The protein repeat units give nine characteristic IR absorption bands, namely, amide A, B, and I−VII. Of these, the amide I and II bands are the two most prominent vibrational bands of the protein backbone (Figure 2.13)

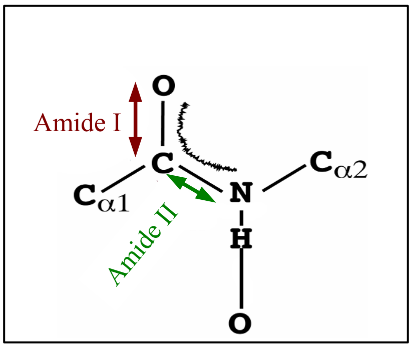

Figure 2.13 Amide I and Amide II vibration types

Bandekar described the nine amide vibration modes and some standard conformations in detail in his review (Bandekar, 1992). Here presented only the most important of them (Figure 2.14)

The ***Amide A*** band (about 3500 cm^{-1}) and ***Amide B*** (about 3100 cm^{-1}) originate from a Fermi resonance between the first overtone of amide II and and the N-H stretching vibration.

Amide I is the most intense absorption band in proteins. It is a band (between 1600 and 1700 cm^{-1}) which is mainly associated with the C=O stretching vibration (70-85%) and is directly related to the backbone conformation.

Amide II is found in the 1510 and 1580 cm^{-1} region and is more complex than amide I. Amide II derives mainly from in-plane N-H bending (40-60% of the potential energy). The rest of the potential energy arises from the C-N (18-40%) and the C-C (about 10%) stretching vibrations. ***Amide III, V*** are very complex bands dependent on the details of the force field, the nature of side chains and hydrogen bonding. Therefore these bands are of little use from in-plane NH bending (40−60% of the potential energy) and from the CN stretching vibration (18−40%), showing much less protein conformational sensitivity than its amide I counterpart (Krimm and Bandekar, 1986). Other amide vibrational bands are very complex depending on the details of the force field, the nature of side chains and hydrogen bonding, which therefore are of little practical use in the protein conformational studies.

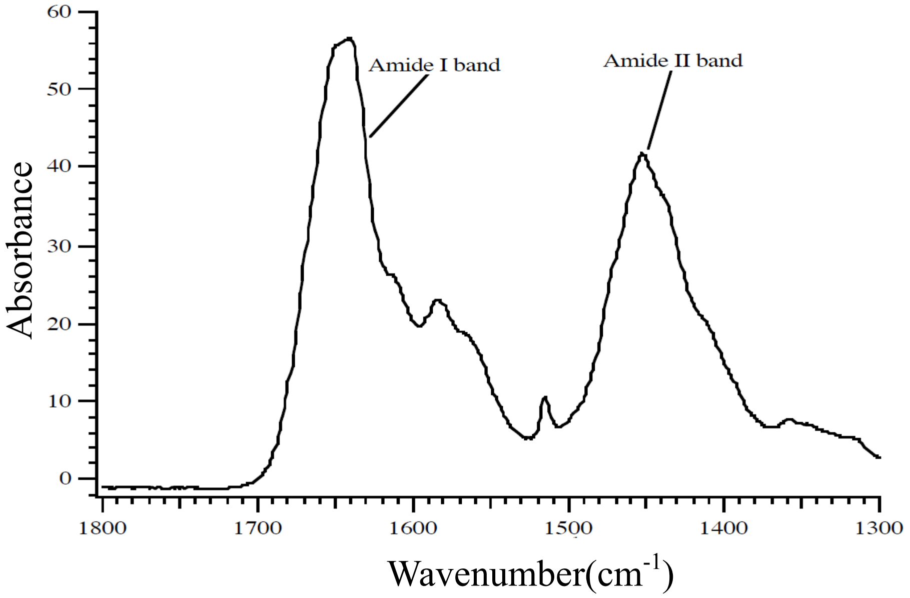

Figure 2.14 Amide vibrations. FTIR spectrum of bovine pancreatic trypsin inhibitor showing the Amide I and Amide II bands.

A spectrum of single bands (each narrow band is characteristic for a secondary structure) is broadened in the liquid or solid state. Therefore, the bands overlap and can not be distinguished in the amide envelope. A curve fitting procedure can be applied to estimate quantitatively the area of each component representing a type of secondary structure. In the pioneering work by (Susi and Byler, 1986) the amide I was deconvoluted with a Lorentzian line shape function and a resolution enhancement factor was applied. The deconvoluted spectrum was fitted with Gaussian band shapes by an iterative curve fitting procedure (Figure 2.15).

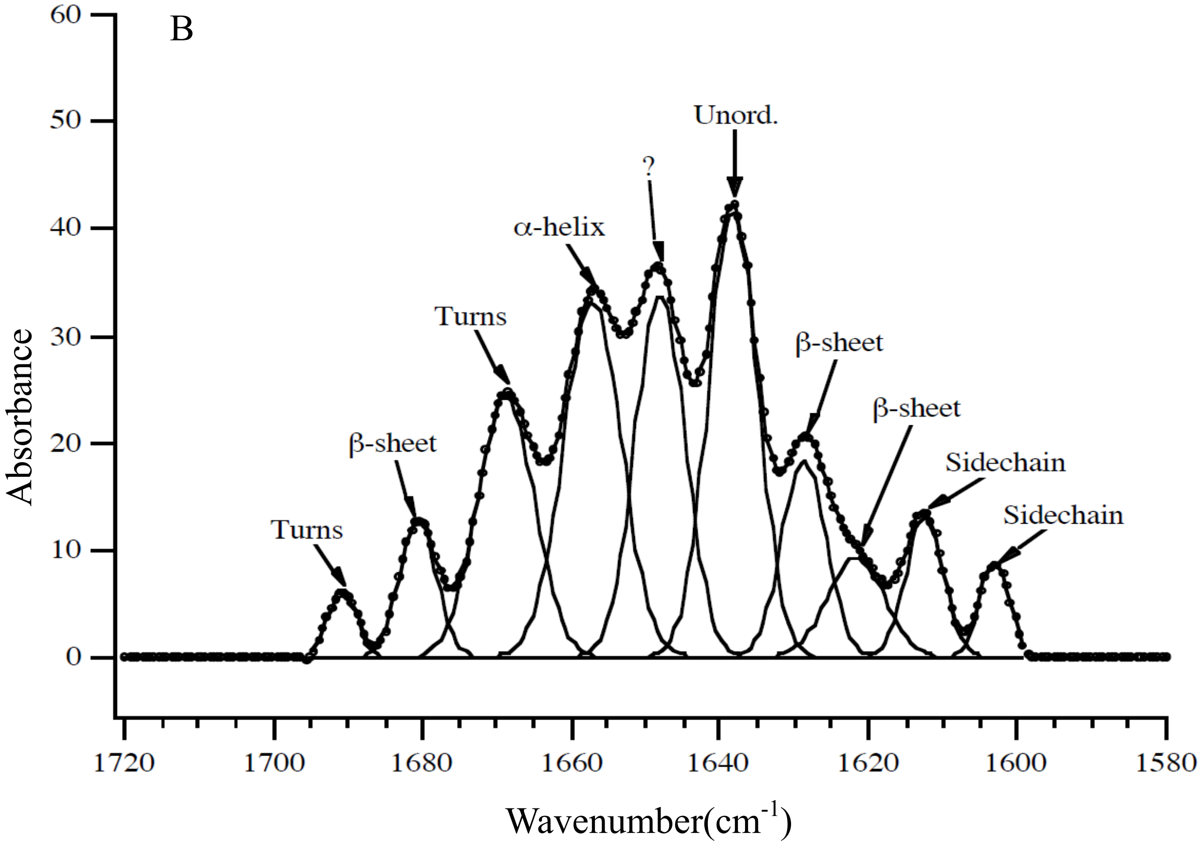

Figure 2.15 Amide vibrations. Results of a Fourier self-deconvolution analysis on the Amide I band for bovine pancreatic trypsin inhibitor. The assignments of the various peaks to the different elements of secondary structure are shown (Tong, Li, and Lin 1999).

The results are in good agreement with the secondary structure information obtained from X-ray crystallographic structures of the proteins under study. High sensitivity to small variations in molecular geometry and hydrogen bonding patterns makes the amide I band uniquely useful for the analysis of protein secondary structural composition and conformational changes (Bandekar and Yu, 2007), each type of secondary structure gives rise to a somewhat different C=O stretching frequency due to unique molecular geometry and hydrogen bonding pattern. (Table 2.2.1)

Structure	Wawenumber (cm^{-1})		
	Amide I	Amide II	Amide III
a- helix	1654-1660	1650-1660	1290-1335
b-sheet	1690-1698	1675-1695	1215-1250
	1624-1642	1625-1640	
b-sheet [aggregation]	1690-1698	1675-1695	1215-1250
	1610-1628	1610-1628	
unordered (random coil)	1645-1653	1640-1650	1250-1290

Table 2.2.1 Proteins in solution. The frequency of Amide component (Susi and Byler, 1986).

The infrared spectra of proteins exhibit absorption bands associated with their characteristic amide group, the structural unit common to all molecules of this type (Arrondo et al., 1993). The characteristic bands of the amide groups of protein chains are similar to the absorption bands exhibited by secondary amides in general, and proteins generally possess a variety of domains containing polypeptide fragments in different conformations. As a consequence, the observed amide I band is usually a complex composite, consisting of a number of overlapping component bands representing helices, beta-structures, turns and random structures. In D_2O solution, it has been revealed that the broad protein amide I band contours can be decomposed into a number of components. A component centred between approximately 1658 and 1650 cm^{-1} has been assigned to the α-helix, which is consistent with both theoretical calculation and the observation of bands in the spectra of α-helical proteins. Bands near 1663 cm^{-1} are assigned to right-handed α helices, although this structure is rarely found in proteins. More than one β-component has been observed in the spectra of many β-sheet proteins. Bands in the regions of 1640−1620 cm^{-1} and 1695−1690 cm^{-1} have been assigned to β-sheet by many authors. Theoretical calculation of β-sheets also predicts an IR active mode between approximately 1695 and 1670 cm^{-1}. These β-components are often complicated by the presence of more than one band above 1670 cm^{-1}. The assignment of bands around 1670, 1683, 1688 and 1694 cm^{-1} to β-turns has been proposed. Turns are also associated with a characteristic band around 1665 cm^{-1}. The unordered conformation (usually referred to as random coil) is usually associated with the IR band between 1640 and 1648 cm^{-1} (Krimm and Bandekar 1986).

The intrinsic width of the single bands characteristic of the secondary structure is often greater than the separation between the bands. Hence, the single bands overlay and they cannot be separated in the whole spectrum. Having spectra with a high signal/noise ratio and very innovative softwares, it has been possible to develop methods to determine the secondary structure components of a protein from an IR spectrum. The best method to use for the estimation of protein secondary structure involves band-fitting of the amide I band. The fractional areas of the fitted component bands are directly proportional to the relative amounts of structure that they represent. The percentages of helices, beta- structures and turns are estimated by addition of the areas of all of the component bands assigned to each of these structures and then expressing the sum as a fraction of the amide I area.

2.2.2.4 Advantages and limitations of FTIR

The main advantage of FTIR over other techniques is convenience. IR spectra can be obtained for proteins in a wide range of environments with a small amount of sample. Other than estimating the protein secondary structures, IR can also provide information on protein structural stability and dynamics.

The FTIR spectrum is also complex, and some characteristic bands of secondary structure elements might overlap. The background subtraction procedure could also bring experimental error. Estimation of side-chain absorption must be taken into account in the analysis of protein spectra.

2.2.2.5 FTIR sample preparation

Infrared spectra were acquired in a Mattson-Polaris Fourier-transform spectrometer purged with dry air and equipped with an MCT detector. Instrumental resolution was 2 cm^{-1}. For FTIR experiments 250 μM Aβ40/Aβ28 peptide were dissolved in HEPES buffer at pD12 and sonicated for 30 seconds (Benseny-Cases et al. 2007). Before measurements, the pD of the solution was adjusted with 10-100 mM DCl solution. The final concentration of peptide was 80 μM. Samples were inserted between CaF_2 windows using a 50-μm-thick mylar spacers. In order to obtain the infrared spectra of the peptide apo and holo forms, for each spectrum, water vapour was subtracted, a spectrum of the solvent was subtracted from the sample (peptide+solvent). In order to obtain the infrared spectra of the peptide, a spectrum of the solvent was subtracted from the sample and baseline corrected. Temperature was 37°C. For each experiment at least two independent measurements were done.

2.2.3 **SAXS**

2.2.3.1 Introduction to SAXS

Small-angle scattering (SAS) of X-rays (SAXS) is a powerful method for the analysis of biological macromolecules in solution. Great progress has been made over the years in applying this technique to extract structural information from non-crystalline samples in the fields of physics, materials science and biology. SAXS is a technique that can probe structure on an extremely broad range of macromolecular sizes (Svergun, 1987). Small proteins and polypeptides in the range of 1–10 kDa, macromolecular complexes and large viral particles up to several hundred MDa can all be measured with modern instrumentation under near native conditions. It is often attractive to laboratory based researchers as the amount of material required for a complete study is relatively low (typically 1–2 mg protein), and almost any biologically relevant sample conditions can be used. The effect of changes to sample environment (pH, temperature, salt concentration and ligand/co-factor titration) can be easily measured and, moreover, at high-brilliance synchrotron beamlines time-resolved experiments can be conducted (Lamb et al., 2008).

Below is presented a short discussion of SAS focussed on the elastic scattering of X-rays, SAXS, where dissolved macromolecules are exposed to a collimated and (for synchrotrons) focussed X-ray beam and the scattered intensity *I* is recorded by a detector as a function of the scattering angle (Figure 2.16). For an in-depth review of the theory behind SAXS the reader is directed to text-books and recent review (Glatter 1982; D. Svergun 1987; Mertens and Svergun 2010).

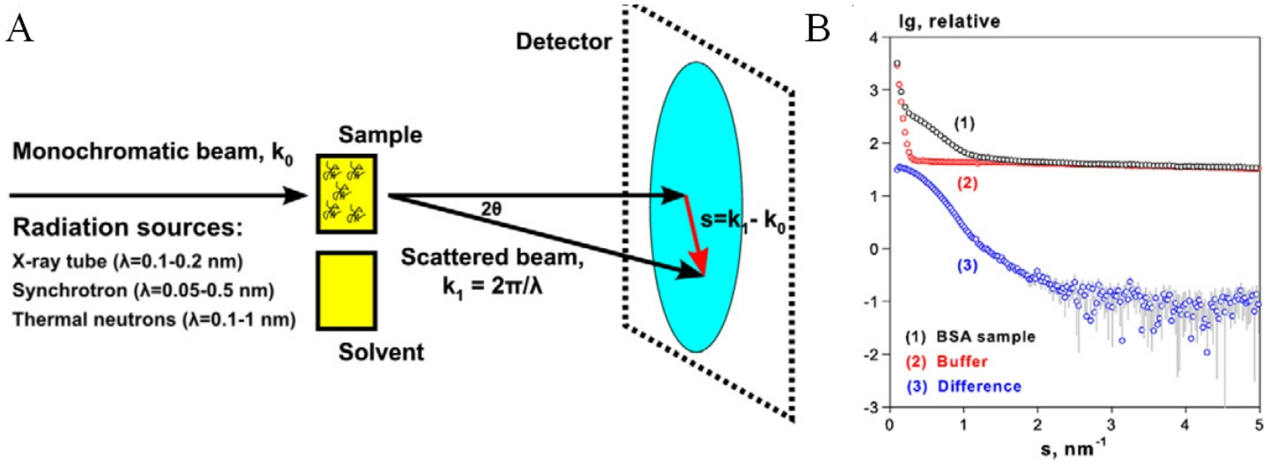

Figure 2.16 Schematic representation of a typical SAS experiment and radially averaged data. (A) Standard scheme of a SAS experiment. (B) X-ray scattering patterns from a solution of BSA measured at X33 (DORIS, Hamburg) in 50 mM HEPES, pH 7.5, solvent scattering and the difference curve (containing the contribution from the protein alone, scaled for the solute concentration, 5 mg/ml). Figure adapted from (Mertens and Svergun, 2010).

Although sophisticated approaches have now been developed for the determination of three-dimensional structure from scattering data, several overall invariant shape and weight parameters can be extracted directly from scattering curves enabling fast sample characterization. These parameters include: the molecular mass (MM), radius of gyration (R_g), hydrated particle volume (V_p) and maximum particle diameter ($D_{\max}$). The Guinier analysis developed by A. Guinier in the 1930s is still the most straightforward method for the extraction of the forward scattering intensity $I(0)$ and the radius of gyration, R_g. For a monodisperse solution of globular macromolecules the Guinier equation is defined as:

$$I(s)=I(0)\exp\left(-\frac{1}{3}R_g^2 s^2\right)$$

In principle, $I(0)$ and R_g can be extracted from the y-axis intercept and the slope of the linear region of a Guinier plot ($\ln[I(s)]$ versus s^2), respectively (Figure 2.17 A and B). However, the range ($s_{\min}$ to s_1) over which the Guinier approximation is valid for each measured scattering curve must be considered. The lower limit of this range, $s_{\min}$, is usually restricted by the experimental set-up, and for an ideal sample is taken to be the minimum angle for which intensity is recorded. The Guinier approximation is based on a power law expansion, used to describe the linear dependence of $\ln[I(s)]$ on s^2 (Mertens and Svergun, 2010). When extended to larger values of s, the higher order terms in the expansion begin to significantly contribute to the scattering intensity, breaking this linear dependence. Given that the power value $(sR_g)^n$ decreases with n for $sR_g < 1$ and increases for $sR_g > 1$, $s_1 < 1/R_g$ is a reasonable estimate for the upper limit of the Guinier fit. However, it is often the case that the range $s_{\min} < s < 1/R_g$ contains too few points, especially in the case of very large macromolecules. It is common in biological SAXS to extend this range up to $s_1 < 1.3/R_g$, so that a sufficient number of data points are available for the estimation of $I(0)$ and R_g. Practice shows that $1.3/R_g$ is a safe estimate for s_1, which does not introduce systematic deviations from linearity. A non-linear Guinier plot is a strong indicator of poor sample quality. Improper background subtraction, the presence of attractive or repulsive inter-particle effects and sample polydispersity result in deviations from linearity (Figure 2.17 C and D). For example, samples that contain a significant proportion of non-specific aggregates yield scattering curves and Guinier plots with a sharp increase in intensity at very small values of s, while samples containing significant inter-particle repulsion yield curves and Guinier plots that show a decrease in intensity at small values of s.

With knowledge of the limitations of the Guinier approximation in mind, the method is an essential first step in sample characterization by SAXS. From visual inspection of the Guinier plot samples can be screened for non-specific aggregation (Figure2.17 A and B, curve 1), the presence of inter-particle repulsion (Figure 2.17 A and B, curve 3), the prevalent oligomerisation state in solution estimated and the invariant shape and weight parameters, R_g and $I(0)$ extracted. In the past, Guinier analysis was always done interactively; recently, automated procedures have become available. In particular, the program AUTORG (Petoukhov and Svergun, 2007) employs statistical methods to optimize the range of s, to detect possible aggregation or repulsive interactions and, based on this, to evaluate the quality and reliability of the extracted parameters. Following from the Guinier analysis the MM can be estimated based on knowledge of the forward scattering intensities and concentrations of both the macromolecule of interest and a standard such as bovine serum albumin. This estimate requires normalization against the solute concentrations for the two measurements, and the accuracy of the MM estimate is limited (Bernadó et al., 2007).

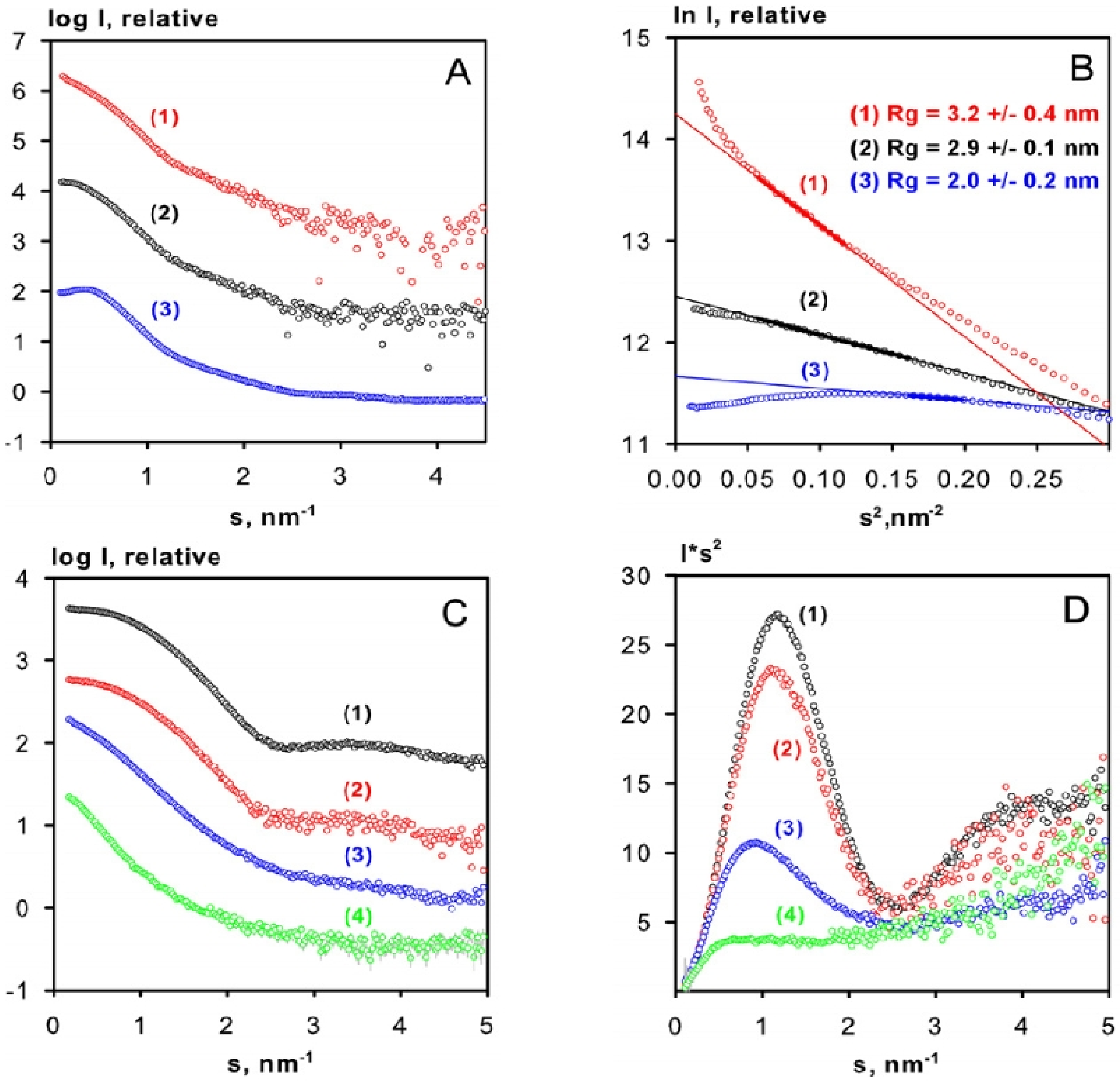

Figure 2.17 Standard plots for characterization by SAXS. (A and B) SAXS curves and Guinier plots for BSA samples measured at X33 (DORIS, Hamburg) in different buffers showing (1) aggregation, (2) good data and (3) inter-particle repulsion. The Guinier fits for estimation of R_g and $I(0)$ are displayed, with the linear regions defining s_{min} and s_{max} used for parameter estimation indicated by the thick lines. (C and D) SAXS curves and Kratky plots for lysozyme samples measured at X33 (DORIS, Hamburg) showing (1) folded lysozyme, (2) partially unfolded lysozyme (in 8M urea), (3) partially unfolded lysozyme at 90 C and (4) unfolded lysozyme (in 8M urea at 90ºC). Plots are arbitrarily displaced on the vertical axis for clarity with the exception of (D), where all curves have been scaled to the same forward scattering intensity, $I(0)$.

An alternative approach to MM estimation that is more suited to solutions with significant lipid, carbohydrate or nucleic acid content (including for example, glycoproteins or protein–lipid complexes) involves the use of water as a standard (Orthaber and Glatter, 2000). Independent from the Guinier analysis, the hydrated particle volume (V_p) can be obtained from the data on a relative scale, avoiding inaccuracies in parameter estimation caused by errors in concentration measurement. Assuming a uniform electron density inside the particle, V_p is estimated following Porod's equation (Mertens and Svergun, 2010):

$$V_p = 2\pi^2 I(0)/Q, \qquad Q = \int_0^\infty s^2 I(s)\, ds$$

where Q is the so-called Porod invariant. For real macromolecules the electron density is of course not uniform, however, at sufficiently high MM (>30 kDa), the subtraction of an appropriate constant from the scattering data generates a reasonable approximation to the scattering of the corresponding homogenous body. The particle volume, V_p allows one to make an alternative estimate of the MM with the added advantage that this estimate is independent of errors in the sample concentration.

Due to the limitations of the Guinier approximation, the extraction of R_g and $I(0)$ from scattering data is also routinely done through the use of indirect Fourier transform methods. Fourier transformation of the scattering intensity yields the distance distribution function, $p(r)$:

$$p(r) = \frac{r^2}{2\pi^2} \int_0^\infty s^2 I(s) \frac{\sin(sr)}{sr}\, ds$$

of the scattering data and allows one to graphically display the peculiarities of the particle shape (Figure 2.18). For example, globular particles yield bell-shaped profiles with a maximum at approximately $D_{\text{max}}/2$ and multi-domain particles often yield profiles with multiple shoulders and oscillations corresponding to intra and inter-subunit distances. Computation of $p(r)$ is not straightforward as a limited range of $I(s)$ is available (from s_{min} to s_{max}), and direct Fourier transformation of the scattering curve from this finite number of points is not possible. A solution to this problem is the indirect Fourier transformation method first proposed by O. Glatter in the 1970s (Glatter, 1982).

In the indirect transform program GNOM (Svergun, 1992), the solution yielding the $p(r)$ function is evaluated using perceptual criteria, providing the user with the means to easily identify reliable solutions and to obtain an optimal value of D_{max}. This procedure has also been automated in the program AUTOGNOM (Petoukhov and Svergun, 2007), where multiple GNOM runs are performed without user intervention across a range of D_{max} values. The parameters estimated from the indirect Fourier transform approach, $I(0)$ and R_g are typically more accurate than those obtained from a Guinier analysis as the entire scattering curve is used for their estimation. For the study of protein folding the Kratky plot ($s^2I(s)$ vs s) can be used as an indication of the folded/unfolded state (Doniach, 2001). Folded globular proteins typically yield a prominent peak at low angles (Figure 2.18C and D, curve 1), whereas unfolded proteins show a continuous increase in $s^2I(s)$ with s (Figure 2.18 C and D, curve 4). Flexible multi-domain proteins can also potentially be identified from the Kratky plot, displaying a mixture of characteristic features of both folded and unfolded proteins similar to that observed for a partially unfolded state (Figure 2.18C and D, curves 2 and 3).

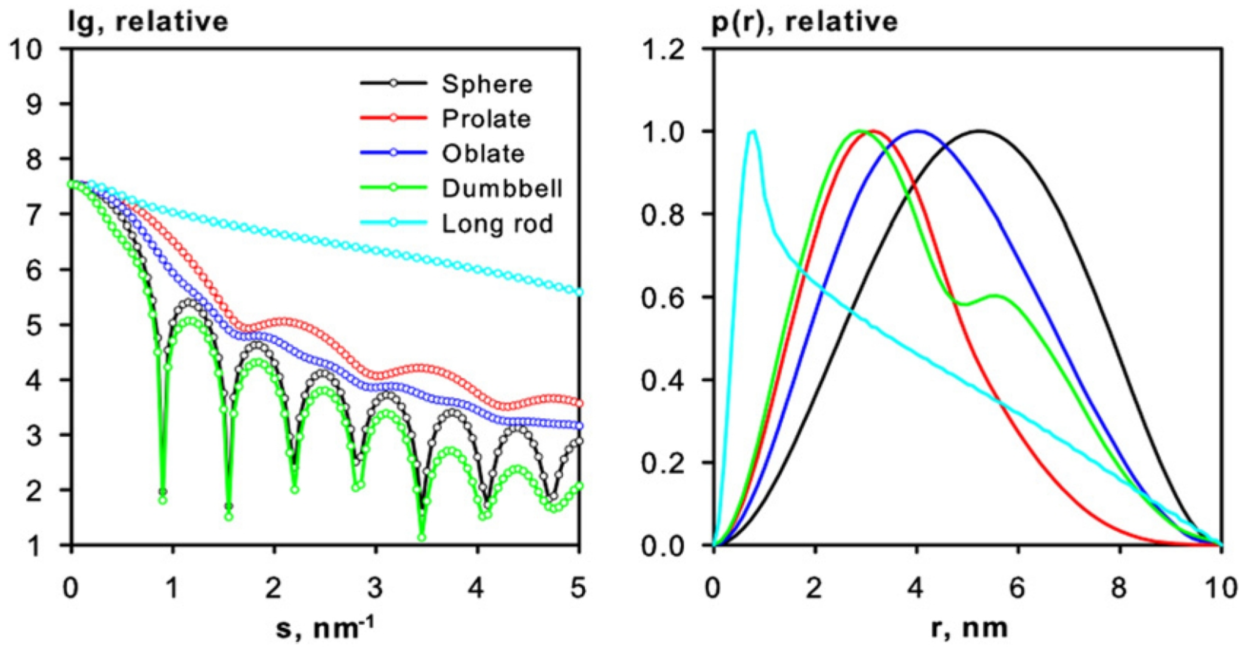

Figure 2.18. Scattering intensities and distance distribution functions. The $p(r)$ calculated for typical geometric shapes: Solid sphere (black), prolate ellipsoid (red), oblate ellipsoid (blue), two-domain (green) and long rod (cyan). The bead models used for the calculation of scattering intensities are shown above the plots.

2.2.3.2 *Ab initio*

The reconstruction of low-resolution 3D models from SAXS data alone is now a standard procedure and as such can also be considered a rapid characterization tool. The basic principles behind shape determination from 1D SAXS data were established in the 1960s, where scattering patterns were computed from different geometrical shapes and compared with experimental data. In the initial *ab initio* approach, the shape of particles was described by an angular envelope function, the latter developed into a series of spherical harmonics. This method was further developed into the first publicly available program SASHA (Svergun et al., 1996). While this method was a major breakthrough in the determination of low-resolution structure from SAXS it was restricted to particles without internal cavities. More detailed ab initio reconstructions became possible through the development of automated bead-modeling. The most popular ab initio bead-modeling program in current use is DAMMIN (Dummy Atom Model Minimisation) (Svergun, 1999). The algorithm represents a particle as a collection of M (>>1) densely packed beads inside a constrained (usually spherical) search volume, with a maximum diameter defined by the experimentally determined $D_{\max}$ (Figure 2.19). The shape reconstruction is conducted starting from a random initial approximation by simulated annealing (Kirkpatrick et al., 1983)

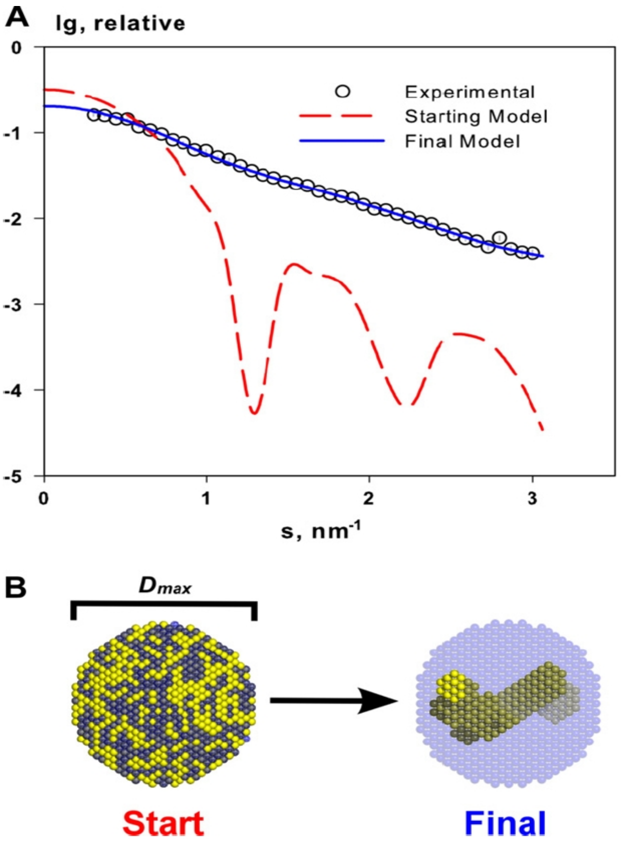

Figure 2.19 ***Ab initio* modelling procedure using DAMMIN.** (A) Starting from a spherical search volume a fitting procedure is conducted until a final model is generated satisfying not only a fit to the experimental data, but also forming a compact and connected model of dummy atoms/beads. (B) The spherical search volume with beads assigned to the particle (yellow) and solvent (blue).

2.2.3.3 Sample preparation

All samples were measured at several solute concentrations ranging from 0.5 to 1.2 mg/ml in 10 mM HEPES buffer at pH 11. Aβ40 peptide-Cu(II) ratio was 1 to 1. The sample concentrations were determined as precise as possible to normalize the scattering data. A single SAXS measurement on X33 was 50 µl of sample, and exposed about 2 minutes to synchrotron radiation (data collection time). The data were processed by the program PRIMUS (Konarev et al., 2003) by using standard procedures (Svergun and Koch, 2003) to compute the radius of gyration R_g, excluded (Porod) volume V_p, and maximum dimension D_{max}. The distance distribution function $p(r)$ was computed by using the program GNOM (Svergun, 1992). The molecular masses (MM) of the solutes were evaluated by scaling against reference solutions of BSA and further verified by comparison with the excluded particle volume (for globular proteins, V_p in nm^3 is about twice the MM in kDa). Particle shapes at low resolution were reconstructed *ab initio* by the bead-modeling programs DAMMIN (D I Svergun 1999). For each condition at least two independent measurements were done.

Synchrotron SAXS data were collected at the EMBL X33 beamline on the storage ring DORIS III [Deutsches Elektronen-Synchrotron (DESY), Hamburg, Germany]. General beamline characteristic are described in Table 2.2.2.

Wavelength	0.15 nm
Flux at sample	5 x 10^{11} ph/s/100mA
Sample to detector distances	Standard: 2.7 m
Resolution SAXS	From s = 0.06 nm^{-1} to 6 nm^{-1}
Small automated sample changer	8 samples (30-200 µl) 3 buffers (1.5 ml)

Table 2.2.2 General characteristics of X33 Beamline at EMBL Hamburg (Roessle et al., 2007).

2.2.4 Microscopy Techniques

2.2.4.1 *Basic principles*

The microscope is used to create an enlarged view of an object such that we can observe details not otherwise possible with the human eye. Since its invention, the microscope has been a valuable tool in the development of scientific theory. Magnifying lenses have been known for as long as recorded history, but it was not until the advent of the modern compound light microscope that the device was used in biology. A compound microscope is composed of two elements; a primary magnifying lens and a secondary lens system, similar to a telescope. Light is caused to pass through an object and is then focused by the primary and secondary lenses. If the beam of light is replaced by an electron beam, the microscope becomes a transmission electron microscope. If light is bounced off of the object instead of passing through, the light microscope becomes a dissecting scope. If electrons are bounced off of the object in a scanned pattern, the instrument becomes a scanning electron microscope.

Macromolecules and their complexes are usually too small to be directly observed by optical microscopy, because their size is insufficient to diffract light of wavelengths with $\lambda >$ 400nm. The resolving power of conventional light microscopes is narrowed down to approx. 0.2µm by Abbe’s equation. The achievable resolution for a wavelength λ is often given by the diffraction limit δ as:

$$\delta = 0.61 \frac{\lambda}{NA} \quad ,$$

with numerical aperture NA, which can be approximated by the angle of incidence $NA \approx \alpha \approx r_a/r_{wd}$ where r_a is the radius of the objective lens and r_{wd} is the working distance. Since $\alpha \ll 1$ for the present purposes, $\sin \alpha \approx \tan \alpha \approx \alpha$.

Optical microscopes can reach a resolution of about δ = 200nm. Unfortunately this is not sufficient for the imaging of the amyloid fibrils, since they have smaller diameters.

Early twentieth century scientists theorized ways of getting around the limitations of the relatively large wavelength of visible light (wavelengths of 400–700 nm) by using electrons. Like all matter, electrons have both wave and particle properties (as theorized by Louis-Victor de Broglie), and their wave-like properties mean that a beam of electrons can be made to behave like a beam of electromagnetic radiation. The wavelength of electrons is found by equating the de Broglie equation to the kinetic energy of an electron:

$$\lambda = \frac{h}{\sqrt{2 m_0 E}} \approx \frac{12.3}{E[\mathrm{keV}]} \ [\mathrm{\mathring{A}}],$$

where, h is Planck's constant, m_0 is the rest mass of an electron and E is the energy of the accelerated electron, it will have a wavelength of 1 nm at 1 eV decreasing to 1 pm at 100 keV.

2.2.4.2 Electron microscopy

Electron Microscopy (EM) technique is based on the same principles as light microscopy that uses electrons instead of light. Electrons are small charged particles, which also exhibit a wave nature in the free state. Their wavelength, which depends upon the inverse of their momentum, is very short (less than 1Å) at the voltages used in electron microscopy. Because electrons are charged particles, they can be deflected by electrostatic or electromagnetic fields. Thus they can be accelerated, bent in their flight path, and focused so that they used in electron optics as photons are used in light optics.

Electrons are usually generated in an electron microscope by electron gun, in the same manner as a light bulb, or alternatively by field electron emission. The electrons are then accelerated by an electric potential and focused by electrostatic and electromagnetic lenses onto the sample. A beam of electrons is passed through the specimen of interest and the interactions with the molecules in the sample will cause some of the electrons to scatter (Hubbard, 1995). With an electron beam several things may happen: (a) If the electron does not strike an atom in the sample it will continue to travel in a straight line until it hits the imaging screen. If the electron gets in contact with the sample, it can either (b) bounce off elastically, without any loss of energy, or (c) inelastically (because of interactions with the electrons of the object) transferring some of its energy to the atom. If the electron is bounced elastically (usually by Coulomb interactions with the nucleus of the object), its energy is constant, and the law of conservation of momentum will determine the angle at which it will bounce. This effect is used for electron diffraction experiments. Electrons with a scattering angle above 90° are termed “back reflected electrons” and are generally not used in EM. The electron microscope extracts structural information carried by the scattered electrons. The elastically scattered electrons, those which have changed their direction but not lost any energy on interaction with the specimen, interfere with the unscattered electrons to produce a phase contrast image. The inelastically scattered electrons, which have changed both direction and energy on interaction with the specimen, generate a diffuse background image that is in some EMs eliminated by an energy filter.

During the work on this thesis, electron microscopy was used for the ultra-structural characterization of the oligomeric aggregates and the more complex prefibrillar structures eventually growing into protofibrils, mature amyloid fibrils and cells in the presence of amyloid aggregates.

2.2.4.3 Transmission electron microscope

The transmission electron microscope (TEM) was the first type of Electron Microscope to be developed and is patterned exactly on the light transmission microscope except that a focused beam of electrons is used instead of light to "see through" the specimen. The first prototype instrument, a so-called transmission electron microscope (TEM), was developed in 1931 by the German engineer Ernst Ruska and honored with the Noble Prize in physics in 1986 (Heidenreich, 1964). The first commercially available instrument was introduced in 1939 by Siemens. To date, TEM is one of the most powerful microscopy techniques used for the visualization and characterization of amyloid fibril structure (Serpell and Smith, 2000).

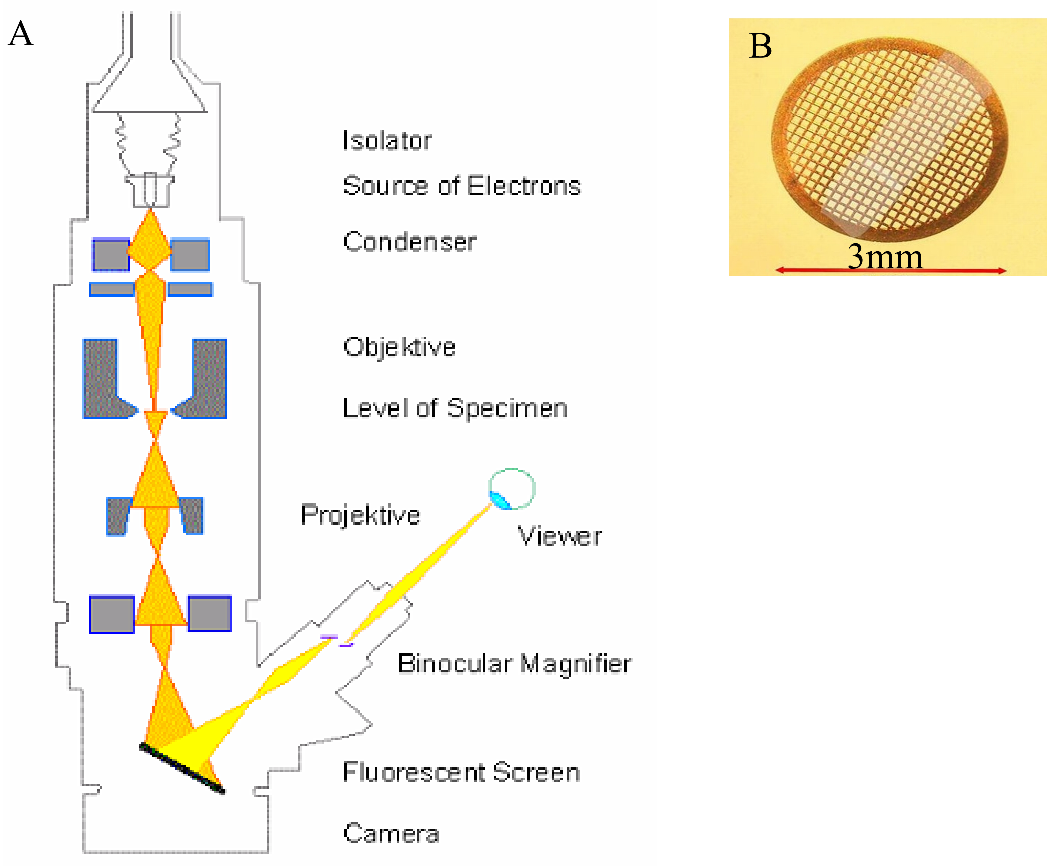

Figure 2.20 Schematic representation of a transmission electron microscope. (A) The electron beam is highlighted in yellow, the electron-optical lenses are depicted in gray. (B) Grid for TEM with a band of thin carbon coating.

Electrons are usually generated in an electron microscope by electron gun, in the same manner as a light bulb, or alternatively by field electron emission. The electrons are then accelerated by an electric potential and focused by electrostatic and electromagnetic lenses onto the sample. A beam of electrons is passed through the specimen of interest and the interactions with the molecules in the sample will cause some of the electrons to scatter (Hubbard 1995). An example of electron microscope is shown in Figure 2.20 A. The energy of the monochromatic electron beam is somewhere between (100 - 400) keV, special instruments go up to 1,5 MeV (at a price of ca. 8 M€). Keeping inelastic scattering of the electrons small has supremacy, this demands specimen thicknesses between 10 nm to ca. 1 µm. The resolution depends on the thickness; high-resolution TEM (*HRTEM*) demands specimens thicknesses in the nm region.

Specimens for TEM analysis are placed on special micro-meshed conductive metals such a as Cu. Au or Ni. The typical dimensions of TEM grids are 3 mm in diameter, and 10-25 µm thick. The mesh number of grids indicates the number of opening per linear inch. The smaller the grid number, the larger the hole size and consequently the greater the ratio of open area to covered area. For example 400-mesh grid (used in this work) has 400 holes, this translates to hole sizes of *ca.* 42 µm. Grids covered with thin layer of carbon (about 10nm) is used to put the sample under electron beam (Figure 2.20B).

2.2.4.4 ***Sample preparation for TEM***

For TEM analysis the sample needs to be thin enough to allow the electrons to pass and contain molecules that diffract electrons. Biological samples are composed mainly of atoms of low electron density (e.g. carbon, hydrogen and nitrogen) and will therefore allow most electrons to pass undisturbed, resulting in poor contrast. In order to improve contrast, negative staining of the samples can be employed. The stains used are usually heavy metal salts, e.g. uranyl acetate $UO_2(CH_3COO)_2 2H_2O$, which will easily interact with the electron beam. The stain will not bind to the sample but will instead surround it so that the edges of the specimen will absorb most electrons – in the end creating a “negative” image.

For current TEM examinations the protein suspensions were adsorbed onto formval/carbon-coated 400 mesh copper grids by coating the grids of 10 ml drops of the protein sample for 10 min. An excess of sample was removed by touching the grid with a filter paper then 10 ml drop of 2.0% uranyl acetate in water was applied to the grids. After 40 sec the excess stain was removed by touching the edge with a filter paper. The grids were allowed to air-dry and examined using a Hitachi H-7000 microscope Jeol JEM 2011 with LaB6 filament as the electron source. Voltage was 75 kV.

2.2.4.5 *Limitations of TEM*

There are a number of drawbacks of the TEM. The negative staining provides the picture of only the outer sample structure. Many materials require extensive sample preparation to produce a sample thin enough to be electron transparent. The structure of the sample may be changed during the preparation process or over-stained. Also the field of view is relatively small, raising the possibility that the region analysed may not be characteristic of the whole sample. The sample or grid carbon coating can be easily damaged by the electron beam, particularly in the case of biological materials. Since accelerated electrons possess a very small cross-section, high vacuum (10^{-8} Torr) is required within the instrument, this condition is very extremal for biological samples study.

2.2.5 **Atomic force microscopy**

2.2.5.1 *Basic principles*

In 1986 the AFM or scanning force microscope (SFM) was invented by Binnig et al.. This microscope, the most widely used and versatile modification of the STM microscope, has undergone much advancement since its initial development. The AFM is one of the most powerful tools for determining the surface topography of biomolecules in their native state at sub-nanometer resolution (Gosal et al., 2006). AFM has been successful in imaging DNA, where the helical pitch of DNA has been shown to be 3.4 nm (Hansma et al., 1993, 1995; Mou et al., 1995), cellulose in plant cell walls (Kirby et al., 1996), a wide range of proteins including globular proteins such as chaperonin proteins (Mou et al., 1996), muscle protein such as myosin and titin, lipid bilayers (Mou et al., 1994; Grandbois et al., 1998), and many other systems.

Unlike X-ray crystallography and electron microscopy, AFM allows biomolecules to be imaged not only under physiological conditions, but also while biological processes are at work. Because of the high signal-to-noise (S/N) ratio, the detailed topological information is not restricted to crystalline specimens. Hence, single biomolecules lacking inherent symmetry can be directly monitored in their native environment (Möller et al., 1999; Santos and Castanho, 2004).

The AFM works in the same way as our fingers in the dark which touch and probe the environment we cannot see. The use of a finger to “visualize” an object leads our brain to deduce its topography while touching it. The resolution of AFM is determined by the radius of the fingertip. To achieve atomic scale resolution, a sharp stylus (radius ~1–2 nm) attached to a cantilever is used in the AFM to scan an object point by point and contouring it while a constant small force is applied to the stylus. The forces (e.g., Van der Waals, electrostatic, magnetic, etc.)

generated between the AFM tip and the sample are transmitted to an attached flexible cantilever, causing it to bend. The bending of the cantilever is monitored by the defection of a laser beam refected by the cantilever. In the AFM, the role of the brain is taken over by a computer, while scanning the stylus is accomplished by a piezoelectric tube. The basic characteristics of AFM are as follows: (1) nearly no limits to samples; (2) high-resolution sample morphology in three dimensions; (3) working in various environments, such as vacuum, air, fluid and low temperature; (4) enabling dynamic observation in physiological environment. In the fluid, biological samples can maintain their native state avoiding any damage.

2.2.5.2 Imaging modes

The primary modes of operation for an AFM are static mode and dynamic mode. In static mode, the cantilever is "dragged" across the surface of the sample and the contours of the surface are measured directly using the deflection of the cantilever. In the dynamic mode, the cantilever is externally oscillated at or close to its fundamental resonance frequency or a harmonic. The oscillation amplitude, phase and resonance frequency are modified by tip-sample interaction forces. These changes in oscillation with respect to the external reference oscillation provide information about the sample's characteristics.

The basic operating principle of the AFM is simple in theory (Figure 2.21); a sharp probe mounted at the end of a flexible cantilever raster-scans over the sample surface in a series of horizontal movements. Deflections of this cantilever caused by interactions between the probe and the sample are monitored by an optical detector which measures the signal from a laser beam that is positioned on the cantilever surface above the probe. This signal is then used by a feedback system to alter the force applied to the sample by the tip by controlling the movements of a piezo crystal. A so called topographic image can then be created from the vertical movements of this crystal.

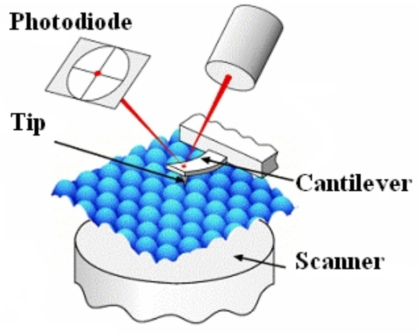

Figure 2.21 A general scheme showing the basic operating principles of the AFM

2.2.5.3 *Modes of operation*

According to the different ways of interaction between the AFM tip and the sample, the operation modes are classified as contact-mode, non-contact mode and semi-contact mode:

1) Contact mode is when the tip scans the sample in close proximity to the surface; the deflection of the cantilever is measured by the detector and compared in a feedback loop to a desired value of deflection. If the measured deflection is different from the desired value the feedback amplifier applies a voltage to the piezo to raise or lower the sample relative to the cantilever to restore the desired value of deflection. The voltage that the feedback amplifier applies to the piezo is a measure of the height of features on the sample surface.

2) Non-contact mode is used in situations where tip contact might alter the sample in subtle ways. In this mode the cantilever is vibrated at its resonant frequency and the tip hovers 50 - 150Å above the sample surface. Long range attractive Van der Waals forces acting between the tip and the sample are detected, and topographic images are constructed by scanning the tip above the surface, whereby the amplitude or phase of the oscillating lever.

3) Keeping the probe tip close enough to the sample for short-range forces to become detectable while preventing the tip from sticking to the surface, dynamic contact mode (also called semi contact or tapping mode) was developed. Tapping mode is a key technique in AFM; it allows high resolution topographic imaging of sample surfaces that are easily damaged by the lateral forces in contact mode or loosely held to their substrate, such as many biomolecules. Tapping mode imaging is implemented by oscillating the cantilever assembly at or near the cantilever's resonant frequency using a piezoelectric crystal. The piezo motion causes the cantilever to oscillate with a high amplitude (typically greater than 20 nm) when the tip is not in contact with the surface. The oscillating tip is then moved toward the surface until it begins to lightly touch, or tap the surface. During scanning, the vertically oscillating tip alternately contacts the surface and lifts off, generally at a frequency of 50,000 to 500,000 cycles per second (50k - 500k Hz). As the oscillating cantilever begins to intermittently contact the surface, the cantilever oscillation is necessarily reduced due to energy loss caused by the tip contacting the surface. The reduction in oscillation amplitude is used to identify and measure surface features. During tapping mode operation, the cantilever oscillation amplitude is maintained constant by a feedback loop. Selection of the optimal oscillation frequency is software-assisted and the average force on the sample is automatically set and maintained at the lowest possible level. When the tip passes over a bump in the surface, the cantilevers amplitude of oscillation decreases. Conversely, when the tip passes over a depression, the cantilever amplitude of oscillation increases (approaching the maximum free air amplitude). The oscillation amplitude of the tip is measured by the detector and input to the AFM controller

electronics. The digital feedback loop then adjusts the tip-sample separation to maintain a constant amplitude and force on the sample.

Because the tip is in hard contact with the surface, the stiffness of the lever needs to be less than the effective spring constant holding atoms together, which is on the order of 1–10 nN/nm. Most contact mode levers have a spring constant of <1 N/m.

AFM has three main advantages over other high resolution microscopic techniques. Firstly it is generally non-destructive, for example the sample preparation does not involve any negative staining or metal coating like in electron microscopy, and secondly the microscope can be operated in liquid, mimicking the in vivo situation as close as possible. Thirdly the AFM has a high signal to noise ratio that allows single proteins to be imaged at a resolution better than 1nm. Unlike the electron microscope which provides a two-dimensional projection or a two-dimensional image of a sample, the AFM provides a three-dimensional surface profile. Additionally, an electron microscope needs an expensive vacuum environment for proper operation.

2.2.5.4 *Limitations of AFM*

The AFM is susceptible, as are all high resolution microscopic techniques to temperature variation and vibration. Temperature drift caused by the AFM is reduced by careful selection of the materials that compose components of the AFM and temperature control around the instrument. Building vibrations (15-20Hz) that may affect imaging can be reduced by isolation of the AFM on a mechanical anti vibration air table or active piezo isolation platforms. There are also some limitations of AFM related to its imaging capabilities. The relatively slow rate of scanning during AFM imaging often leads to thermal drift, especially apparent when imaging liquids with temperature difference between the liquid and the liquid cell, causing the cantilever to bend. This can be reduced by allowing the AFM to equilibrate (Lapshin 2009).

Tip convolution is an imaging artefact that occurs because of the large size of the AFM probe in relation to the samples imaged. In many cases the sides of the AFM probe will interact with the sample leading to a broadening of the image (Figure 2.22). AFM samples have a limited range of roughness that cannot be too high or the sample will touch the underside of the cantilever severely reducing image quality. A typical AFM tip is 3µm tall, though rougher samples can be imaged by using higher aspect ratio tips (though the z direction piezo range is normally about one micron) or imbedding the rough sample in a matrix.

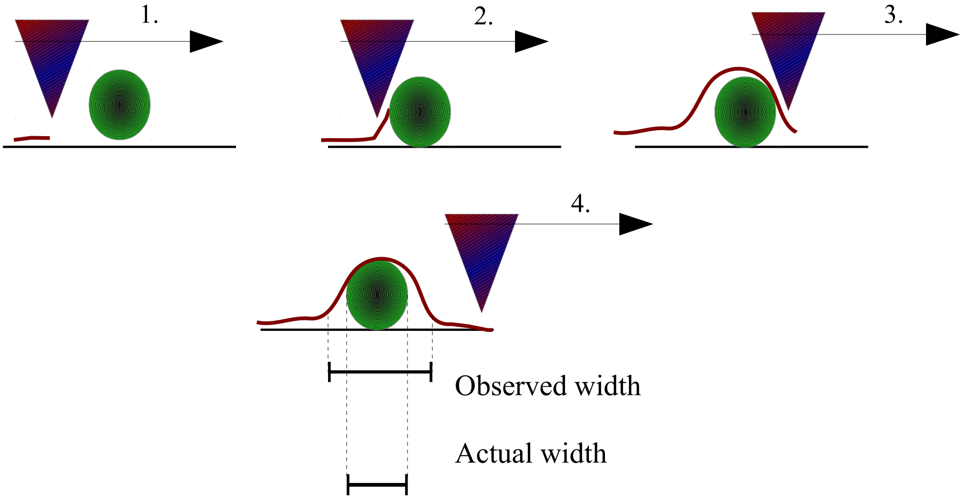

Figure 2.22 **Tip convolution.** As the tip (▼) approaches the scanned object (●), the side of the tip hits first, causing the premature raising of the cantilever, Numbers 1 – 4 correspond to the tip movements. The difference between observed width and actual width can be seen.

2.2.5.5 *Substrate for AFM*

The samples for atomic force microscopy imaging should be immobilized on a rigid support. Since AFM does not require the substrate to be conductive, the choice of substrates is almost unlimited. Both glass cover slips and cleaved mica sheets have been used to adsorb various macromolecules and organelles with varying degrees of success. Biological specimens like cells, molecules (proteins) are usually bound to a fat substrate like mica or glass.

The most commonly used substrate for AFM is mica. Mica is a non-conducting layered material, atomically flat, clean after cleavage, easy to cut to desired sizes,relatively inexpensive, negatively charged but it can be modified to make the surface positive.

The most common form of mica is Muscovite $KAl_2(OH)_2AlSi_3O_{10}$. Mica's property to be highly charged at the surface leads to the fact that it is always covered with a thin (0.5 nm) layer of water when exposed to ambient air. This water layer leads to a continuous adhesion between AFM tip and sample (Jena and Hörber, 2002).

Despite the widespread use of mica, the mechanism of adsorption is not well understood. For both glass and mica in aqueous media, it is known that positive ions tend to dissociate from the surface to make it negatively charged. It is also known that most protein surfaces contain both positively and negatively charged residues at neutral pH and that the neutrality can be altered by changing the pH of the buffer solution. For example, ferritin has an isoelectric point of about 5 and is positively charged at pH < 5 and negatively charged at pH > 5. Therefore it seems plausible to assume that electrostatic interaction is primarily responsible for adsorption. However, it must be also realized that most of these charged groups are shielded by counter-ions in solution. It is not clear whether it is the direct interaction between the oppositely charged groups or the salt bridges between like charged groups that is responsible for surface adsorption in each case (Jena and Hörber 2002).

2.2.5.6 *Sample preparation and image analysis*

AFM analysis was performed with an AFM Integra Probe Nanolaboratory (NT-MDT, Russia). A closed-loop sample scanning (100 mm scanner) and the semi-contact resonance mode were used in all measurements.

Freshly cleaved surface of muscovite mica, obtained from NanoandMore GmbH (Germany), was used as the atomically smooth substrate. The samples were prepared by dropping 10 µl of 10 mM HEPES solution of the Aβ40 peptide 30nM on mica and by subsequent solvent evaporation at room temperature. The analysis was performed with high accuracy non-contact composite (HA NC) etalon silicon tip cantilevers (NT-MDT, Russia) with a resonant frequency of 120 kHz, a tip radius of 10 nm and a spring constant of 3.4 N/m in air and at ambient temperature and humidity. A grain analysis as a part of the Nova™ image processing software was performed on scans with min. 200 counts with a 3 nm threshold. The z dimension of individual particles was used for the histogram analysis and the average particle diameter calculation (Malý et al., 2009).

2.2.6 **Cell biology techniques**

2.2.6.1 **In vitro toxicity models**

In vitro models and tests have been developed in response to the complexity of the *in vivo* cellular environment, and the difficulties and expense with conducting tests *in vivo*. Commonly used models in Alzheimer’s disease include primary neuronal cultures (Whitson et al., 1989; White et al., 1999; Opazo et al., 2002) and immortal cell lines, including human neuroblastomas (SH-SY5Y) (Hughes et al., 2010), mouse albino neuroblastomas (Neuro-2A) (Dahlgren, et al. 2002) and (PC12), a cell line derived from a pheochromocytoma of the rat adrenal medulla.(Poduslo et al., 2010).

Cell lines differ in their sensitivity to Aβ. Aβ(25-35) was over 200 fold more toxic to PC12 cells than Neuro-2A cells (Calderón et al., 1999). Aβ showed a higher propensity to bind to PC12 cell membranes than a range of other models, including a neuronal cell line, cortical primary neurons and hippocampal primary neurons (Simakova and Arispe 2007).

In order to study the possible biological significance of the current study two different cell lines were chosen: SH-SY5Y, a neuroblastoma cell line and PC12. According to what has been previously described, PC12 have a negatively charged outer surface of the cell membrane because they chronically express PS onto the outer leaflet of the bilayer (they are chronically pre-apaoptotic) (Lee et al. 2002; Simakova and Arispe 2007).

SH-SY5Y is one of three serially isolated neuroblast clones (SH-SY, SH-SY5, SH-SY5Y) of the human neuroblastoma cell line SK-N-SH which was established in 1970 from a bone marrow biopsy of a metastatic neuroblastoma site in a four year-old girl (Biedler et al., 1973). The SH-SY5Y cell line has become a popular cell model for neurodegenerative disease research because this cell line possesses many characteristics of DAergic neurons. For example, these cells express tyrosine hydroxylase and dopamine-beta-hydroxylase, as well as the dopamine transporter. Moreover, this cell line can be differentiated into a functionally mature neuronal phenotype in the presence of various agents. (Xie, Hu, and Li 2010).

2.2.6.2 Cell culturing

Cell line PC12, derived from apheocromocytoma of the rat adrenal medula, was grown at 37^0C with $5\%CO_2$ in DMEM, containing 7.5% of Horse HS and 7.5% of FBS, 2 mM Glutamine and penicilin/streptomycin(100 U/ml / 100 µg/ml)

Cell line SH-SY5Y, derived from human neuroblasome bone metastatic tumor, was grown at 37^0C with $5\%CO_2$ in DMEM/Ham's F12 medium, containing 10% of inactivated FBS, 2 mM Glutamine and penicilin/streptomycin(100 U/ml / 100 µg/ml)

Dulbecco’s Modified Eagle Medium (DMEM) was developed in 1969 and is a modification of Basal Medium Eagle buffered with HEPES and sodium bicarbonate sodium pyruvate (source of energy) and L-glutamine (amino acid). DMEM has twice the amino acid concentrations of BEM, has four times the vitamin concentrations, 1000 mg/L of glucose and uses twice the HCO_3- and CO_2 concentrations to achieve better buffering. DMEM is suitable for most types of cell (Freshney, 2000). It was shown that the levels of albumin (possible Cu chelator) in blood plasma, e.g. in FBS and HS, is much higher than found in the CSF and brain interstitium, where Aβ-Cu(II) interactions are thought to take place. For example in humans albumin is present at 600 µM in blood plasma, but only at ~3 µM in the CSF (Carter and Ho, 1994), which could be achieved by reducing of FBS content to 1%. Consequently, DMEM media (Gibco) with only 1 % of FBS added was used for all Aβ treatment experiments.

Cultures were incubated in a 5% CO_2 humidified atmosphere at 37°C. Cells were seeded at a density of 1.2×10^5 cells/cm^2 and starved in 1% (v/v) FBS for 24 h before any treatment. Medium was changed every 3 days and cells were passaged every 4-5 days. Cells were seeded at a $2.0*10^4$ cells/cm^2 density onto poly-D-lysine–precoated wells and starved at 1% (vol/vol) FCS for 24h before treatments.

2.2.6.3 Toxicity assay

The toxic effects of spontaneous Aβ fibrillation and Cu(II)-induced-aggregation of Aβ on cell cultures were assessed.

There are numerous methods to evaluate the toxicity of a compound to cells. Although none of these assays can reliably predict toxicity *in vivo* they are useful tools to compare different treatments and are widely used to indicate toxicity at a basic level. An overview is given below:

The number of surviving cells are quantified as a percentage of the number of live cells counted after plating (Whitson et al., 1989). Counting cells stained with trypan blue can also be used as a measure of cell viability (Pike et al., 1993).

The 3-(4,5-Dimethylthiazol-2-yl)-2,5-Diphenyltetrazolium Bromide Assay 3-(4,5-dimethylthiazol-2-yl)-2,5-diphenyltetrazolium bromide (MTT) is traditionally the most widely used measure of cell viability since it was developed by Mosmann in 1983 (Mosmann, 1983). MTT is a tetrazolium salt that produces a yellow solution when dissolved in water. Active mitochondrial dehydrogenases in metabolically active cells will convert MTT to insoluble purple formazan crystals. This change will not occur in dead cells. The insoluble formazan is solubilized by the addition of cell lysis buffer, and the absorbance at 570 nm was measured.

For cell viability assay MTT solution (5 mg/ml in PBS, pH 7.4) were added to all wells. The plates were covered in aluminum foil and incubated at 37°C for 4 h. The fluorescence was read at 570 nm on a VICTOR3™ multilabel reader. Where percentage of cell viability (or percentage of cell growth), was calculated as:

$$\frac{F - F_{\text{buffer}}}{F_{\text{cells}} - F_{\text{buffer}}} \cdot 100\,\%,$$

where F is the MTT fluorescence, F_{buffer} is the buffer fluorescence only F_{cells} is the fluorescence of cells with no treatments.

Peptide and its derivatives were added in different conditions and was incubated with cells 24 hours. After incubation cell metabolism was measured using the MTT test. Cells were incubated with MTT 0.5mg/ml in culture medium for 2 hours, then the medium was removed and cells dissolved in DMSO. The absorbance was measured using a Victor's 3 plate reader (Perkin Elmer).

Before experiments, the cells were plated at a density of approximately 2×10^4 viable cells per well in 96-well plates (for MTT assay).Thiazolyl Blue Tetrazolium Bromide (MTT) assay performed as previously described by Hansen et al. 1989, with minor modifications. MTT was added 24 hours after cell treatment at a final concentration of 0.5 g/L for cells or 0.2 g/L and incubated at 37ºC in a CO_2 incubator for 45 min. Then, MTT medium was removed and the resulting formazan dye was solubilised with dimethylsulfoxide.

All protocols used in this thesis for culturing cells were taken from “Culture of animal cells" (Freshney, 2000). In the Figure 2.23 is indicated the scheme of experiment used to evaluate the cell viability.

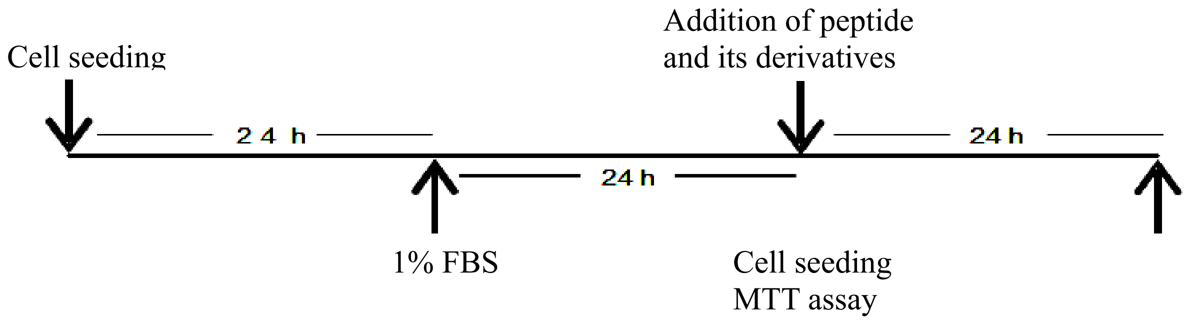

Figure 2.23. Cell treatment procedure. Sequence of events: 24 hours after seeding, FCS was reduced to 1% ; the MTT test was run 24 hours after treatment with peptide and its derivatives.

To compare either several different treatments or the influence of two or more factors at the same time the most appropriate method of statistical analysis of such experiments is analysis of variance (ANOVA)(Miller and Brown, 1997).

3 RESULTS

3.1 INFLUENCE OF CU(II) ON Aβ AGGREGATION

3.1.1 Introduction

Alzheimer disease is characterized by extracellular amyloid plaques, composed predominately of 39-43 amino acids β -amyloid peptides. Soluble Aβ40 and Aβ42 (the major components of plaques) are present in the cerebrospinal fluid (CSF) and blood plasma from birth (Vigo-Pelfrey et al., 1993; Lambert et al., 1998), but the trigger that promotes oligomerisation and fibril formation is a subject of hot debate.

A notable characteristic of AD is also altered metal ion concentration in the brain and disrupted metal ion homoeostasis (Dong et al., 2003). Physiological levels of Cu(II) induce aggregation of Aβ (Atwood et al., 1998, 2002; Bush, 2003). Copper interactions with the Aβ are believed to play a role in Alzheimer's disease (AD), in particular due to production of reactive oxygen species and Cu(II)-mediated oligomerization (Bush, 2003; Barnham and Bush, 2008, 2008; Jiang et al., 2010; Sarell, Wilkinson, and Viles, 2010b). To understand the role that copper might play in these processes, a detailed knowledge of the fundamental Cu(II)/Aβ interactions is essential. Growing evidence suggests that copper ions play an important role in the pathogenesis of AD by inducing protein misfolding and generating reactive oxygen species (Drew et al., 2010). Numerous mechanisms of possible Aβ and Cu(II) interactions proposed often come into conflict and still remain inconclusive. Some reports find that Cu(II) acts as a neuroprotectant by preventing formation of toxic Aβ species (Yoshiike et al. 2001; Zou et al. 2002), whereas others suggest that Cu(II) induces Aβ structures that are neurotoxic (Kirkitadze, Bitan, and Teplow 2002). One proposal for explaining a neurotoxicity induced by interaction with Cu(II) is that it results from changes in the Cu(II) coordination environment during Aβ oligomerization or as a function of Cu(II) concentration (Smith et al. 2007). So it is important to characterize the interaction of Cu(II) cations with Aβ monomers, that area has not been yet explored in detail and unravelling the influence of copper on Aβ oligomerization is potentially important in understanding of AD.

One of the aims of the present work was to establish the link between the influence of Cu(II) ions on Aβ40 monomer morphology and fibrillation properties and as well the effect of Aβ40-Cu(II) complexes on cell toxicity. For this study, spectroscopy techniques, SAXS, AFM, TEM and toxicity assays were applied. The present chapter reports that initially Cu(II) anchors to the Aβ40 monomers favouring the the formation of 330±50 kDa oligomers, which after additional protonation aggregate into amorphous non-fibrillar toxic aggregates.

Recent x-ray absorption fine structure (EXAFS) provided a similar x-ray absorption spectra for the full-length Aβ42 and a Aβ16 Cu(II) binding site. Cu(II) binds to the three histidines (His-6, His-13 and His-14) and a carboxylate oxygen from either Glu-11 or Asp-1 residue (Streltsov et al., 2008). It has been also shown that the full-length Aβ40 and Aβ42 and also truncated Aβ28 and Aβ16 peptides bind Cu(II) in the same coordination environment (Karr 2007). Previous studies of Aβ42 aggregation in the presence of Cu(II) were compatible with the conclusions for Aβ40 (Pedersen et al., 2011). On this basis it has been proposed that under the same experimental conditions Aβ42 will bind Cu(II) in a similar way as Aβ40.

Aβ is constitutively anabolised and catabolised in the brain throughout life in all humans. The conditions or agents that prevent Aβ monomers from oligomerisation and fibril formation is unknown but it was shown previously that Aβ40 peptide had no tendency to aggregate at alkaline pH 11 (Wood et al., 1996). In suspension at pH 11, Aβ40 peptide is present in equilibrium of monomers and low molecular weight oligomers. At this pH the secondary structure of Aβ40 peptide can be described as a mixture of unordered and α-helical structures. Diluting the alkaline pH 11 to the neutral pH 7.4 brings a slow self-association of monomeric Aβ40 peptide in a random coi1 conformation to form an oligomeric nucleus with intermolecular non-fibrillar β-structures and after that fibril growing with a β-sheet secondary structure undergoes in a nucleation-dependent pathway (Benseny-Cases et al., 2007; Roychaudhuri et al., 2009).

In the present work pH 11 was used to model *in vitro* the conditions favouring the equilibrium for the monomeric Aβ40 species. In order to investigate the effect of Cu(II) ions on the morphology of monomeric Aβ species, loading of Aβ40 with Cu(II) was performed at pH 11.

In this study Aβ40 at pH 11 is denominated as Aβ40_{pH11}, Aβ40 equilibrium of monomers and low molecular weight oligomers: (Aβ$40_{m\leftrightarrow o}$), Aβ40 loaded with Cu(II) at pH 11 hereinafter is referred to as Cu(II)-Aβ40_{pH11}.

3.1.2 Structure and morphology of Cu(II)- Aβ40_{pH11} complex at basic pH

3.1.2.1 AFM

Atomic Force Microscopy (AFM) was used in order to investigate the effect of Cu(II) ions on monomeric Aβ$40_{m\leftrightarrow o}$ morphology.

AFM provides a means to image without the need for negative staining and allowed to estimate the shape and size (height) of the particles. Aβ40 and Cu(II)-Aβ40_{pH11} species were imaged on a mica surface at ambient conditions and the non-contact scanning mode. The images were collected after dilution by a factor 10^4 of 250 μM stock suspension of Aβ40.

The AFM morphology analysis of the Aβ40 at pH 11 (Aβ40_{pH11}) in the absence of Cu(II) revealed only small spherical objects which can be described as a population of monomers and low molecular weight oligomers. No fibrillar or amorphous assemblies were detected at this pH. The average height and standard deviation of 191 Aβ40 particles are 2.4 and 0.3 nm respectively (Figure 3.1).

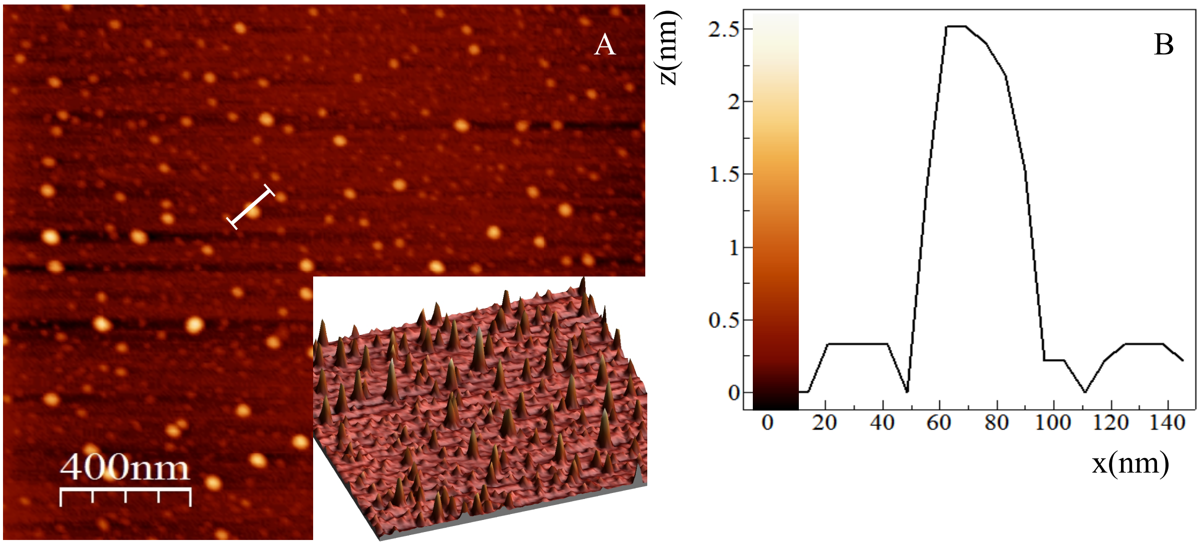

Figure 3.1 AFM characterization of morphology of Aβ40 at pH 11. (A) The planar and 3D look image of Aβ40 peptide. (B) The heigh of an average Aβ40 particle. Pixels with a height below 0.5 nm are considered as noise.

The AFM morphology analysis of the Cu(II)-Aβ40$_{pH11}$ shows a significant difference with respect to the Aβ40$_{pH11}$. (Figure 3.2). The average height and standard deviation of 89 Cu(II)-Aβ40 Aβ40$_{pH11}$ particles makes 13 nm and 4.8 nm respectively. This is up to 5 times greater than those of Aβ40$_{pH11}$. The number of particles seen on the mica surface is reduced compared with Aβ40$_{pH11}$ alone. Significantly that no fibrillar or amorphous assemblies were detected at this condition.

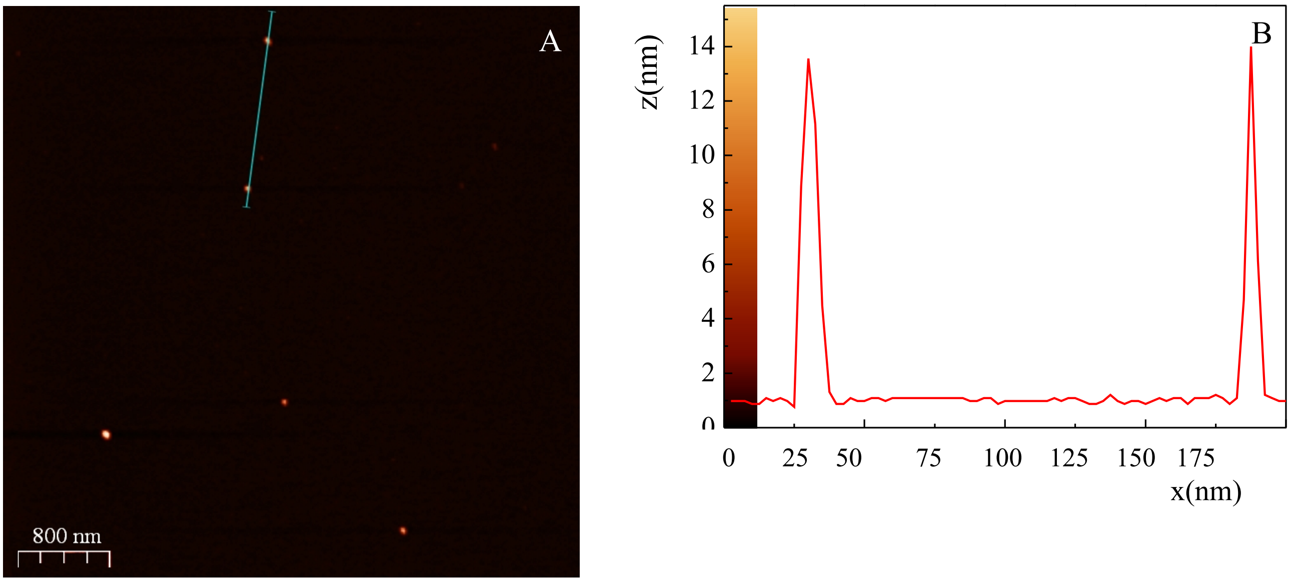

Figure 3.2 AFM characterization of morphology of Cu(II)-Aβ40$_{pH11}$ particles. (A)The planar images of of Cu(II)-Aβ40$_{pH11}$. (B) The heights of the aggregates. Pixels with a height below 1 nm are considered as noise.

The results of the AFM analysis are summarized in the histogram and presented in Figure 3.3. The population of Cu(II)- Aβ40$_{pH11}$ is presented by the particles of bigger size than that of Aβ40$_{pH11}$. This indicates that Cu(II) causes the oligomerization of Aβ40 at high pH.

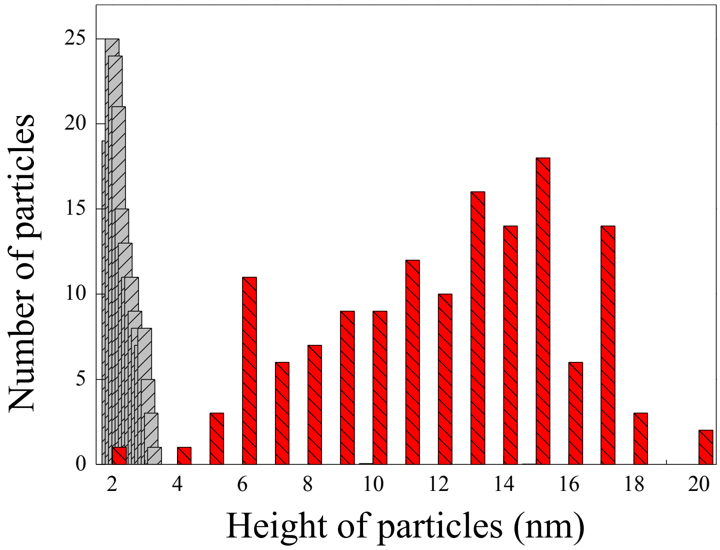

Figure 3.3 The height distribution of Aβ40$_{pH11}$ and Cu(II)-Aβ40pH11 particles. Red columns correspond to Cu(II)-Aβ40$_{pH11}$, dashed grey columns represent the height distribution of Aβ40$_{pH11}$.

3.1.2.2 SAXS

SAXS probes the structure of native biological macromolecules in solutions at a low (1–2 nm) resolution. The SAXS patterns directly provide parameters such as molecular weight (MW), maximum diameter (D_{max}) and particle excluded volume.

SAXS patterns are shown for Cu(II)-Aβ40$_{pH11}$ and Aβ40$_{pH11}$ in Figure 3.11. As it can be seen, the nature of two solutions is different. As a step for SAXS data treatment, a Guinier plateau has to be calculated (see section 2.2.3.1). A Guinier plot can indicate the aggregation that primarily affect the further SAXS data treatment. From the obtained SAXS data Guinier plateau was found and $p(r)$ was calculated only for Cu(II)-Aβ40$_{pH11}$. For Aβ40 peptide no Guinier plateau was possible to find. Guinier plots with a sharp increase in intensity at very small values of s mean that samples contain significant inter-particle repulsion. This can indicate that the oligomerization of Aβ40 induced by Cu(II) weakens the inter-particle repulsion.

In the indirect transform program GNOM (Svergun, 1992), the solution yielding the p(r) function is evaluated using perceptual criteria, providing with the means to easily identify reliable solutions and to obtain an optimal value of D_{max}. This procedure has also been automated in the program AUTOGNOM (Petoukhov and Svergun, 2007), where multiple GNOM runs are performed across a range of D_{max} values. The parameters estimated from the indirect Fourier transform approach I(0)

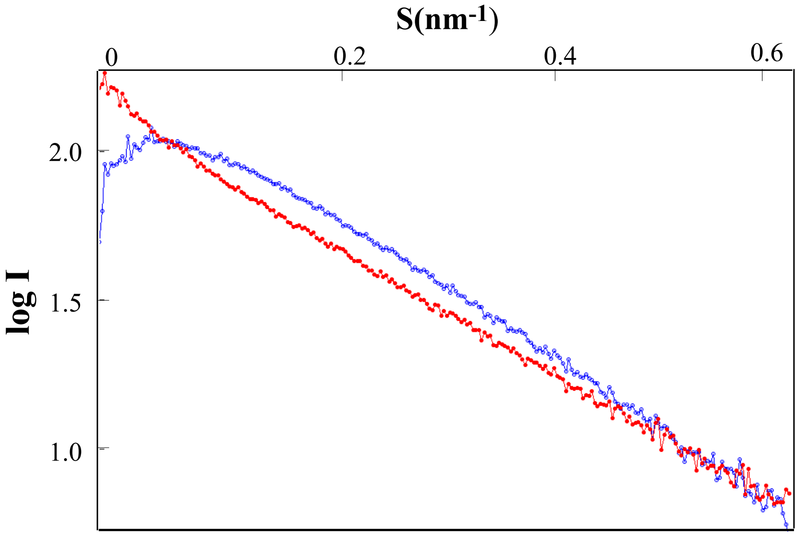

Figure 3.4 The experimental SAXS profiles. SAXS patterns of Aβ40 alone and Cu(II)-Aβ40$_{pH11}$. The concentration of peptide of each sample was 1.2 mg/ml in 10m M HEPES at pH 11, the temperature was 37^{0}C.

and, R_g, are more accurate than those obtained from a Guinier analysis as the entire scattering curve is used for their estimation. Figure 3.5 represent the best fit of the theoretical model calculated using GNOM to the experimental data and $p(r)$ calculated for Cu(II)-Aβ40$_{pH11}$. The distance distribution function $p(r)$ gives the maximum length in the particle, D_{max}, by the position where $p(r)$ smoothly returns to zero at large values of r. In the Figure 3.6 a theoretical example of distance distribution function $p(r)$ is presented indicating that globular macromolecules have a $p(r)$ function with a single peak, while elongated macromolecules have a longer tail at large r and can have multiple peaks (Putnam, Hammel, Hura, and Tainer, 2007a).

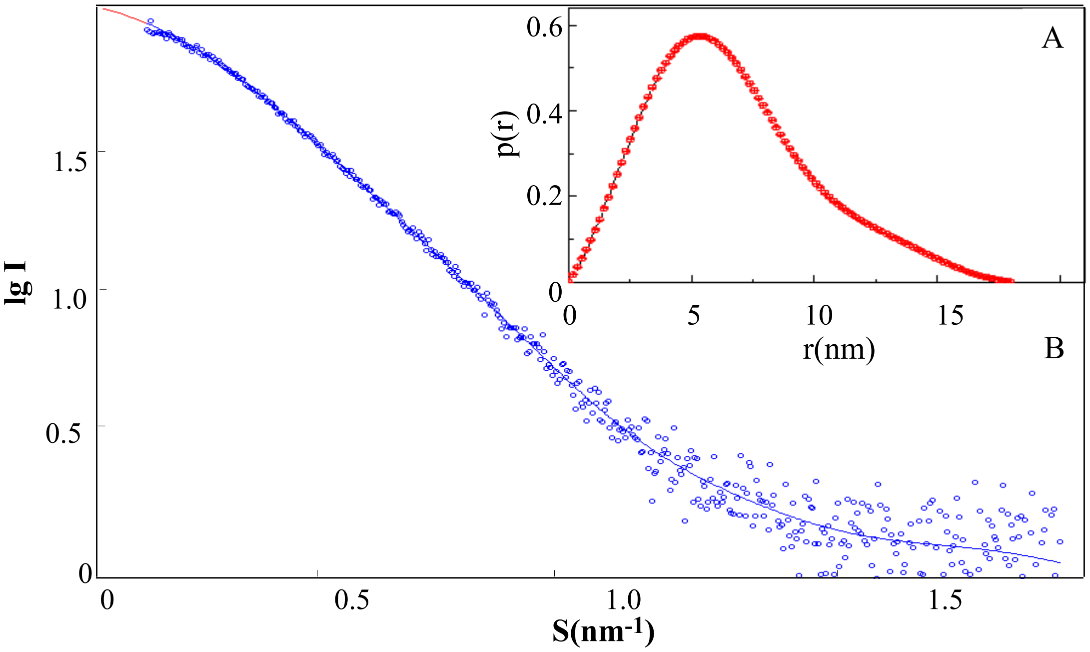

Figure 3.5 The distance distribution function. (A) The distance distribution function p(r) Cu(II)-Aβ40$_{pH11}$ with a single peak corresponds to the quasi globular shape with D_{max}≈17 nm. (B) The best fit for the model calculated shown here as a blue line, blue circles correspond to the experimental data.

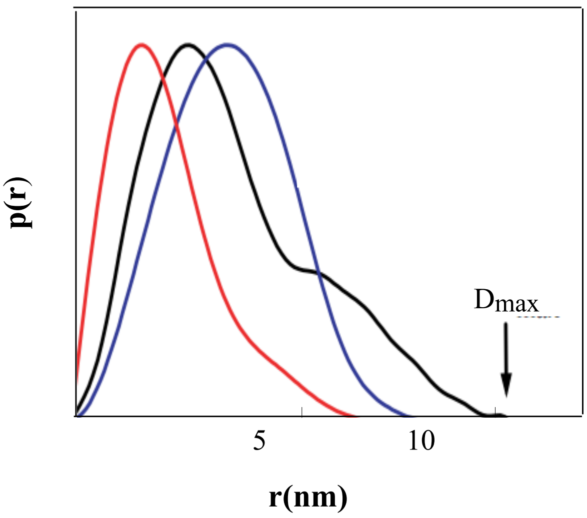

Figure 3.6 The distance distribution function. Theoretical $p(r)$ calculated for proteins with different structures. Red line corresponds to the $p(r)$ of unfolded, black: multidomen, blue: globular proteins. Adapted from Putman at al. 2007.

The reconstruction of low-resolution 3D models from SAXS data alone is a procedure where scattering patterns were computed from different geometrical shapes starting from a random initial approximation by simulated annealing and compared with experimental data using DAMMIN (for more details see chapter 2.2.3.2). From ten independent reconstruction runs a 3D model of Cu(II)-Aβ40$_{\mathrm{pH11}}$ particle was calculated. Maximum diameter is 16.8 ± 0.8 nm, a molecular weight is 330 ± 50 kDa. This suggests that Cu(II)- Aβ40$_{\mathrm{pH11}}$ particle consists of 80±10 Aβ40 monomers (Figure 3.7).

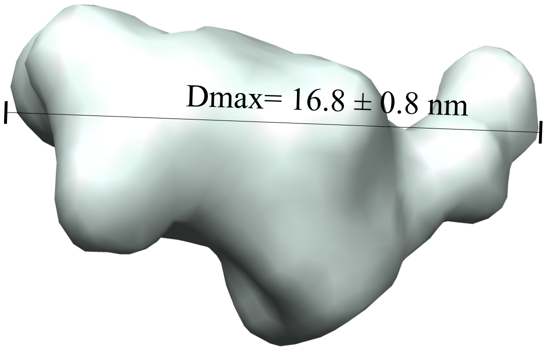

Figure 3.7 3-Dimensional model of the Cu(II)-Aβ40pH11 particle. Here is presented an average model of of the Cu(II)-Aβ40pH11 particle in solution after 10 independent DAMMIN reconstructions.

For the study of protein folding the Kratky plot can be used as an indication of the folded/unfolded state. Folded globular proteins typically yield a prominent peak at low angles whereas unfolded proteins show a continuous increase in $s^2I(s)$ with s (for more details see section 2.2.3.1). Globular macromolecules follow Porod's law and have bell-shaped curves. Extended molecules, such as unfolded peptides, lack this peak and have a plateau or are slightly increasing in the larger s-range (Putnam, Hammel, Hura, and Tainer, 2007b). Kratky plot calculated using GNOM shows that Aβ40 peptide in the presence of Cu(II) is not identically folded as peptide alone (Figure 3.8).

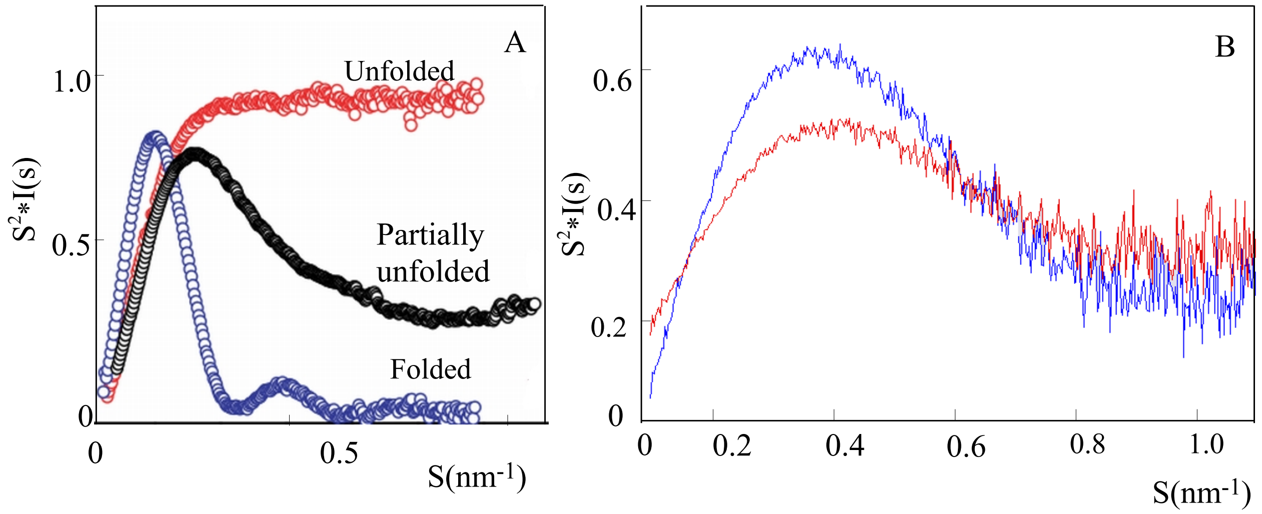

Figure 3.8 Gradations of folding as monitored by SAXS. Kratky plots have the form of $I(s)s^2$ against s, where $I(s)$ is the scattering intensity and s is related to the scattering angle. In a Kratky plot, an inverted parabola indicates a well-folded structure. (blue curve) More pronounced peaks indicate more folded structures. A plot with a tail rising "to the right" (increasing x-axis) indicates unfolding, a black curve corresponds to partially unfolded protein, red one to unfolded protein. (A) Red plot corresponds to the $s^2I(s)$ of unfolded, black: partialy unfolded, blue: folded proteins. Adapted from (Putnam, Hammel, Hura, and Tainer, 2007a). (B) Blue pattern corresponds to Cu(II)-Aβ40pH11, red pattern: to Aβ40 alone.

3.1.2.3 TEM

To complete the SAXS data with morphology data the sample of Cu(II)-Aβ40$_{pH11}$ was analysed under transmission electron microscope. The particle dimensions of Cu(II)- Aβ40$_{pH11}$ assumed by SAXS match those observed by TEM. On the electron micrograph Cu(II)- Aβ40$_{pH11}$ can be described as a multitude of particles with diameters close to 20 nm. The presence of fibrillar forms was not detected. (Figure 3.9). It was not possible to detect any object in the case of Aβ40$_{pH11}$ under the same conditions due to restriction of TEM resolution.

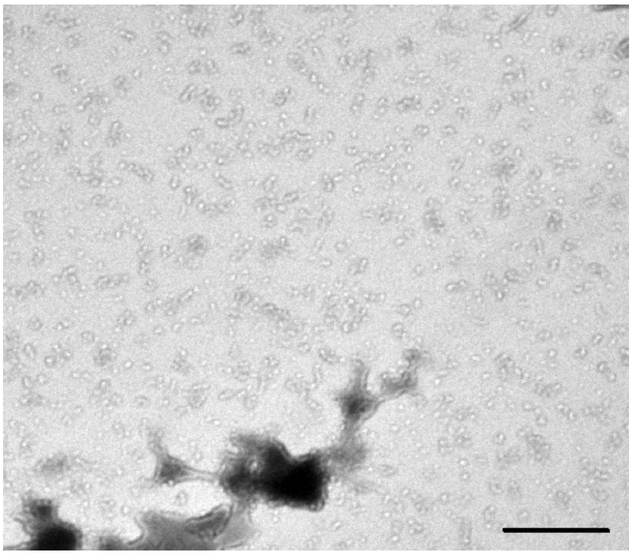

Figure 3.9 Electron micrograph of granular non-fibrillar aggregates of Cu(II)-Aβ40Aβ40$_{pH11}$. Representative TEM micrograph image shows Cu(II)- Aβ40$_{pH11}$. The sample aliquots for EM images were collected after 24 hours of incubation at 37^{o}C at pH 11. 200 nm is an equivalent of the bar scale.

3.1.2.4 **FTIR**

In order to get information on conformational changes of Aβ40 caused by Cu(II) binding at pH 11, the FTIR spectral changes were measured in amide region I. The Fourier Transform of Infra Red (FTIR) spectra of Aβ40$_{pH11}$ and Cu(II)-Aβ40$_{pH11}$ were measured (Figure 3.10).

FTIR spectra show that Aβ40$_{pH11}$ has a maximum around 1642 cm^{-1}. This band can be assigned to a mixture of structures corresponding to unordered (1640-45 cm^{-1}) and α-helical (≈1650 cm^{-1}) structures (Figure 3.10). The infrared band of Cu(II)-Aβ40pH11 shows its maxima at 1635 cm^{-1} that can be assigned to β- structures. There is also a shoulder a 1650 cm^{-1} that can be assigned to the absorption of unordered structures. FTIR proves that at pD11 Aβ40 alone was not aggregated since none band around 1620 cm^{-1}, typical for aggregated, either fibrillar or non-fibrillar structures, was detected.

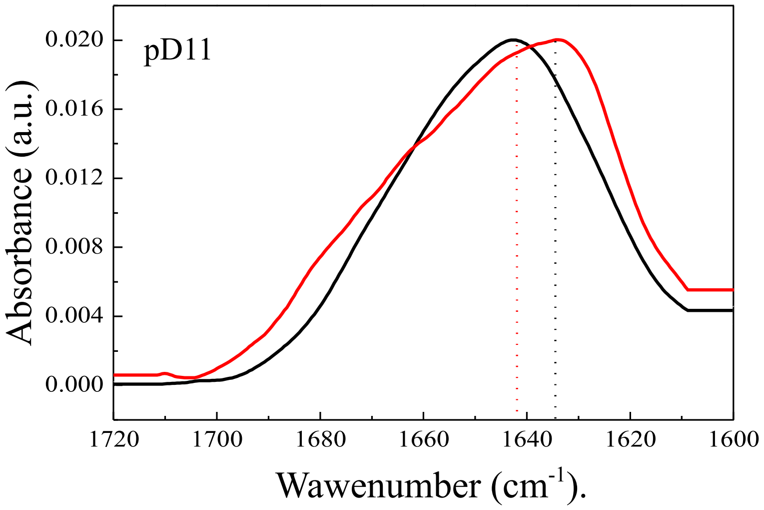

Figure 3.10 Conformational characterization of Aβ40 and Cu(II)-Aβ40 Aβ40$_{pH11}$. The FTIR spectra of Aβ40$_{pH11}$ and Cu(II)-Aβ40pH11 in the amide I region at alkaline pD. Black curve: a freshly prepared 80 µM Aβ40 peptide. Red curve: Cu(II)-Aβ40pH11. Spectra are normalized against their area. No time evolution of the FTIR spectra of the amide I region was observed for both samples.

Brief summary of results obtained

The data provided with three different techniques such as AFM, TEM and SAXS evidence that at basic pH Cu(II)- Aβ40$_{pH11}$ formed small aggregates with approximately 20-nm-diameter, molecular weight 330 ± 50 kDa (equivalent of 80±10 Aβ40 monomers). Complemented with FTIR data it can be suggested that those aggregates characterized by a mixture of β- and unordered structures.

3.1.3 Structure and morphology of Cu(II)-Aβ40 aggregates at pH 7.4

3.1.3.1 ThT fluorescence spectroscopy

In order to investigate the effect of Cu(II) ions on Aβ40 fibril formation capacity, ThT assay was applied to monitor the β-sheet formation. ThT is a highly selective dye the fluorescence of which depends on the formation of amyloid fibrils but does not detect amorphous non fibrillar aggregates, presumably because of the lack of repetitive structures (LeVine, 1993).

As it was reported previously, a typical fibril growth curve, monitored by ThT fluorescence characterizes aggregation of Aβ40 at pH7.4. Lowering the pH from 11 to 7.4 sets the reaction of fibrillization: first Aβ40 forms small oligomers which rapidly combine to form nuclei and after a lag phase fibrils start to grow exponentially. Inspection of the Aβ40 aggregation ThT curve indicates that all typical fibril grow features are available: the nucleation, elongation and saturation phases (Benseny-Cases et al., 2007).

When Cu(II) ions are added to Aβ40 and then pH is diluted to pH 7.4 no ThT fluorescence characterizing ThT positive β-sheet fibrils since no variation of the ThT fluorescence for this sample was found (Figure 3.11).

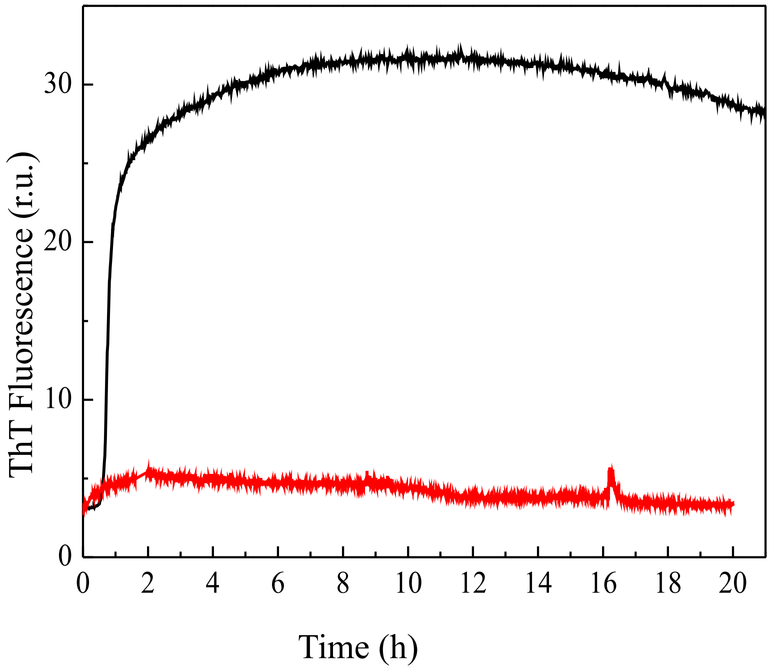

Figure 3.11 Time course studies of Cu(II)-Aβ40$_{pH11}$ aggregation by ThT fluorescence assay. The aggregation assay reaction mixtures containing 25μM Aβ40 alone (black graph) and 25μM Cu(II)-Aβ40$_{pH11}$ (red graph). Red graph shows that no fibrils grew in case of Cu(II)- Aβ40$_{pH11}$ and with time no variation of the ThT fluorescence was detected. Cu(II) was added to the Aβ40 suspension at pH 11 (peptide-to-metal ratio was 1 to 1), then the peptide-metal suspension was incubated at pH 7.4. Black graph reveals that the fibrillar structures grow from Aβ40. Graph shows the results from the real time ThT fluorescence measurements. Samples were incubated at pH 7.4, at least 20 hours, at 37°C with gentle agitation.

3.1.3.2 **TEM**

In order to study the morphology of Cu(II)-Aβ40$_{pH11}$ at pH 7.4, for TEM study the aliquots were taken from the corresponding Cu(II)-Aβ40$_{pH11}$ and Aβ40$_{pH11}$ ThT aggregation mixtures after 24 hours of incubation at pH 7.4, at 37 °C. Figure 3.12 represents images of the Aβ40 and Cu(II)-Aβ40$_{pH11}$. Incubation of Cu(II)-Aβ40$_{pH11}$ at pH 7.4 has been show to favour the formation of large amorphous granular aggregates.

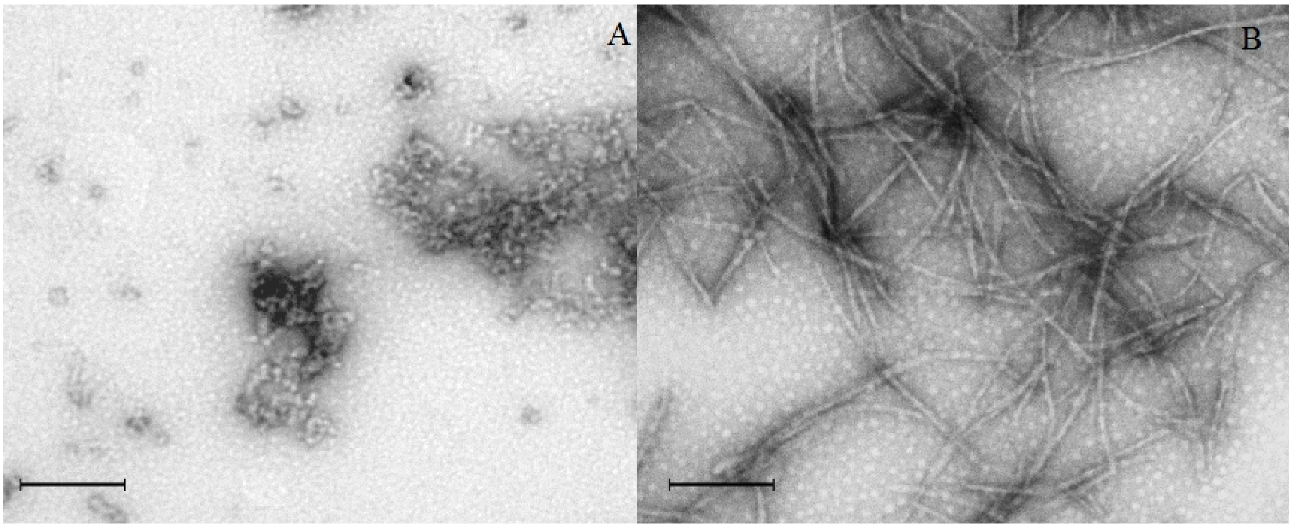

Figure 3.12. Morphology of Aβ40 and Cu(II)-Aβ40pH11. Representative TEM micrographs show that Cu(II)-Aβ40$_{pH11}$ after incubation at pH 7.4 during 24 hours formed amorphous granular aggregates (A) meanwhile Aβ40 formed fibrils(B).

3.1.3.3 **FTIR**

In order to get information on conformational changes of Cu(II)-Aβ40$_{pH11}$ caused by pH 7.4, the FTIR spectra of Cu(II)-Aβ40$_{pH11}$ were measured at pD7.6.

As it was previously shown by our research group, the FTIR spectra of the Aβ40 alone at pD 7.6 are dominated by an amide I vibration at 1623 cm^{-1} characteristic of β-sheet secondary structure and characterized by a kinetic of structural changes during a time. The absorbance corresponding to the band at 1623 cm^{-1} increases meanwhile the absorbance corresponding to the band centred at 1640 cm^{-1} (unordered and helical structures) decreases. That means that there is a change of conformation from unordered to a β-sheet structure (Benseny-Cases et al., 2007).

In Figure 3.13 shown are the FTIR spectra of the Cu(II)-Aβ40pH11, all spectra represent a broad band centred at 1633 cm^{-1}. that can be assigned to a β-structure. Basing on this band shift it is assumed that the hydrogen bounds involved in the β- structures of Cu(II)-Aβ40pH11 are weaker than those in β-sheet structure of Aβ40.

It is important to note that from the infrared spectra it is not possible to distinguish fibrillar from non-fibrillar β-structures. However, when equivalent samples to those used for infrared spectroscopy where analysed using the fluorescent dye ThT (Figure 3.11) and complemented by transmission electron microscopy (Figure 3.12), the conclusion is drawn that the β-intermolecular structures of Cu(II)-Aβ40$_{pH11}$ correspond to non-fibrillar amorphous aggregates.

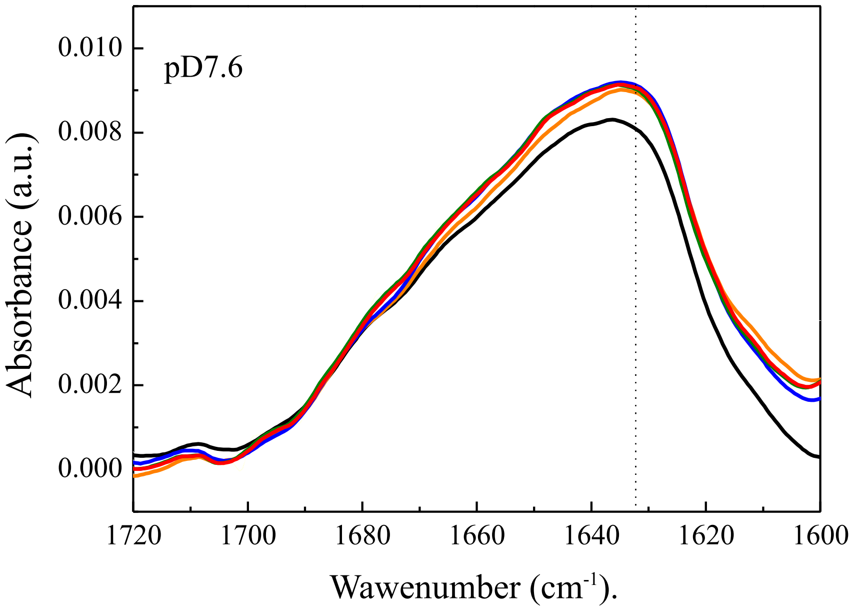

Figure 3.13 The FTIR spectra of Cu(II)-Aβ40$_{pH11}$ in the amide I region. The variation of the amount of β-structure as a function of time. FTIR spectra of Cu(II)-Aβ40$_{pH11}$ were acquired in 30 min. steps. Cu(II) was added to suspension of Aβ40 at pD11, then the mixture was adjusted to the neutral pD 7.6 (pH=7.4). Black spectrum corresponds to Cu(II)-Aβ40$_{pH11}$ at pD11, spectra presented by other colours were measured after adjusting to pD 7.6.

3.1.3.4 Tyrosine intrinsic fluorescence

Changes in intrinsic fluorescence can be used for studying the structural changes (Lakowicz 2006). Monitoring intrinsic tyrosine fluorescence during fibril formation revealed changes in the shape and intensity of the tyrosine emission spectrum. The decrease in tyrosine intensity parallels the assembly of Aβ40 into fibrils, due to the formation of β-sheet, which leads to the changing of neighbourhood of tyrosine 10 (Munishkina and Fink, 2007).

It was shown previously that Cu(II) causes quenching of the tyrosine fluorescence signal if added to the Aβ40 at pH 7.4. (Karr et al., 2005; Sarell, Wilkinson, and Viles, 2010a).

To examine the effect of Cu(II) binding on local conformational changes near the tyrosine 10 of Cu(II)-Aβ40$_{pH11}$ complex, the intrinsic fluorescence of tyrosine 10 was investigated. In these studies the final concentration of Aβ40 was 25 µM. For the studies with monomeric Aβ40, Cu(II) was added to the peptide at pH 11. Then just before measurements the pH of samples was diluted to pH 7.4. For the studies with fibrillar Aβ40, Cu(II) was added after fibril formation had occurred, after 24 hours incubation at pH 7.4. For the fluorescence quenching experiments a four cells SLM-aminco 800 fluorescence spectrometer was used with an excitation of 285 nm and emission wavelength staring at 290 nm and finishing at 400 nm. 1 cm path length quartz cuvettes were uses with always the same set of stirrers.

First, the effect of pH and Cu(II) on tyrosine fluorescence for l-tyrosine was studied. The results show that one mole equivalent of Cu(II) ions did not cause significant quenching of intrinsic fluorescence of l-tyrosine. At pH 11 tyrosine is deprotonated, no tyrosine emission is possible. After protonation (dilution of pH from 11 to 7.4) l-tyrosine in the presence/absence of Cu(II) recovered its intrinsic fluorescence (Figure 3.14).

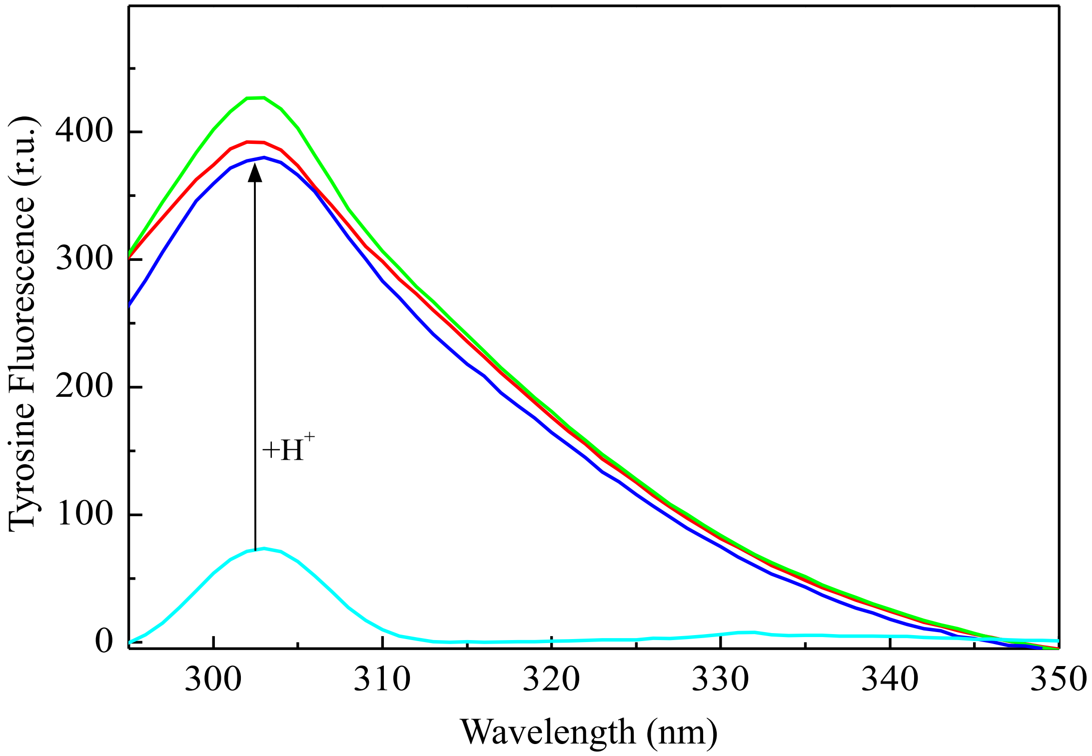

Figure 3.14 Tyrosine intrinsic fluorescence. Intrinsic fluorescence of l tyrosine is sensitive to the pH but not to Cu(II). Cyan spectrum corresponds to l-tyrosine at pH 11. Blue spectrum shows the recovery of intrinsic emission of l-tyrosine after changing pH 11 to 7.4. Green spectrum: Emission signal of l-tyrosine fluorescence at pH 7.4. Green, cyan and blue spectra were measured in the presence of Cu(II). Red spectrum: Intrinsic fluorescence of l-tyrosine alone at pH 7.2. λ_{exc} was 286 nm, λ_{em} was 290-350nm.

Next, the intrinsic tyrosine 10 of Cu(II)-Aβ40$_{pH11}$ was investigated. The results indicate that the florescence signal of the tyrosine 10 of Cu(II)-Aβ40$_{pH11}$ complex at pH7.4 was weaker by up to 80% contrary to the subsequent signal of Aβ40. The recovery of tyrosine fluorescence after protonation was not detected. Interestingly that no characteristic tyrosinate peak at ≈345 nm was detected on fluorescence spectra of the tyrosine 10 of aggregated Aβ40-Cu(II) complex (Figure 3.15).

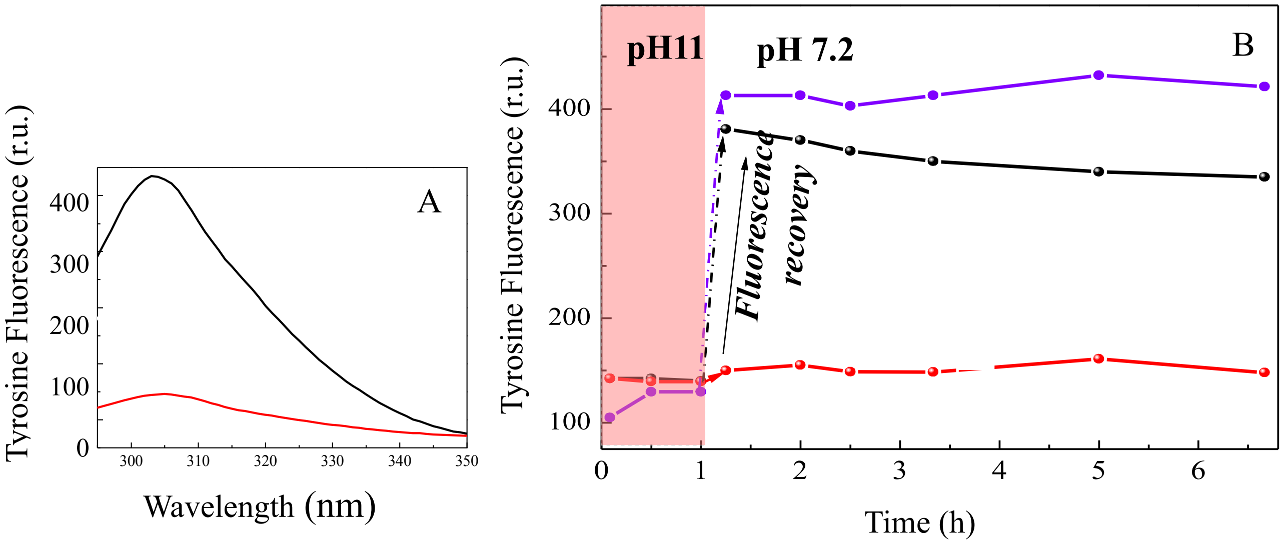

Figure 3.15 Effect of Cu(II) on Aβ40 tyrosine 10 intrinsic fluorescence. (A) Tyrosine intrinsic fluorescence is sensitive to Aβ40 secondary structure. Black spectrum: tyrosine 10 fluorescence signal of Aβ40. Red spectrum: tyrosine 10 fluorescence signal of Cu(II)-Aβ40$_{pH11}$. (B) Intrinsic tyrosine fluorescence is sensitive to the pH. Red dashed area shows the measurements at pH 11. White area corresponds to measurements at pH 7.4. Black line: intrinsic tyrosine 10 fluorescence signal of Aβ40. Red line : Cu(II)-Aβ40$_{pH11}$. Violet line: L-tyrosine in the presence of Cu(II). For these measurements λ_{exc} was 286 nm, λ_{em} was 290-350nm.

It was recently shown that even fibrils of Aβ40 once formed, retain their structure after Cu(II) additions *(Sarell et al., 2009)*. In the present work it was shown that at pH7.4 Cu(II) ions, without affecting the morphology of Aβ40 preformed fibrils, induce quenching of their tyrosine intrinsic fluorescence (Figure 3.16).

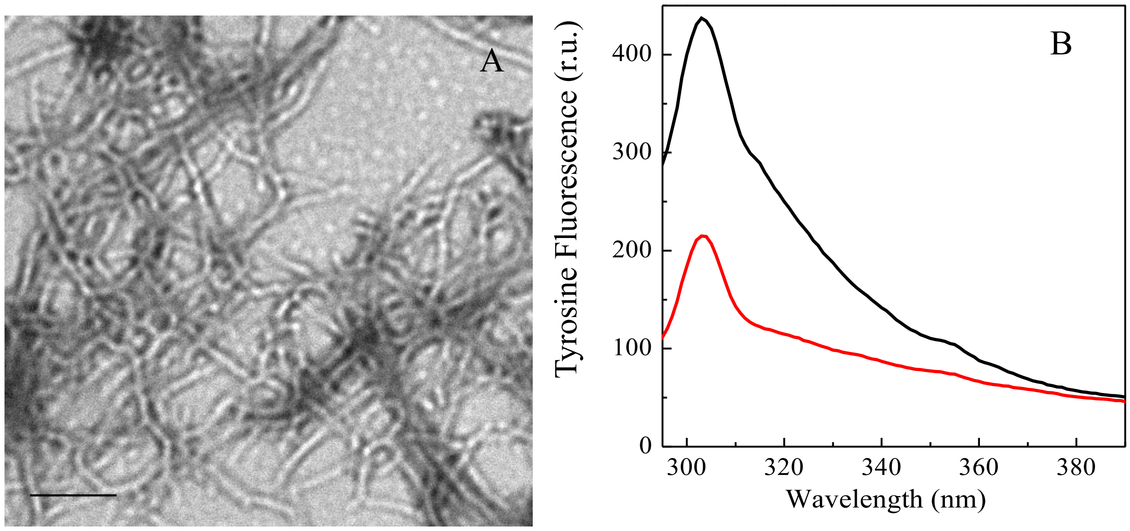

Figure 3.16 Morphology of preformed Aβ40 fibrils in the presence of Cu(II) and effect of Cu(II) on Aβ40 fibrillar tyrosine 10 fluorescence. (A) Aβ40 fibrils in the stoichiometric presence of Cu(II). Electron micrograph representative image reveals that Cu(II) ions did not disaggregated the performed Aβ40 fibrils. (Scale bar, 200 nm). (B) Intrinsic Tyrosine fluorescence spectra of Aβ40 fibrils alone (black curve) and Aβ40 fibrils in the presence of Cu(II) (red curve) show a significant tyrosine fluorescence decay. λ_{exc} was 286 nm, λ_{em} was 290-380nm.

3.1.3.5 Metal chelating effect on the structure of **Cu(II)-Aβ40$_{pH11}$**

To examine the possibility to convert the conformation of Cu(II)-Aβ40$_{pH11}$ amorphous aggregates to the fibrillar ones the ThT and tyrosine fluorescence of Aβ40$_{pH11}$ in the presence of a strong metal chelator was investigated. EDTA has a 10^{18} affinity for Cu(II) ions compared to the 10^{10} of Aβ (Sarell et al., 2009). EDTA was added to Cu(II)-Aβ40$_{pH11}$ at the peptide-metal-EDTA ratio 1:1:1 to compete for the Cu(II) ions. In the presence of EDTA no significant alteration in ThT fluorescence of Cu(II)-Aβ40$_{pH11}$ was detected. The tyrosine 10 fluorescence signal did not reappeared as well. Thus it seems unlikely that the Cu(II) ions were bond to Aβ in the presence of EDTA but Cu(II) ions clearance does not help to recuperate fibrillar conformation if amorphous aggregates once formed.

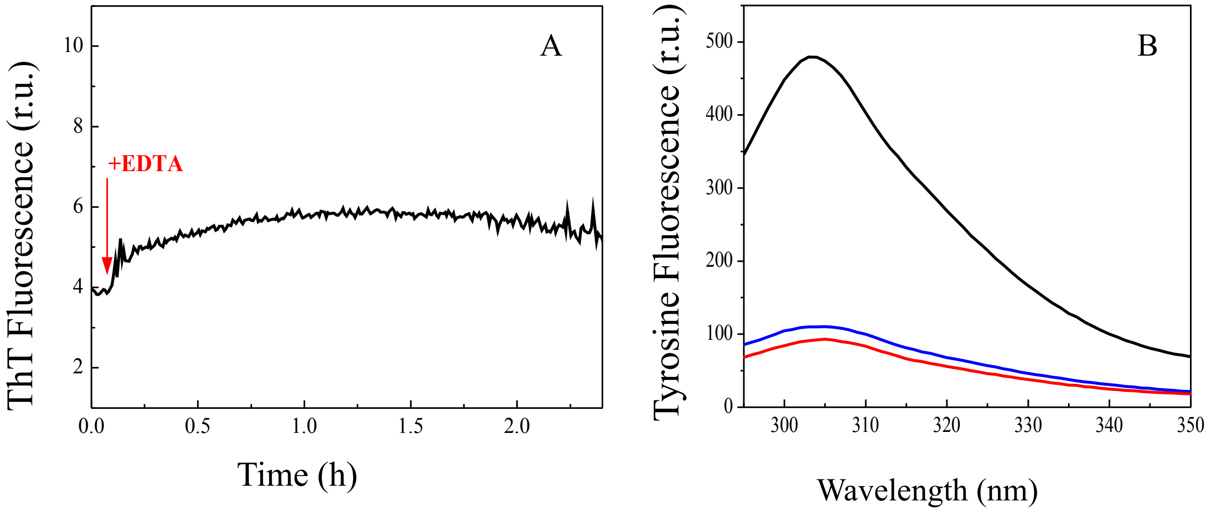

Figure 3.17 ThT fluorescence of Cu(II)-Aβ40$_{pH11}$ in the presence of EDTA. (A) No recovery of ThT emission was detected after adding EDTA to Cu(II)-Aβ40$_{pH11}$ in ratio 1 to 1. (B) No recovery of tyrosine 10 fluorescence signal was detected after adding EDTA. Black spectrum: Aβ40 fibrils, red spectrum: Cu(II)-Aβ40$_{pH11}$, blue spectrum: Cu(II)-Aβ40$_{pH11}$ in the presence of EDTA. Al measurement were done at pH 7.4.

Brief summary of results obtained

At pH 7.4 Cu(II)-Aβ40$_{pH11}$ form amorphous aggregates with non ThT positive β-structure. Basing on FTIR band shift it is assumed that the hydrogen bonds involved in the β-structures of Cu(II)-Aβ40pH11 are weaker than those in β-sheet structure of Aβ40.

Cu(II) ions cause alteration of Aβ secondary structure and irreversible decrease of the Tyrosine 10 intrinsic fluorescence.

Amorphous conformation of Cu(II)-Aβ40$_{pH11}$ complex is resistant: Cu(II) ions clearance does not let Aβ40 to recuperate its fibrillar conformation if amorphous aggregates already formed.

3.1.4 Structure and morphology of Cu(II)- Aβ28$_{pH11}$ complex at neutral pH

3.1.4.1 Introduction

Aβ has a hydrophilic N-terminal region and a more hydrophobic C-terminal region. Aβ has been investigated using its fragments. The C-terminal region, including residues 28-42, is significant for nucleation in fibril formation, but not essential. In contrast, the amino terminal region around residues 1-9 is not important for amyloid fibril formation (Hilbich et al., 1991). In the central region, Aβ(16-22) comprises a central hydrophobic core that is thought to be crucial in Aβ assembly. Aβ(11-25) has been found to form ordered amyloid fibrils, exhibiting similar morphology to that of the full-length Aβ (Takano, 2008). Aβ28 lacks the C-terminus. The aggregation of the Aβ28 peptide induced by the pH jump from neutral to <6 yields an antiparallel β-sheet structure (Perálvarez-Marín, Barth, and Gräslund 2008).

In the present work the use of Aβ28 was a particularly good model of the soluble Aβ at pH 7.4 because at neutral pH the Aβ28 peptide shows no tendency to aggregate (no fluorescence variation was observed at pH7.4 by our research group previously (Cortijo-Arellano, Ponce, Durany, and Cladera 2008b; Klajnert et al. 2006).). Cu(II) binds to Aβ28 with the same affinity and coordination geometry (Karr, 2007; Drew et al., 2010) as to the full length Aβ. Aβ28 peptide is not toxic to PC12 and SH-SY5Y cells.

The Aβ28 peptide morphology and structure analysis was done under the same condition and for the same purpose as for Aβ40.

3.1.4.2 AFM measurements

AFM was used in order to investigate the effect of Cu(II) ions on Aβ28 morphology. Aβ28 and Cu(II)-Aβ28$_{pH11}$ species were imaged on a mica surface at ambient conditions and a non-contact scanning mode. The images were collected after dilution by a factor $10^4$of a 250 µM stock suspension of Aβ28. In Figure 3.18 (A and B) shown is an example of the AFM image of Aβ28. The objects seen at this pH have heterogeneous shapes. The average height and standard deviation of 112 Aβ28 particles are 0.8 nm and 0.2 nm respectively. C and D images of Figure 3.18 represent a planar view and a height analysis of Cu(II)-β28$_{pH11}$. The average height and standard deviation of 79 Cu(II)-Aβ28$_{pH11}$ particles are 1.4 nm and 0.3 nm respectively. As the image shows, Cu(II)-Aβ28$_{pH11}$ peptide forms globular objects. No significant increase of the object size was observed with the respect to Aβ28 alone. Interestingly that the images obtained reveal that Aβ28$_{pH11}$ particles were heterogeneously shaped, Cu(II)-Aβ28$_{pH11}$ had a globular shape. Importantly that in the both cases no fibrillar or big aggregated assemblies were detected.

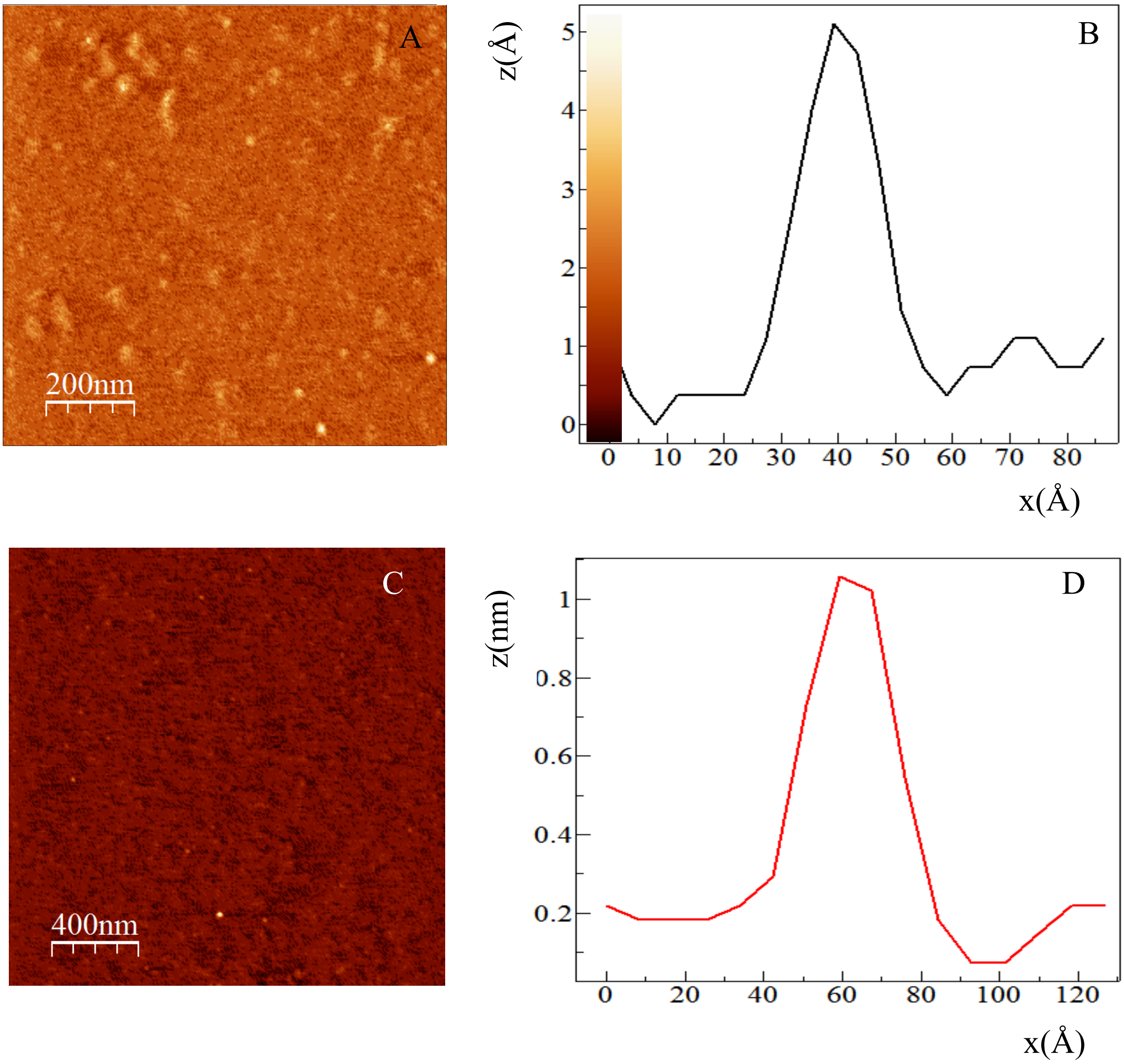

Figure 3.18 AFM characterization of morphology of Cu(II)-$A\beta28_{pH11}$ at pH11. Representative images of Aβ28 peptide in absence/presence of Cu (II) are shown. (A) The image of $A\beta28_{pH11}$. (B) The height of the $A\beta28_{pH11}$ particle. The signal below 1.2 Å was considered as a noise. (C) The image of Cu(II)-$A\beta28_{pH11}$. (D) The size (height) of an Cu(II)-$A\beta28_{pH11}$. The image was collected after dilution of a 250 µM solution at pH 11 by a factor 10^4. The signal below 0.2 nm was considered as a noise.

The results of the AFM analysis of Cu(II)-$A\beta28_{pH11}$ are summarized in the histogram presented in Figure 3.19.

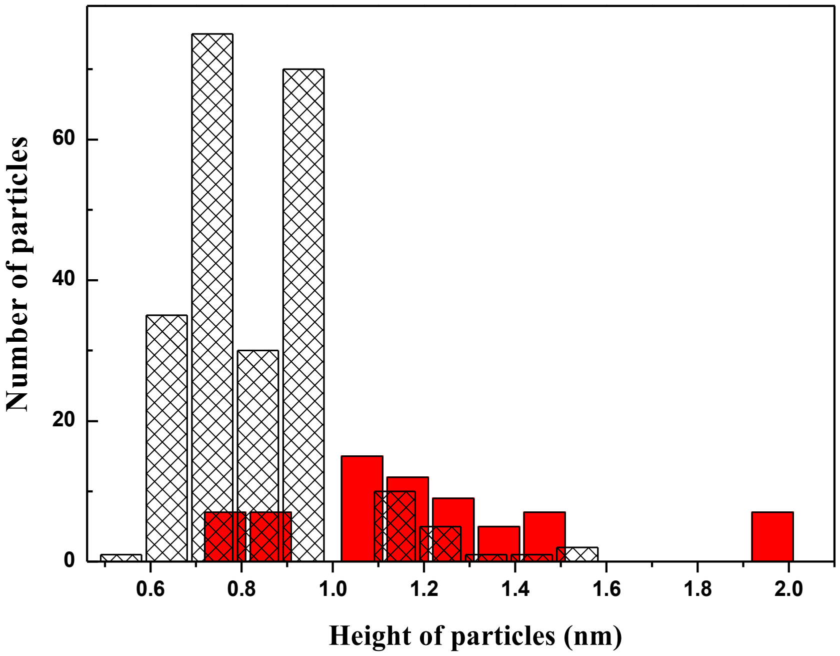

Figure 3.19 The heights distribution of Aβ28$_{pH11}$ and Cu(II)-Aβ28$_{pH11}$. Bars are presented by hatched columns correspond to Aβ28, red columns represent the height distribution of Cu(II)-Aβ28$_{pH11}$.

The results of the AFM analysis for Aβ28$_{pH11}$ and Aβ40$_{pH11}$ are summarized in Table 3.1.1. The particle sizes of the Cu(II)-Aβ40$_{pH11}$ are up to 6 times bigger than those of Aβ40$_{pH11}$. Second, the particle sizes of the Cu(II)-Aβ28$_{pH11}$ do not significantly differ from those of Aβ28$_{pH11}$. The particles of Aβ40$_{pH11}$ are up to 3 times higher than those of Aβ28$_{pH11}$ and in the presence of Cu(II) ions, the difference in heights are 10 times larger than that of the full length peptide.

	Aβ40$_{pH11}$	Cu(II)-Aβ40$_{pH11}$	Aβ28$_{pH11}$	Cu(II)-Aβ28$_{pH11}$
Particle height (nm)	2.4±0.3	13±4.8	0.8±0.2	1.4±0.3

Table 3.1.1. The summarized results (sizes) of the AFM analysis.

3.1.4.3 TEM

No objects to image were possible to detect in the case of Aβ28$_{pH11}$. It can be suggested that the objects were to small to be detected by the present TEM resolution.

3.1.4.4 SAXS

For Aβ28 and Aβ40$_{pH11}$ Guinier plateau was not possible to find. Both Guinier plots had a sharp increase in intensity at very small values of s. This can be explained if samples contain significant inter-particle repulsion, which can indicate that Cu(II) does not cause aggregation of Aβ40 at pH 11.

Brief summary of results obtained

Aβ28 does not aggregate in the presence of Cu(II) at basic pH.

3.1.5 Structure and morphology of Cu(II)-Aβ28 aggregates at pH 5.5

3.1.5.1 FTIR

For the study of secondary structure of Aβ28 the FTIR was collected and reported (Cortijo-Arellano, Ponce, Durany, and Cladera 2008b). The FTIR spectra of Aβ28 at pD 5.7 at the amide I band showed a kinetic of structural changes in time presented by 1) the decreasing of the broad bands centred at ~1640 cm^{-1} which correspond to unordered and helical structures and 2) by the increasing of the band at at a wave-number around 1616 cm^{-1}, a band assigned as typical one of a β-sheet structure.

FTIR spectra collected at the amide I band of Cu(II)-Aβ28 at pD 5.7 show a well defined peak around 1622 cm^{-1} which can be assigned to a β-structure,. The peak forms in the very beginning with no further time evolution during 24 hours incubation at 37^0C, pD 5.7 (Figure 3.20).

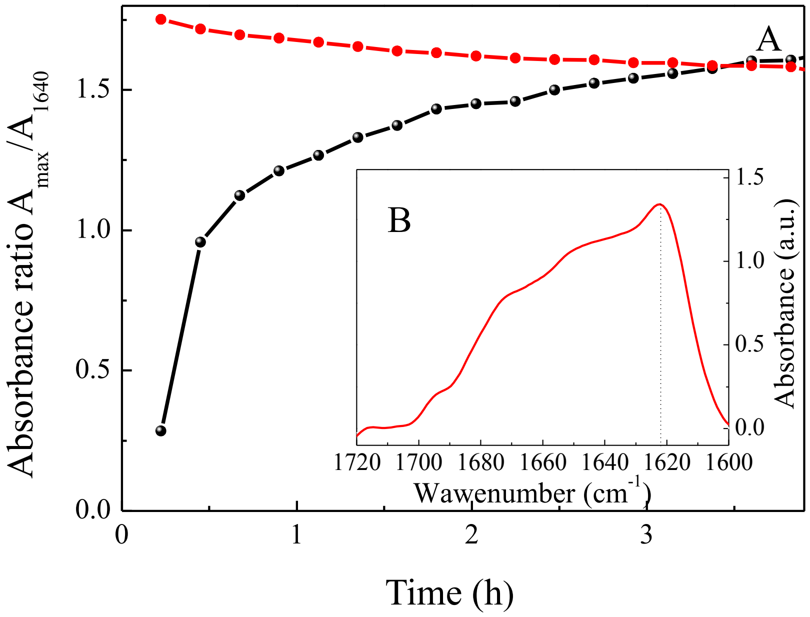

Figure 3.20 The FTIR spectra of Aβ28- Cu(II) in the amide I region. (A) Variation with time of the amount of β-structure of Cu(II)-Aβ28 shown by the red curve and Aβ28 shown by the black curve is expressed as a ratio of absorbances of unordered/helical structures (1640 cm^{-1}) versus β-sheet secondary structure (1622 cm^{-1}) as a function of time. (B) FTIR spectra of Cu(II)-Aβ28.

3.1.5.2 ThT fluorescence spectroscopy

In order to investigate the effect of Cu(II) ions on Aβ28 fibril formation, ThT assay was applied to monitor the β-sheet formation using ThT fluorescence spectroscopy. Because the aggregation of the Aβ28 peptide induced by the pH jump from neutral to <6 yields an antiparallel β-sheet structure (Perálvarez-Marín, Barth, and Gräslund 2008) the experiments was done at pH5.5. First, was studied the importance for Aβ28 fibril formation of the tyrosine 10. It has been suggested that Aβ tyrosine 10 plays a role in the stabilization of amyloid fibrils due to aromatic stacking interactions (one of the forces holding together the amyloid structure). The results show that tyrosine 10 is crucial for fibril formation: the Aβ28 Tyr10Ala mutant does not show the alteration of ThT emission signal.

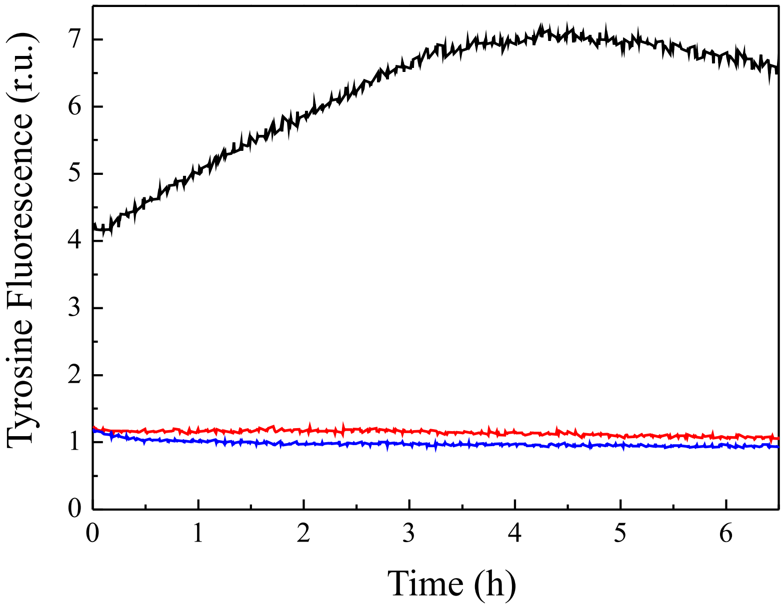

Figure 3.21 Thioflavin T fluorescence variation for Aβ28 and Aβ28Y10A. Thioflavin T fluorescence variation Black gpaph: Aβ28 at pH 5.5, blue graph: mutant Aβ28Y10A at pH 5.5, red graph: Aβ28 at pH 7.4 Peptides concentration was 25 μM. Temperature was 37°C.

Since tyrosine 10 is so important for Aβ28 peptide aggregation, and is thought to be involved to some extent in the binding of metal ions to the Aβ peptide (although not as direct ligand) (Streltsov et al., 2008), it was decided to study how the presence of Cu(II) would affect the Aβ28 aggregation.As it is shown in Figure 3.22, the presence of a stoichiometric concentration of the Cu(II) ions inhibited the formation of ThT positive Aβ28 fibrils. The results obtained show that the presence of Cu(II) hampers the formation of Aβ28 fibrillar structures.

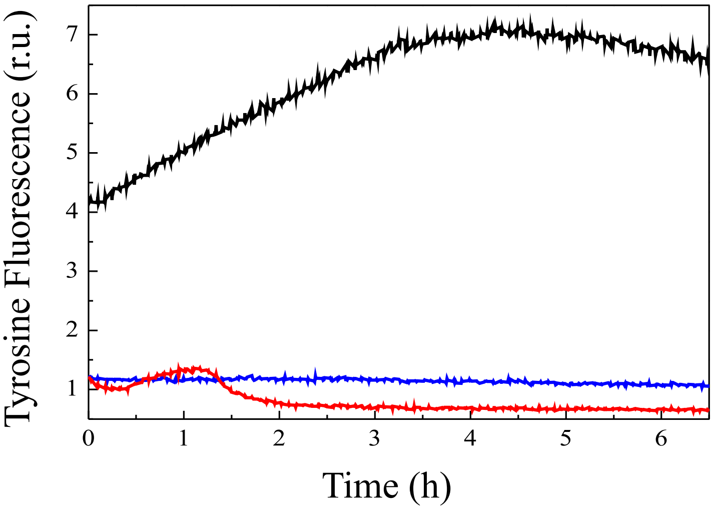

Figure 3.22 Time course studies of Aβ28 in the presence of Cu(II) aggregation by ThT fluorescence assay. Graphs show the results from the real time ThT fluorescence measurements. The aggregation assay reaction mixture contains 25μM Cu(II)-Aβ28 at pH 5.5. Black graph : Aβ28, red graph:Cu(II)-Aβ28, Blue:t Aβ28Y10A

3.1.5.3 TEM

In order to study the morphology of Cu(II)-Aβ28, the aliquots for TEM studies were taken from corresponding Cu(II)-Aβ28 and Aβ28 ThT aggregation mixtures after 24 hours of incubation at 37°C. In Figure 3.23 the representative images of the Aβ28 and Cu(II)-Aβ28 are shown. It is documented that Cu(II)-Aβ28 after 24 hours at pH 5.5 formed amorphous non-fibrillar aggregates meanwhile Aβ28 alone formed fibrils.

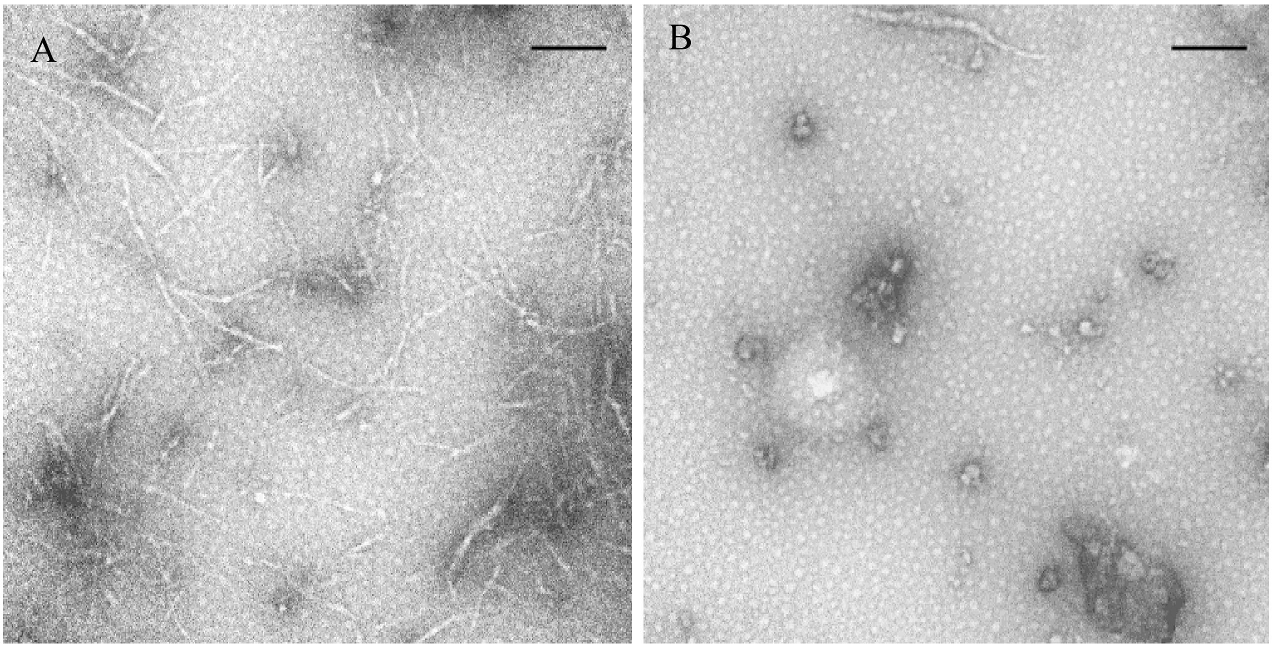

Figure 3.23 Morphology of Aβ28 in the presence of Cu(II) observed by TEM. Electron micrograph images of the Aβ28 in the presence of Cu(II). The TEM images show: (A) Aβ28 fibrils, (B) Cu(II)-Aβ28 granular amorphous aggregates. Scale bar is equal to 200 nm.

3.1.5.4 **Tyrosine 10 intrinsic fluorescence**

To monitor the variation of intrinsic tyrosine fluorescence in the presence of Cu(II), the intensity of the tyrosine emission spectrum was inspected. As reported in Figure 3.24 the presence of Cu(II) caused a clear decrease in the intensity of intrinsic tyrosine fluorescence. This observation is in agreement with the Tyrosine 10 fluorescence variation measured in the presence of Cu(II) for the fragment Aβ(1-16) by Maiti et al.(Maiti et al., 2008). These authors point out that the oxidation state and coordination geometry of the bound copper ion both affect the Aβ28 fluorescence behaviour, indicating close association between tyrosine 10 residue and the ion. Tyrosine 10 does not become a tightly bound ligand to Cu(II) but is influenced by a charge transfer process which may rationalize the fluorescence quenching observations.

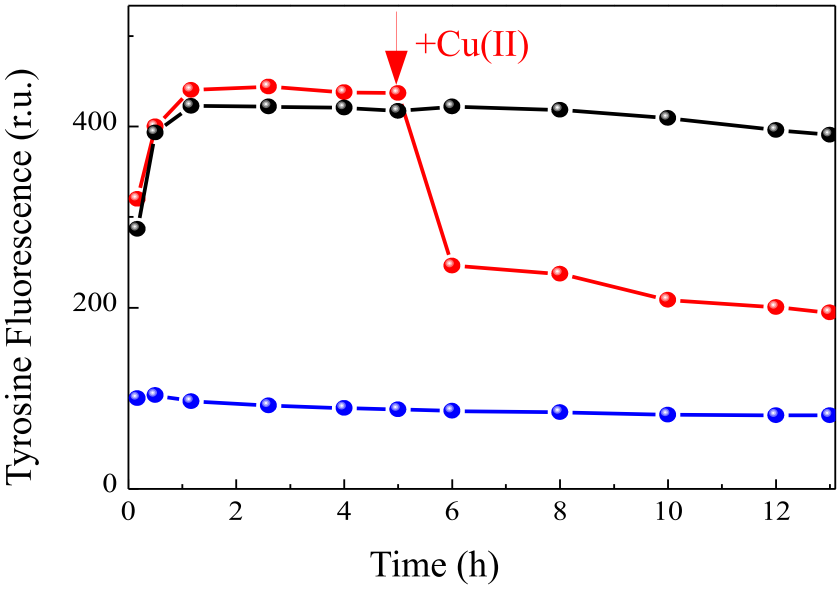

Figure 3.24 Effect of Cu(II) on Aβ28 Tyrosine 10 intrinsic fluorescence. Aβ28 Tyrosine 10 fluorescence is sensitive to the presence of Cu(II). Black curve: Intrinsic Tyrosine fluorescence spectra of Aβ28, red curve: Aβ28 fibrils in the presence of Cu(II), blue curve: Cu((II)-Aβ28. All measurements were done for solutions diluted to the pH 5.5 after several hours of incubation at 37^{0}C with gentle agitation. λ_{exc} was 286 nm, λ_{em} was 290-350 nm.

The addition of Cu(II) to a suspension of preformed Aβ28 amyloid fibrils dissembled the fibrillar structures (Figure 3.25). This fact was detected by a rapid decrease of the ThT fluorescence upon addition of Cu(II), concomitant with a decrease in the intensity of the tyrosine 10 intrinsic fluorescence. As shown in Figure 3.25E after Cu(II) addition, large non-fibrillar aggregates were detected by electron microscopy. The alteration of fibril morphology also was confirmed by DLS. One signal peak of Aβ28 fibrils hydrodynamic diameter (D_H) after intervention of Cu(II) converted in to two peaks. This suggests that Cu(II) ions aggregate the Aβ28 fibrils.

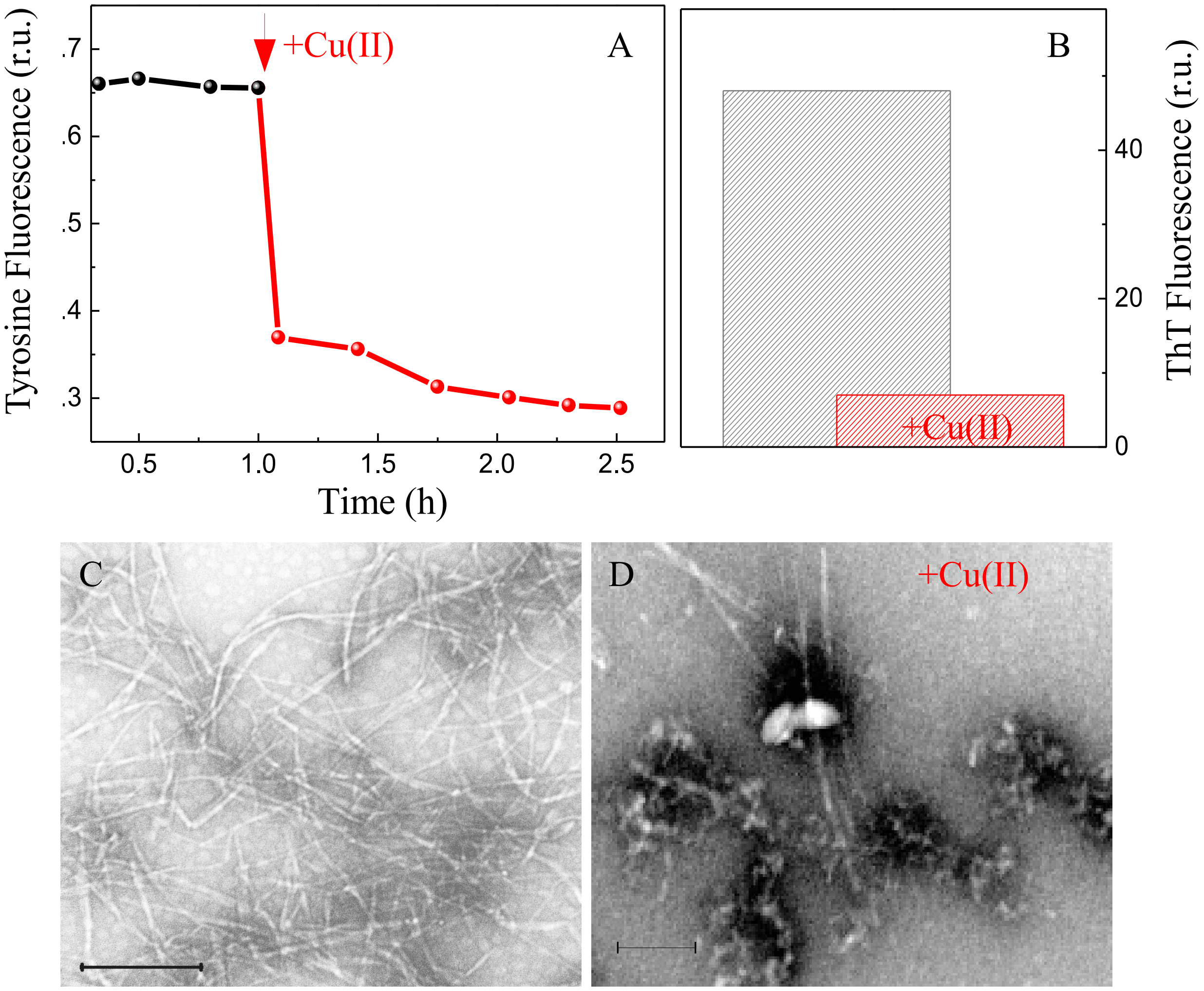

Figure 3.25 Aβ28 fibrils in presence of Cu(II). (A) Grey curve Tyrosine 10 intrinsic fluorescence intensity of Aβ28 fibrils. (B) ThT fluorescence signal of Aβ28 fibrils: grey bar, ThT fluorescence signal of Aβ28 fibrils in the presence of Cu(II): red bar. Grey curve Tyrosine intrinsic fluorescence intensity of Aβ28 fibrils. Red bar:Tyrosine intrinsic fluorescence intensity of Aβ28 fibrils in the presence of Cu(II). (C) TEM image of Aβ28 fibrils. (D) TEM image of non-fibrillar aggregates and rests of Aβ28 fibrils after Cu(II) addition. (Scale bar, 200 nm).

Brief summary:

1. Tyrosine 10 is crucial for Aβ28 fibril formation: the Aβ28 Tyr10Ala mutant does not aggregate.
2. The presence of Cu(II) hampers the formation of Aβ28 fibrillar structures.
3. Incubation of the Cu(II)-Aβ28 at pH 5.5 has been shown to favor the formation of amorphous aggregates forms amorphous non-fibrillar aggregates.
4. Cu(II) disassembles the Aβ28 fibrillar structures.

3.1.6 Effect of Cu(II) on Aβ toxicity

In order to study the possible biological significance of the current study, to assay toxicity of

Cu(II)-Aβ40$_{pH11}$ and Cu(II)-Aβ28 amorphous aggregates two different cell lines were chosen: SH-SY5Y, a neuroblastoma cell line, and PC12. Both cell lines have been previously described as neural cell models to test amyloid peptides toxicity (Simakova and Arispe 2007; Bieschke et al. 2008).

PC12 have a negatively charged outer surface of the cell membrane because they chronically express phosphatidylserine (PS) onto the outer leaflet of the bilayer (PC12 cells are chronically pre-apoptotic). SH-SY5Y cells do not chronically express PS, their outer cell surface membrane is neutral. Thus the PC12 and SHSY5Y cell lines, a pair of cell lines differing in cell surface charge, were chosen to be the model for Aβ toxicity in this thesis.

Solutions containing either Aβ alone or Cu(II)-Aβ were prepared as described for the ThT assay. For the experiments using pre-incubated Aβ samples, the relative degree of β-aggregation in each sample was regularly monitored using the ThT assay until β-aggregation reached a maximum. At this point, the samples were transferred into wells containing either the PC12 or SH-SY5Y cultures as described above.

3.1.7 Cu(II)-Aβ40$_{pH11}$ toxicity

PC12 and SH-Sy5Y cell lines were used to determine the toxicity of Cu(II)-Aβ40$_{pH11}$ and Cu(II)-Aβ28 complexes. The results are summarized in the Figure 3.26 and 3.28. Control used: 100% cell activity corresponds to that of the cells in the absence of either peptide, Cu(II) or peptide-metal complexes. Agents were added into the cell culture 48 hour after the cell seeding and 24 hour after FCS reduction to 1%. Cell metabolic activity was measured using the MTT test 24 hours after the addition of the Aβ loaded with Cu(II) at pH 11. The starting concentrations of PC12 and SH-SY5Y cell were $2*10^4$ cells per well in a 96-well plate.

Figure 3.26 shows cell viability measured using MTT test after 24 hours incubation with Cu(II)-Aβ40$_{pH11}$, Aβ40 and Aβ40 fibrils. The results obtained are the following: There is no significant differences between Aβ40 added at pH7.4 or at pH11 to the cell culture. When Aβ40 was added after pH adjusting to pH7.4 (Aβ40$_{pH7.4}$: oligomeric species) a reduction of 28 ± 2% and 22 ± 2.5% in metabolic activity was observed for PC12 and SH-SY5Y, respectively. When Aβ40 was added without pH adjusting (Aβ40$_{pH11}$: monomeric species) a reduction of 25 ± 2.4% and 15 ± 1.5 % in metabolic activity was observed for PC12 and SH-SY5Yrespectively. When fibrillar Aβ40 (Aβ40 fibrils: the peptide was preincubated for 24 hours at pH 7.4) was added to the cell culture, the cell metabolism was reduced by 22 ± 3.5 % and 20 ± 2 % for PC12 and SH-SY5Y respectively. Cu(II)-Aβ40$_{pH11}$ amorphous aggregates are more toxic than Aβ40 fibrils and Aβ40 peptide alone. Cu(II)-Aβ40$_{pH11}$ reduced cell viability, by 51 ± 2.4 % and 46 ± 4.3 % for PC12 and SH-SY5Y respectively. Before the addition to the cell culture, Aβ40$_{pH11}$ was preincubated with Cu(II) for 24 hours at a metal-peptide ratio of 1 to 1. Incubation of the Cu(II)-Aβ40$_{pH11}$ at pH7.4

has been shown to favor the formation of amorphous aggregates (Figure 3.12). Such aggregates are therefore shown to be toxic.

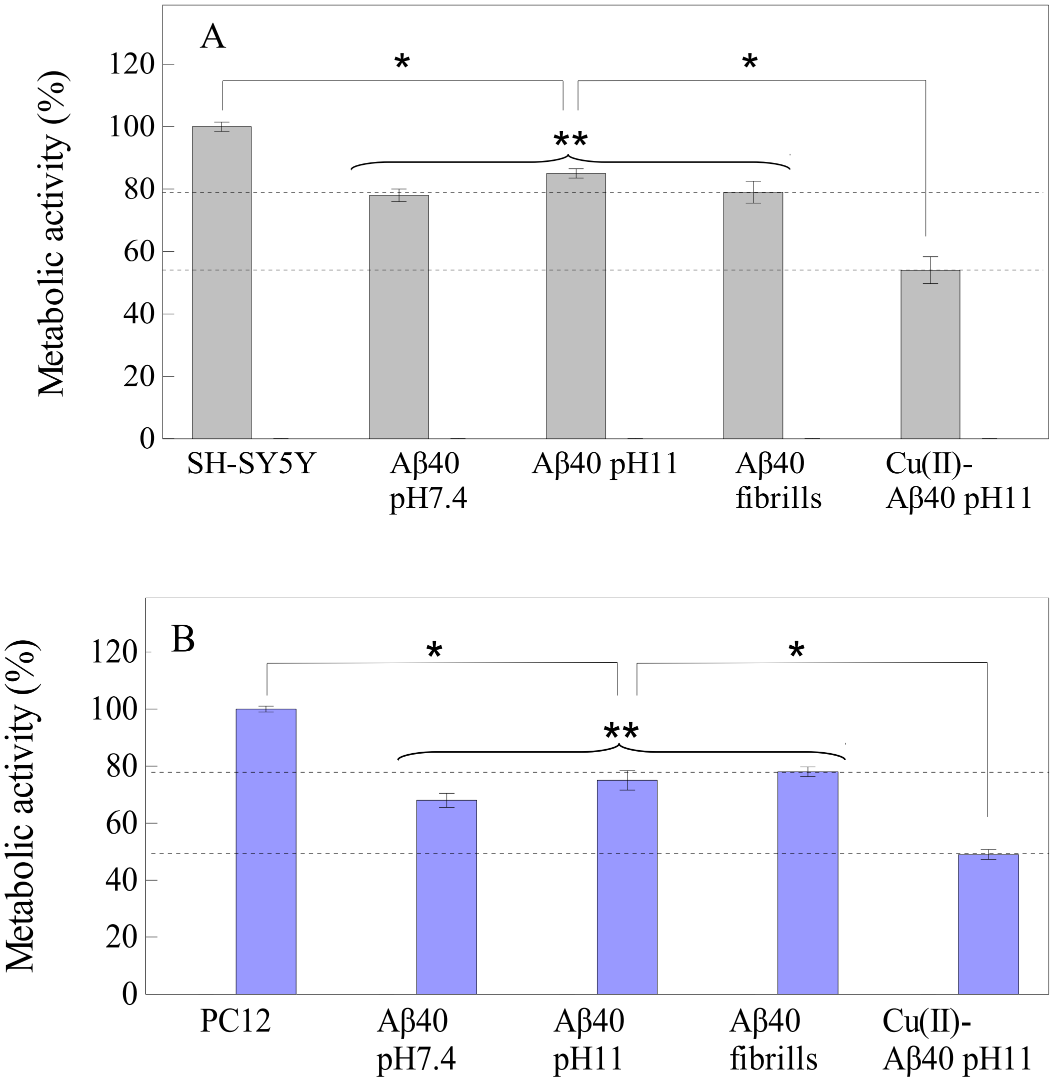

Figure 3.26 Cu(II)-Aβ40$_{pH11}$ cell toxicity. Metabolic activity was measured by MTT assay. (A) Metabolic activity of the SH-SY5Y cells in the presence of Cu(II)-Aβ40$_{pH11}$. (B) Metabolic activity of the PC12 cells in the presence of Cu(II)-Aβ40$_{pH11}$. The metal-free and metal-complexed peptide concentration was 25 μM. Statistics: **- Not significantly different, *- significantly different (ANOVA analysis, $p < 0.05$, $n_{SH\text{-}SY5Y}=4$, $n_{PC12}=2$). Error bars are standard errors.

To evaluate if the DMEM dilution with Cu(II) in HEPES at different pH 11 would have an effect on cells survival, the PC12 and SH-SY5Y cells were grown for 24 hours in DMEM diluted with Cu(II) in HEPES (pH 11, pH 7.4) and their metabolic activity was examined. The results are summarized in Figure 3.27 showing that the 25 μM concentration of free Cu(II) in HEPES at pH 11 or at pH 7.4 had no detectable effect neither for PC12 nor for SH-SY5Y cells. The 100% cell metabolic activity corresponds to that of cells in the absence of any dilution.

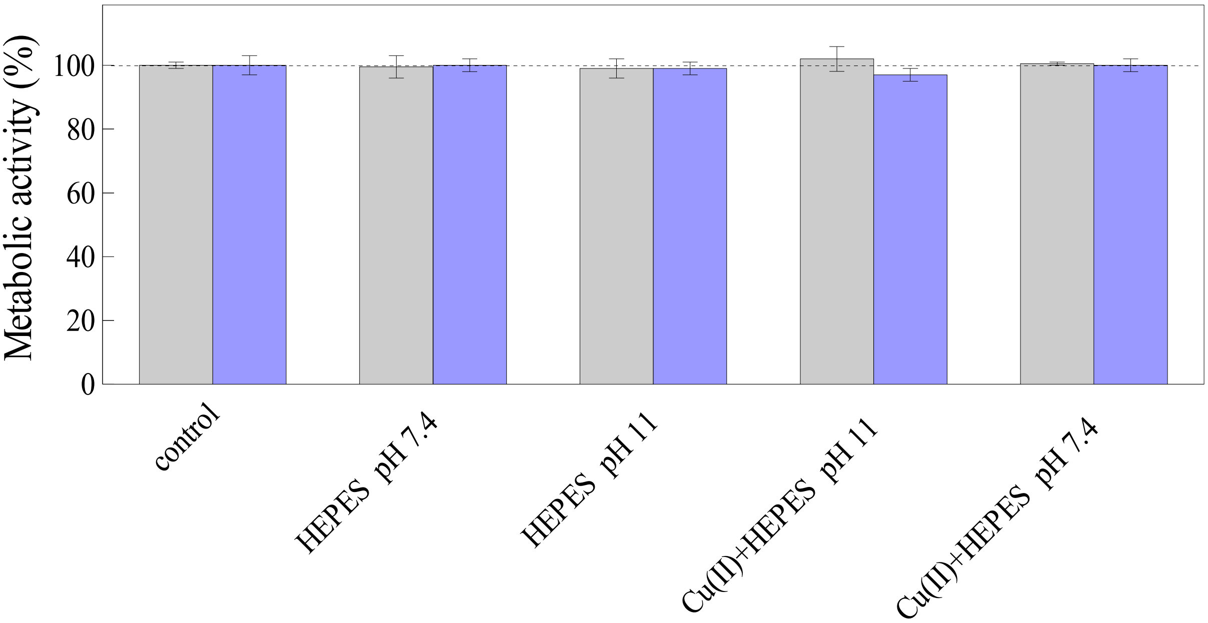

Figure 3.27 Effect of free Cu(II) ions and pH of HEPES on cell metabolic activity. Cu(II) concentration was 25 μM. Cell metabolic activity was measured by MTT assay. Light gray bars correspond to the SH-SY5Y cells, blue bars represent the PC12 cells. Statistics: Error bars are the standard errors. No significant difference exists between any of the experimental points and the control (ANOVA analysis, $p < 0.05$, n=4).

As well PC12 and SH-SY5Y were used to determine the the toxicity of Cu(II)-Aβ28$_{pH11}$. The results are summarized in Figure 3.28. Control used: 100% cell metabolic activity corresponds to that of cells in the absence of either peptide, Cu(II) or peptide-metal complex. The results obtained are the following: for PC12 and SH-SY5Ycells Aβ28$_{pH7.4}$ (monomeric species) had no toxic effect. Cu(II)-Aβ28$_{pH7.4}$ significantly reduced metabolic activity of SH-SY5Y and PC12cells, by 35 ± 5.1% and 41 ± 7.8 % respectively. Before the addition, Aβ28 was preincubated with Cu(II) for 24 hours at a metal-peptide ratio of 1 to 1.

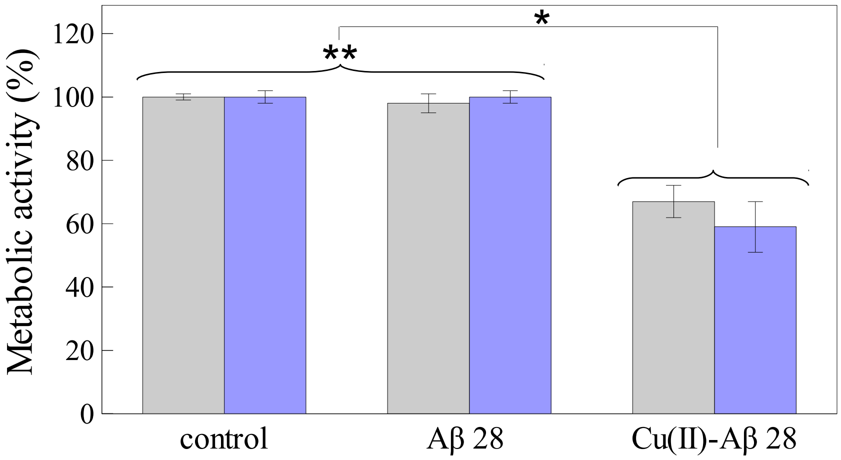

Figure 3.28 Cu(II)-Aβ28$_{pH11}$ cell toxicity. Metabolic activity was measured by MTT assay. The metal-free and metal-complexed peptide concentration was 25 μM. Light gray bars correspond to the SH-SY5Y cells, blue bars represent the PC12 cells. Statistics: **- Not significantly different, * - significantly different. (ANOVA analysis, $p < 0.05$, $n_{SH\text{-}SY5Y}=3$, $n_{PC12}=2$). Error bars are standard errors.

Brief summary:

Four findings are evident from this data:

1. Amorphous aggregates of Cu(II)-Aβ40$_{pH11}$ are significantly toxic than Aβ40 in its fibrillar, oligomeric or monomeric conformations for PC12 and SH-SY5Y cells .
2. Aβ28 peptide is not toxic for PC12 and SH-SY5Ycells.
3. Incubation of the Aβ28 in the presence of Cu(II) has been shown to favor the formation of amorphous aggregates (Figure 3.23). Such aggregates are therefore shown to be toxic.

3.2 INFLUENCE OF DENDRIMERS ON AB AGGREGATION

3.2.1 Introduction

It has been shown that the globular branched polymers known as dendrimers have a great potential as antiamiloydogenic agents PAMAM and cationic phosphorus-containing dendrimers to be able to modulate Aβ β formation (Klajnert, Cortijo-Arellano, Cladera, et al., 2006; Wasiak et al., 2011). Dendrimers have been proven to interact with amyloids, although most of dendrimers assayed in amyloidogenic systems are toxic to cells. The development of glycodendrimers, poly (propylene imine) (PPI) dendrimers decorated with maltose (Mal), represents the possibility of using dendrimers with a low intrinsic toxicity. In the present chapter we show that fourth (PPI-G4) and fifth (PPI-G5) generation glycodendrimers have the capacity to interfere with Alzheimer's amyloid peptide Aβ 40 fibrillization. The interaction is generation dependent: PPI-G5 blocks amyloid fibril formation generating granular non-fibrillar amorphous aggregates whereas PPI-G4 generates clumped fibrils at low dendrimer-Aβ ratios and amorphous aggregates at high ratios. Both PPI-G4 and PPI-G5 are non-toxic to PC12 and SH-SY5Y cells. PPI-G4 reduces amyloid toxicity by clumping fibrils together, whereas amorphous aggregates are more toxic than Aβ fibrils to PC12 cells. The results show that glycodendrimers are promising non-toxic agents in the search for antiamyloidogenic compounds. Fibril clumping may be an anti-amyloid toxicity strategy.

3.2.2 Effect of dendrimers on Aβ40 fibril formation kinetics and on Aβ40 aggregated species morphology

In this study, the effect of surface chemistry of different dendrimers on Aβ40 aggregation was investigated. In Figure 3.29 positively charged PAMAM (PAMAM_+), neutral PAMAM (PAMAM_0), cationic phosphorus-containing dendrimers and PPI glicodenrimer are schematically presented. These are dendrimers of similar size and molecular geometry but with different surface groups.

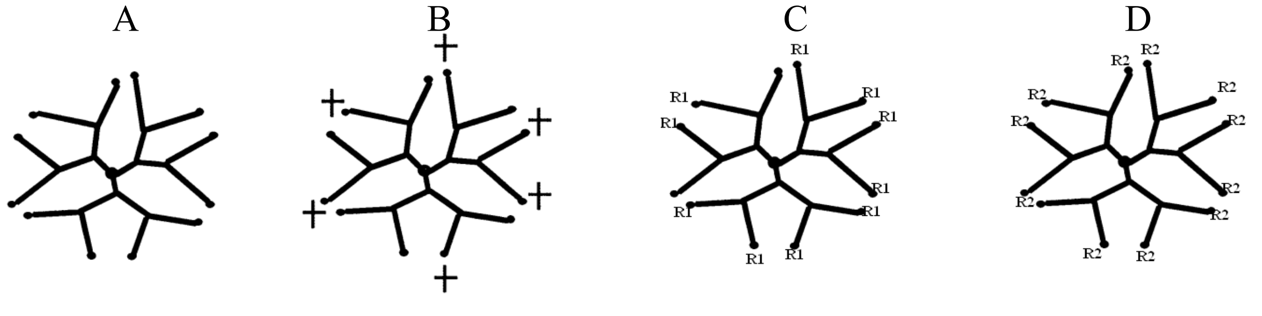

Figure 3.29 **Schematic drawing of dendrimer structur**e: (A) neutral, hydroxyl-terminated PAMAM_0; (B) cationic, amine-terminated PAMAM_+. (C) cationic phosphorus-containing dendrimers , R1 is tetravalent thiophosphoryl trichloride, (D) glicodenrimer, R2 is maltose.

3.2.2.1 PAMAM dendrimers

In Figures 3.30 and 3.31, are shown the results from the real time ThT fluorescence measurements of Aβ40 fibrillization in the presence of PAMAM. For this study were chosen cationic PAMAM-NH_2 and neutral hydroxyl-terminated PAMAM of the fourth generation in order to study how PAMAM dendrimer's surface charge determine their effect on amyloid formation. The graphs clearly indicate the variation of ThT fluorescence in the presence of different Aβ40-$PAMAM_+$ ratios confirming the alteration of fibrillization kinetics. TEM images (Figure 3.30) reveal the structures observed after 24 hours of aggregation which were fibrillar or amorphous and granular depending of Aβ-$PAMAM_+$ ratio. This finding is in agreement with previous studies concerning aggregation of other amyloid peptides and PAMAM dendrimers. (M. Cortijo-Arellano, Ponce, et al. 2008; Rekas et al. 2009).

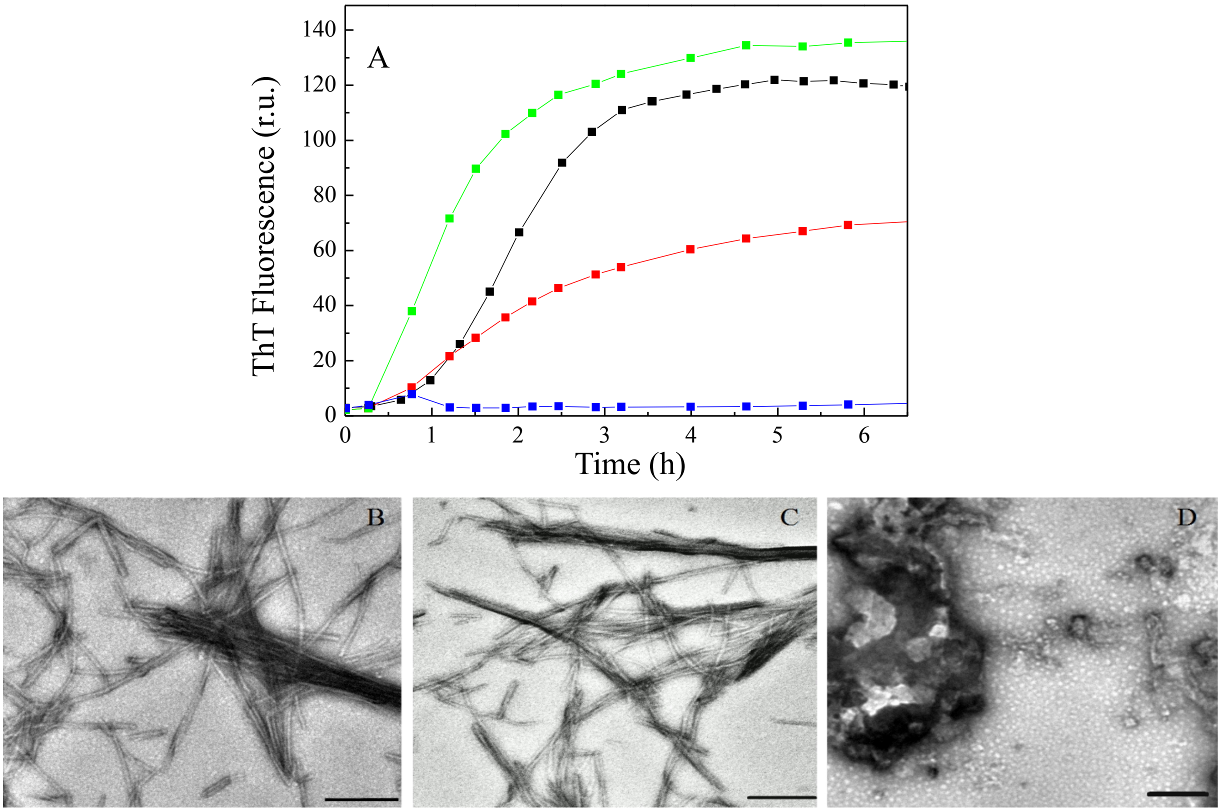

Figure 3.30 Morphology and time course studies of Aβ40 fibrillization in the presence of $PAMAM_+$ **using ThT fluorescence assay and morphology observed by TEM.** The aggregation assay reaction mixture containing 25µM Aβ40 in the presence of $PAMAM_+$ and 35µM ThT dye was incubated at pH 7.4, 37°C with stirring. (A) ThT fluorescence assay. The coloured curves clearly indicate the differences in ThT fluorescence signal of different peptide-$PAMAM_+$-ratios confirming the alteration of fibrillization kinetics. The black curve corresponds to the control, Aβ40 alone; the green curve shows Aβ40 in the presence of $PAMAM_+$ at peptide-dendrimer ratio 1 to 0.1; the red curve represents peptide-dendrimer ratio 1 to 1 and the blue curve corresponds to the peptide-dendrimer ratio 1 to 10. No significant changes in ThT fluorescence were observed up to 24 h. **Electron micrograph images:** (B) Aβ40 fibrils formed in the presence of $PAMAM_+$ dendrimers at ratio 1 to 0.1. (C) TEM image Aβ40 fibrils formed in the presence of $PAMAM_+$ dendrimers at ratio 1 to 1 and (D) Aβ40 amorphous non-fibrilar aggregates formed in the presence of $PAMAM_+$ at ratio 1 to 10. The sample aliquots for all EM images of the Aβ40 in the presence of $PAMAM_+$ dendrimers were collected from the corresponding ThT aggregation assay reaction mixtures after 24 hours of incubation. The scale bars are 200 nm.

In Figure 3.31, there are the results from the real time ThT fluorescence measurements of Aβ40 fibrillization in the presence of PAMAM dendrimers with neutral surface charge PAMAM_0. Here as well was documented a clearly seen effect of different Aβ40-dendrimer ratios on ThT fluorescence signal confirming the alteration of fibrillization kinetics. TEM images reveal the structures observed after 24 hours of aggregation which were fibrillar or amorphous depending on peptide-dendrimer ratio.

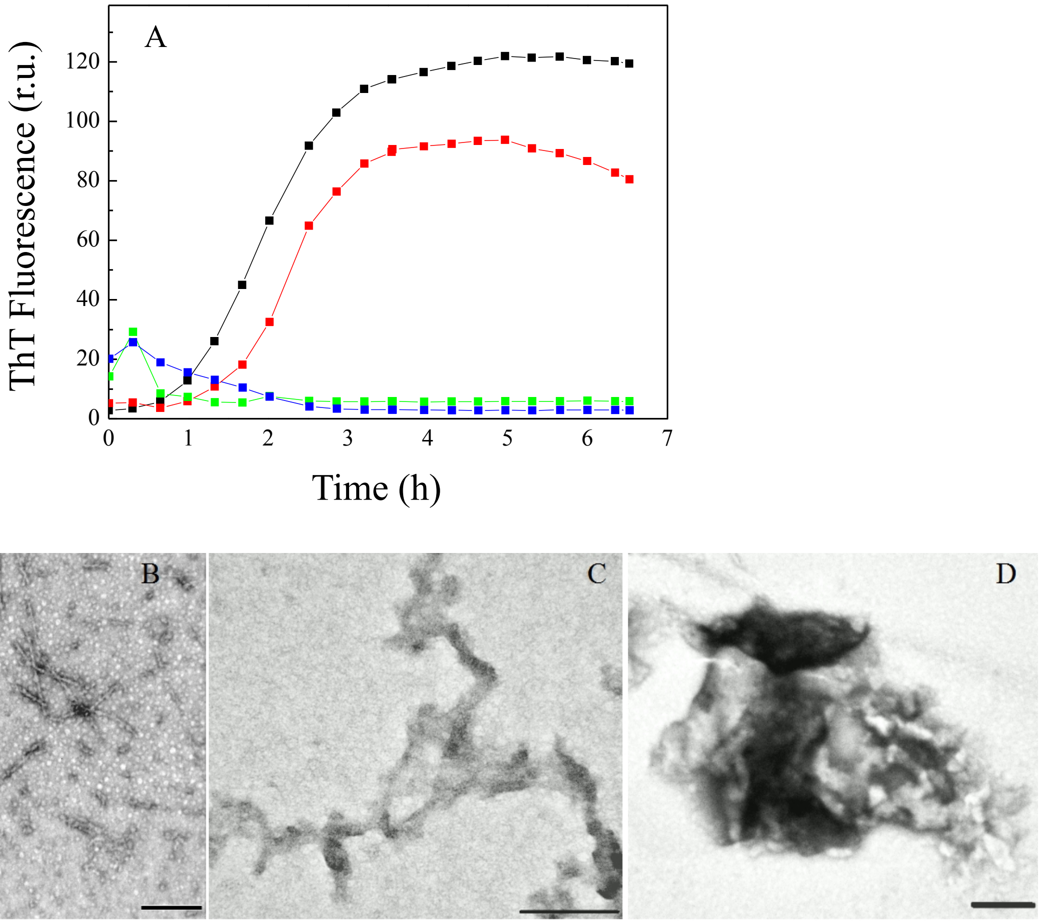

Figure 3.31 Morphology and time course studies of Aβ40 fibrillization in the presence of PAMAM_0 using ThT fluorescence assay and aggregates morphology observed by TEM. The aggregation assay reaction mixture containing 25µM Aβ40 in the presence of PAMAM_0 and 35µM ThT dye was incubated at pH 7.4, 37°C with stirring. (A) ThT fluorescence assay. The coloured curves clearly indicate the differences in ThT fluorescence of different peptide-PAMAM_0 ratios confirming the alteration of fibrillization kinetics. The black curve corresponds to the control, Aβ40 alone; the blue curve serves for peptide-dendrimer ratio 1 to 0.1; the green curve shows Aβ40 in the presence of PAMAM_0 at peptide-dendrimer ratio 1 to 1; the red curve represents the peptide-dendrimer ratio 1 to 10. No significant changes in ThT fluorescence were observed up to 24 h. **Electron micrograph images:** (B) Aβ40 fibrils formed in the presence of PAMAM_0 dendrimers at ratio 1 to 0.1. (C) TEM image of Aβ40 aggregates formed in the presence of PAMAM_0 dendrimers at ratio 1 to 1 and (D) Aβ40 amorphous non-fibrilar aggregates formed in the presence of PAMAM_0 at ratio 1 to 10. The sample aliquots for all EM images of the Aβ40 in the presence of PAMAM_0 dendrimers were collected from the corresponding ThT aggregation assay reaction mixtures after 24 hours of incubation. The scale bars are 200 nm.

3.2.2.2 Cationic phosphorus-containing dendrimers

PCD are a unique family of dendrimers, which use a tetravalent thiophosphoryl trichloride as branching point and aromatic rings as repeating unit. The usefulness of these dendrimers for elaboration of highly sensitive bio-sensors and for *in vitro* drug delivery (for instance as transfection agents, or against HIV-1 and the scrapie form of prions) was described (Caminade, Turrin, and Majoral 2010). For this research the 4th generation of PCD was used. In Figure 3.32 shown are the results from the real time ThT fluorescence measurements of Aβ40 fibrillization in the presence of PCD. Because of high noise -to-signal ratio no measurements were possible for dendrimer concentrations more than 25μM. Here as well was documented a clearly seen decelerating effect of PCD on ThT fluorescence signal of Aβ40 aggregation at peptide-dendrimer ratio 1 to 1. TEM images reveal the structures observed after 24 hours of aggregation which were fibrillar for all exterminated peptide-dendrimer ratios.

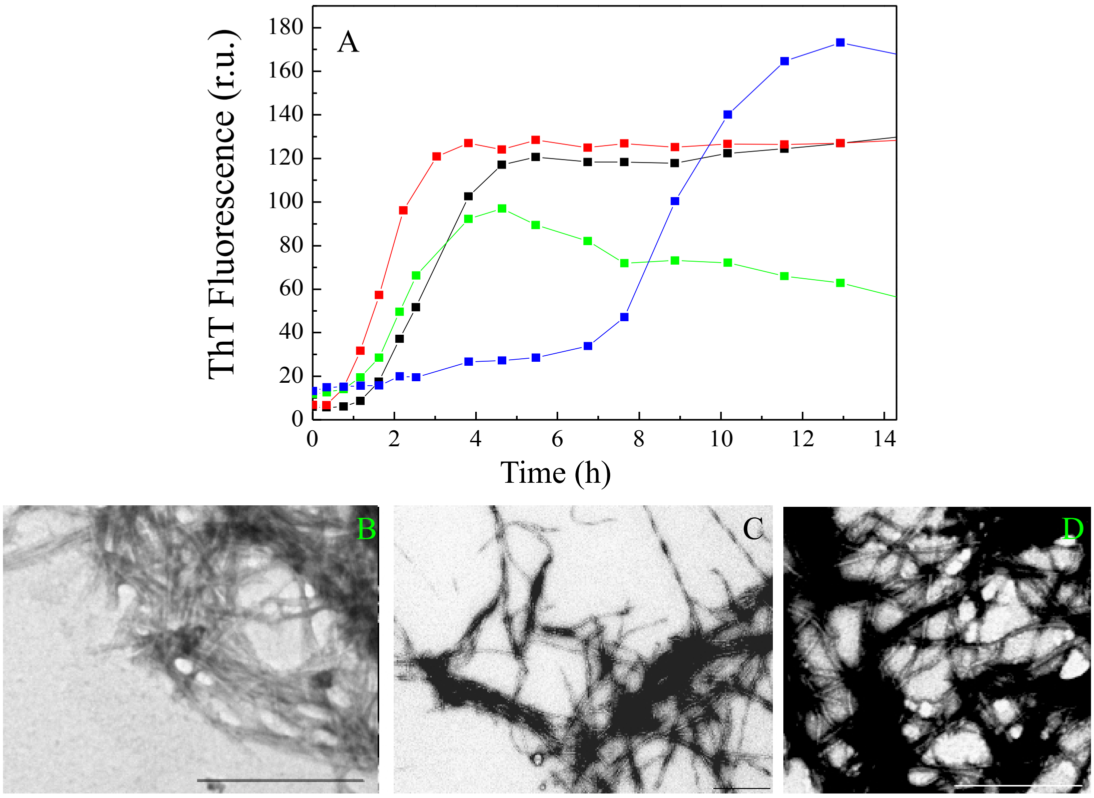

Figure 3.32 Morphology and time course studies of Aβ40 fibrillization in the presence of PCD using ThT fluorescence assay and aggregates morphology observed using TEM. The aggregation assay reaction mixture containing 25μM Aβ40 in the presence of PCD and 35μM ThT dye was incubated at pH 7.4, 37°C with stirring. (A) ThT fluorescence assay. The coloured curves indicate the differences in ThT fluorescence signal of different peptide-PCD ratios. The black curve corresponds to the control, Aβ40 alone; the blue curve is for peptide-dendrimer ratio 1 to 1; the green curve shows Aβ40 in the presence of PCD at peptide-dendrimer ratio 1 to 0.1; the red curve represents at peptide-dendrimer ratio 1 to 0.01. **Electron micrograph images:** (B) Aβ40 fibrils formed in the presence of PD at ratio 1 to 0.01. (C) TEM image of Aβ40 aggregates formed in the presence of PCD dendrimers at ratio 1 to 0.1 and (D) Aβ40 amorphous non-fibrilar aggregates formed in the presence of PCD at ratio 1 to 1. The sample aliquots for all EM images of the Aβ40 in the presence of PCD dendrimers were collected from the corresponding ThT aggregation assay reaction mixtures after 24 hours of incubation. The scale bars are 200 nm.

3.2.2.3 PPI-maltose dendrimers

The effect of PPI-maltose dendrimers G4 and G5 on Aβ40 fibril formation kinetics is shown in Figures3.33A and 3.34A respectively. Both PPI-G4 and PPI-G5 have the capacity to inhibit fibril formation. PPI-G4 inhibits Aβ40 fibril formation at 1 to 10 peptide-dendrimer ratio. At lower peptide-dendrimer ratios an effect of clumping fibrils together was observed Figures (3.33 B and C).

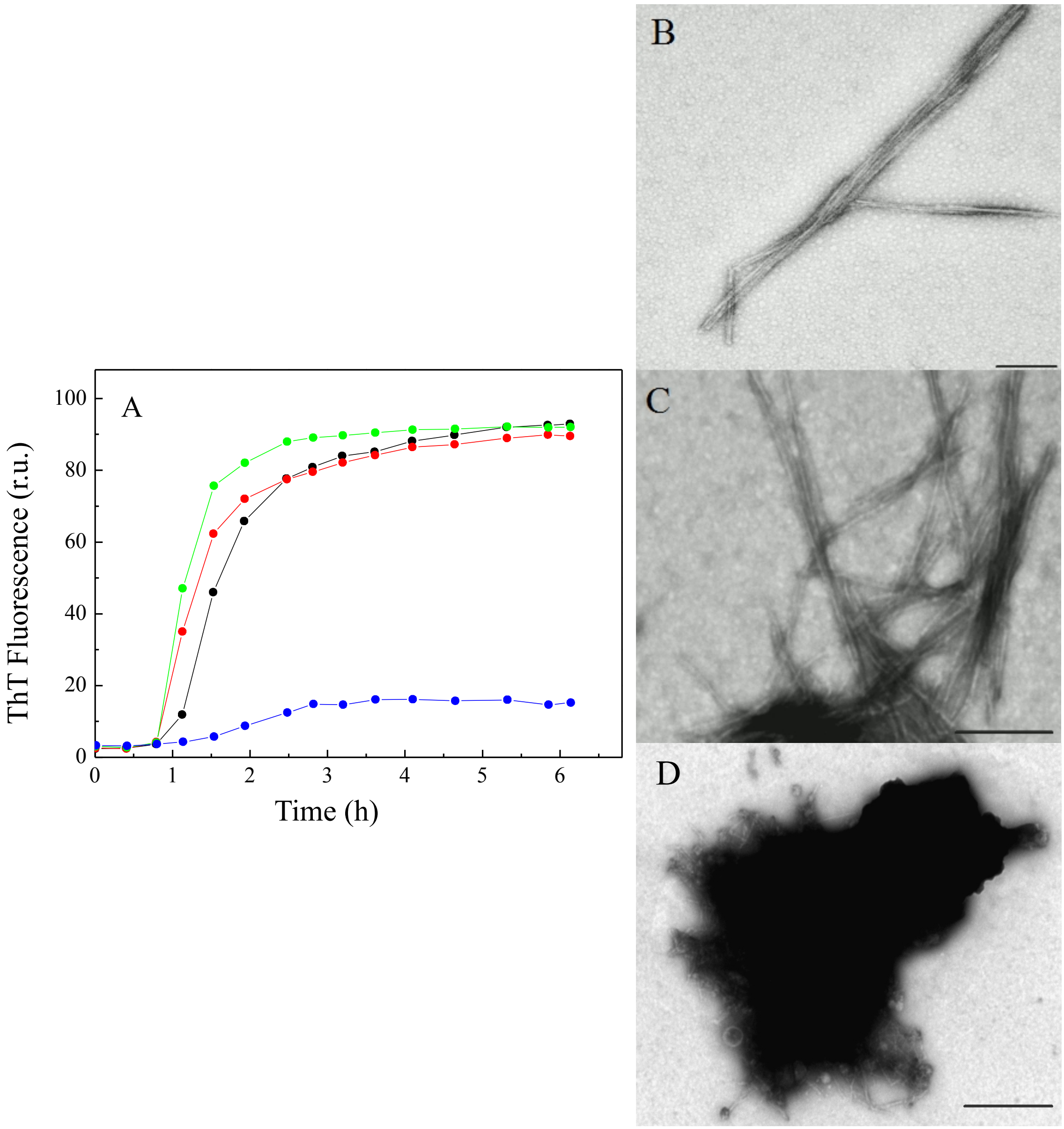

Figure 3.33 Time course studies of Aβ40 fibrillization in the presence of maltose dense shell dendrimers (PPI G4) using Thioflavin T (ThT) fluorescence assay and morphology observed by TEM. The aggregation assay reaction mixture containing PPI-G4 dendrimers, 25μM Aβ40 and 35μM ThT dye was incubated during 24 hours with stirring at 37 °C. (A) The graphs show the results from the real time ThT fluorescence measurements. The curves clearly indicate the differences in ThT fluorescence of different peptide-PPI-G4 ratios confirming the alteration of fibrillization kinetics. The black curve corresponds to the control, Aβ40 alone; green shows Aβ40 in the presence of dendrimers at the peptide-dendrimer ratio 1 to 0.1; the red curve represents the peptide-dendrimer ratio 1 to 1 and the blue one is for the peptide-dendrimer ratio 1 to 10. **Electron micrograph images of the Aβ40 in the presence of PPI-G4 dendrimers**: sample aliquots from ThT aggregation assay collected after 24 hours of incubation. (B) Aβ40 fibrillar clumps in the presence PPI-G4 dendrimers in ratio 1 to 0.1. (C) Aβ40 fibrillar clumps at the Aβ40-PPI-G4 ratio 1 to 1; (D) Aβ40 fibrillar clumps at the pept Aβ40 I-G4 1 to 10. The scale bars are 200 nm.

Ppi-G5 has been found to be more effective at inhibiting fibril formation than PPI-G4. PPI-G5 completely inhibits Aβ40 fibril formation at much lower peptide-dendrimer ratios than PPI-G4 (Figure 3.34A). Aβ40 in the presence of PPI-G5 forms non ThT positive amorphous aggregates (Figure 3.34B,C and D).

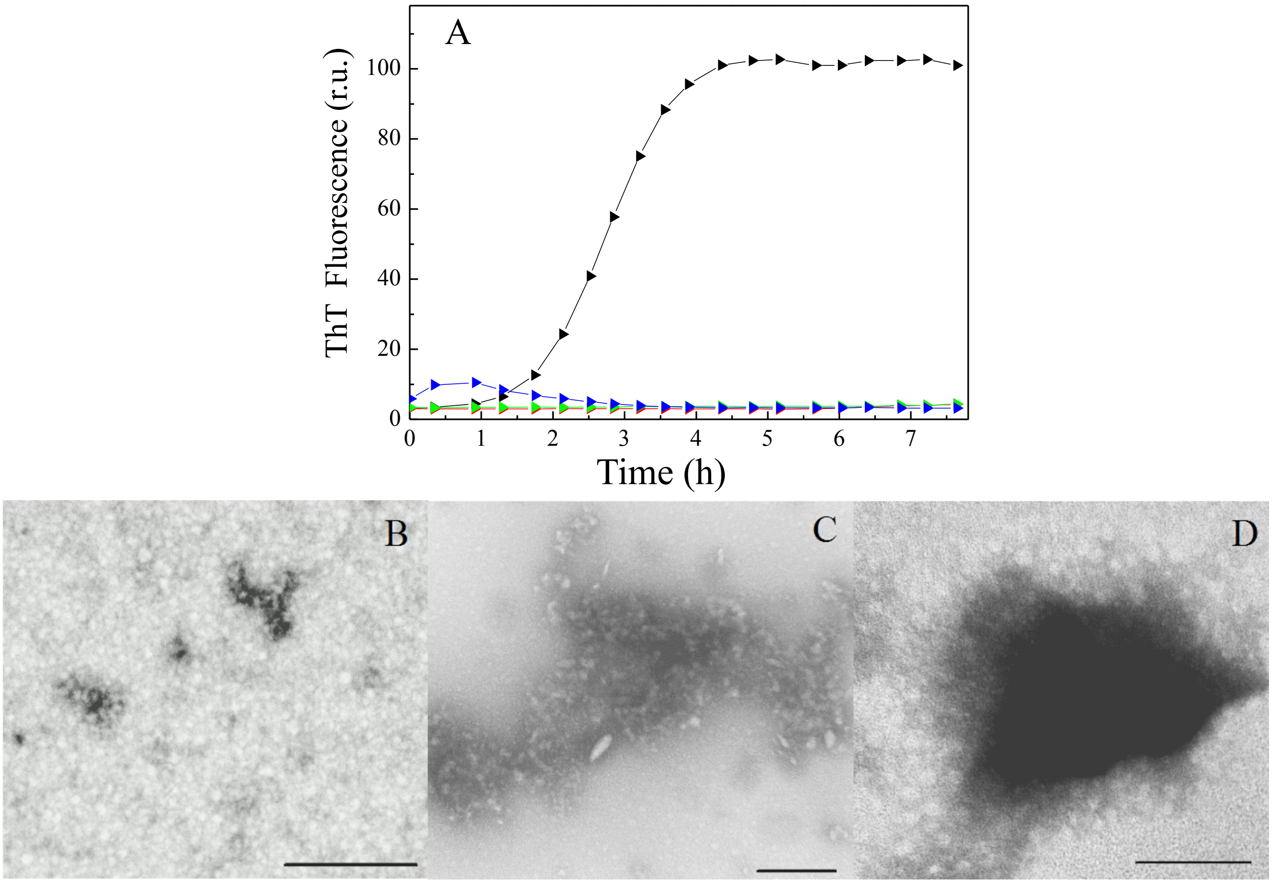

Figure 3.34 Time course studies of Aβ40 fibrillization in the presence of maltose dense shell dendrimers (PPI G5) using Thioflavin T (ThT) fluorescence assay and morphology observed by TEM. The aggregation assay reaction mixture containing PPI-G5 dendrimers, 25µM Aβ40 and 35µM ThT dye was incubated during 24 hours with stirring at 37°C. (A) The graphs show the results from the real time ThT fluorescence measurements. The curves clearly indicate the differences in ThT fluorescence of different peptide-PPI-G5 ratios confirming the alteration of fibrillization kinetics. The black curve corresponds to the control, Aβ40 alone; the green curve shows Aβ40 in the presence of dendrimers at the peptide-dendrimer ratio 1 to 0.1; the red curve represents the peptide-dendrimer ratio 1 to 1 and the blue one is for the peptide-dendrimer ratio 1 to 10. Electron micrograph images of the Aβ40 in the presence of PPI-G5 dendrimers: sample aliquots from ThT aggregation assay collected after 24 hours of incubation. (B) Aβ40 in the presence of PPI-G5 dendrimers at ratio 1 to 0.1.(C) Aβ40 aggregates at the peptide-PPI-G5 ratio 1 to 1; (D) Aβ40 aggregtes at the peptide- PPI-G5 ratio 1 to 10. The scale bars are 200 nm.

How peptide-dendrimer ratios modulate Aβ40 β formation becomes clear when representing the percentage of fibril formation (100% fibril formation is given by the value of the ThT fluorescence at the plateau of the control samples in Figure 3.35) as a function of peptide-dendrimer ratio.

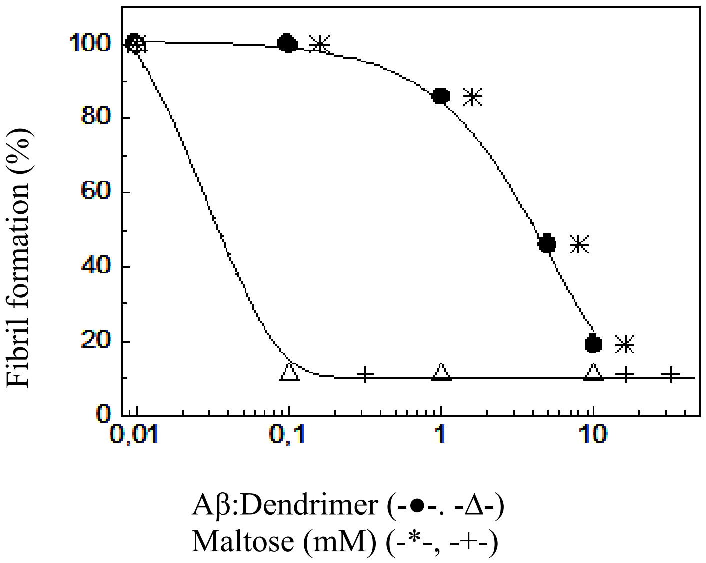

Figure 3.35 Differential effect of PPI-G4 and PPI-G5 dendrimers on Aβ40 fibril formation inhibition. Percentage of fibril formation is represented as a function of dendrimer-peptide ratio and total maltose concentration. (-●-) Effect of PPI-G4 as a function of the dendrimer-peptide ratio; (-*-) Effect of PPI-G4 as a function of maltose concentration. (-Δ-) Effect of PPI-G5 as a function of the dendrimer-peptide ratio; (-+-) Effect of PPI-G5 as a function of maltose concentration. Percentage of fibril formation was determined from the ThT fluorescence values at the plateaus of the curves in Figures 3.33and 3.34.

PPI-G5 inhibits fibril formation at much lower dendrimer-peptide ratios than PPI-G4 (dendrimer-peptide ratio: 0.1 for G5 versus 10 for G4). Only at a dendrimer-peptide ratio of ten and above, both PPI-G4 and PPI-G5 completely inhibit fibril formation. However, at dendrimer-peptide ratios up to 1 amyloid fibrillar structures which cause a high level of ThT fluorescence, still form in the presence of PPI-G4. Because for the same dendrimer-peptide ratio the concentration of maltose in the sample is higher in the presence of PPI-G5 than in the presence of PPI-G4, the percentage of fibril formation has been represented as well in Figure 3.35 as a function of maltose concentration. It can be clearly appreciated that at the PPI-G5-peptide ratio corresponding to 0.3 mM maltose, fibril formation is completely inhibited, whereas at the PPI-G4-peptide ratio corresponding to 2 mM maltose, fibril formation is still above 80% of the control. Thus, a higher sugar concentration does not explain the higher fibril-formation inhibition efficiency observed for PPI-G5 (see discussion).

At this point a possible explanation to such a difference could reside on the actual level of maltose concentration in each case. Representing the percentage of fibril formation as a function of maltose concentration however, gave a very similar result to that shown for dendrimer/peptide ratios. The explanation must lie, therefore, elsewhere, probably on the density of maltose molecules on the dendrimer's surface. As it can be seen in Table 3.2.1 together with other characteristic parameters of PPI-G4 and PPI-G5 maltose dendrimers, the maltose surface density is nearly 50% higher in PPI-G5.

	Mol mass (g/mol)	Maltose units attached	Diameter
PPI-G4	23400	64	6 nm
PPI-G5	44500	114	7 nm

Table 3.2.1 PPI Maltose dense shell dendrimers. Number of attached maltose units in PPI-G4 and PPI-G5, mol masses of glycodendrimers determined by 1H NMR and diameter (Appelhans et al., 2007).

In the electron microscope micrographs shown in Figure 3.36 it can be seen that Aβ40 fibrils are ‘clumped’ together in the presence of PPI-maltose G4 at a dendrimer/peptide ratios of 1 to 1 and 0.1 to 1 (Figures 3.36 C and D respectively). Moreover, in contrast to what is observed for Aβ40, no globular aggregates are observed in coexistence with the fibrils (3.36 A, B), when PPI-G4 is present. In the presence of PPI-G5 at any of the tested dendrimer-peptide ratios, no fibrillar but amorphous aggregates were detected (Figures 3.36 E and F, dendrimer-peptide ratios of 1 to 1 and 0.1 to 1).

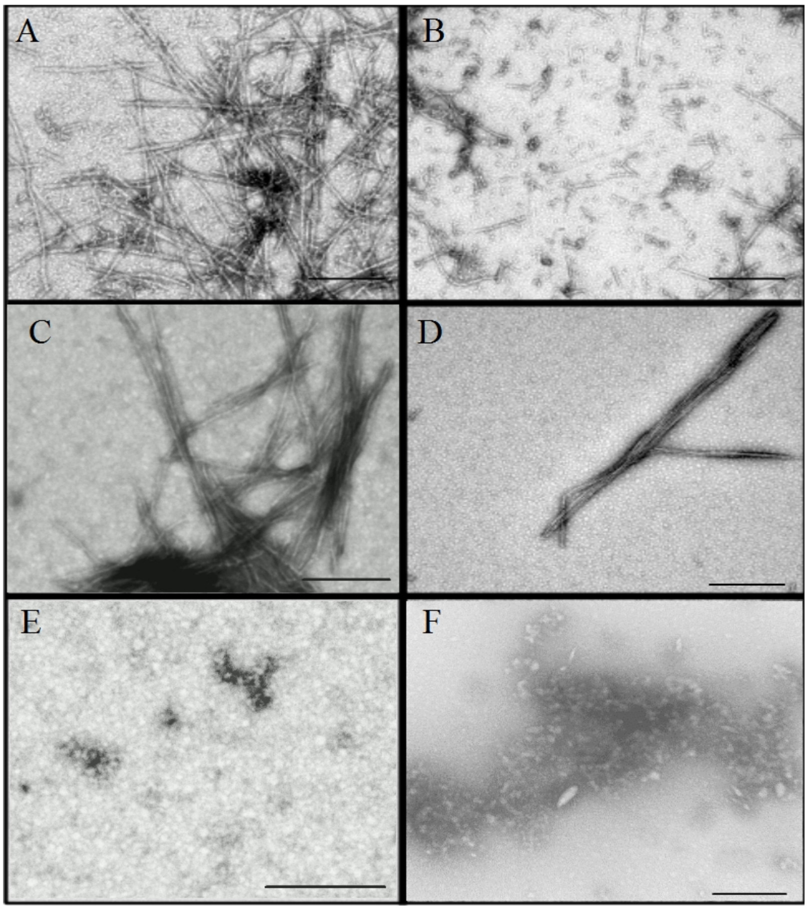

Figure 3.36 Morphology of Aβ40 and dendrimer-Aβ40 amyloid aggregates. Transmission electron microscopy images: (A and B) Aβ40 incubated at pH 7.4 .Coexistence of fibrils and globular oligomers. (C, D) Detection of clumped fibrils of Aβ40 incubated at pH 7.4 in the presence of PPI-G4. (E,F) Detection of amorphous non-fibirlar aggregates of Aβ40 incubated at pH 7.4 in the presence of PPI-G5. Aβ40 and Aβ40-dendrimer complexes were incubated for 12 hours at pH 7.4 and 37°C before the preparation of the microscopy grids.

Brief summary:

All tested types of dendrimers have dose-dependent effect on Aβ40 peptide aggregation.

Low concentration of dendrimers causes fibril grow, high concentration causes amorphous aggregates formation.

PPI-G4 causes clumping of fibrils, $PAMAM_0$ and PPI-G5 inhibit fibrillization at much lower peptide-dendrimer ratios than others.

PCD slow down the reaction of fibril formation at peptide-dendrimer ratio 1 to 1.

3.2.3 Effect of dendrimers on cell metabolic activity

3.2.3.1 PAMAM

For PAMAM and phosphorous dendrimers to be considered plausible antiamyloid molecules there is a fundamental aspect that needs being addressed: dendrimers biocompatibility (cell toxicity). In general, cationic dendrimers that have been shown to interfere with amyloid fibril formation are known to be toxic to cells due to the effect on the cell membrane structure on the strong electrostatic interactions between the dendrimers' positive charges and the negative charges on the membrane (K. Jain et al. 2010).

To determine effects of the dendrimers on metabolic activity of PC12 and SH-SY5Y cells, the MTT test was used. All polymers affected the metabolic activity in a concentration dependent manner when they were added in the concentration range 0–50 μM for 24 hours to the cells. Cytotoxicity of the PAMAM is surface charge dependent and increased in relation to the increasing concentrations as presented in Figure 3.37 and 3.38. Control used: 100% cell activity corresponds to that of cells in the absence of dendrimers. The results show that 25 μM concentration of PAMAM after 24 h significantly lowered the metabolic activity SH-SY5Y and PC12. 25 μM concentration of $PAMAM_+$ lowered the metabolic activity by 29 ± 4.0 % and 25 ± 3.1 % for SH-SY5Y and PC12 cell lines respectively. 25 μM $PAMAM_0$ lowered the metabolic activity by 28 ±2.5 % and 48 ±4.2 % for SH-SY5Y and PC12 cell lines respectively.

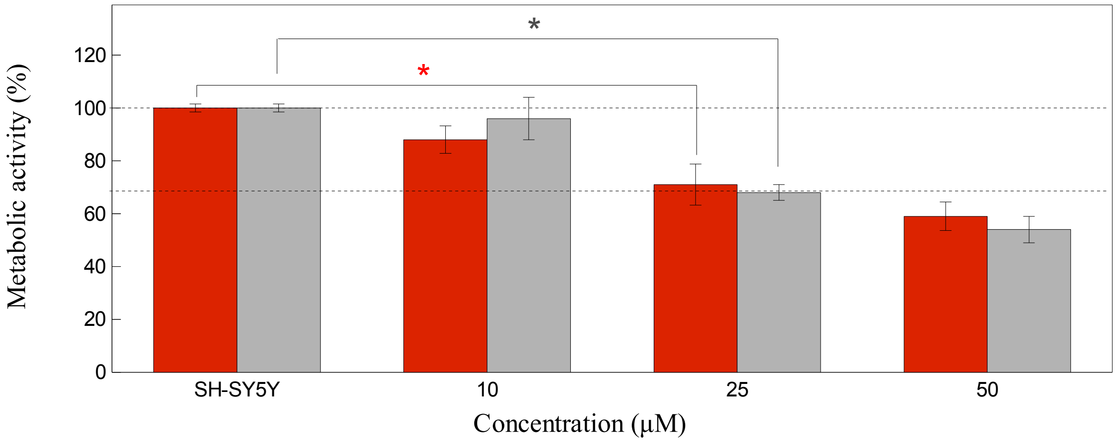

Figure 3.37 Metabolic activity of SH-SY5Y cells after the treatment with PAMAM dendrimers. Cell metabolic activity was measured by MTT assay. Red bars show SH-SY5Y cell metabolic activity after the treatment with PAMAM$_+$ dendrimers, the gray bars show metabolic activity after the treatment with PAMAM$_0$. 100% cell metabolic activity corresponds to that of cells in the absence of dendrimers. Statistics: * significant difference exists between controls and cells treated with PAMAM dendrimers at concentrations ≥ 25 µM (*- PAMAM$_{+,}$ *- PAMAM$_0$). (ANOVA analysis, $p < 0.05$, n =3). Error bars are standard errors.

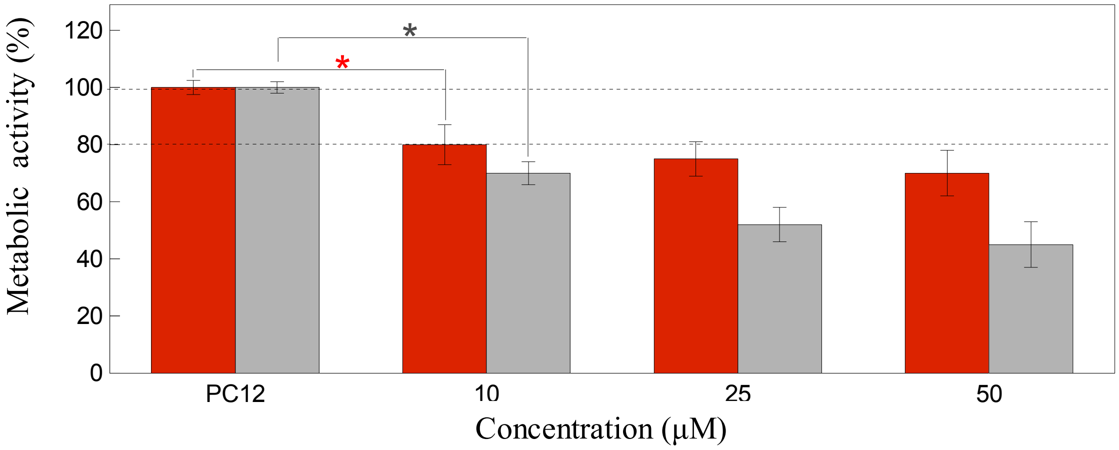

Fiure 3.38 Metabolic activity of PC12 cells after the treatment with PAMAM dendrimers. Cell metabolic activity was measured by MTT assay Red bars show PC12 cell metabolic activity after the treatment with PAMAM$_+$ dendrimers, the grey bars show metabolic activity after the treatment with PAMAM$_0$. 100% cell metabolic activity corresponds to that of cells in the absence of dendrimers. Statistics: * significant difference exists between controls and cells treated with PAMAM dendrimers at concentrations ≥ 10 µM (*- PAMAM$_{+,}$ *- PAMAM$_0$). (ANOVA analysis, $p < 0.05$, n =3). Error bars are standard errors.

3.2.3.2 Cationic phosphorus-containing dendrimers

Cytotoxicity of the PCD increases in relation to the increasing concentrations as presented in Figure 3.39. As well, PC12 and SH-SY5Y were used to determine the the toxicity of PCD.

Control used: 100% cell activity corresponds to that of cells in the absence of dendrimers. The results obtained are the following: 25 µM concentration of PCD caused significant cell death after 24 h, lowered the metabolic activity up to 35 %.

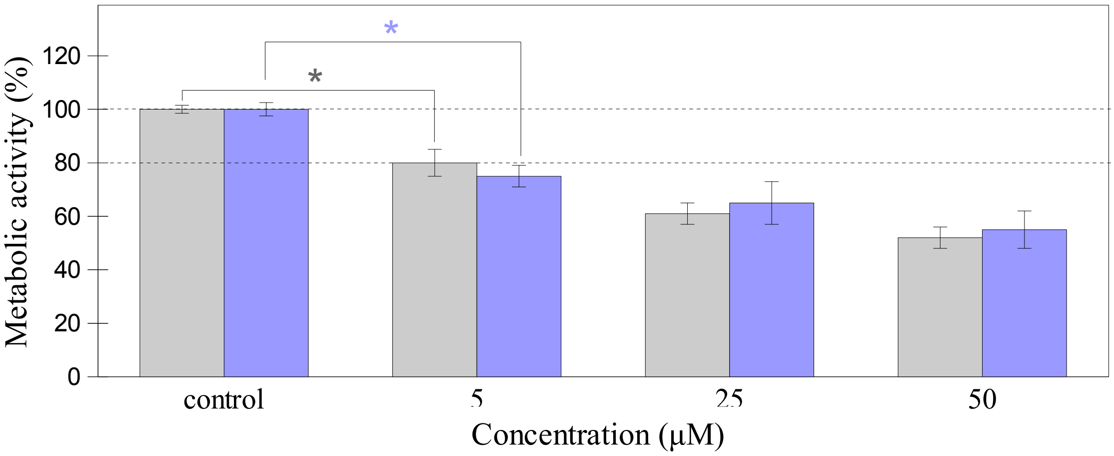

Figure 3.39 Metabolic activity of PC12 and SH-SY5Y cells after the treatment with PCD. Cell metabolic activity was measured by MTT assay Grey bars show metabolic activity of SH-SY5Y, violet bars show metabolic activity of PC12 cells. 100% cell activity corresponds to that of cells in the absence of dendrimers. Statistics: * significant difference exists between controls and cells treated with PCD at concentrations ≥ 5 µM for both cell lines (SH-SY5Y: *, PC12: *). (ANOVA analysis, $p < 0.05$, n =3). Error bars are standard errors.

3.2.3.3 PPI maltose dense shell dendrimers

One way of overcoming this problem with at the same time preserving the capacity of dendrimers to interfere with biological systems, has been the derivatization of the amino groups on the dendrimer's surface with oligosaccharide molecules. Glycodendrimers have already been shown to have a decreased toxicity with respect to charged dendrimers. They are promising structures for use, through the formation of hydrogen bonds, as multivalent ligands for various bio-interactions and have been shown to effectively interfe with the propagation of the scrapie prion protein (Bush et al., 1994; Klajnert et al., 2008). Cytotoxicity of the PPI dendrimers does not depend on dendrimer generation and concentrations used for experiments. As presented in Figure 3.40, PPI induced induced only a light decrease in metabolic activity and are considered as dendrimers with a good compatibility.

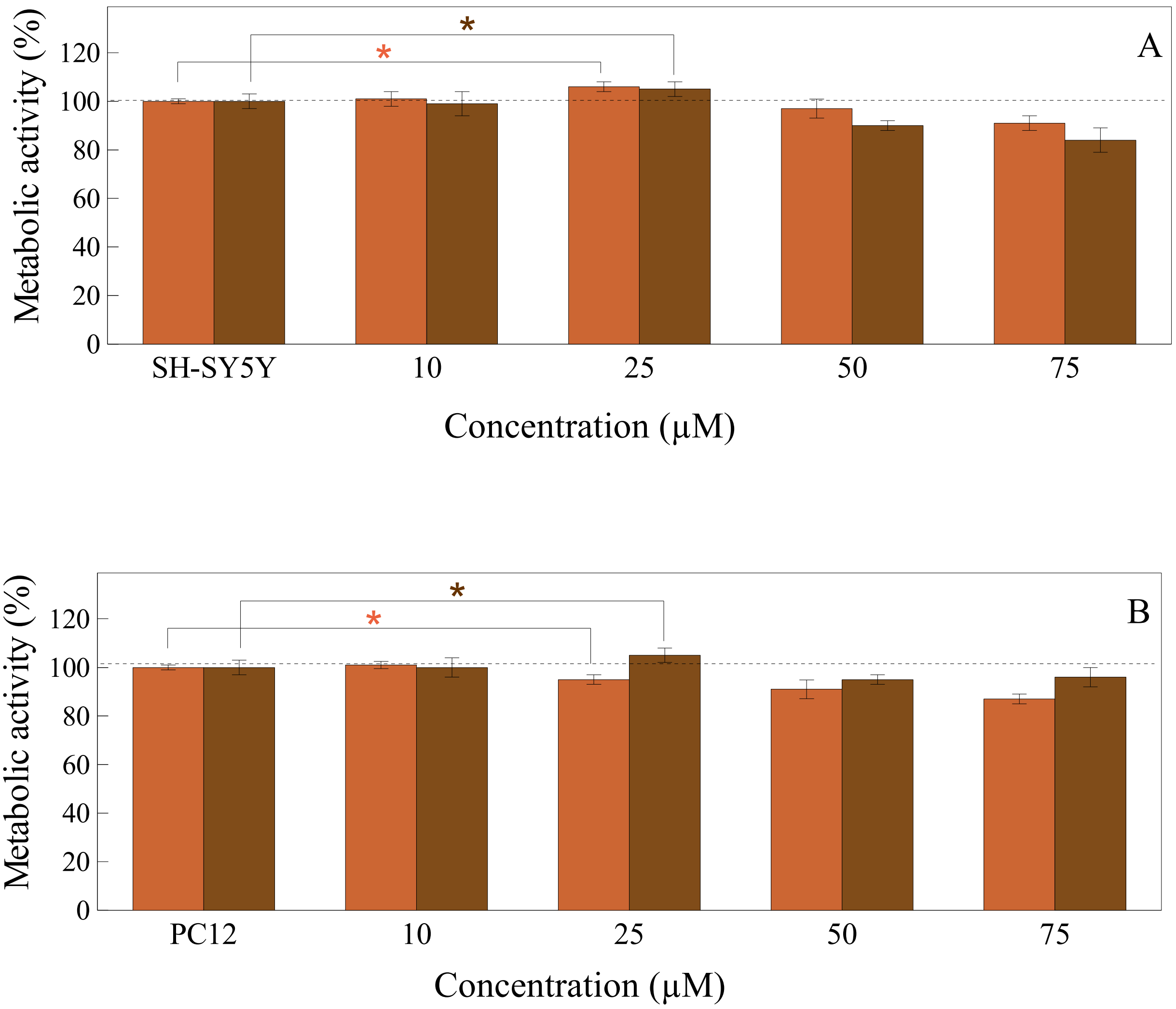

Figure 3.40 Metabolic activity of PC12 and SH-SY5Y cells after the treatment with with PPI dendrimers. Cell metabolic activity was measured by MTT assay. (A) Metabolic activity of SH-SY5Y cells. (B) Metabolic activity of PC12 cells. Orange bars show metabolic activity of cells treated with PPI-G4, brawn bars show metabolic activity of cells treated with PPI-G5.Statistics: * no significant difference exists between controls and cells treated with PPI dendrimers at concentrations 25 µM for both cell lines (PPIG4:*, PPIG5:*). (ANOVA analysis, $p < 0.05$, n =4). Error bars are standard errors.

Brief summary:

Both PPI-G4 and PPI-G5 are non toxic at 25 µM concentration and become mildly toxic at concentrations between 50 and 75 µM to PC12 and SH-SY5Y cell lines. PAMAM and phosphorus dendrimers have an increased toxicity level with respect to glycodendrimers.

3.2.3.4 Effect of maltose dendrimers on Aβ40 cell toxicity.

The effect of PPI-G4 and G5 on the cell toxicity of Aβ40 was studied on PC12 cells as a more sensitive cell type to Aβ40. For this cell line, Aβ40 peptide added as a monomer and as fibrils is shown to be toxic. The results show, however, that when the peptide is incubated in the presence of PPI-G4 dendrimers at peptide-dendrimers ratios at which clumped fibrils are formed, when added into the cell culture, these peptide-dendrimers complexes are non-toxic. This is not the case when the peptide is added after incubation with PPI-G5 (or G4 at peptide-dendrimers ratios higher than 1 to 1), under our experimental conditions these peptide-dendrimers complexes form amorphous aggregates, which result in a substantial degree of cell toxicity.

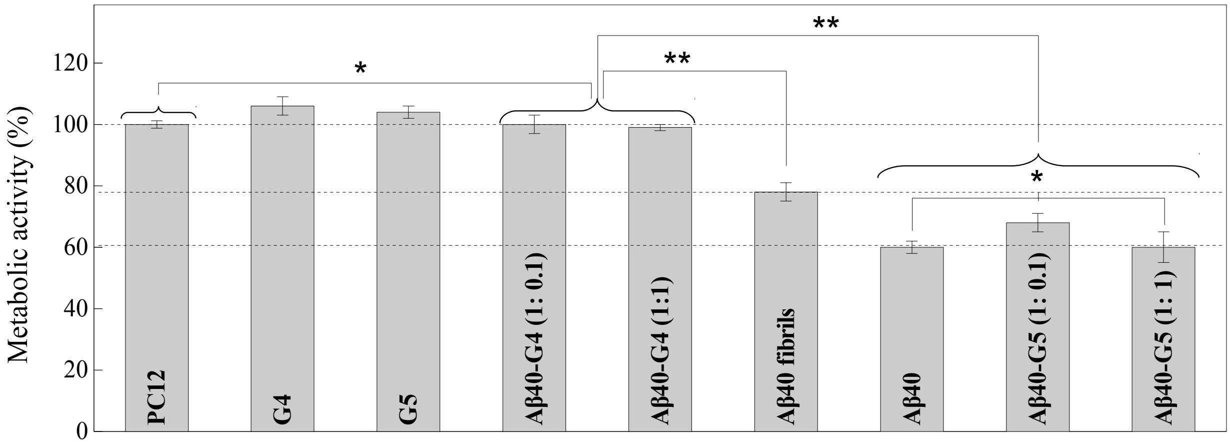

Figure 3.41 Aβ40 toxicity in the presence of PPI-maltose dendrimers. Cell metabolic activity was measured by MTT assay. (PC12): a control, cells in the absence of dendrimers and/or Aβ40. (G4): effect of PPI-G4 25μM in the absence of peptide; (G5): effect of PPI-G5 25μM in the absence of peptide. (Aβ40-G4 (1:0.05)): PPI-G4-Aβ40 at peptide-dendrimer ratio 1 to 0.05. (Aβ40-G4 (1:1)): of PPI-G4-Aβ40 at peptide-dendrimer ratio 1 to 1. (Aβ40 fibrils): fibrillar Aβ40. (Aβ40-G5 (1:0.1)): PPI-G5- Aβ40 at peptide-dendrime ratio 1 to 0.1. (Aβ40-G5 (1:1)): Mixtures of PPI and Aβ40 and Aβ40 alone were incubated for 12 hours at pH 7.4 at different dendrimer-peptide ratios previous addition to the cell culture. (Aβ40): Aβ40 was added into the cell culture without incubation. The final peptide concentration was in all cases 25 μM.
Statistics: * : not significantly different, **: significantly different. (ANOVA analysis, $p < 0.05$, n=3).

Brief summary:

In the present work is shown that :

1. PPI maltose dense shell dendrimers of the fourth generation are confirmed to inhibit Alzheimer's amyloid peptide Aβ40 cell toxicity. "Clumped" fibrils (Figure 3.36) of Aβ40-G4 at peptide-dendrimer ratio up to 1 to 1 are not toxic for the PC12 cells.
2. Amorphous aggregated of of Aβ40-G5 (Figure 3.36) are toxic for the PC12 cells.

4 DISCUSSION

4.1 Influence of Cu(II) on Aβ40 aggregation

According to the amyloid cascade hypothesis, amyloid peptides should play a central role in triggering cell toxicity in Alzheimer's disease. However, amyloid formation is a complex phenomenon involving many different intermediate aggregated species. The specific toxic agent or agents have not yet been identified. The mechanism by which Aβ is toxic is nowadays hotly debated (Yankner and Lu, 2009). By the foregoing versions, the insoluble Aβ fibrillar deposits were considered to be the cause of disease, triggering pathogenic processes leading to neuronal death and synaptic dysfunction. How Aβ peptide assembles into fibrils, a complex highly organized structure, in detail is still unknown. A number of soluble Aβ peptide oligomers different in size (ranging from dimers to larger aggregates and protofibrils which are bigger than oligomers but still not fibrils) are described and considered to be true intermediates in the assembly of Aβ fibrils and have been shown to be neurotoxic (Lansbury and Lashuel, 2006), thereby the focus has been shifted from mature fibrils to Aβ assemblies other than fibrils, these oligomers have been proposed as therapeutic targets (Klein et al., 2001) and now Aβ oligomers are believed to play important causal roles in AD (Glabe, 2008). Amyloid aggregation, however, is a process extremely sensitive to different physicochemical parameters, the presence of metal ions such as Cu(II) and other molecules or macromolecular assemblies, such as biological membranes (Benseny-Cases et al 2011). All these factors can greatly influence and modify the way in which the peptides aggregate and, very importantly, they are factors which have full physiological significance, especially under certain pathological conditions. In the present work the amorphous non-fibrillar aggregates of Cu(II)-$A\beta40_{pH11}$ are characterized as possible toxic species in Alzheimer's disease. These toxic amorphous non-fibrillar aggregates are the end product of the interaction of Cu(II) with monomeric Aβ40 ($A\beta40_{m \leftrightarrow o}$). Together with previous descriptions of granular aggregates with poly-glutamine peptides related to Huntington's disease and the SH3 domain of PI3, Aβ amorphous aggregates related to Alzheimer's disease (Benseny-Cases et al. 2011) are a further example of a possible common aggregation and toxicity mechanism in conformational diseases. Cu(II)-$A\beta40_{pH11}$ amorphous aggregates may represent a pharmacological target in Alzheimer's disease.

A notable characteristic of AD is altered Cu(II) ion concentration in the brain. It is known that Cu(II) level in the brain increases with age (Barnham and Bush, 2008), thus the loss of Cu(II) homeostasis is a possible risk factor in AD and the role of copper abnormalities in the pathogenesis of AD is under discussion (Squitti et al., 2004).

It has been shown that Aβ monomers develop into various non-fibrilar Aβ assemblies and may represent distinct structural variants (Yang et al., 2010). It can be assumed that for fibrillization *in vitro* the sequence specificity is less important than conditions leading to polymorphism of amyloid aggregates. It was shown that amyloid fibrils grown in different experimental conditions have different morphology because the oligomers they grow from have different initial conformation and this starting point of fibrillation can be modulated by changing the solution conditions (Takano, 2008). If the Aβ peptides can adapt diverse structures and are capable of aggregating into a variety of structures under slightly different conditions, metals including Cu(II) are certainly contributing to this structural variability. For the truncated Aβ(17-21) peptide it was already shown that different metal coordination structures result in a range of distinct self-assembled morphologies. (Dong et al., 2007).

The aim of of the present work was to elucidate how Cu(II) ions affect the process of aggregation, in view of a strong association of Aβ oligomers toxicity with AD pathogenesis.

The results shows that Cu(II) has a great influence on the kinetics, aggregate morphology and toxicity of Aβ40.

In the present work it was shown that in presence of Cu(II) monomeric $A\beta40_{m\leftrightarrow o}$ form peptide-metal complex (Cu(II)-$A\beta40_{pH11}$).

It was estimated using SAXS technique that Cu(II)-$A\beta40_{pH11}$ complex has spheroidal shape with a diameter around 17 nm (Figure 3.7). Using SAXS it was calculated that the molecular weight of the Cu(II)-$A\beta40_{pH11}$ complex is 330 ± 50 kDa, indicating that one Cu(II)-$A\beta40_{pH11}$ particle consists of 80-100 Aβ40 molecules. The presence of 15-20-nm-size objects was also detected from TEM and AFM images of Cu(II)-$A\beta40_{pH11}$ (Figures 3.2, 3.9). AFM analysis shows that Cu(II)-$A\beta40_{pH11}$ aggregates are up to 6 times bigger than monomeric $A\beta40_{m\leftrightarrow o}$. Interestingly, in the presence of Cu(II), in the same pH conditions, the the complex of Cu(II)-$A\beta28_{pH11}$ is not significantly bigger than monomeric $A\beta28_{pH11}$. (Figure 3.18). Aβ28 does not have C-terminus, so this can indicate that hydrophobic C-terminus plays an important role in the collapse of 80-100 Aβ40 molecules happened at pH11 in the presence of Cu(II).

As the FTIR study shows, after Cu(II) anchors the monomeric $A\beta40_{m\leftrightarrow o}$, within a few minutes the secondary structure of Cu(II)-$A\beta40_{pH11}$ changes from a mixture of unordered and α-helical structures to non-fibrillar β-structure without forming fibrillar β-structure after lowering the pH to 7.4. In the Figure 4.1 is shown the way of Aβ40 secondary stricture evolution in the presence of Cu(II): at pH 11 Aβ40 exist as an equilibrium of monomers and low molecular weight oligomers ($A\beta40_{m\leftrightarrow o}$), a protonation (lowering the pH to pH 7.4) of $A\beta40_{m\leftrightarrow o}$ triggers the amyloid fibril formation through the nucleation phase described by Aβ40 nuclei ($A\beta40_{N}$) with non-fibrillar β-structure (Benseny-Cases et al., 2007). Cu(II)-$A\beta40_{pH11}$ complex after lowering the pH to 7.4 does not form fibrillar aggregates with β-sheet secondary structure, it evolution ends by forming amorphous aggregates with non-β-fibrillar secondary structure. For truncated Aβ28 peptide FTIR study shows, after Cu(II) anchors the monomeric $A\beta28_{m\leftrightarrow o}$, the secondary structure of Cu(II)-

$A\beta280_{pH11}$ rapidly changes from a mixture of unordered and α-helical structures to non-fibrillar β-structure without forming fibrillar β-structure after lowering the pH to 5.5.

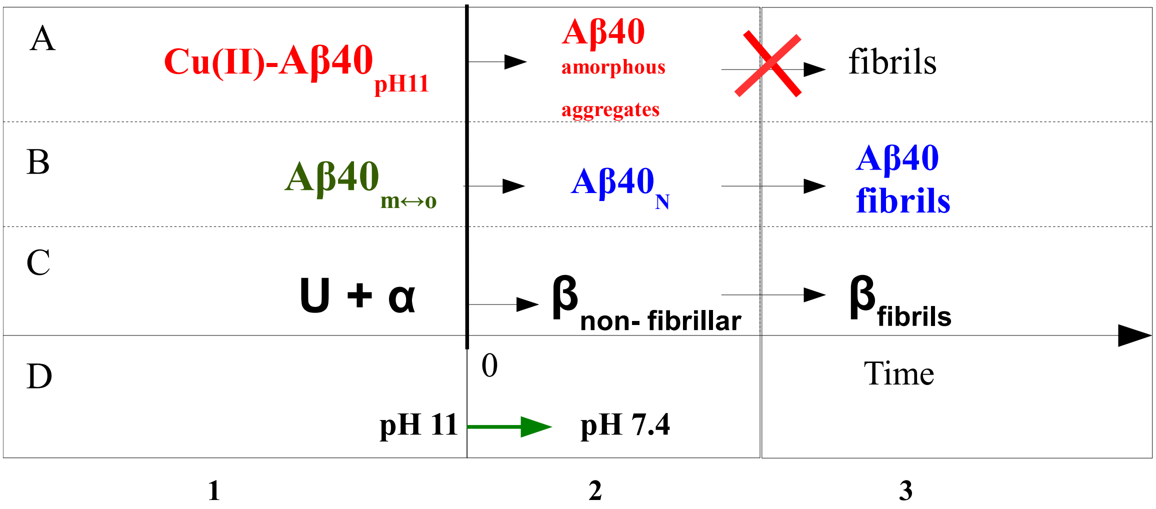

Figure 4.1 The Aβ secondary stricture evolution. The arrows denote the changes. The background corresponds to the secondary structure content: the green dashed area indicates a mixture of unordered and α-helical structures, the light brown dashed area indicates β-non-fibrillar structure, the light blue dashed area indicates β-fibrillar structure. (A) In the presence of Cu(II)-$A\beta40_{pH11}$ after lowering the pH becomes aggregated with non fibrillar β-structure content. without forming fibrillar β-structure. (B) Monomeric $A\beta40_{m\leftrightarrow o}$ in the absence of Cu(II) after lowering the pH first forms Aβ40 nuclei ($A\beta40_N$) with non-fibrillar β-structure and than forms the amyloid fibrils. (C) The content of a mixture of unordered and α-helical structures (column 1) after lowering the pH changes to the content of β-non-fibrillar structure (column 2) and than, with time, changes to the content of β-fibrillar structure (column 3). (D) According to the green arrow it is shown the pH changing from pH11 to 7.4 at time point 0 .

The alteration of Aβ40 secondary structure cause bu Cu(II) is irreversible. This conclusion has been drawn after Cu(II) clearance with a strong chelator EDTA (affinity of EDTA to Cu(II) is 10^8 times stronger than affinity to Cu(II) of Aβ (Sarell et al., 2009)) did not restore the formation of fibrillar structures (Figure 3.17). This results show that if amorphous aggregates once formed further fibrillization is not possible. The results obtained using FTIR, THT fluorescence and TEM confirmed that at pH 7.4 Cu(II)-$A\beta40_{pH11}$ forms amorphous aggregates (Figures 3.11, 3.12, 3.13).

For truncated Aβ peptide it was also shown that Cu(II) ions disaggregate mature Aβ28 fibrils giving place to amorphous aggregates (Figure 3.25). In the case of Cu(II)-Aβ28 complex a Cu(II) clearance with a (EDTA) restores the formation of fibrillar structures. These facts give a support for a suggestion that C-terminus of Aβ40 plays a key role in secondary structure stabilization.

We have shown that those amorphous aggregates of Cu(II)-$A\beta40_{pH11}$ are significantly toxic than fibrillar or monomeric $A\beta40_{m\leftrightarrow o}$ forms of Aβ40 peptide as it was shown in the Figure 3.26.

Aβ40 as it has been previously described that at neutral pH Cu(II)ions can promote Aβ fibril formation (Karr et al., 2004; Sarell, Wilkinson, and Viles, 2010b). Taking into account the results obtained during this study and together with data from the literature we suggest that at least two distinct pathways exist of Aβ40 peptide aggregation in the presence of Cu(II): one pathway is amiloidogenic, the other favors amorphous aggregate formation. The key moment determining the scenario is the conformation of Aβ40 at the moment of Cu(II) binding as it shown in Figure 4.2. First scenario: After protonation monomeric Aβ40$_{m\leftrightarrow o}$ forms nuclei Aβ40$_N$, which are β-structured aggregates composed of tightly packed Aβ40 peptides that have β-sheet secondary structure and with time will form the protofibrilar precursors to Aβ fibrils and finally amyloid fibrils. Second scenario leads to the formation of amorphous aggregates. Cu(II) binds to monomeric Aβ40$_{m\leftrightarrow o}$ forming Cu(II)-Aβ40$_{pH11}$ species with β-non-fibrilar secondary structure. Basing on FTIR band shift it is assumed that hydrogen bonds involved in the formation of β-structure of Cu(II)-Aβ40$_{pH11}$ are weaker than those in β- sheet structure of Aβ40, this can be explained the Aβ40 molecules composition of metal-peptide complex is not regular and this structural irregularity does not fit for fibril formation requirements.

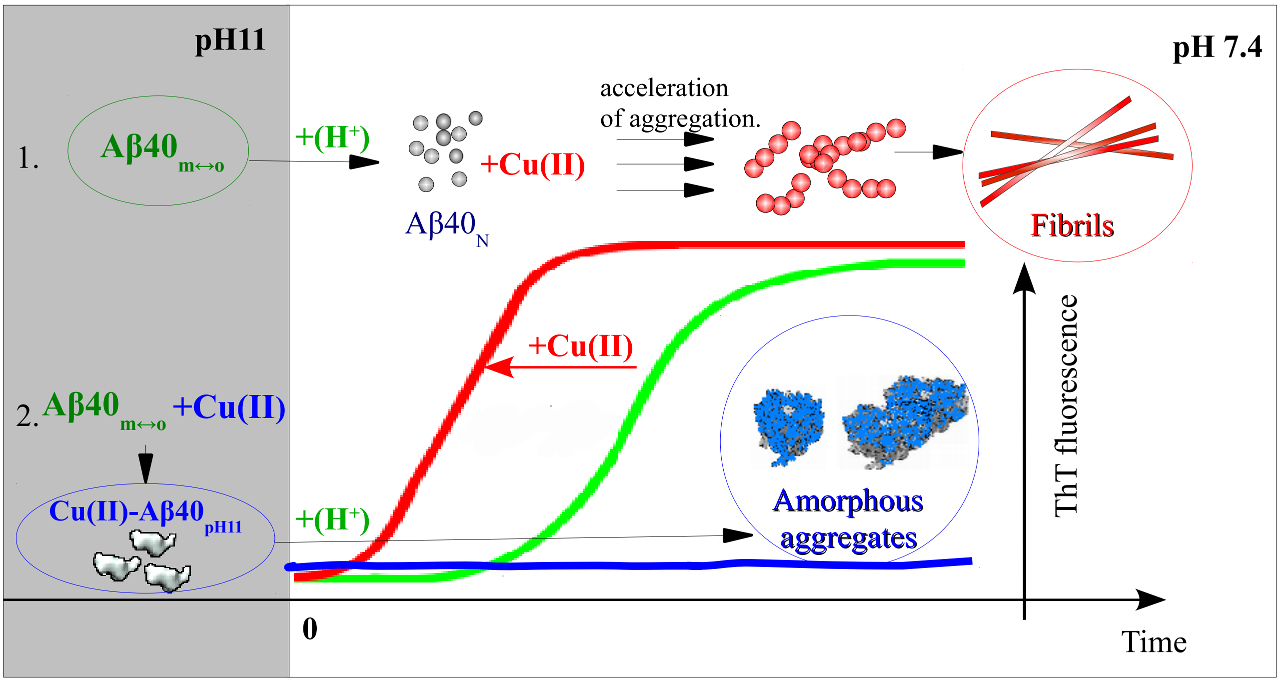

Figure 4.2 In the presence of Cu(II) there are at least two different aggregation pathways for Aβ 40. (1) Pathway leading to ThT positive aggregates: in the absence of Cu(II) after lowering the pH to pH 7.4 (whit area) monomeric Aβ40$_{m\leftrightarrow o}$ forms Aβ40 nuclei (Aβ40$_N$), if Cu(II) binds those “fibril wiling” Aβ40$_N$ nuclei acceleration of fibril formation is observed (red curve). (2) If Cu(II) binds monomeric Aβ40$_{m\leftrightarrow o}$ at pH 11 (gray area) forming Cu(II)-Aβ40$_{pH11}$ species, after lowering a pH to pH 7.4 Cu(II)-Aβ40$_{pH11}$ complex forms non-ThT positive amorphous aggregates (Blue curve). Aβ40 in the absence od Cu(II) ions indicated by green curve.

Based on the data from the literature the following hypothesis can be suggest for the explanation of amorphous aggregates pathway: Alies and co-workers (Alies et al. 2011) described the pH-dependent

Cu(II) coordination to Aβ. It was found that Aβ binds Cu(II) depending on pH conditions. Using EPR, CD, and NMR techniques four possible Cu(II) coordinations in the Cu(II)-Aβ complex were found and described corresponding to the four intervals of pH 6-7.8, pH 7.9-8.3, pH 8.4-10.2 and pH 10.2-12 namely, components I, II, III and IV. The predominant Cu(II) equatorial sites are presented in Figure 4.3.

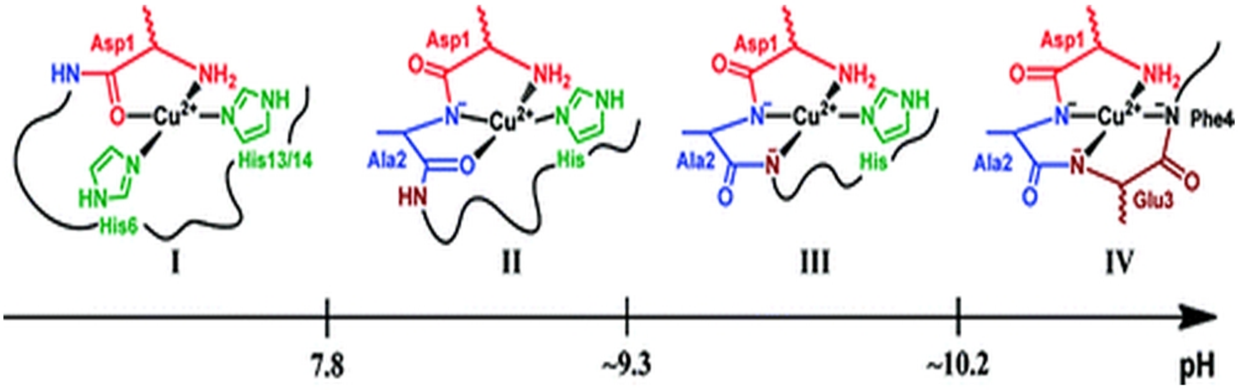

Figure 4.3 Proposed Equatorial Cu(II) binding sites of Aβ-Cu(II) as a function of pH. Depending on pH Cu(II) ion is coordinated by the different residues of Aβ:

I. {−NH2, CO (Asp1–Ala2), Nim (His6), Nim (His13 or His14)},
II. {−NH2, N– (Asp1–Ala2), CO (Ala2–Glu3), Nim},
III. {−NH2, N– (Asp1–Ala2), N–(Ala2–Glu3), Nim}
IV. {-NH(2), N(-) (Asp1-Ala2), N(-) (Ala2-Glu3), N(-) (Glu3-Phe4)}. The scheme was adapted from (Alies et al. 2011).

At neutral pH Cu(II) ion is coordinated by Asp 1, Ala2 and tree His 6, 13, 14 but at pH 11 instead of three His 6, 13 and 14 there are Glu3 and Phe 4 (Figure 4.4).

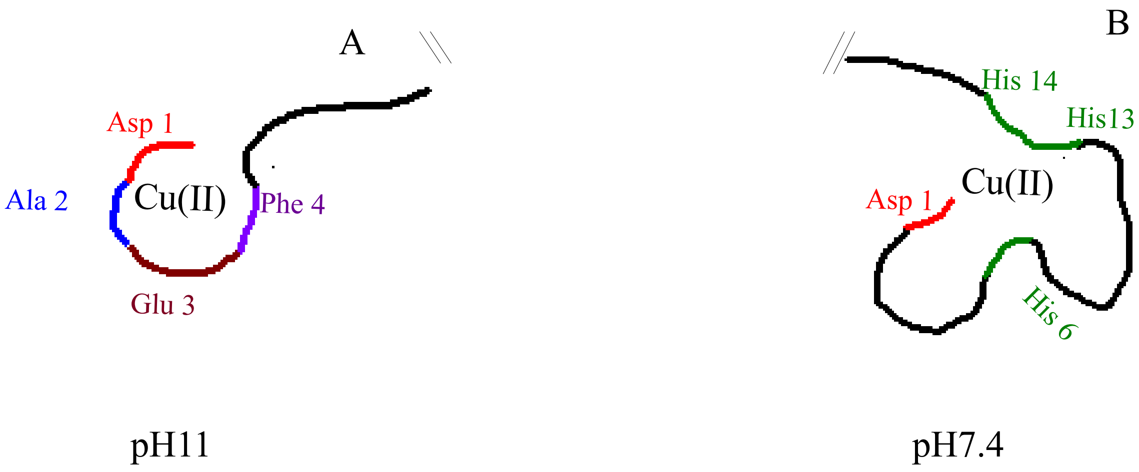

Figure 4.4 The pH induced conformational changes of Aβ-Cu(II) coordination. Black line indicate the Aβ peptide out of the Cu(II)-binding site. (A) pH11 [Asp1-Ala2 -Glu3 -Phe4]-Cu(II) ion coordination (B) pH7.4 [Asp1-Ala2-His6-His13- His14)]-Cu(II) ion coordination.

For fibril assembly Cu(II) has to be coordinated by His 6, 13 and 14. Both, electrostatic and hydrophobic interactions have been recognized as playing a fundamental role in the formation and stabilization of the fibrillar proteinaceous structures known as amyloids (Gazit 2002). Electrostatic interactions take place, within the sequence, between acidic and alkaline residues. Hydrophobic interactions may imply, among others, aromatic residues such as tyrosine 10 and phenylalanine 4. Both have been related on the one hand, to the stabilization of amyloid fibrils through stacking ring to ring interactions; on the other hand, tyrosine 10 residues have been implicated in the binding of metal cations (Karr, 2007; Maiti et al., 2008; Minicozzi et al., 2008; Streltsov et al., 2008). Aromatic stacking interactions, have been previously proposed as amyloid structure stabilizers and are in general recognized as a relevant kind of interaction in protein chemistry (Gazit, 2002; Tjernberg et al., 2002). If Cu(II) coordinated not by His 6, 13 and 14, this makes impossible the formation of the oligomeric species “correctly structured for fibril assembly”and the formation of amorphous aggregates of Aβ take place. As results show this new structure significantly hampers the Aβ tyrosine stacking, therefore affecting the tyrosine intrinsic fluorescence (Figure 3.15).

The results obtained with truncated Aβ28 peptide show that binding of Cu(II) to Aβ peptide may imply the interaction of Cu(II) with tyrosine 10. There are several reasons for this suggestion:

1. Tyrosine 10 is situated closely to the main coordinators of Cu(II) ion: His 6, His 13 and His 14, so it can be assumed that Tyrosine 10 is close to Cu(II) to be involved into metal-peptide interaction.
2. Tyrosine 10 is crucial for fibril formation: the Aβ28 Tyr10Ala mutant does not aggregate.
3. The presence of Cu(II) inhibits the formation of Aβ28 fibrils.

Even if tyrosine 10 does not directly coordinate Cu(II) ion (Streltsov et al. 2008), tyrosine is very important “witness” of interaction of Aβ peptide with Cu(II) because the decrease in its intrinsic fluorescence reflects the changes of peptide secondary structure in the presence of Cu(II). It could be suggested that tyrosine 10 as charged residue may be implicated in electrostatic interactions for example due to the importance of rotational angle of phenoxyl ring (Figure 4.5).

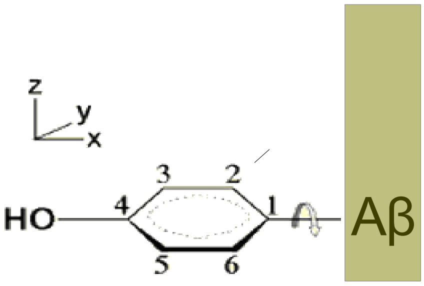

Figure 4.5. This figure defines dihedral angle in tyrosine. The arrow describes possible rotation of the phenol ring of tyrosine residue . Brown strip schematically indicates Aβ40 peptide.

Thus it can be suggested that cytotoxicity of Cu(II)-Aβ40$_{pH11}$ can be explained by the supramolecular organization of the amyloid aggregates. The mature fibrils of Aβ40 and Ab28 were tested to besignificantly harmless to cells than amourphous aggregates (Figure 3.26). One of possible explanation for the augmented toxicity of Aβ-Cu(II) aggregates could be an increased oxidative stress at the membrane by catalysing the production of ROS (reactive oxygen species) in the presence of physiological reducing agents (e.g. ascorbate). Generation of harmful reactive oxygen species by the Cu-Aβ complexes requires the reduction of Cu(II) to Cu(I) by ascorbate followed by O_2 or H_2O_2 activation, which finally leads to neuronal death. Additionally the accumulation of Aβ-Cu(II) at the neuronal cell surface, could generate toxic hydrogen peroxide and hydroxil radicals. Lipid peroxidation of the membrane will compromise membrane integrity and result in cell death.

4.2 Influence of dendrimers on Aβ40 aggregation

PAMAM and phosphorous dendrimers have been previously shown to be able to modulate amyloid peptide aggregation by interfering in different ways (fibril breaking, inhibition of fibril formation, acceleration of fibril formation) with the amyloid polymerization process. The interaction of dendrimers with amyloid peptides has been found to depend on dendrimer structure, generation, pH of the medium and the dendrimer-peptide ratio (Bush et al., 1994; Klajnert, Cladera, et al., 2006; Klajnert et al., 2007, 2007). However, the intrinsic toxicity of PAMAM and phosphorous dendrimers had until now prevented the evaluation of these branched structures as antiamyloidogenic agents by measuring their potential to reduce the amyloid peptides cell toxicity. The situation has changed with the establishment of biocompatible PPI glycodendrimers (Klajnert, Cortijo-Arellano, Bryszewska, et al., 2006) in which each peripheral amino group at the dendritic PPI surface is derivated preferably with twice the amount of sugar molecules. Thus, the resulting dendritic glycostructures have a neutral surface made of a dense maltose shell. With these characteristic structural features, PPI glycodendrimers exhibit a specific interaction capacity with biological molecules governed by hydrogen bonding, and have already been proven to be effective as antiprion agents in cell culture (Barbara Klajnert et al. 2008). In the present study, we have shown that PPI-maltose dendrimers have the capacity to interfere with the fibril formation process of the amyloid peptide Aβ40, related to Alzheimer's disease (Figures 3.33 and 3.34) in two main ways: (1) by inhibiting fibril formation; (2) by clumping amyloid fibrils together. PPI-G5 has been found to be more effective at inhibiting fibril formation than PPI-G4. PPI-G5 completely inhibits fibril formation at much lower dendrimer-peptide ratios (1 to 0.1) than PPI-G4 (1 to 10) (Figure 3.35). The analysis of the results permits to rule out maltose concentration as the key parameter. The conclusion is based on the fact that, at any given maltose concentration up to 10 mM, PPI-G4 and PPI-G5 have a different effect on fibril formation (Table 3.2.1). Within this concentration range PPI-G5 clearly inhibits fibril formation, whereas PPI-G4 does not. In terms of size, PPI-G5 diameter is only 1 nm larger than that of PPI-G4 (Figure 1.18). Thus, the maltose surface density is clearly higher in the case of PPI-G5 (64 Mal units for PPI-G4 and 114 Maltose units for PPI-G5; about 78% more Maltose units on the PPI-G5 surface). Maltose surface density can therefore be the predominant parameter that may explain the highly different amyloid-interfering properties of PPI-G4 and PPI-G5. A higher maltose surface density would correlate with a higher density of any kind of hydrogen bonds (OH-COOH, OH- and OH-N-heterocycles etc.) between the PPI glycodendrimer and the peptides.

The results on the interaction of PPI glycodendrimers and Aβ40 can be interpreted in terms of the possible molecular mechanisms leading to fibrillar or amorphous structures as shown in Figure 4.6. It has been previously described by (Benseny-Cases, Cócera, and Cladera 2007) that Aβ40-Cl (chloride as a counter-ion, as is the case in the present work) forms, very quickly, a mixture of monomers ($A\beta40_m$) and low and high molecular weight oligomers ($A\beta40_o$) when the fibril formation process is triggered by lowering the pH of the peptide solution from 11 (stock solution) to 7.4 (triggering of the fibril formation process). In contact with this mixture PPI-G4 would favor the formation of fibrillar dendrimer-peptide complexes ($G4{\cdot}A\beta40_{Fibrils}$) at dendrimer-peptide ratios below 1. At dendrimer-peptide ratios above 1, PPI-G4 gives amorphous aggregates ($G4{\cdot}A\beta40_{Amorphous}$). Furthermore, the same type of granular aggregates is observed at any of the PPI-G5-peptide ratios measured.

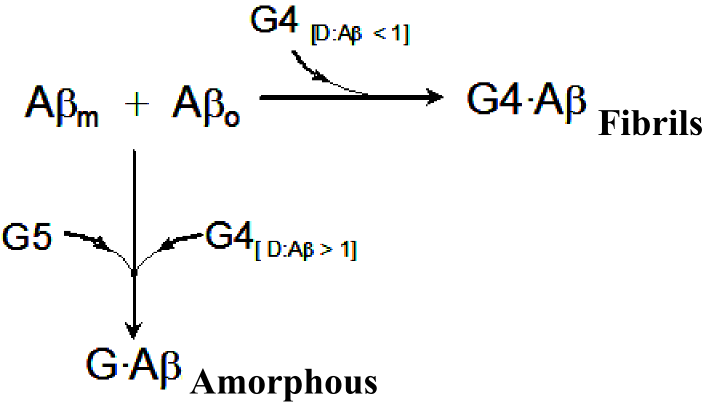

Figure 4.6 Schematic proposal of a molecular mechanism explaining the formation of the different PPI-maltose dendrimers-Aβ40**) aggregates described in the present work**. $A\beta_m$: Monomeric Aβ40; $A\beta_o$: oigomeric (low and high molecular weight oligomers) Aβ40; $G4_{[D:A\beta < 1]}$: PPI-G4 added at dendrimer-peptide ratio below 1; $G4_{[D:A\beta > 1]}$: PPI-G4- Aβ40 at dendrimer-peptide ratio above 1; G5: PPI-G5; $G4{\cdot}A\beta40_{Fibrils}$: PPI-G4- Aβ40 fibrillar complex; $G{\cdot}A\beta40_{amourphous}$: PPI-maltose- Aβ40 non-fibrillar complex. Since Aβ40 with chloride as a counter ion was used in the present work, low and high molecular weight oligomers form very quickly when lowered the pH of the solution from 12 to pH 7.4 (Benseny-Cases et al., 2007) PPI dendrimers were therefore added into these mixtures of monomeric and oligomeric Aβ40.

Morphologically, the interaction of PPI-maltose dendrimers can be schematized as shown in Figure 4.7. In the absence of dendrimers, formation of amyloid fibrils proceeds via a nucleation dependent polymerization process (Figure 4.7a): peptide monomers combine into oligomers of low and high molecular weight; these oligomeric species combine into prefibrillar structures, which finally convert into amyloid fibrils. According to our results, at dendrimer-peptide ratios below 1, PPI-G4 cannot hamper the formation of the prefibrillar structures, so the dendrimer cannot prevent the formation of fibrils, but can glue together the formed fibrils, forming the observed fibril clumps (Figure 4.7b). At dendrimer-peptide ratios higher than 1, PPI-G4 may, due to its high concentration, effectively interfere with oligomer formation from monomeric peptide and/or small oligomeric structures and with oligomer-oligomer interaction, hampering the formation of amyloid prefibrils and therefore preventing the formation of fibrils and favoring instead the formation of amorphous aggregates (Figure 4.7c). Formation of granular aggregates can be accomplished as well with PPI-G5 at any of the tested dendrimer-peptide ratios (Figure 4.7d). In this case and probably due to a higher maltose surface density, the interaction of PPI-G5 with the peptide oligomers can, even at low dendrimer-peptide ratios, change their structure in a way that impedes the correct combination for fibril formation.

One more possible mechanism explaining the formation of amorphous aggregates in the presence of PPI-G5 can be suggested. Assuming that maltose dendrimers catalyze fibril formation at low dendrimer-peptide ratios, PPI dendrimers attract Aβ peptides thereby favoring fibril grow. The increment in catalyzing groups augments the velocity of fibrillation. The “overcatalization” results in insufficiency of time for regular fibril structure grow and chaotic clamping of Aβ peptides happen.

In terms of cell toxicity, we have shown that PPI-G4 used at low dendrimer-peptide ratios inhibits fibril toxicity by clumping the fibrils together, whereas granular, non-fibrillar, amorphous dendrimer-peptide complexes are found to be toxic for the cultured cells. These results will allow a better understanding of the potential use of dendrimers as antiamyloidogenic agents and call the attention towards the necessity to carefully evaluate the toxicity of the different antiamyloid compound-peptide complexes. In this sense, the results may represent a sign of encouragement in the search for antiamyloid strategies based on the use of substances that would clean the medium of oligomeric non-fibrillar (toxic) aggregates by stabilizing fibrillar (non-toxic) structures. At the same time, the results point out the possibility that fibril formation inhibitors can generate very toxic aggregated species. A more detailed physico-chemical characterization of the toxic glycodendrimer-peptide complexes (size, surface potential, etc.), currently under way in our labs, will permit a better understanding of the mechanisms through which they exert the toxic effect. Moreover, together with the present results it will allow the design of new glycodendrimers decorated with additional functional groups in order to try to achieve the formation of non-fibrillar and non-toxic aggregates, increasing in this way the number of antiamyloidogenic strategies.

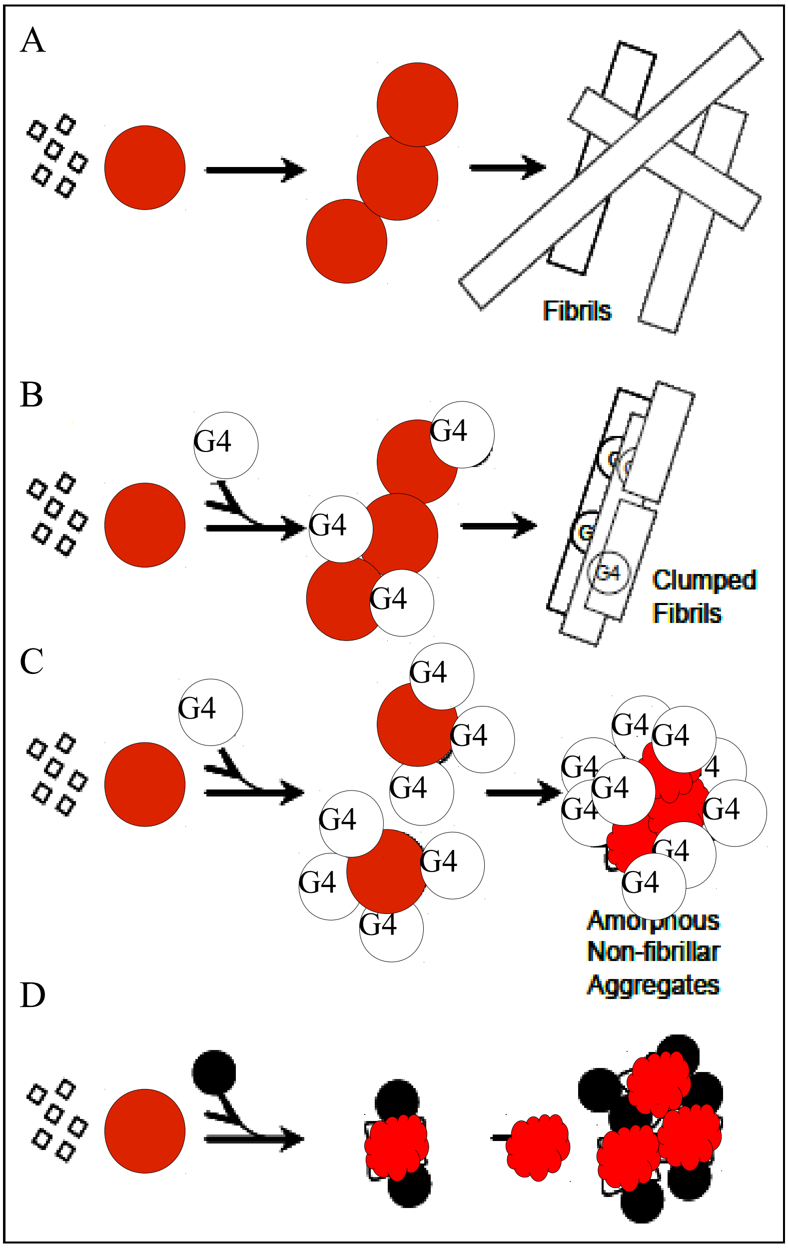

Figure 4.7 Graphic schematically representing the morphology of different dendrimer-amyloid aggregated species and the interactions that can explain their formation. (A) Nucleation-dependent polymerization process of Aβ40: monomeric peptide (◊) assembles as lower and higher molecular weight peptide oligomers (●) (rapid formation under our experimental conditions); prefibrillar structure forms by combination of peptide oligomers (●●●) and finally converts into fibrils (□). (B) In the presence of PPI-G4 dendrimer at low dendrimer-peptide ratios, the interaction of the dendrimer with the monomeric peptide does not prevent the formation of prefibrillar and fibrillar structures but the fibrils are clumped, possibly glued together by the dendrimer; (C) PPI-G4 at high dendrimer-peptide ratios does prevent the formation of prefibrillar structures by interfering with oligomer formation (the dendrimer can interfere by interacting with the peptide monomers, small oligomers and big oligomers) forming dendrimer-peptide oligomer complexes that combine in the form of granular non-fibrillar amorphous aggregates (red cloud); (D) PPI-G5 (●) is able to alter the peptide oligomeric structures (probably due to its capacity to form a higher number of hydrogen bonds per dendrimer) even at low dendrimer-peptide ratios, impeding in this way the formation of prefibrillar structures and leading to the formation of amorphous aggregates.

4.3 Amorphous aggregates in AD.

From our results, a relationship emerges between Cu(II), PPI dendrimers and amorphous aggregates. Both Cu(II) and PPI dendrimers can produce toxic amorphous aggregates (Figure 4.8).

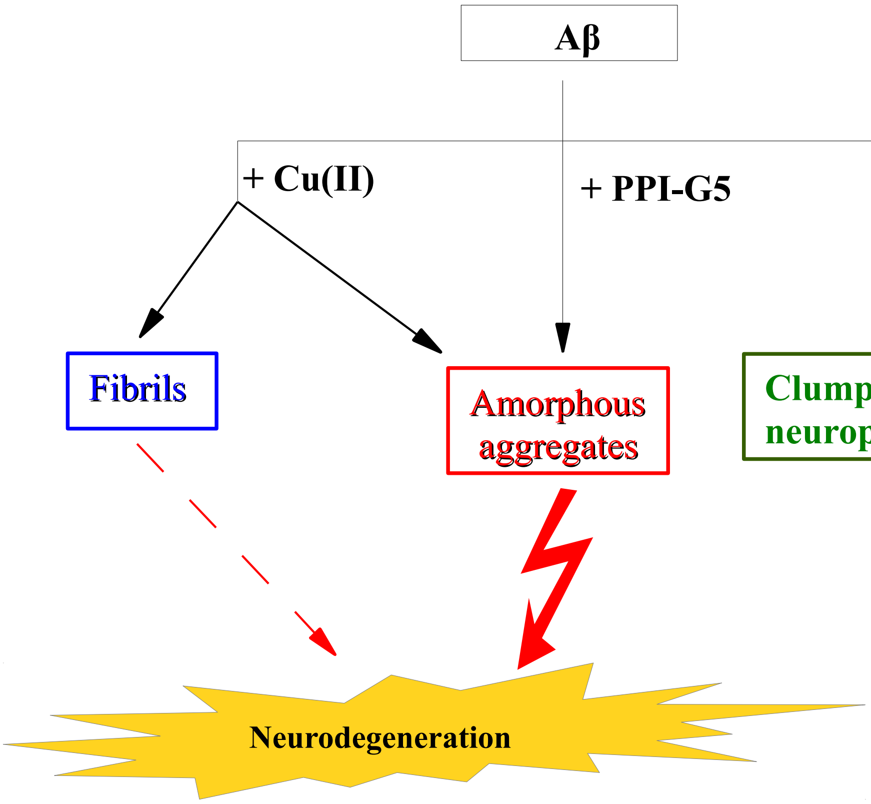

Figure 4.8 Effects of influence on Aβ40 aggregation. The mechanisms of amorphous aggregates formation in those cases could be distinct but the end product will cause neuronal death.

The formation of Aβ40 and Aβ42 non-fibrillar aggregates has been previously described in relation to pH (Kremer et al., 2000) and the presence of metal ions (Ha et al., 2007) although they have not attracted the attention of researchers as possible central players in Alzheimer's disease. Amorphous aggregates, however, have been described in some previous works: one by the group of Ron Kopito with poly-glutamine peptides related to Huntington disease (Mukai et al., 2005) and others by the groups of M. Stefani and C.M. Dobson with the SH3 domain of PI3 (Bush et al. 1994; Bucciantini et al. 2005). In these works the authors point to the possibility of amorphous aggregates implying a common mechanism for protein misfolding diseases. These same type of aggregates are the ones that we identify as Aβ-Cu(II) aggregates forming at pH 11 and PPI-G5-Aβ40.

In summary, from the results obtained during this study we propose the hypothesis of amorphous non-fibrillar Aβ aggregates playing a central role in amyloid toxicity. In relation to neurodegeneration, we have placed amorphous Aβ aggregates in a general scheme in which they represent a possible link between possible causes and risk factors associated to Alzheimer's disease and neurotoxicity, thus becoming, in our view, a molecular target for future pharmacological approaches to the treatment of the pathology (Figure 4.9).

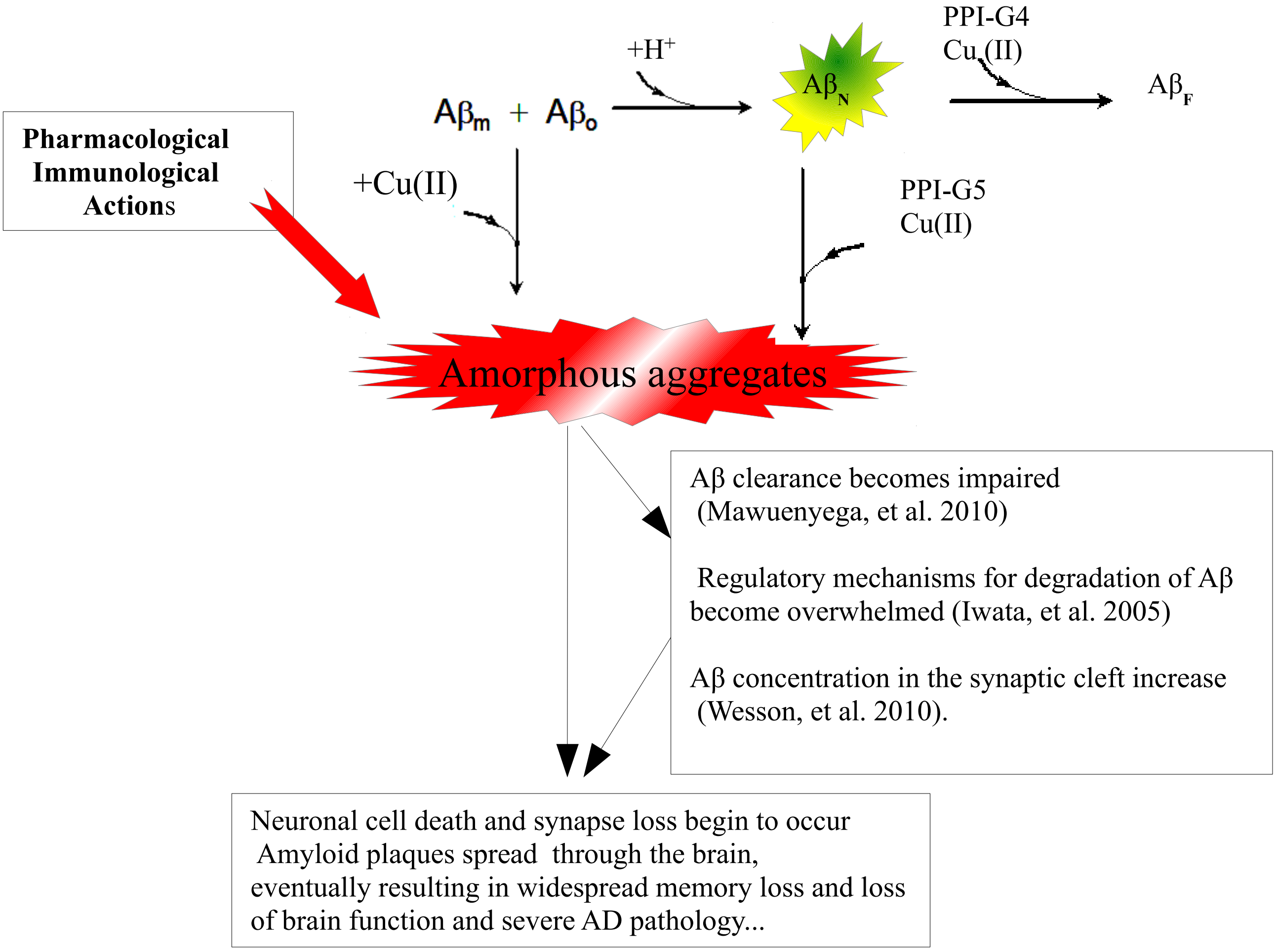

Figure 4.9 **Role of of amorphous aggregates in Alzheimer's disease**. Amorphous aggregates may play a central role in amyloid toxicity related to neurodegeneration by representing a common link between several different possible causes (amyloid peptide hypothesis) enhancement and neurotoxicity. Monomeric Aβ40; $A\beta_{O}$: oigomeric (low and high molecular weight oligomers) Aβ40;·$A\beta40_{F}$: fibrillar complex; $A\beta_{N}$: fibril producing nuclei of Aβ40. Cu(II) and PPI have several ways of interaction with Aβ. Peptide protonation, secondary structure of $A\beta_{N}$ intermediates and the concentration of the additives (Cu(II), PPI dendrimers) results in different aggregation pathways.

5 CONCLUSIONS

The data provided by the experimental part of this thesis allow to make the following conclusions:

INFLUENCE OF CU(II) ON β AGGREGATION

Aβ peptide in the presence of Cu(II) at pH 11 originates the following changes:

- Irreversible decrease of the tyrosine 10 intrinsic fluorescence. Tyrosine 10 is essential for fibril formation (the Aβ28Tyr10Ala mutant does not form amyloid fibrils).

- Irreversible alteration of the Aβ secondary structure promoting the formation of toxic amorphous aggregates which are significantly toxic than Aβ40 as its fibrillar, oligomeric or monomeric forms .

The results of this study suggest that amorphous aggregates may represent a new pharmacological target in Alzheimer's disease. It can be also suggested that metal chelators have no pharmacological potential in AD treatment because if the complex of Cu(II)-amorphous aggregates once formed Cu(II) ions clearance does not change its amorphous conformation.

INFLUENCE OF DENDRIMERS ON β AGGREGATION

- PPI glycodendrimers of generations 4 (PPI-G4) and 5 (PPI-G5) have capacity to interfere with the Alzheimer's amyloid peptide Aβ fibril formation process.

- PPI-peptide interaction is generation dependent: PPI-G5-peptide effectively block amyloid fibril formation generating granular non-fibrilar amorphous aggregates. PPI G4 have the capacity to interfere with the fibril formation process of the amyloid peptide Aβ40 by clumping amyloid fibrils together.

- PPI maltose dendrimers of generations 4 and 5 are non-toxic to neuronal cells at the concentration up to 50 μM.

- Amorphous aggregated of of Aβ40-PPI G5 are toxic for PC12 cells.

- PPI-G4 dendrimers can be efficiently used to inhibit Alzheimer's amyloid peptide Aβ40 cell toxicity by the facilitation of clustering the amyloid fibrils. Those maltose dendrimers are confirmed to inhibit the normal degree of toxicity of Aβ40 fed to the cells in its fibrillar form.

6 RESUM

6.1 Influència del coure i dels dendrímers sobre el procés d'agregació del pèptid beta-amiloide

Una de les característiques principals dels malalts afectats d'Alzheimer (AD) és la presència de plaques senils en el cervell. Aquestes plaques es troben formades pels anomenats pèptids amiloides com l'Aβ40 i l'Aβ42. Sovint, en aquestes plaques, els ions metàl·lics com el Cu(II) o el Fe(III) es troben a concentracions altes i units als pèptids amiloides. L'homeòstasi dels metalls com el Cu(II) es veu afectada en l' etiologia de la malaltia d'Alzheimer. De tota manera, el rol dels ions Cu(II) en la malaltia és encara un fet controvertit.

El primer capítol d'aquesta tesi recull l'estudi de la influència del Cu(II) en l'agregació del pèptid amiloide. Amb aquesta finalitat s'han utilitzat les tècniques de microscòpia de força atòmica (AFM), microscòpia electrònica de transmissió (TEM), dispersió de raigs X a angles petits (SAXS), i espectroscòpia d'infraroig amb transformada de Fourier (FTIR) i espectrometria de fluorescència per a l'estudi de la morfologia i de l'estructura secundària dels agregats amiloides formats en presència de Cu(II). A més a més, els efectes sobre la toxicitat d'aquests agregats s'ha estudiat en les línies cel·lulars PC12 i SH-SY5Y, utilitzades com a model neuronal. Els resultats obtinguts mostren que aquests agregats són no fibril·lars i presenten una toxicitat més alta que les fibres amiloides. Recolzant la hipòtesi de que una alteració de l'homeòstasi del coure pot tenir un rol important en la malaltia d'Alzheimer.

En el segon capítol d'aquesta tesi s'ha estudiat, dintre del marc general de la cerca de compostos per a bloquejar o eliminar les espècies amiloides citotòxiques, els dendrimers de maltosa com a possibles moduladors de l'agregació i de la toxicitat del pèptid amiloide. En aquest treball s'han utilitzat dendrimers de maltosa de les generacions 4 i 5. S'ha confirmat que, contràriament al que passa amb la majoria d'altres compostos dendrimèrics, aquests dendrimers no són tòxics en cèl·lules PC12 i SH-SY5Y i que són capaços de modular l'agregació del pèptid Aβ40. Els dendrimers de cinquena generació interaccionen amb el pèptid amiloide fent que aquest formi agregats no fibril·lars, més tòxics que el pèptid sol. Per altra banda, els dendrimers de generació 4 afecten l'agregació del pèptid en funció de la relació dendrimer-pèptid. A altes relacions de dendrimers, el pèptid forma estructures equivalents a les formades pel dendrimer de generació 5. En canvi, per a relacions dendrimer-pèptid baixes, el pèptid forma fibres que, degut al dendrimer, s'agrupen. En aquestes condicions el pèptid no és tòxic. Aquests resultats permeten considerar als dendrimers de maltosa com a possibles eines per a reduir la toxicitat dels pèptids amiloides.

6.2 Introducció

6.2.1 Impacte de la malaltia d'Alzeimer

A causa de l'augment de l’esperança de vida i de la proporció de gent gran en les poblacions, un dels principals problemes relacionats amb la salut en les pròximes dècades, seran les malalties neurodegeneratives (demències) relacionades amb l'edat. La demència és una disminució de la capacitat mental que en general avança lentament, en què la memòria, el pensament i el judici es deterioren, i la personalitat també ho pot fer. És una de les causes més importants de discapacitat en els ancians. D'acord amb la iniciativa Europea sobre la malaltia d’Alzheimer i altres demencies[3], els tipus més comuns de demència són:

- La malaltia d'Alzheimer (AD) (50 a 70% dels casos, un nombre segurament subestimat a causa de les dificultats en el diagnòstic).
- La demència vascular
- La demència causada per cops freqüents al cervell;
- La demència frontotemporal;
- La malaltia de Pick;
- La malaltia de Binswanger;
- La demència amb cossos de Lewy.

La malaltia d’Alzheimer és una de les més freqüents en les societats occidentals i es preveu un augment dels casos en els pròxims anys. El principal factor de risc és l’edat i per tant, l’envelliment de la població agreuja el nombre de casos de la malaltia i actualment és una de les que té un el món impacte social més elevat. Estudis estadístics mostren que 35,6 milions de persones a tot patia demència, en alguna de les seves formes al 2010, i que questa xifra gairebé es duplicarà cada 20 anys, possiblement arribant als 65 milions de persones l’any 2030 (Informe de 2010 de l’associació ‘Alzheimer’s Disease International’). El nombre de persones que pateixen actualment de demència a Europa s'estima en 9,9 milions (segons una resolució del Parlament Europeu del 19 de gener de 2011 sobre una ‘*Iniciativa Europea sobre la malaltia d’Alzheimer i altres demències*’)[4]. El total de costos mèdics i socials de la malaltia d'Alzheimer a Europa pugen a aproximadament 99.7 mil millions d'euros per l’any 2010. Pel que fa a Espanya, és una de les societats que envelleixen més ràpid en el món. D'acord amb l'índex d'envelliment, la proporció de la població espanyola de 65 anys o més era del 16,8% l’any 2004 i aquest percentatge s'ha duplicat en els últims 30 anys. Es

---

[3] http://europa.eu/legislation_summaries/public_health/health_determinants_lifestyle/sp00 14_en.htm

[4] http://www.europarl.europa.eu/sides/getDoc.do?pubRef=-//EP//TEXT+TA+P7-TA-2011-0016+0+DOC+XML+V0//EN

troba en el setè lloc del rànquing d'envelliment dels països europeus. Per tant, la càrrega de les malalties neurodegeneratives, en especial la malaltia d'Alzheimer, s'espera que creixi de manera exponencial. Segons Pedro-Cuesta et al. (2009) entre 600.000 i 400.000 persones pateixen demència i Alzheimer a Espanya respectivament.

Aquestes dades i xifres demostren la necessitat de millorar els tractaments actuals per a la malaltia d'Alzheimer i sobretot la necessitat d'introduir tecnologies innovadores.

La malaltia d'Alzheimer és una patologia complexa de la qual, avui en dia, encara no se n'ha determinat la causa o les causes. La malaltia porta a la mort neuronal i, per tant, a la pèrdua de part del teixit cerebral. L'estudi histològic de les regions afectades ha portat a la descripció de les dues característiques principals dels cervells dels malalts d'Alzheimer: els garbuixos neurofibril·lars i les plaques neurítiques (Yamaguchi et al. 1991). Aquestes plaques es troben, especialment, en regions de l'hipocamp (que té un paper clau en la formació de nous records) i del còrtex frontal (àrea dedicada a pensar, planejar i recordar), acompanyades de pèrdua de sinapsi i mort neuronal. Les neurones que utilitzen glutamat i acetilcolina com a neurotransmissors, són les més afectades per la pèrdua de sinapsi, tot i que també es poden veure afectades les que produeixen serotonina i norepinefrina (Honer 2003; Mattson 2004). Els garbuixos neurofibril·lars són agregats intracel·lulars de la proteïna tau. Aquesta proteïna, normalment soluble, s'associa als microtúbuls i els estabilitza. Ara bé, en la malaltia d'Alzheimer, la proteïna tau es troba hiperfosforil·lada i agregada formant fibres. Les plaques neurítiques són dipòsits de fibres i agregats amorfs del pèptid β-amiloide (Aβ) de 10 a 120 μm de diàmetre, que presenten un centre més dens de pèptid Aβ rodejat de neurites.

Seguint mecanismes encara poc coneguts, les fluctuacions conformacionals que experimenten els intermediaris del plegament en el procés que porta a l'estat natiu de les proteïnes poden, en determinades condicions, generar agregats moleculars estables. Aquests agregats, poden ser amorfs, o bé, adoptar una estructura fibril·lar molt ordenada i poden existir en equilibri termodinàmic amb l'estat natiu i desnaturalitzat. Algunes mutacions puntuals en la seqüència peptídica (amiloïdosi d'origen hereditari o esporàdic), l'aparició d'espècies que afavoreixin la formació de nuclis i que incloguin la seqüència nativa (malaltia d'Alzheimer i Encefalopaties Espongiformes) i canvis en el pH local poden afavorir la formació de les formes agregades. Aquests agregats són especialment importants degut a la relació directa que tenen amb algunes malalties, com la d'Alzhimer, ja que constitueixen les plaques neurítiques.

6.2.2 Model d'agregació dels pèptids amiloides

El pèptid amiloide present a les plaques senils, prové del processament proteolític d’una proteïna precursora, l’APP, i té de 39 a 43 residus aminoacidics, però la població majoritaria està formada per un fragment de 40 residus (Aβ40), i un de 42 residus (Aβ42).

El pèptid amiloide es secretat a l'espai extracel·lular en forma de monòmer on, mitjançant un procés de polimerització, forma les fibres típiques de les plaques senils. Aquest procés d'associació, a més, comporta canvis en l'estructura secundaria del pèptid. Així, el pèptid monomèric en forma desordenada adopta una estructura ordenada de fulla beta quan es troba formant fibres. La cinètica de formació de les fibres té una forma típicament sigmoidal, la qual s'interpreta com a un procés de polimerització nucleada. En aquests tipus de processos, es defineixen dues fases. La primera, anomenada de latència o nucleació, és la més lenta i consisteix en la progressiva associació de monòmers per a formar oligòmers de baix pes molecular, el quals també poden associar-se formant oligòmers d'alt pes molecular. En una segona fase, aquests oligòmers serveixen de nucli per a la formació de fibres, tant per acoblament d'oligomers com per addició de monòmers.

El detall molecular que defineix aquestes dues fases està encara per aclarir i existeixen diferents interpretacions pel que fa al nombre i l'estructura dels intermediaris que portarien a la formació de nuclis i fibres. Entre els monòmers i les fibres s'han definit a la literatura diferents intermediaris de baix pes molecular (2-8 monòmers) i d'alt pes molecular (20-40 monòmers). Els mecanismes de formació d'oligòmers pels pèptids amiloides Aβ42 porten a una formació ràpida de pentàmers i hexàmers d'Aβ per a la posterior formació de protofibres. En canvi, està descrit que per al pèptid Aβ40 es manté un equilibri de monòmers, dímers, trímers i tetràmers. Hi ha molts estudis dedicats a la caracterització morfològica dels oligomers i sembla haver-hi consens en què presenten una morfologia esfèrica. La importància de la caracterització d'aquestes formes intermediàries rau en les evidències que la toxicitat del pèptid amiloide està lligat a la presència d'aquestes estructures oligomériques.

6.2.3 Influència del coure sobre l'agregació del pèptid amiloide

La malaltia d’Alzheimer es caracteritza per plaques extracel·lulars amiloides, compostes predominantment per pèptids β-amiloides de 39 a 43 aminoàcids. Els Aβ40 i Aβ42 solubles (components principals de les plaques) són presents al líquid cefaloraquidi (LCR) i al plasma sanguini des del naixement (Lambert et al. 1998;.Vigo-Pelfreyet et al. 1993), però el detonant que promou l'oligomerització, la formació de fibres o altres agregats és un tema de discussió.

Una característica notable de la malaltia d'Alzheimer és la concentració alterada d'ions metàl·lics al cervell i una alteració de l'homeòstasi d'aquests (Dong et al. 2003). Els nivells fisiològics de Cu(II) indueixen l'agregació d'Aβ (Atwood et al. 2002; Atwood et al. 1998; Bush 2003). Es pensa que les interaccions del coure amb l'Aß tenen un rol important en la malaltia d'Alzheimer, en particular a causa de la producció d'espècies altament reactives derivades del oxigen i per l'oligomerització del pèptid induïda per Cu(II) (Bush 2003; Barnham i Bush 2008; Balland, Hureau i Savéant 2010, Jiang et al. 2010;. Sarell, Wilkinson i Viles 2010b; Drew, Màsters i Barnham 2010). Per comprendre el rol que el coure podria representar en aquests processos, és essencial tenir un coneixement detallat de les interaccions fonamentals entre Cu(II) i Aß. Els nombrosos mecanismes proposats per a possibles interaccions entre Cu(II) i Aß entren sovint en conflicte i encara no són concloents. Alguns resultats indiquen que el Cu(II) actua com a neuroprotector, prevenint la formació d'espècies Aβ tòxiques (Yoshiike et al 2001; Zou et al. 2002), mentre que d'altres suggereixen que el Cu(II) indueix estructures Aβ que són neurotòxiques (Kirkitadze, Habiten i Teplow 2002). Una de les propostes per explicar la neurotoxicitat induïda per la interacció amb Cu(II) és que aquesta resulta dels canvis produïts a l'entorn de coordinació del Cu(II) durant l'oligomerització del pèptid Aβ (Smith et al. 2007). Ja que aquesta àrea no ha estat encara explorada en detall, és important caracteritzar la interacció del Cu(II) amb monòmers Aβ. Com que a més, la toxicitat del pèptid pot estar relacionada amb la morfologia dels agregats que forma en presència de Cu(II), és important dilucidar la influència del coure en l'oligomerització d'Aβ és potencialment important per a la comprensió de la malaltia d'Alzheimer.

6.2.4 Els dendrímers i el pèptid beta-amilode

Els dendrímers són una nova classe de polímers globulars, molt ramificats que, gràcies a la seva estructura, permeten un gran ventall d'aplicacions biomèdiques, com per exemple l'encapsulament de fàrmacs o la teràpia gènica. El terme dendrímer deriva del grec dendron, que significa "arbre", fent referència a la seva forma hiperramificada i arborescent. El primer dendrímer va ser sintetitzat per D.A. Tomalia i col·laboradors (Tomalia et al., 1985). Al mateix temps i de manera independent, el grup de Newkome (Newkome et al., 1999) va donar a conèixer la síntesi i, des d'aleshores els dendrímers han estat àmpliament estudiats degut a la seva forma única.

Els primers dendrímers sintetitzats van ser els de tipus PAMAM (poliamidoamines), que estan formats per un nucli central d'amoni. Actualment, existeixen diferents companyies especialitzades en la síntesi de dendrímers a gran escala com Dendritech i també es poden adquirir del catàleg de productes de la companyia Sigma, com qualsevol altre compost químic.

El procés de síntesi té lloc mitjançant una seqüència de reaccions iteratives, de tal manera que cada etapa de la reacció dóna lloc a una nova i major generació. La síntesi es pot donar de manera divergent (el dendrímer creix a partir d'un nucli central, per addició de monòmers) o convergent (el dendrímer creix per etapes, des de les branques cap al nucli central). Al final de cada branca hi ha tres grups amino lliures, els quals poden reaccionar amb dues molècules de metil acrilat i dues molècules d'etilendiamina. Cada seqüència de reaccions completa dóna lloc a una nova generació del dendrímer, amb unes propietats definides, podent arribar fins a 10 generacions. El nombre de grups reactius a la superfície es duplica amb cada generació, mentre que la massa molecular augmenta més de dues vegades.

Els dendrímers són macromolècules monodisperses, a diferència dels polímers lineals, ja que la seva massa i mida molecular són controlades de manera específica durant el seu procés de síntesi. Degut a la seva arquitectura, els dendrímers en solució presenten una certa viscositat que augmenta a mida que augmenta la generació. La seva solubilitat ve determinada per la presència de grups terminals, de tal manera que els dendrímers amb grups terminals hidrofílics són més solubles en dissolvents polars mentre que els que tenen grups hidrofòbics són més solubles en dissolvents orgànics. La seva forma globular i la presència de cavitats internes confereixen als dendrímers unes propietats úniques, com la possibilitat d'encapsular fàrmacs en el seu interior i el seu posterior redireccionament cap a òrgans i teixits específics en el cas de la teràpia gènica.
La recerca i caracterització de molècules que interfereixin en el procés d'agregació de pèptids i proteïnes amiloides resulta del màxim interès en el desenvolupament d'estratègies per a combatre els mecanismes desencadenants de les patologies. En aquest sentit, s'ha descobert que els dendrímers amb grups amino a la seva superfície, com els PAMAM (poliamidoamina) o el PPI (polipropilenimina) són capaços d'eliminar les molècules de PrP^{SC} de cultius neuronals infectats per prions (Supattapone et al., 1999, 2001; Heegaard et al., 2004) i que la capacitat d'eliminació dels prions augmenta amb el nombre de generacions del dendrímer. J. Solassol et al. han estudiat l'efecte de 3 generacions (3ª, 4ª i 5ª) de P-dendrímers (dendrímers que contenen grups fosfats) com a agents anti priònics(Supattapone et al., 1999, 2001). Els resultats obtinguts demostren una capacitat d'eliminació dels prions existents en les cèl·lules infectades i de pèrdua de la infectivitat amb el tractament amb P-dendrímers.

D'altra banda, se sap que els dendrimers PAMAM i els P-dendrimers tenen una elevada capacitat d'interferir en el procés d'agregació de fragments del pèptid amiloide relacionat amb la malaltia d’Alzheimer. Segons la relació dendrimer-pèptid, pden ocasionar una accelaració del procés de formació de fibres o una inhibició del mateix (les nostres referències sobre el tema).

En general, un dels principals problemes de la utilització de dendrimers com a agents antiamiloidogènics, es la toxicitat intrínseca d’estructures dendrimèriques com els PAMAM o els de fòsfor. El desenvolupament de glicodendrímers, decorats per exemple amb maltosa, representa la possibilitat d'utilitzar els dendrímers amb una baixa toxicitat intrínseca.

6.3 Hipòtesi

D'acord amb la hipòtesi de la cascada amiloide, els pèptids amiloides tenen un paper central en l'aparició i desenvolupament de la malaltia d'Alzheimer. La toxicitat del pèptid depèn fortament del seu estat d'agregació i, a la vegada, l'agregació del pèptid depèn de diversos factors fisicoquímics, com la presència de cations metàl·lics divalents. La interacció dels cations metàl·lics divalents amb el pèptid amiloide afectarà la conformació dels agregats peptídics i influirà fortament en la toxicitat del pèptid.

Avui una de les principals estratègies per lluitar contra la malaltia d'Alzheimer és el disseny de compostos capaços de bloquejar o inhibir les espècies agregades tòxiques dels pèptids amiloides.

6.4 Objectius

El pèptid amiloide és un dels principals components de les plaques senils dels cervells afectats per la malaltia d'Alzheimer. Els nivells fisiològics de coure indueixen l'agregació d'Aβ i per tant, les interaccions del coure amb l'Aß tenen un rol important en la malaltia d'Alzheimer, en particular a causa de la producció d’espècies altament reactives derivades del oxigen i per l'oligomerització induïda per coure.

L'objectiu general d'aquest treball és la caracterització molecular de la interacció del pèptid beta-amiloide amb el coure i els dendrimers.

Aquest objectiu general s'ha d’assolir a partir dels següents objectius específics:

- Caracterització molecular dels intermediaris formats durant el procés de formació de fibres en presència de coure.

- Determinació de la influència de les característiques moleculars dels intermediaris formats amb coure en la capacitat tòxica del pèptid amiloide en cultius cel·lulars.

- Caracterització molecular dels intermediaris formats durant el procés de formació de fibres en presència de diferents dendrímers.

- Determinació de la influència de les característiques moleculars dels intermediaris formats amb els dendrimers en la capacitat tòxica del pèptid amiloide en cultius cel·lulars.

6.5 Resultats

6.5.1 Influència del coure en el procés d'agregació del pèptid beta-amilode

Un dels objectius d'aquest treball va ser caracteritzar la influència del Cu(II) en la conformació d'Aβ40 i en la capacitat del monòmer d'Aβ40 per formar fibres i, tanmateix, l'efecte dels complexos Aβ40-Cu(II) en la toxicitat cel·lular. Per a aquest estudi s'han aplicat un gran nombre de tècniques com ara SAXS, AFM, TEM i assaigs de toxicitat. En aquest capítol s'ha trobat que, inicialment, el Cu(II) s'enllaça amb els monòmers Aβ40 (el pèptid es te en estat monomèric a pH 11) els quals afavoreixen la formació d'oligòmers de 330 ± 50 KDa, que s'agreguen en compostos amorfes no fibril·lars i tòxics després d'una protonació addicional (baixada del pH de 11 a 7.4 desprès d'incubar el pèptid amb coure).

Per avaluar el possible paper dels agregats amorfs formats en presencia de Cu(II) en la toxicitat del pèptid β-amiloide, es van realitzar experiments de citotoxicitat amb dues línies cel·lulars amb característiques diferents:

1. Cèl·lules PC12: Línia cel·lular derivada d'un feocromacitoma (tumor neuroendocrí) de la medul·la de rata (Arispe etal. 2004).
2. Cèl·lules SH-SY5Y: Línia cel·lular de tercera generació de neuroblastomes, clonada a partir d'altres línies provinents d'una línia cel·lular original de feocromacitoma.

Es va utilitzar la prova del MTT per mesurar la viabilitat cel·lular. El pèptid es va incubar a pH 11 en presencia de Cu(II) o es va ajustar el pH a 7.4 abans d'afegir-lo a les cèl·lules. Els agregats es van deixar 24 hores al cultiu cel·lular. L'addició d'agregats formats a pH 11 en presencia de Cu(II) als cultius cel·lulars redueix un 42 % el metabolisme de les cèl·lules SH-5YSY i un 49 % el metabolisme de les cèl·lules PC12, la reducció del metabolisme provocada pels agregats amorfs en les dues línies cel·lulars és molt més elevada que la provocada pel pèptid s'ha afegit sense Cu (II) a pH 7.4 i pH 7.4l cultiu cel·lular, en aquest cas el metabolisme cel·lular es va reduir en un 20%.

Aß té un extrem N-terminal hidrofílic i una regió C-terminal més hidrofòbica. El fragment peptídic Aβ28 no té la regió C-terminal i no mostra cap tendència a agregar-se a un pH neutre. La formació de fibres del pèptid Aβ28 és induïda pel salt de pH de neutre a <6 (Perálvarez-Marín, Barth i Gräslund 2008). Els resultats dels estudis sobre la interacción del Cu(II) amb el fragment Aβ28 varen demonstrar que:

1. La reducció del metabolisme provocada pels Cu(II)-Aβ28 en cèl·lules PC12 i SH-SY5Y és molt elevada (45%), mentre que Aβ28 sol no és tòxic.
2. Per Aβ28 la tirosina 10 és crucial en la formació de fibres: la Aβ28 mutant Tyr10Ala no s'agrega.
3. La presència de Cu (II) inhibeix la formació d'estructures fibril·lars de Aβ28.
4. L'adició de Cu (II) provoca la desestructuració de fibres de Aβ28 preformades.

6.5.2 Influència dels dendrímers en el procés d'agregació del pèptid beta-amilode

Es coneguda la capacitat dels dendrimers per interactuar amb els amiloides, encara que la majoria dels dendrímers assajats en els sistemes amiloidogènics són tòxics per les cèl·lules. El desenvolupament de glicodendrímers de poli(propilenimina) o PPI decorat amb maltosa (Mal), representa la possibilitat d'utilitzar els dendrímers amb una baixa toxicitat intrínseca. En aquest treball s'ha demostrat que la quarta (PPI-G4) i cinquena (PPI-G5) generació tenen la capacitat d'interferir en el procés d'agregació del pèptid amiloide. Això es fa evident, al mesurar tant la fluorescència de la ThT com el percentatge de fibres generades.

La interacció és depenent de la generació: PPI-G5 anul·la la formació d'estructures fibril·lars, afavorint la formació d'estructures granulars no fibril·lars (agregats amorfs) mentre que els dendrimers de quarta generació PPI-G4 té un comportament dual, ja que generen l'agrupació de les fibres del pèptid a baixes relacions dendrímer:peptid amiloide i la formació d'agregats amorfs en altes relacions dendrímer:petid. El següent pas va ser investigar la morfologia dels diferents Aβ40-dendrímers agregats mitjançant microscòpia electrònica de transmissió. Al microscopi electrònic es pot observar que al final del procés d'agregació s'observen fibres d'Aβ40 típiques. En presència de PPI-G4 en una proporció de dendrímers-pèptid de 0,1 les fibres trobades són mes grans i es troben agrupades i no s'observa la presencia de cap agregat amorf, mentre que en presència de PPI-G5 s'originen agregats amorfs. Aquesta formació d'agregats no fibril·lars es va observar en totes les relacions de PPI-G5 i pèptid estudiades i només quan la relació era de 10 per al dendrimer PPI-G4. Per avaluar l'efecte dels dendrímers sobre la viabilitat cel·lular i sobre la toxicitat del pèptid Aβ40 en cultiu cel·lular, es van realitzar experiments de citotoxicitat amb dues línies cel·lulars: PC12 i SH-SY5Y.

Es va utilitzar la prova del MTT per mesurar la viabilitat cel·lular. Així, es va demostrar que tots dos dendrimers de maltosa (PPI-G4 i PPI-G5) no eren tòxics per a qualsevol de les dues línies cel·lulars fins a una concentració de 50 μM. Posteriorment, es van utilitzar les cèl·lules PC12 per determinar la influència de glicodendrímers PPI sobre la toxicitat de Aβ40. Quan es van afegir les fibres d' Aβ40 al cultiu cel·lular, el metabolisme cel·lular es va reduir en un 20%. En canvi, quan es va afegir el monòmer d'Aβ40, es va observar que l'activitat metabòlica baixava al voltant del 40%. En presència de PI-G4-Mal amb una relació de dendrímers-pèptid de 0,05:1 la viabilitat cel·lular no es veia reduïda en absolut, mentre que l'addició de PPI-G4 incubades amb el pèptid amiloide (relació de dendrímers-pèptid de 0,1:1) va reduir el metabolisme cel·lular poc més del 10%. Els resultats indiquen que el dendrímer PPI-G4 origina fibres d'Aβ40 no tòxiques mitjançant l'aglutinació d'aquestes. Per altre banda, PPI-G4 per si sol no va mostrar cap toxicitat cel·lular en l'assaig. No obstant això, quan PPI-G5 es va incubar durant 12 hores en la presència d'Aβ40 en una proporció de dendrímers-pèptid de 1:1, el metabolisme cel·lular es va reduir en un 40%, un efecte molt similar a l'observat per el monòmer d'Aβ40. Per tant, els dendrímers PPI-G5 afavoreixen la generació de grans agregats amorfs que resulten ser molt mes tòxics. En conjunt, podem concloure que glicodendrímers són prometedors agents no tòxics en la recerca de compostos anti-amiloidogènics.

6.6 Discussió general

Dels resultats d'aquest treball, s'infereix, en primer lloc que tant el coure com el dendrimers poden generar agregats amorfs (Figura 1). Aquest fet resulta tenir una transcendència específica en relació a la morfologia de les espècies agregades que resulten ser citotòxiques. Actualment es coneixen diverses malalties de les anomenades conformacionals, causades pel plegament incorrecte i l'agregació de pèptids i proteïnes que es troben normalment a l'organisme. El fenomen d'agregació és especialment rellevant quan es tracta de pèptids ja que els intermediaris parcialment plegats són més abundants que en proteïnes (Dobson 2004; Jahn i Radford 2005). Sovint i independentment de la proteïna o pèptid implicat, l'agregació és en forma de fibres molt similars en aparença i estructura secundària (estructura β perpendicular a l'eix fibril·lar). Les bases del plegament de proteïnes mostren com estats parcialment plegats poden afavorir, en determinades circumstàncies, contactes intermoleculars favorables a l'associació, causant la formació que poden ser fibril·lars o amorfs. De fet, es coneixen seqüències peptídiques i residus que afavoreixen l'agregació del pèptid.

Com ja s’ha dit, una de les anomenades malalties conformacionals és la malaltia d’Alzheimer en la qual és el pèptid β-amiloide el que agrega formant fibres. Ara bé, aquest procés de formació de fibres és altament depenent de factors físicoquímics com la temperatura o el pH (Sunde i Blake 1997; Dobson 1999). La formació d’agregats amorfs, com a ruta alternativa a la formació de fibres, ja s'ha descrit anteriorment en relació al pH (Kremer et al. 2000) i la presència d'ions metàl·lics (Ha, Ryu, i el Parc de 2007) tot i que no va atreure l'atenció dels investigadors com a possibles actors centrals en la malaltia d'Alzheimer. En quant a la seva toxicitat, els agregats amorfs s'han descrit en alguns treballs anteriors: una pel grup de Ron Kopitar amb pèptids de poli-glutamina relacionats amb la malaltia de Huntington (Mukai et al 2005). I altres, pels grups de Stefani i Dobson amb pèptids del domini SH3 de la PI3 (Bucciantini et al 2002; Bucciantini et al 2005). En aquests treballs els autors apunten la possibilitat d'agregats amorfs que implica un mecanisme comú per a les malalties de mal plegament de proteïnes. Aquests mateix tipus d'agregats son tòxics per les cèl·lules neuronals.

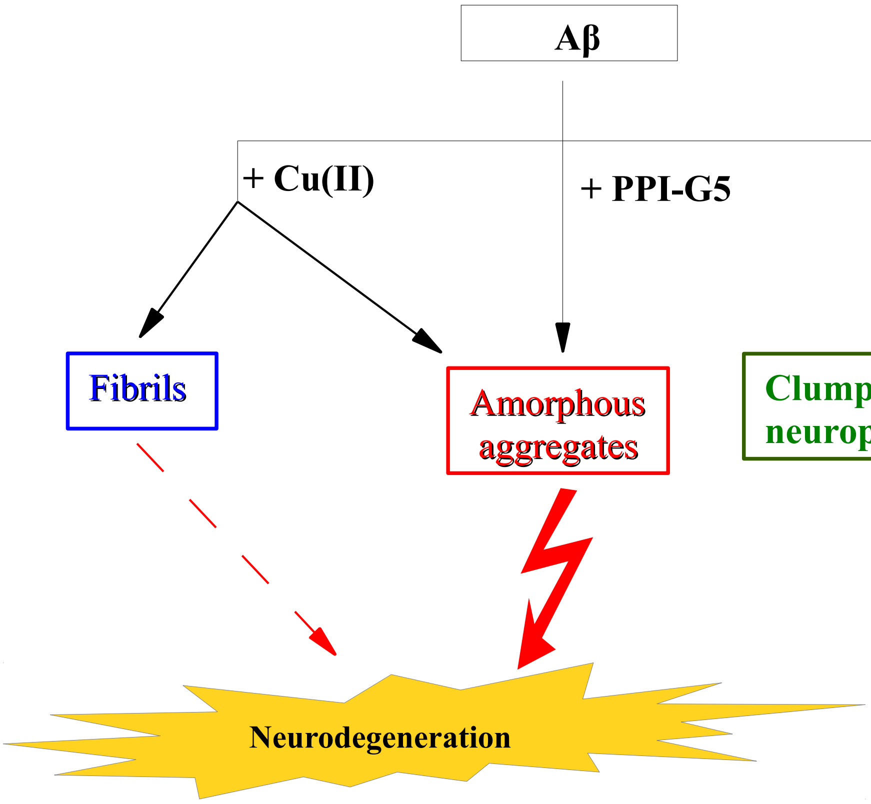

Figura 6.1 Relació entre el coure i els dendrimers en la generació de agregats amorfs tòxics.

Els resultats presentats en aquesta memòria els agregats amorfs formats pel pèptid l’Aβ40, en presència de coure i en presència de dendrimers, s’afegeix a la formació d’agregats amorfs descrita pel nostre grup a pH 5.5 (Benseny et al. Curr Azl Res), com a possibles protagonistes de la citotoxicitat del pèptid, si més no, en un nivell semblant al que es dóna actualment a les estructures oligomèriques que es formen durant la fase de latència a pH neutre, com possibles agents citotòxics.

En resum, a partir d'aquests resultats proposem la hipòtesi que els agregats amorfs juguen un rol central en la toxicitat de la proteïna amiloide. En relació a la neurodegeneració, tal i com es mostra a la següent figura6.1, els agregats amorfs representen un possible vincle entre les possibles causes i factors de risc associats a la malaltia d'Alzheimer (estrès oxidatiu, els esdeveniments vasculars, els pèptids amiloide) i neurotoxicitat, convertint-se així, en una diana molecular per al futur dels enfocaments farmacològics per al tractament de la patologia.

Els resultats obtinguts en el present treball pel que fa a la interacció dels dendrímers de maltosa amb el pèptid amiloide, assenyalen també que aquestes estructures polimèriques es poden utilitzar per a reduir la citotoxicitat de les formes agregades del pèptid. S'ha demostrat que la utilització de la generació 4 de dendrímers de maltosa genera la formació de fibres enganxades (clumped fibrils), unes estructures que resulten no ser citotòxiques. Els dendrímers de maltosa per tant, resulten ser una eina potencialment útil en la recerca d'agents antiamiloidogènics, que permetin bloquejar la formació de les formes citotòxiques del pèptid amiloide relacionat amb la malaltia d'Alzheimer.

6.7 CONCLUSIONS

Les dades obtingudes de la part experimental d'aquesta tesi permet realitzar les següents conclusions:

INFLUÈNCIA DEL COURE EN EL PROCÉS D'AGREGACIÓ DEL PÈPTID Aß............................

El pèptid Aß en presència de Cu(II) a pH 11 origina canvis estructurals, com ara:

- Causar una disminució irreversible de la fluorescència intrínseca de la tirosina 10. La tirosina 10 és essencial per a la formació de fibres (el mutant Aβ28Tyr10Ala no forma fibres d'amiloide) i, que condueixen a una major citotoxicitat.

- Provocar una alteració de l'estructura secundària Aß, afavorint la generació de grans agregats amorfs els quals son molt més tòxics que les fibres.

El resultats obtinguts en aquest primer estudi suggereixen que els agregats amorfs poden representar una diana farmacològica interessant. També es pot suggerir que els quelants de metalls no poden oferir un bon potencial terapèutic per al tractament d'AD perquè un cop format el complex Cu(II)-agregats amorfs, aquest conserva la seva estructura.

INFLUÈNCIA DELS DENDRÍMERS EN EL PROCÉS D'AGREGACIÓ DEL PÈPTID Aß40.

- El dendrimers de maltosa de quarta (PPI-G4) i cinquena (PPI-G5) generacions tenen la capacitat d'interferir el procés de formació de fibres amiloides.

- La interacció dendrímer:pèptid amiloide és depenent de la generació: PPI-G5 és molt eficaç en el bloqueig de la formació de fibres d'amiloide, generant estructures granulars no fibril·lars o agregats amorfs. Mentre que PPI-G4 genera fibres de pèptid més agrupades a relacions dendrímers:pèptid baixes i agregats amorfs a altes relacions.

- PPI-G4 i PPI-G5 no són tòxics per les cèl·lules PC12 i SH-SY5Y fins a concentracions de 50 µM.

- Els agregats amorfs han demostrat ser tòxics per les cèl·lules PC12

- PPI-G4 a una baixa relació afavoreix la generació de fibres aglutinades que resulten ser menys tòxiques que els agregats amorfs i les fibres d’Aß.

BIBLIOGRAPHY

Alies, B., Eury, H., Bijani, C., Rechignat, L., Faller, P., Hureau, C., 2011. Inorganic Chemistry 50, 11192-11201.

Al-Jamal, K.T., Ramaswamy, C., Florence, A.T., 2005. Advanced Drug Delivery Reviews 57, 2238-2270.

Alper, J., 1991. Science 251, 1562 -1564.

Alzheimer, A., Stelzmann, R.A., Schnitzlein, H.N., Murtagh, F.R., 1995. Clin Anat 8, 429-431.

Appelhans, D., Zhong, Y., Komber, H., Friedel, P., Oertel, U., Scheler, U., Morgner, N., Kuckling, D., Richter, S., Seidel, J., Brutschy, B., Voit, B., 2007. Macromol Biosci 7, 373-383.

Arispe, Z., Diaz, J.C., Simakova, O., 2007. Biochim. Biophys. Acta 1768, 1952-1965.

Arrondo, Z., Muga, A., Castresana, J., Goñi, F.M., 1993. Prog. Biophys. Mol. Biol. 59, 23-56.

Artavanis-Tsakonas, S., Matsuno, K., Fortini, M.E., 1995. Science 268, 225-232.

Atwood, C.S., Perry, G., Zeng, H., Kato, Y., Jones, W.D., Ling, K.-Q., Huang, X., Moir, R.D., Wang, D., Sayre, L.M., Smith, M.A., Chen, S.G., Bush, A.I., 2004. Biochemistry 43, 560-568.

Atwood, G., Moir, R.D., Huang, X., Scarpa, R.C., Bacarra, N.M., Romano, D.M., Hartshorn, M.A., Tanzi, R.E., Bush, A.I., 1998. J. Biol. Chem. 273, 12817-12826.

Atwood, C., Martins, R.N., Smith, M.A., Perry, G., 2002. Peptides 23, 1343-1350.

Augy, T., Bonin-Guillaume, S., Blin, O., 2006. Encephale 32 Pt 5, S641-649.

Avila, J., 2006. FEBS Lett. 580, 2922-2927.

Balbach, J., Petkova, A.T., Oyler, N.A., Antzutkin, O.N., Gordon, D.J., Meredith, S.C., Tycko, R., 2002. Biophys. J. 83, 1205-1216.

Bandekar, J., 1992. Biochim. Biophys. Acta 1120, 123-143.

Bandekar, J., Yu, S., 2007. Acta Biochim. Biophys. Sin. (Shanghai) 39, 549-559.

Barnham, K., Bush, A.I., 2008. Curr Opin Chem Biol 12, 222-228.

Barnham, K., McKinstry, W.J., Multhaup, G., Galatis, D., Morton, C.J., Curtain, C.C., Williamson, N.A., White, A.R., Hinds, M.G., Norton, R.S., Beyreuther, K., Masters, C.L., Parker, M.W., Cappai, R., 2003. J. Biol. Chem. 278, 17401-17407.

Barth, A., Zscherp, C., 2002. Q. Rev. Biophys. 35, 369-430.

Bartzokis, G., Sultzer, D., Cummings, J., Holt, L.E., Hance, D.B., Henderson, V.W., Mintz, J., 2000. Arch. Gen. Psychiatry 57, 47-53.

Bayer, T., Schäfer, S., Breyhan, H., Wirths, O., Treiber, C., Multhaup, G., 2006. Clin. Neuropathol. 25, 163-171.

Bellingham, S.A., Lahiri, D.K., Maloney, B., La Fontaine, S., Multhaup, G., Camakaris, J., 2004. J. Biol. Chem. 279, 20378-20386.

Benedek, G., Fuller, S., Atwood, C.S., Laws, S.M., Gandy, S.E., Martins, R.N., 2004. Pharmacol. Res. 50, 397-409.

Benseny-Cases, N., Cócera, M., Cladera, J., 2007. Biochem. Biophys. Res. Commun. 361, 916-921.

Benseny-Cases, N., Klementiev O., Malý J., Cladera J. Alz. Curr. Res., 2011(accepted)

Bernadó, P., Mylonas, E., Petoukhov, M.V., Blackledge, M., Svergun, D.I., 2007. J. Am. Chem. Soc. 129, 5656-5664.

Biedler, J., Helson, L., Spengler, B.A., 1973. Cancer Research 33, 2643 -2652.

Bieschke, J., Siegel, S.J., Fu, Y., Kelly, J.W., 2008. Biochemistry 47, 50-59.

Boix, R., 2006. Q. Rev. Biophys. 39, 1-55.

Bowen, D.M., Smith, C.B., White, P., Flack, R.H., Carrasco, L.H., Gedye, J.L., Davison, A.N., 1977. Brain 100, 427-453.

Braak, H., Braak, E., 1991. Acta Neuropathol. 82, 239-259.

Van Broeck, B., Van Broeckhoven, C., Kumar-Singh, S., 2007. Neurodegener Dis 4, 349-365.

Brookmeyer, R., Gray, S., Kawas, C., 1998. Am J Public Health 88, 1337-1342.

Bryngelson, J.D., Onuchic, J.N., Socci, N.D., Wolynes, P.G., 1995. Proteins 21, 167-195.

Bucciantini, M., Rigacci, S., Berti, A., Pieri, L., Cecchi, C., Nosi, D., Formigli, L., Chiti, F., Stefani, M., 2005. FASEB J. 19, 437-439.

Bush, A., 2003. Trends Neurosci. 26, 207-214.

Bush, A., Pettingell, W.H., Multhaup, G., d Paradis, M., Vonsattel, J.P., Gusella, J.F., Beyreuther, K., Masters, C.L., Tanzi, R.E., 1994. Science 265, 1464-1467.

Bush, A.I., Tanzi, R.E., 2008. Neurotherapeutics 5, 421-432.

Calderón, F.H., Bonnefont, A., Muñoz, F.J., Fernández, V., Videla, L.A., Inestrosa, N.C., 1999. J. Neurosci. Res. 56, 620-631.

Camargo, L.M., Oddo, S., Green, K.N., McGaugh, J.L., LaFerla, F.M., 2005. Neuron 45, 675-688.

Caminade, A.-M., Turrin, C.-O., Majoral, J.-P., 2010. New J. Chem. 34, 1512-1524.

Carter, D.C., Ho, J.X., 1994. Adv. Protein Chem. 45, 153-203.

Chabre, Y.M., Roy, R., 2008. Curr Top Med Chem 8, 1237-1285.

Cheng, Y., Xu, Z., Ma, M., Xu, T., 2008. J Pharm Sci 97, 123-143.

Choi, B.-S., Zheng, W., 2009. Brain Res. 1248, 14-21.

Cookson, M.R., Shaw, P.J., 1999. Brain Pathology 9, 165-186.

Corder, E.H., Saunders, A.M., Strittmatter, W.J., Schmechel, D.E., Gaskell, P.C., Small, G.W., Roses, A.D., Haines, J.L., Pericak-Vance, M.A., 1993. Science 261, 921-923.

Cortijo-Arellano, M., Ponce, J., Durany, N., Cladera, J., 2008a. Biochem. Biophys. Res. Commun. 368, 238-242.

Cortijo-Arellano, M., Ponce, J., Durany, N., Cladera, J., 2008b. Biochem Biophys Res Commun 368, 238-42.

Cuajungco, M.P., Lees, G.J., 1997. Brain Res. Brain Res. Rev. 23, 219-236.

DeMattos, R.B., Bales, K.R., Cummins, D.J., Dodart, J.C., Paul, S.M., Holtzman, D.M., 2001. Proc. Natl. Acad. Sci. U.S.A. 98, 8850-8855.

Donaldson, C., Tarrier, N., Burns, A., 1998. Int J Geriatr Psychiatry 13, 248-256.

Dong, A., Huang, P., Caughey, W.S., 1992. Biochemistry 31, 182-189.

Dong, J., Atwood, C.S., Anderson, V.E., Siedlak, S.L., Smith, M.A., Perry, G., Carey, P.R., 2003. Biochemistry 42, 2768-2773.

Dong, J., Canfield, J.M., Mehta, A.K., Shokes, J.E., Tian, B., Childers, W.S., Simmons, J.A., Mao, Z., Scott, R.A., Warncke, K., Lynn, D.G., 2007. Proc. Natl. Acad. Sci. U.S.A. 104, 13313-13318.

Doniach, S., 2001. Chem. Rev. 101, 1763-1778.

Drew, S.C., Masters, C.L., Barnham, K.J., 2010. PLoS ONE 5, e15875.

DuBay, K.F., Pawar, A.P., Chiti, F., Zurdo, J., Dobson, C.M., Vendruscolo, M., 2004. J. Mol. Biol. 341, 1317-1326.

Eanes, E.D., Glenner, G.G., 1968. J. Histochem. Cytochem. 16, 673-677.

Elliot, A., Ambrose, E.J., 1950. Nature 165, 921-922.

Eriksen, J.L., Sagi, S.A., Smith, T.E., Weggen, S., Das, P., McLendon, D.C., Ozols, V.V., Jessing, K.W., Zavitz, K.H., Koo, E.H., Golde, T.E., 2003. J. Clin. Invest. 112, 440-449.

Francis, P.T., Palmer, A.M., Snape, M., Wilcock, G.K., 1999. J. Neurol. Neurosurg. Psychiatr. 66, 137-147.

Fraser, P.E., McLachlan, D.R., Surewicz, W.K., Mizzen, C.A., Snow, A.D., Nguyen, J.T., Kirschner, D.A., 1994. J. Mol. Biol. 244, 64-73.

Fréchet, J.M., 1994. Science 263, 1710-1715.

Freshney, R.I., 2000. Culture of Animal Cells: A Manual of Basic Technique, 4th Edition, 4th ed. Wiley-Liss.

Gasparini, L., Gouras, G.K., Wang, R., Gross, R.S., Beal, M.F., Greengard, P., Xu, H., 2001. J. Neurosci. 21, 2561-2570.

Gazit, E., 2002. FASEB J. 16, 77-83.

Giehm, L., Christensen, C., Boas, U., Heegaard, P.M.H., Otzen, D.E., 2008. Biopolymers 89, 522-529.

Glabe, C.G., 2008. J. Biol. Chem. 283, 29639-29643.

Glatter, O., 1982. Small angle x-ray scattering. Academic Press, London ;;New York.

Glenner, G.G., Wong, C.W., 1984. Biochem. Biophys. Res. Commun. 120, 885-890.

Gosal, W.S., Myers, S.L., Radford, S.E., Thomson, N.H., 2006. Protein Pept. Lett. 13, 261-270.

Gouras, G.K., Tsai, J., Naslund, J., Vincent, B., Edgar, M., Checler, F., Greenfield, J.P., Haroutunian, V., Buxbaum, J.D., Xu, H., Greengard, P., Relkin, N.R., 2000. Am. J. Pathol. 156, 15-20.

Grandbois, M., Clausen-Schaumann, H., Gaub, H., 1998. Biophys. J. 74, 2398-2404.

Grant, W.B., Campbell, A., Itzhaki, R.F., Savory, J., 2002. J. Alzheimers Dis. 4, 179-189.

Gregersen, N., Bross, P., Vang, S., Christensen, J.H., 2006. Annu Rev Genomics Hum Genet 7, 103-124.

Grundke-Iqbal, I., Iqbal, K., Quinlan, M., Tung, Y.C., Zaidi, M.S., Wisniewski, H.M., 1986. J. Biol. Chem. 261, 6084-6089.

Guilbault, G., 1973. Practical fluorescence theory, methods, and techniques,. M. Dekker, New York.

Ha, C., Ryu, J., Park, C.B., 2007. Biochemistry 46, 6118-6125.

Haass, C., Schlossmacher, M.G., Hung, A.Y., Vigo-Pelfrey, C., Mellon, A., Ostaszewski, B.L., Lieberburg, I., Koo, E.H., Schenk, D., Teplow, D.B., 1992. Nature 359, 322-325.

Haass, C., Selkoe, D.J., 2007. Nat. Rev. Mol. Cell Biol. 8, 101-112.

Hansma, H.G., Laney, D.E., Bezanilla, M., Sinsheimer, R.L., Hansma, P.K., 1995. Biophys J 68, 1672-1677.

Hansma, H.G., Sinsheimer, R.L., Groppe, J., Bruice, T.C., Elings, V., Gurley, G., Bezanilla, M., Mastrangelo, I.A., Hough, P.V., Hansma, P.K., 1993. Scanning 15, 296-299.

Hardy, J., 1997. Trends Neurosci. 20, 154-159.

Hardy, J., Allsop, D., 1991. Trends Pharmacol. Sci. 12, 383-388.

Hardy, J.A., Higgins, G.A., 1992. Science 256, 184-185.

Harrison, S.M., Harper, A.J., Hawkins, J., Duddy, G., Grau, E., Pugh, P.L., Winter, P.H., Shilliam, C.S., Hughes, Z.A., Dawson, L.A., Gonzalez, M.I., Upton, N., Pangalos, M.N., Dingwall, C., 2003. Mol. Cell. Neurosci. 24, 646-655.

Hartley, D.M., Walsh, D.M., Ye, C.P., Diehl, T., Vasquez, S., Vassilev, P.M., Teplow, D.B., Selkoe, D.J., 1999. J. Neurosci. 19, 8876-8884.

Hartley, D.M., Zhao, C., Speier, A.C., Woodard, G.A., Li, S., Li, Z., Walz, T., 2008. J. Biol. Chem. 283, 16790-16800.

Heegaard, P.M.H., Pedersen, H.G., Flink, J., Boas, U., 2004. FEBS Lett. 577, 127-133.

Heidenreich, R., 1964. Fundamentals of transmission electron microscopy. Interscience publ. ;J. Wiley, London ;;New York ;;Sydney.

Hensley, K., Carney, J.M., Mattson, M.P., Aksenova, M., Harris, M., Wu, J.F., Floyd, R.A., Butterfield, D.A., 1994. Proc. Natl. Acad. Sci. U.S.A. 91, 3270-3274.

Hilbich, C., Kisters-Woike, B., Reed, J., Masters, C.L., Beyreuther, K., 1991. J. Mol. Biol. 218, 149-163.

Holmes, C., Boche, D., Wilkinson, D., Yadegarfar, G., Hopkins, V., Bayer, A., Jones, R.W., Bullock, R., Love, S., Neal, J.W., Zotova, E., Nicoll, J.A.R., 2008. Lancet 372, 216-223.

Huang, X., Atwood, C.S., Hartshorn, M.A., Multhaup, G., Goldstein, L.E., Scarpa, R.C., Cuajungco, M.P., Gray, D.N., Lim, J., Moir, R.D., Tanzi, R.E., Bush, A.I., 1999. Biochemistry 38, 7609-7616.

Hubbard, A., 1995. The Handbook of surface imaging and visualization. CRC Press, Boca Raton.

Hughes, M., Snetkov, V., Rose, R.-S., Trousil, S., Mermoud, J.E., Dingwall, C., 2010. J. Neurochem. 114, 832-842.

Hunt, C.E., Turner, A.J., 2009. FEBS J. 276, 1845-1859.

Hussain, I., Hawkins, J., Harrison, D., Hille, C., Wayne, G., Cutler, L., Buck, T., Walter, D., Demont, E., Howes, C., Naylor, A., Jeffrey, P., Gonzalez, M.I., Dingwall, C., Michel, A., Redshaw, S., Davis, J.B., 2007. J. Neurochem. 100, 802-809.

Jahn, T.R., Radford, S.E., 2005. FEBS J. 272, 5962-5970.

Jain, K., Kesharwani, P., Gupta, U., Jain, N.K., 2010. Int J Pharm 394, 122-142.

Jansen, J.F., de Brabander-van den Berg, E.M., Meijer, E.W., 1994. Science 266, 1226-1229.

Jena, B.P., Hörber, J.K.H., 2002. Atomic force microscopy in cell biology. Academic Press.

Jiang, D., Li, X., Liu, L., Yagnik, G.B., Zhou, F., 2010. J Phys Chem B 114, 4896-4903.

Jiménez, J.L., Guijarro, J.I., Orlova, E., Zurdo, J., Dobson, C.M., Sunde, M., Saibil, H.R., 1999. EMBO J. 18, 815-821.

Johansson, A.-S., Berglind-Dehlin, F., Karlsson, G., Edwards, K., Gellerfors, P., Lannfelt, L., 2006. FEBS J. 273, 2618-2630.

Jorgensen, L., Nielson, H.M., 2010. Delivery Technologies for Biopharmaceuticals: Peptides, Proteins, Nucleic Acids and Vaccines. John Wiley and Sons.

Kajava, A.V., Aebi, U., Steven, A.C., 2005. J. Mol. Biol. 348, 247-252.

Kang, J., Lemaire, H.G., Unterbeck, A., Salbaum, J.M., Masters, C.L., Grzeschik, K.H., Multhaup, G., Beyreuther, K., Müller-Hill, B., 1987. Nature 325, 733-736.

Karr, J.W., 2007. Copper(II) and the amyloid beta peptide of Alzheimer’s disease. ProQuest.

Karr, J.W., Akintoye, H., Kaupp, L.J., Szalai, V.A., 2005. Biochemistry 44, 5478-87.

Karr, J.W., Kaupp, L.J., Szalai, V.A., 2004. J. Am. Chem. Soc. 126, 13534-13538.

Kirby, A.R., Gunning, A.P., Morris, V.J., 1996. Biopolymers 38, 355-366.

Kirkitadze, M.D., Bitan, G., Teplow, D.B., 2002. J. Neurosci. Res. 69, 567-577.

Kirkitadze, M.D., Condron, M.M., Teplow, D.B., 2001. J. Mol. Biol. 312, 1103-1119.

Kirkpatrick, S., Gelatt, C.D., Jr, Vecchi, M.P., 1983. Science 220, 671-680.

Klajnert, B., Appelhans, D., Komber, H., Morgner, N., Schwarz, S., Richter, S., Brutschy, B., Ionov, M., Tonkikh, A.K., Bryszewska, M., Voit, B., 2008. Chemistry 14, 7030-7041.

Klajnert, B., Cladera, J., Bryszewska, M., 2006. Biomacromolecules 7, 2186-2191.

Klajnert, B., Cortijo-Arellano, M., Bryszewska, M., Cladera, J., 2006. Biochem. Biophys. Res. Commun. 339, 577-582.

Klajnert, B., Cortijo-Arellano, M., Cladera, J., Bryszewska, M., 2006. Biochem. Biophys. Res. Commun. 345, 21-28.

Klajnert, B., Cortijo-Arellano, M., Cladera, J., Majoral, J.-P., Caminade, A.-M., Bryszewska, M., 2007. Biochem. Biophys. Res. Commun. 364, 20-25.

Klein, W.L., Krafft, G.A., Finch, C.E., 2001. Trends Neurosci. 24, 219-224.

Konarev, P.V., Volkov, V.V., Sokolova, A.V., Koch, M.H.J., Svergun, D.I., 2003. Journal of Applied Crystallography 36, 1277-1282.

Koo, E., Squazzo, S.L., 1994. J. Biol. Chem. 269, 17386-17389.

Kremer, J.J., Pallitto, M.M., Sklansky, D.J., Murphy, R.M., 2000. Biochemistry 39, 10309-10318.

Krimm, S., Bandekar, J., 1986. Adv. Protein Chem. 38, 181-364.

Kumar, C.S.S.R., 2007. Nanomaterials for cancer diagnosis. Wiley-VCH.

Lakowicz, J.R., 2006. Principles of fluorescence spectroscopy. Springer.

Lamb, J.S., Zoltowski, B.D., Pabit, S.A., Crane, B.R., Pollack, L., 2008. J. Am. Chem. Soc. 130, 12226-12227.

Lambert, M.P., Barlow, A.K., Chromy, B.A., Edwards, C., Freed, R., Liosatos, M., Morgan, T.E., Rozovsky, I., Trommer, B., Viola, K.L., Wals, P., Zhang, C., Finch, C.E., Krafft, G.A., Klein, W.L., 1998. Proc. Natl. Acad. Sci. U.S.A. 95, 6448-6453.

Lannfelt, L., Blennow, K., Zetterberg, H., Batsman, S., Ames, D., Harrison, J., Masters, C.L., Targum, S., Bush, A.I., Murdoch, R., Wilson, J., Ritchie, C.W., 2008. Lancet Neurol 7, 779-786.

Lansbury, P.T., Lashuel, H.A., 2006. Nature 443, 774-779.

Lapshin, R.V., 2009. Astrobiology 9, 437-442.

Lazo, N.D., Grant, M.A., Condron, M.C., Rigby, A.C., Teplow, D.B., 2005. Protein Sci. 14, 1581-1596.

Lee, J.H., Won, S.M., Suh, J., Son, S.J., Moon, G.J., Park, U.J., Gwag, B.J., 2010. Exp. Mol. Med. 42, 386-394.

Lee, S., Fernandez, E.J., Good, T.A., 2007. Protein Sci. 16, 723-732.

Leissring, M.A., Murphy, M.P., Mead, T.R., Akbari, Y., Sugarman, M.C., Jannatipour, M., Anliker, B., Müller, U., Saftig, P., De Strooper, B., Wolfe, M.S., Golde, T.E., LaFerla, F.M., 2002. Proc. Natl. Acad. Sci. U.S.A. 99, 4697-4702.

Leopold, P.E., Montal, M., Onuchic, J.N., 1992. Proc. Natl. Acad. Sci. U.S.A. 89, 8721-8725.

LeVine, H., 3rd, 1993. Protein Sci. 2, 404-410.

Levy-Lahad, E., Wasco, W., Poorkaj, P., Romano, D.M., Oshima, J., Pettingell, W.H., Yu, C.E., Jondro, P.D., Schmidt, S.D., Wang, K., 1995. Science 269, 973-977.

Lin, M.-S., Chen, L.-Y., Tsai, H.-T., Wang, S.S.-S., Chang, Y., Higuchi, A., Chen, W.-Y., 2008. Langmuir 24, 5802-5808.

Linder, M.C., Wooten, L., Cerveza, P., Cotton, S., Shulze, R., Lomeli, N., 1998. Am. J. Clin. Nutr. 67, 965S-971S.

Lomakin, A., Chung, D.S., Benedek, G.B., Kirschner, D.A., Teplow, D.B., 1996. Proc. Natl. Acad. Sci. U.S.A. 93, 1125-1129.

Lombardi, V.R.M., García, M., Cacabelos, R., 1998. Journal of Neuroscience Research 54, 539-553.

Loup, C., Zanta, M., Caminade, A., Majoral, J., Meunier, B., 1999. Chemistry - A European Journal 5, 3644-3650.

Lovell, M.A., Robertson, J.D., Teesdale, W.J., Campbell, J.L., Markesbery, W.R., 1998. J. Neurol. Sci. 158, 47-52.

Lundkvist, J., Näslund, J., 2007. Curr Opin Pharmacol 7, 112-118.

Maiti, N.C., Jiang, D., Wain, A.J., Patel, S., Dinh, K.L., Zhou, F., 2008. J Phys Chem B 112, 8406-8411.

Majoros, I.J., Myc, A., Thomas, T., Mehta, C.B., Baker, J.R., Jr, 2006. Biomacromolecules 7, 572-579.

Makin, O.S., Serpell, L.C., 2005a. Methods Mol. Biol. 299, 67-80.

Makin, O.S., Serpell, L.C., 2005b. FEBS J. 272, 5950-5961.

Malý, J., Lampová, H., Semerádtová, A., Stofik, M., Kovácik, L., 2009. Nanotechnology 20, 385101.

Masters, C.L., Simms, G., Weinman, N.A., Multhaup, G., McDonald, B.L., Beyreuther, K., 1985. Proc. Natl. Acad. Sci. U.S.A. 82, 4245-4249.

Mattson, M., 1997. Physiol. Rev. 77, 1081-1132.

McDonald, R., 2002. Can J Exp Psychol 56, 221-239.

McDonald, R.J., Craig, L.A., Hong, N.S., 2010. Behav. Brain Res. 214, 3-11.

McGrath, D.V., 2005. Mol. Pharm. 2, 253-263.

Mertens, H.D.T., Svergun, D.I., 2010. Journal of Structural Biology 172, 128-141.

Meyer-Luehmann, M., Spires-Jones, T.L., Prada, C., Garcia-Alloza, M., de Calignon, A., Rozkalne, A., Koenigsknecht-Talboo, J., Holtzman, D.M., Bacskai, B.J., Hyman, B.T., 2008. Nature 451, 720-724.

Miller, L.M., Wang, Q., Telivala, T.P., Smith, R.J., Lanzirotti, A., Miklossy, J., 2006. J. Struct. Biol. 155, 30-37.

Miller, R.G., Brown, B.W., 1997. Beyond ANOVA: basics of applied statistics. Chapman & Hall.

Minicozzi, V., Stellato, F., Comai, M., Dalla Serra, M., Potrich, C., Meyer-Klaucke, W., Morante, S., 2008. J. Biol. Chem. 283, 10784-10792.

Minogue, A.M., Stubbs, A.K., Frigerio, C.S., Boland, B., Fadeeva, J.V., Tang, J., Selkoe, D.J., Walsh, D.M., 2009. Brain Res. 1262, 89-99.

Möller, C., Allen, M., Elings, V., Engel, A., Müller, D.J., 1999. Biophys. J. 77, 1150-1158.

Mölsä, P.K., Marttila, R.J., Rinne, U.K., 1986. Acta Neurol. Scand. 74, 103-107.

Mosmann, T., 1983. J. Immunol. Methods 65, 55-63.

Mou, J., Czajkowsky, D.M., Zhang, Y., Shao, Z., 1995. FEBS Lett. 371, 279-282.

Mou, J., Sheng, S., Ho, R., Shao, Z., 1996. Biophys. J. 71, 2213-2221.

Mou, J., Yang, J., Huang, C., Shao, Z., 1994. Biochemistry 33, 9981-9985.

Mukai, H., Isagawa, T., Goyama, E., Tanaka, S., Bence, N.F., Tamura, A., Ono, Y., Kopito, R.R., 2005. Proc. Natl. Acad. Sci. U.S.A. 102, 10887-10892.

Munishkina, L.A., Fink, A.L., 2007. Biochim. Biophys. Acta 1768, 1862-1885.

Munoz, D.G., Feldman, H., 2000. CMAJ 162, 65-72.

Naiki, H., Higuchi, K., Hosokawa, M., Takeda, T., 1989. Anal. Biochem. 177, 244-249.

Nelson, R., Sawaya, M.R., Balbirnie, M., Madsen, A.Ø., Riekel, C., Grothe, R., Eisenberg, D., 2005. Nature 435, 773-778.

Newkome, G.R., Childs, B.J., Rourk, M.J., Baker, G.R., Moorefield, C.N., 1999. Biotechnology and Bioengineering 61, 243-253.

Nichols, M.R., Moss, M.A., Reed, D.K., Lin, W.-L., Mukhopadhyay, R., Hoh, J.H., Rosenberry, T.L., 2002. Biochemistry 41, 6115-6127.

Nunomura, A., Perry, G., Pappolla, M.A., Wade, R., Hirai, K., Chiba, S., Smith, M.A., 1999. J. Neurosci. 19, 1959-1964.

Onuchic, J.N., Luthey-Schulten, Z., Wolynes, P.G., 1997. Annu Rev Phys Chem 48, 545-600.

Onuchic, J.N., Wolynes, P.G., Luthey-Schulten, Z., Socci, N.D., 1995. Proc. Natl. Acad. Sci. U.S.A. 92, 3626-3630.

Opazo, C., Huang, X., Cherny, R.A., Moir, R.D., Roher, A.E., White, A.R., Cappai, R., Masters, C.L., Tanzi, R.E., Inestrosa, N.C., Bush, A.I., 2002. J. Biol. Chem. 277, 40302-40308.

Orgogozo, J.-M., Gilman, S., Dartigues, J.-F., Laurent, B., Puel, M., Kirby, L.C., Jouanny, P., Dubois, B., Eisner, L., Flitman, S., Michel, B.F., Boada, M., Frank, A., Hock, C., 2003. Neurology 61, 46-54.

Orthaber, D., Glatter, O., 2000. Chem. Phys. Lipids 107, 179-189.

Paris, D., Town, T., Parker, T., Humphrey, J., Mullan, M., 2000. Ann. N. Y. Acad. Sci. 903, 97-109.

Parvathy, S., Hussain, I., Karran, E.H., Turner, A.J., Hooper, N.M., 1999. Biochemistry 38, 9728-9734.

Pearson, H.A., Peers, C., 2006. J. Physiol. (Lond.) 575, 5-10.

Pedersen, J.T., Østergaard, J., Rozlosnik, N., Gammelgaard, B., Heegaard, N.H.H., 2011. Journal of Biological Chemistry 286, 26952 -26963.

de Pedro-Cuesta, J., Virués-Ortega, J., Vega, S., Seijo-Martínez, M., Saz, P., Rodríguez, F., Rodríguez-Laso, A., Reñé, R., de las Heras, S.P., Mateos, R., Martínez-Martín, P., Manubens, J.M., Mahillo-Fernandez, I., López-Pousa, S., Lobo, A., Reglà, J.L., Gascón, J., García, F.J., Fernández-Martínez, M., Boix, R., Bermejo-Pareja, F., Bergareche, A., Benito-León, J., de Arce, A., del Barrio, J.L., 2009. BMC Neurol 9, 55.

Perczel, A., Hudáky, P., Pálfi, V.K., 2007. J. Am. Chem. Soc. 129, 14959-14965.

Petkova, A.T., Leapman, R.D., Guo, Z., Yau, W.-M., Mattson, M.P., Tycko, R., 2005. Science 307, 262-265.

Petoukhov, M.V., Svergun, D.I., 2007. Curr. Opin. Struct. Biol. 17, 562-571.

Pfeifer, M., Boncristiano, S., Bondolfi, L., Stalder, A., Deller, T., Staufenbiel, M., Mathews, P.M., Jucker, M., 2002. Science 298, 1379.

Pike, C.J., Burdick, D., Walencewicz, A.J., Glabe, C.G., Cotman, C.W., 1993. J. Neurosci. 13, 1676-1687.

Pimplikar, S.W., 2009. Int J Biochem Cell Biol 41, 1261-1268.

Poduslo, J.F., Gilles, E.J., Ramakrishnan, M., Howell, K.G., Wengenack, T.M., Curran, G.L., Kandimalla, K.K., 2010. PLoS ONE 5, e8813.

Price, J.L., Morris, J.C., 1999. Ann. Neurol. 45, 358-368.

Putnam, C.D., Hammel, M., Hura, G.L., Tainer, J.A., 2007a. Q. Rev. Biophys. 40, 191-285.

Putnam, C.D., Hammel, M., Hura, G.L., Tainer, J.A., 2007b. Quarterly Reviews of Biophysics 40.

Racchi, M., Govoni, S., 2003. Experimental Gerontology 38, 145-157.

Rae, T.D., Schmidt, P.J., Pufahl, R.A., Culotta, V.C., O'Halloran, T.V., 1999. Science 284, 805-808.

Ragone, R., Colonna, G., Balestrieri, C., Servillo, L., Irace, G., 1984. Biochemistry 23, 1871-1875.

Rekas, A., Lo, V., Gadd, G.E., Cappai, R., Yun, S.I., 2009. Macromol Biosci 9, 230-238.

Riek, R., Güntert, P., Döbeli, H., Wipf, B., Wüthrich, K., 2001. Eur. J. Biochem. 268, 5930-5936.

Rival, T., Page, R.M., Chandraratna, D.S., Sendall, T.J., Ryder, E., Liu, B., Lewis, H., Rosahl, T., Hider, R., Camargo, L.M., Shearman, M.S., Crowther, D.C., Lomas, D.A., 2009. Eur. J. Neurosci. 29, 1335-1347.

Roessle, M.W., Klaering, R., Ristau, U., Robrahn, B., Jahn, D., Gehrmann, T., Konarev, P., Round, A., Fiedler, S., Hermes, C., Svergun, D., 2007. Journal of Applied Crystallography 40, s190-s194.

Roychaudhuri, R., Yang, M., Hoshi, M.M., Teplow, D.B., 2009. J. Biol. Chem. 284, 4749-4753.

Santos, N.C., Castanho, M.A.R.B., 2004. Biophys. Chem. 107, 133-149.

Sarell, C.J., Wilkinson, S.R., Viles, J.H., 2010a. Journal of Biological Chemistry 285, 41533-41540.

Sarell, J., Syme, C.D., Rigby, S.E.J., Viles, J.H., 2009. Biochemistry 48, 4388-4402.

Sarell, J., Wilkinson, s, Viles, s, 2010b. J. Biol. Chem. 285, 41533-41540.

Sawaya, M.R., Sambashivan, S., Nelson, R., Ivanova, M.I., Sievers, S.A., Apostol, M.I., Thompson, M.J., Balbirnie, M., Wiltzius, J.J.W., McFarlane, H.T., Madsen, A.Ø., Riekel, C., Eisenberg, D., 2007. Nature 447, 453-457.

Schenk, D., Barbour, R., Dunn, W., Gordon, G., Grajeda, H., Guido, T., Hu, K., Huang, J., Johnson-Wood, K., Khan, K., Kholodenko, D., Lee, M., Liao, Z., Lieberburg, I., Motter, R., Mutter, L., Soriano, F., Shopp, G., Vasquez, N., Vandevert, C., Walker, S., Wogulis, M., Yednock, T., Games, D., Seubert, P., 1999. Nature 400, 173-177.

Scheper, W., Nijholt, D.A.T., Hoozemans, J.J.M., 2011. Autophagy 7, 910-911.

Schlief, M.L., Craig, A.M., Gitlin, J.D., 2005. J. Neurosci. 25, 239-246.

Schmitz, C., Rutten, B.P.F., Pielen, A., Schäfer, S., Wirths, O., Tremp, G., Czech, C., Blanchard, V., Multhaup, G., Rezaie, P., Korr, H., Steinbusch, H.W.M., Pradier, L., Bayer, T.A., 2004. Am. J. Pathol. 164, 1495-1502.

Selkoe, D.J., 2001. Physiol. Rev. 81, 741-766.

Serpell, L.C., Fraser, P.E., Sunde, M., 1999. Meth. Enzymol. 309, 526-536.

Serpell, L.C., Smith, J.M., 2000. J. Mol. Biol. 299, 225-231.

Shen, C.L., Murphy, R.M., 1995. Biophys. J. 69, 640-651.

Sherrington, R., Rogaev, E.I., Liang, Y., Rogaeva, E.A., Levesque, G., Ikeda, M., Chi, H., Lin, C., Li, G., Holman, K., Tsuda, T., Mar, L., Foncin, J.F., Bruni, A.C., Montesi, M.P., Sorbi, S., Rainero, I., Pinessi, L., Nee, L., Chumakov, I., Pollen, D., Brookes, A., Sanseau, P., Polinsky, R.J., Wasco, W., Da Silva, H.A., Haines, J.L., Perkicak-Vance, M.A., Tanzi, R.E., Roses, A.D., Fraser, P.E., Rommens, J.M., St George-Hyslop, P.H., 1995. Nature 375, 754-760.

Shukla, D., Schneider, C.P., Trout, B.L., 2011. Advanced Drug Delivery Reviews.

Sigel, A., 2006. Neurodegenerative diseases and metal ions. Wiley, Chichester West Sussex England ;;Hoboken NJ.

Simakova, O., Arispe, N.J., 2007. J. Neurosci. 27, 13719-13729.

Sisodia, S.S., 1992a. Proc. Natl. Acad. Sci. U.S.A. 89, 6075-6079.

Sisodia, S.S., 1992b. Proc. Natl. Acad. Sci. U.S.A. 89, 6075-6079.

Smith, D.P., Ciccotosto, G.D., Tew, D.J., Fodero-Tavoletti, M.T., Johanssen, T., Masters, C.L., Barnham, K.J., Cappai, R., 2007. Biochemistry 46, 2881-2891.

Snyder, E.M., Nong, Y., Almeida, C.G., Paul, S., Moran, T., Choi, E.Y., Nairn, A.C., Salter, M.W., Lombroso, P.J., Gouras, G.K., Greengard, P., 2005. Nat. Neurosci. 8, 1051-1058.

Sokolov, Y., Kozak, J.A., Kayed, R., Chanturiya, A., Glabe, C., Hall, J.E., 2006. J. Gen. Physiol. 128, 637-647.

Soscia, S.J., Kirby, J.E., Washicosky, K.J., Tucker, S.M., Ingelsson, M., Hyman, B., Burton, M.A., Goldstein, L.E., Duong, S., Tanzi, R.E., Moir, R.D., 2010. PLoS ONE 5, e9505.

Soto, C., Castaño, E.M., Frangione, B., Inestrosa, N.C., 1995. J. Biol. Chem. 270, 3063-3067.

Squitti, R., Cassetta, E., Dal Forno, G., Lupoi, D., Lippolis, G., Pauri, F., Vernieri, F., Cappa, A., Rossini, P.M., 2004. Arch. Neurol. 61, 738-743.

Squitti, R., Lupoi, D., Pasqualetti, P., Dal Forno, G., Vernieri, F., Chiovenda, P., Rossi, L., Cortesi, M., Cassetta, E., Rossini, P.M., 2002. Neurology 59, 1153-1161.

Squitti, R., Salustri, C., 2009. Curr Alzheimer Res 6, 476-487.

Squitti, R., Zito, G., 2009. Recent Pat CNS Drug Discov 4, 209-219.

St George-Hyslop, P., Polinsky, R., Haines, J., Nee, L., Tanzi, R., Conneally, P., Growdon, J., Myers, R., Pollen, D., Drachman, D., 1987. J. Neural Transm. Suppl. 24, 13-21.

Stine, W.B., Jr, Dahlgren, K.N., Krafft, G.A., LaDu, M.J., 2003. J. Biol. Chem. 278, 11612-11622.

Streltsov, V., Titmuss, S.J., Epa, V.C., Barnham, K.J., Masters, C.L., Varghese, J.N., 2008. Biophysical Journal 95, 3447-3456.

Strittmatter, W.J., Weisgraber, K.H., Huang, D.Y., Dong, L.M., Salvesen, G.S., Pericak-Vance, M., Schmechel, D., Saunders, A.M., Goldgaber, D., Roses, A.D., 1993. Proc. Natl. Acad. Sci. U.S.A. 90, 8098-8102.

De Strooper, B., 2010. Physiological Reviews 90, 465 -494.

Stuart, B.H., 2004. Infrared spectroscopy: fundamentals and applications. John Wiley and Sons.

Sunde, M., Serpell, L.C., Bartlam, M., Fraser, P.E., Pepys, M.B., Blake, C.C., 1997. J. Mol. Biol. 273, 729-739.

Supattapone, S., Nguyen, H.O., Cohen, F.E., Prusiner, S.B., Scott, M.R., 1999. Proc. Natl. Acad. Sci. U.S.A. 96, 14529-14534.

Supattapone, S., Wille, H., Uyechi, L., Safar, J., Tremblay, P., Szoka, F.C., Cohen, F.E., Prusiner, S.B., Scott, M.R., 2001. J. Virol. 75, 3453-3461.

Susi, H., Byler, D.M., 1983. Biochem. Biophys. Res. Commun. 115, 391-397.

Susi, H., Byler, D.M., 1986. Meth. Enzymol. 130, 290-311.

Svenson, S., Tomalia, D.A., 2005. Adv. Drug Deliv. Rev. 57, 2106-2129.

Svergun, D., 1987. Structure analysis by small-angle x-ray and neutron scattering. Plenum Press, New York.

Svergun, D., 1992. Journal of Applied Crystallography 25, 495-503.

Svergun, D., Koch, M.H., Pedersen, J.S., Serdyuk, I.N., 1996. Basic Life Sci. 64, 149-174.

Svergun, D.I., 1999. Biophys. J. 76, 2879-2886.

Svergun, D.I., Koch, M.H.J., 2003. Reports on Progress in Physics 66, 1735-1782.

Syme, C.D., Nadal, R.C., Rigby, S.E.J., Viles, J.H., 2004. J. Biol. Chem. 279, 18169-18177.

Takano, K., 2008. Curr Alzheimer Res 5, 540-547.

Tanzi, R.E., Haines, J.L., Watkins, P.C., Stewart, G.D., Wallace, M.R., Hallewell, R., Wong, C., Wexler, N.S., Conneally, P.M., Gusella, J.F., 1988. Genomics 3, 129-136.

Teng, F.Y.H., Tang, B.L., 2005. Biochem. Biophys. Res. Commun. 328, 1-5.

Teplow, D., 2006. Meth. Enzymol. 413, 20-33.

Thinakaran, G., Koo, E., 2008. J. Biol. Chem. 283, 29615-29619.

Tjernberg, L., Hosia, W., Bark, N., Thyberg, J., Johansson, J., 2002. J. Biol. Chem. 277, 43243-43246.

Tomalia, D.A., Baker, H., Dewald, J., Hall, M., Kallos, G., Martin, S., Roeck, J., Ryder, J., Smith, P., 1985. Polymer Journal 17, 117-132.

Tomalia, D.A., Majoros, I., 2003. Journal of Macromolecular Science, Part C: Polymer Reviews 43, 411-477.

Tong, Y., Li, W., Lin, Y., 1999. Guang Pu Xue Yu Guang Pu Fen Xi 19, 704-706.

Turnbull, S., Tabner, B.J., El-Agnaf, O.M., Twyman, L.J., Allsop, D., 2001. Free Radic. Biol. Med. 30, 1154-1162.

Valko, M., Morris, H., Cronin, M.T.D., 2005. Curr. Med. Chem. 12, 1161-1208.

Vassar, R., Bennett, B.D., Babu-Khan, S., Kahn, S., Mendiaz, E.A., Denis, P., Teplow, D.B., Ross, S., Amarante, P., Loeloff, R., Luo, Y., Fisher, S., Fuller, J., Edenson, S., Lile, J., Jarosinski, M.A., Biere, A.L., Curran, E., Burgess, T., Louis, J.C., Collins, F., Treanor, J., Rogers, G., Citron, M., 1999. Science 286, 735-741.

Venyaminov, S., Kalnin, N.N., 1990. Biopolymers 30, 1243-1257.

Vigo-Pelfrey, C., Lee, D., Keim, P., Lieberburg, I., Schenk, D.B., 1993. J. Neurochem. 61, 1965-1968.

Waldemar, G., Dubois, B., Emre, M., Georges, J., McKeith, I.G., Rossor, M., Scheltens, P., Tariska, P., Winblad, B., 2007. Eur. J. Neurol. 14, e1-26.

Walsh, D.M., Lomakin, A., Benedek, G.B., Condron, M.M., Teplow, D.B., 1997. J. Biol. Chem. 272, 22364-22372.

Walter, J., Kaether, C., Steiner, H., Haass, C., 2001. Curr. Opin. Neurobiol. 11, 585-590.

Wang, W., Hecht, M.H., 2002. Proc. Natl. Acad. Sci. U.S.A. 99, 2760-2765.

Wang, Y., Hodgkinson, V., Zhu, S., Weisman, G.A., Petris, M.J., 2011. Advances in Nutrition: An International Review Journal 2, 129 -137.

Wasiak, T., Ionov, M., Nieznanski, K., Nieznanska, H., Klementieva, O., Granell, M., Cladera, J., Majoral, J.-P., Caminade, P.A.-M., Klajnert, B., 2011. Molecular Pharmaceutics.

Whalley, L.J., 2001. Br J Psychiatry Suppl 40, s53-59.

White, A.R., Bush, A.I., Beyreuther, K., Masters, C.L., Cappai, R., 1999. J. Neurochem. 72, 2092-2098.

Whitson, J.S., Selkoe, D.J., Cotman, C.W., 1989. Science 243, 1488-1490.

Wolfe, M.S., Citron, M., Diehl, T.S., Xia, W., Donkor, I.O., Selkoe, D.J., 1998. J. Med. Chem. 41, 6-9.

Wood, S.J., Maleeff, B., Hart, T., Wetzel, R., 1996. J. Mol. Biol. 256, 870-877.

Wurth, C., Guimard, N.K., Hecht, M.H., 2002. J. Mol. Biol. 319, 1279-1290.

Xie, H., Hu, L.-sen, Li, G.-yi, 2010. Chin. Med. J. 123, 1086-1092.

Yang, M., Roychaudhuri, R., Deshpande, A., Cole, G.M., Frautschy, S., Teplow, D.B., 2010. Biophysical Journal 98, 457a-457a.

Yankner, B.A., Lu, T., 2009. J. Biol. Chem. 284, 4755-4759.

Yankner, B.A., Lu, T., Loerch, P., 2008. Annu Rev Pathol 3, 41-66.

Yiyun, C., Tongwen, X., 2005. Eur J Med Chem 40, 1188-1192.

Yoshiike, Y., Tanemura, K., Murayama, O., Akagi, T., Murayama, M., Sato, S., Sun, X., Tanaka, N., Takashima, A., 2001. J. Biol. Chem. 276, 32293-32299.

Zagorski, M.G., Barrow, C.J., 1992. Biochemistry 31, 5621-5631.

Zagorski, M.G., Yang, J., Shao, H., Ma, K., Zeng, H., Hong, A., 1999. Meth. Enzymol. 309, 189-204.

Zou, K., Gong, J.-S., Yanagisawa, K., Michikawa, M., 2002. J. Neurosci. 22, 4833-4841.